

Functional analysis of *Hectd2*:
A prion disease modifier associated with incubation
time

A thesis presented in partial fulfilment of the requirements for the
degree of Doctor of Philosophy to the University of London

Rabia Begum
MRC Prion Unit, UCL Institute of Neurology
University College London

Declaration

I, Rabia Begum, confirm that the work presented in this thesis is of my own. Where information has been derived from other sources, I confirm that this has been indicated in the thesis.

Abstract

Prion diseases in mice are characterised by prolonged, clinically silent incubation periods that are distinct in duration and reproducible. Incubation times are influenced by a number of factors with the major genetic determinant being variation within the prion protein gene, *Prnp*, however, different lines of inbred mice with identical *Prnp* genotypes show differences in incubation time indicative of a multi-genic effect. A heterogeneous stock of mice was used for fine mapping studies from which emerged several candidate genes including *Hectd2*, an E3 ubiquitin ligase. A human association study found that this genetic modifier is associated with an increased risk to vCJD and kuru.

To characterise *Hectd2*, a yeast two hybrid screen was performed to search for novel interactors, yielding twenty binding partners. Selected candidates were verified by co-immunoprecipitation in mammalian cells. These included *Sh3glb1*, which has been linked to autophagy in a Parkinson's disease model as well as *Stambp*, which encodes a deubiquitination protein in the CNS, and *Stmn2*, a gene previously associated with susceptibility to vCJD in a genome wide association study. *Pacsin2* and *Sept7*, also emerged as *Hectd2* interactors. These proteins operate in the cytoskeletal network, serving a regulatory role for maintaining neuronal integrity, a pathway not previously recognised in prion pathology. By application of a cell based model of prion propagation, the Scrapie Cell Assay, it has been possible to establish the effect of knocking down candidate genes on cell susceptibility thus providing a direct link with prion pathology. In addition, *Hectd2* knockout and transgenic overexpressing mouse models were challenged with three strains of mouse adapted prions to search for an association with incubation time. In conclusion, this has been the first attempt at interactome mapping of a candidate gene associated with incubation time in mouse and susceptibility to human diseases. We have identified novel gene candidates that are implicated in prion pathology, thus providing an insight into the possible pathways that modulate prion disease.

Acknowledgements

I would like to thank my supervisor, Dr Sarah Lloyd, for her teaching, guidance and continued support throughout my PhD. I would also like to thank Professor Parmjit Jat, my secondary supervisor, for helpful discussions and for his words of wisdom.

A very special thanks to Dr Craig Brown for his contribution to my project, knowledge imparted and comedic value he brought to our lab. Thank you for teaching me how to make stable cell lines and for performing the Scrapie Cell Assays - you have been an absolute pleasure to work with.

I would like to thank the rest of the team, Shaheen Akhtar and Julia Grizenkova, for all the fun times that we shared in the lab. I would like to extend my deepest appreciation to Ray Young for his help with preparation of figures and also thanks to Billy West, my go-to Adobe Illustrator expert following Ray's departure. I would also like to thank all of the staff involved in generating the mouse models of *Hectd2*, in particular Dr Sarah Lloyd for conducting the work, Dr Emmanuel Asante's team and Andrew Tomlinson for their support in generating the Tg260 mice, the BSF staff at Wakefield Street for animal maintenance, Huda Al-Doujaily and Dr Jonathon Wadsworth for preparation of prion inocula and also to the Histology team. Many thanks to Dr Jules Edgeworth for teaching me how to culture cells.

I would like to thank the staff and all the students at the MRC Prion Unit/Department of Neurodegenerative Diseases for their words of encouragement, technical advice and for making my PhD a more enjoyable experience. In particular, a special thanks to Dr Sarah Mizielinska, Rosie Bunton, Chris McKinnon, Savroop Bhamra and Masue Marbiah for their support, entertainment and for being awesome friends throughout this process. I would also like to thank Rumena Begum for being a trooper in patiently enduring my PhD woes! Finally I would like to thank my family for cheering me on with their positivity and especially my parents for being my pillars of support.

“Indeed, in the creation of the heavens and the earth, and the alternation of the night and the day, are signs for those of understanding.” [Qur'an 3:190]

Table of Contents

Abstract	3
Acknowledgements	4
Table of contents.....	5
List of figures	9
List of tables	11
List appendices.....	11
1 Introduction	12
1.1 The prion phenomenon.....	12
<i>1.1.1 Human prion diseases.....</i>	<i>12</i>
<i>1.1.2 Aberrant conversion of PrP^C to PrP^{Sc}</i>	<i>15</i>
<i>1.1.3 Characterisation of the prion protein</i>	<i>17</i>
<i>1.1.4 Prion strains</i>	<i>20</i>
<i>1.1.5 Transmission barrier</i>	<i>23</i>
<i>1.1.6 Genetic susceptibility to prion diseases</i>	<i>24</i>
1.2 Genetic modifiers of prion disease incubation time	26
<i>1.2.1 Incubation time</i>	<i>26</i>
<i>1.2.2 Quantitative trait loci.....</i>	<i>29</i>
<i>1.2.3 Candidate genes.....</i>	<i>30</i>
1.3 HECTD2 is a prion disease modifier linked to incubation time	35
<i>1.3.1 E3 ubiquitin ligases</i>	<i>35</i>
<i>1.3.2 Ubiquitin proteasome system-mediated clearance in prion pathology</i>	<i>39</i>
<i>1.3.3 Autophagy-mediated clearance in prion pathology.....</i>	<i>41</i>
<i>1.3.4 E3 ubiquitin ligases in neurodegenerative diseases</i>	<i>44</i>
1.4 Project outline	48
2 Materials and methods.....	50
2.1 Materials	50
<i>2.1.1 Chemicals and reagents</i>	<i>50</i>
<i>2.1.2 Commercial kits</i>	<i>52</i>
<i>2.1.3 Equipment</i>	<i>53</i>

2.1.4 Software	53
2.1.5 Websites	54
2.2 Methods.....	55
2.2.1 Cloning.....	55
2.2.1.1 Oligonucleotide primer design.....	55
2.2.1.2 PCR amplification of inserts for cloning	56
2.2.1.3 Small-scale plasmid purification	57
2.2.1.4 Large-scale plasmid purification.....	57
2.2.1.5 Vector preparation	57
2.2.1.6 Ligation.....	58
2.2.1.7 shRNA design and generation	59
2.2.2 RNA manipulation and analysis	61
2.2.2.1 RNA recovery from cultured cells	61
2.2.2.2 Reverse transcription	61
2.2.2.3 Real time quantitative PCR.....	62
2.2.3 Transformation.....	62
2.2.3.1 DH5 α E.coli cells	62
2.2.3.2 Y2HGold yeast cells	63
2.2.4 Screening of clones	64
2.2.4.1 Bacterial/yeast colony PCR.....	64
2.2.4.2 Agarose gel electrophoresis.....	65
2.2.4.3 Restriction digestion	66
2.2.4.4 Gel excision and purification.....	66
2.2.5 Bacterial/yeast culture	66
2.2.5.1 Bacterial growth	66
2.2.5.2 Yeast growth	67
2.2.6 Sequencing	67
2.2.7 Yeast-two-hybrid library screen.....	68
2.2.8 Mammalian cell culture.....	69
2.2.8.1 Cell maintenance	69
2.2.8.2 Cryopreservation of cells.....	70
2.2.8.3 Recovery of cells.....	70
2.2.8.4 Transfection of cells.....	70

2.2.9 Protein expression analysis	71
2.2.9.1 <i>Preparation of yeast cell protein extract</i>	71
2.2.9.2 <i>Preparation of mammalian cell protein extract</i>	71
2.2.9.3 <i>SDS PAGE</i>	72
2.2.9.4 <i>Western blotting</i>	72
2.2.9.5 <i>Antibodies used</i>	73
2.2.10 Co-immunoprecipitation	73
2.2.11 Knockdown stable cell lines	74
2.2.11.1 <i>Virus generation</i>	74
2.2.11.2 <i>Transduction</i>	75
2.2.11.3 <i>Drug selection of shRNA-expressing cells</i>	75
2.2.12 Scrapie Cell Assay	75
3 Identification of candidate substrates	76
3.1 <i>The Yeast-Two-Hybrid Principle</i>	77
3.2 <i>Selection of bait constructs</i>	78
3.3 <i>Construction of the Hectd2 bait proteins</i>	79
3.4 <i>Pre-screening preparation of Hectd2 bait constructs</i>	82
3.5 <i>Library screening using the Yeast-Two-Hybrid system</i>	87
3.6 <i>Candidate interactors</i>	93
3.7 <i>Co-transformational confirmation of interactions in yeast</i>	95
3.8 <i>Mapping the region of Hectd2-substrate binding</i>	97
4 Validation of interactions in a mammalian cell system	101
4.1 <i>Candidate gene selection for co-immunoprecipitation assays</i>	101
4.2 <i>Design and construction of c-MYC/HA tagged fusion proteins</i>	102
4.3 <i>Co-expression and co-immunoprecipitation of interacting complexes</i>	106
5 Effect on cell susceptibility to prion infection	117
5.1 <i>shRNA gene knockdown in N2aPK1/2 cells</i>	117
5.2 <i>Construction of the pSUPER.retro.puro recombinant plasmid</i>	118
5.3 <i>Relative quantitation of target gene shRNA knockdown</i>	119
5.4 <i>Effect of target knockdown on the Scrapie Cell Assay, SCA</i>	124
6 Supporting work: mouse models of Hectd2: role in incubation time	128
6.1 <i>Mouse models of Hectd2</i>	128

6.2	<i>Generation of the Hectd2 knockout mice</i>	128
6.3	<i>Transmission of prions to Hectd2^{-/-} mice</i>	132
6.4	<i>Generation of Hectd2-overexpressing mice (Tg260^{+/+})</i>	136
6.5	<i>Transmission of prions to Hectd2-overexpressing transgenic mice</i>	138
6.6	<i>Prion strains in infected mouse brains and histology</i>	142
7	Discussion	149
7.1	<i>Discovery of novel candidate interactors of Hectd2</i>	149
7.2	<i>Mapping the region of Hectd2 binding</i>	154
7.3	<i>Mechanism of action of candidate genes in prion propagation and pathology</i>	155
7.3.1	<i>Sh3glb1 modulates prion propagation</i>	155
7.3.2	<i>Sept7 modulates prion propagation</i>	158
7.3.3	<i>Stamp, Pacsin2 and Stmn2: possible modulators of prion propagation</i>	162
7.4	<i>Evidence from mouse models: is Hectd2 a genetic modifier of prion disease?</i>	165
7.5	<i>Continuing research</i>	167
7.5.1	<i>Does Hectd2 confer E3 ubiquitin ligase activity?</i>	167
7.5.2	<i>Characterisation of the molecular pathway by which prion clearance is mediated</i>	168
7.6	<i>Concluding comments</i>	169
8	References	171
9	Appendices	194

List of figures

- Figure 1.1 Pathogenic mutations and polymorphic variations within the prion protein gene
- Figure 1.2 Prion protein structure
- Figure 1.3 Distinct pattern of bands showing types of prion strains for classical CJD, a novel type describing vCJD and kuru
- Figure 1.4 Mechanism of substrate ubiquitin conjugation by the two main types of ligases, HECT and RING E3s
- Figure 1.5 Family of HECT E3 ligases
- Figure 3.1.1 Principle of yeast-two-hybrid assay
- Figure 3.2.1 Sequence analysis of Hectd2
- Figure 3.3.1 Cloning strategy for construction of bait plasmids
- Figure 3.3.2 Construction of the GAL4 BD tagged fusion proteins
- Figure 3.3.3 Insert release from GAL4 BD fusion constructs
- Figure 3.4.1 Expression of Hectd2 bait proteins
- Figure 3.4.2 Toxicity testing of bait proteins
- Figure 3.4.3 Testing for autoactivation of Hectd2 bait proteins
- Figure 3.5.1 Library screening workflow
- Figure 3.5.2 High stringency selection of library positives
- Figure 3.5.3 Prey plasmids insert screening
- Figure 3.7.1 Representative set of Hect414/prey interactions confirmed in yeast
- Figure 3.8.1 Locating the region of Hectd2-prey interaction
- Figure 3.8.2 Putative binding region
- Figure 4.2.1 Construction of the tagged fusion proteins
- Figure 4.2.2 Insert release from MYC/HA fusion constructs
- Figure 4.3.1 Overview of co-immunoprecipitation assay
- Figure 4.3.2 Sh3glb1 co-immunoprecipitates with Hectd2 in COS-7 cells
- Figure 4.3.3 Stmn2 co-immunoprecipitates with Hectd2 in COS-7 cells
- Figure 4.3.5 Stambp co-immunoprecipitates with Hectd2 in COS-7 cells
- Figure 4.3.4 Pacsin2 co-immunoprecipitates with Hectd2 in COS-7 cells

Figure 4.3.6 Sept7 co-immunoprecipitates with Hect414 in COS-7 cells

Figure 5.2.1 Transcription of shRNA targeting *Sh3glb1*

Figure 5.3.1 Relative mRNA expression of candidate genes

Figure 5.4.1 Effect of candidate gene knockdown in the Scrapie Cell Assay

Figure 6.2.1 Construction of targeting allele to generate *Hectd2* knockout mice

Figure 6.2.2 *Hectd2* mRNA sequence

Figure 6.3.1 Kaplan-Meier curves for onset of first clinical signs for *Hectd2* knockout mice

Figure 6.3.2 Kaplan-Meier survival curves for *Hectd2* knockout mice.

Figure 6.4.1 Relative expression of *Hectd2* overexpressing, Tg260^{+/-}, heterozygous mice

Figure 6.5.1 Kaplan-Meier curves for onset of first clinical signs for Tg260^{+/+}, *Hectd2*-overexpressing mice

Figure 6.5.2 Kaplan-Meier survival curves for Tg260^{+/+}, *Hectd2*-overexpressing mice

Figure 6.6.1 PrP^{Sc} type determination from infected mouse brains

Figure 6.6.2 RML transmission to *Hectd2*^{-/-}: histological analysis

Figure 6.6.3 ME7 transmission to *Hectd2*^{-/-}: histological analysis

Figure 6.6.4 MRC2 transmission to *Hectd2*^{-/-}: histological analysis

Figure 6.6.5 RML transmission to Tg260^{+/+}: histological analysis

Figure 6.6.6 ME7 transmission to Tg260^{+/+}: histological analysis

Figure 6.6.7 MRC2 transmission to Tg260^{+/+}: histological analysis

List of tables

- Table 2.2.1 Primers for cloning into pGBKT7, pCMV-MYC or pCMV-HA
- Table 2.2.2 shRNA oligonucleotides for cloning into pSUPER.retro.puro
- Table 2.2.3 PCR screening primers
- Table 2.2.4 Antibodies
- Table 3.3.1 Molecular weight of Hectd2 fragments
- Table 3.6.1 Candidate genes and proportional match to full length protein
- Table 3.8.1 Locating the region of binding to Hectd2 via co-transformation of bait with prey
- Table 4.2.1 Molecular weight of candidate genes and Hectd2/Hect414
- Table 4.3.1 Construct combinations for co-immunoprecipitations
- Table 5.3.1 shRNA knockdown lines for Scrapie Cell Assay
- Table 6.3.1 Mean incubation times for *Hectd2*^{-/-} and WT mice
- Table 6.5.1 Mean incubation times for *Hectd2*-overexpressing (Tg260^{+/+}) and WT mice

List of appendices

Appendix 1 Solution formulations

- 1.1 Bacterial selection plates
- 1.2 Yeast selection plates
- 1.3 Yeast transformation solutions
- 1.4 Yeast protein extraction solutions and buffers
- 1.5 Mammalian cell lysis buffers
 - 1.5.1 Standard cell lysis buffer
 - 1.5.2 RIPA buffer

Appendix 2 Vectors

Appendix 3 Sequences

1 Introduction

1.1 The Prion Phenomenon

1.1.1 Human prion diseases

Prion diseases, or transmissible spongiform encephalopathies, are a group of fatal neurodegenerative conditions that are transmissible to both humans and animals. These include Creutzfeldt Jacob Disease (CJD), Fatal Familial Insomnia (FFI), Gerstmann Straussler Scheinker syndrome (GSS), variant CJD and kuru in humans. Animal prion diseases include Bovine Spongiform Encephalopathy (BSE), Scrapie, Chronic Wasting Disease (CWD) and Transmissible Mink Encephalopathy, which affect cattle, sheep/goat, mule deer/elk and mink, respectively¹⁻⁴. The histopathological hallmarks by which the disease can be distinguished include spongiform vacuolation of the brain, neuronal loss and astrogliosis, which may be accompanied by brain deposition of an atypical version of the prion protein, PrP^{Sc}^{2, 3, 5}. The prion protein or PrP^C is expressed normally in cells but may undergo post-translational conversion into an aberrant, pathogenic isoform, PrP^{Sc}⁶. This conformation of the prion protein has been found to constitute the principal if not sole component of the infectious agent⁷. Although rare, affecting only one in a million per year worldwide³, intense research has been focused on this field due to the unique biology of the prion agent thought to cause disease. A notable feature that characterises these encephalopathies is their prolonged clinically silent period, or incubation time, which marks the interval between infection and onset of clinical symptoms^{3, 8}.

Distinct from any other disorder, prion diseases present as one of three different forms, sporadic, inherited or acquired⁹⁻¹¹. Sporadic occurrences of the disease constitute ~85% of all cases, where most patients are aged between 45-75. This classical form of CJD manifests as a rapidly progressive dementia, characterised by a diffuse pattern of PrP^{Sc} deposition^{11, 12}. Symptoms characterising the onset of disease include myoclonus, cerebellar ataxia, cortical blindness, depression, insomnia and fatigue. It is speculated that the disease is triggered spontaneously in the brain although its aetiology remains unknown^{9, 11}.

Inherited prion diseases account for ~15% of cases and have been causally linked to autosomal dominant mutations within the prion protein gene, *PRNP*^{13, 14}. Although the molecular basis of how these mutations cause disease is unknown, it is thought that they increase the conversion of PrP^C to PrP^{Sc}¹⁵. Alternative membrane topology of PrP has also been postulated as a possible mechanism by which neurotoxicity may be caused¹⁶. The A117V and G114V mutations associated with familial CJD may generate Ctm-PrP which spans the membrane once with its C terminus facing the cytosol^{16, 17}. This membrane topology of PrP is enhanced following PrP^{Sc} accumulation, giving rise to the notion that Ctm-PrP may represent a neurotoxic species that causes pathogenicity^{17, 18}.

Over 30 pathogenic mutations have been defined, (Figure 1.1), where the E200K mutation is the most common cause of inherited prion disease¹⁹. Knowledge of these mutations makes it possible to perform pre-symptomatic diagnosis through *PRNP* analysis³. The inherited conditions include familial CJD (fCJD), Gerstmann-Straussler Scheinker syndrome (GSS) and fatal familial insomnia (FFI), which show variable clinical and neuropathological presentation depending on the mutation³. fCJD patients are affected by a rapidly progressive dementia including myoclonus; GSS manifests as a chronic cerebellar ataxia with patients suffering later onset of progressive dementia and FFI features include progressive insomnia, dementia, hallucinations, malfunction of the autonomous nervous system and is commonly linked to a missense mutation within *PRNP* at codon 178²⁰.

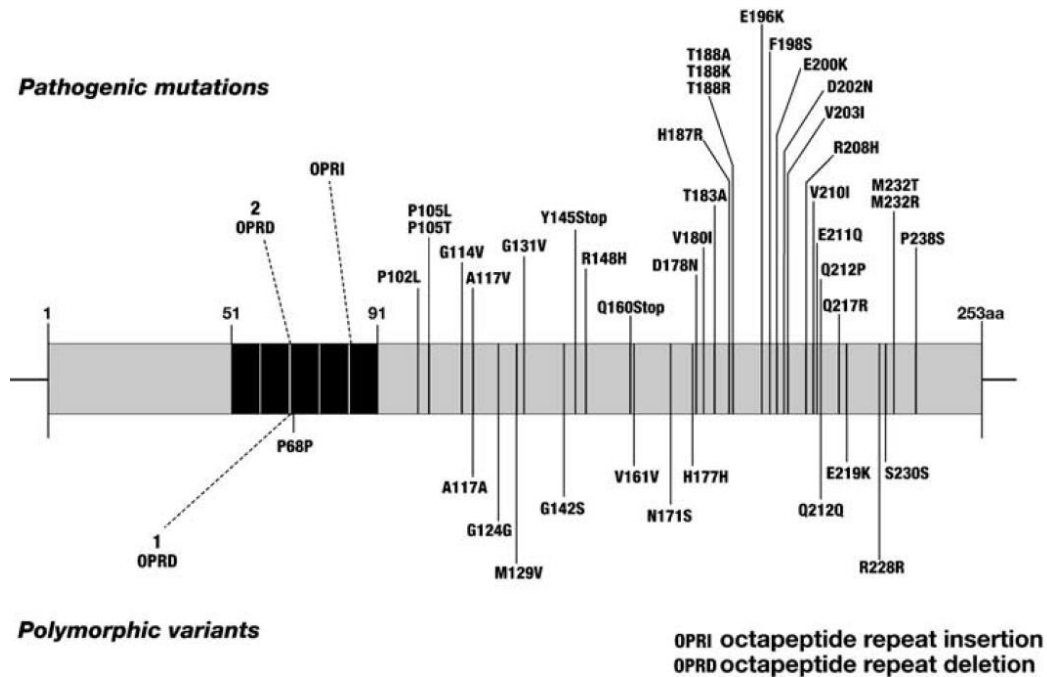


Figure 1.1 Pathogenic mutations and polymorphic variations within the prion protein gene. Amino acid changes representing pathogenic mutations are shown above in the schematic whereas polymorphisms that influence the susceptibility to disease are shown below. *Adapted from Mead et al., 2006.*

Acquired prion diseases are caused by exposure to infectious prion agents and include iatrogenic CJD (iCJD), kuru and vCJD. Iatrogenic CJD arose by accidental transmission of CJD prions through surgical procedures with contaminated instruments and transplantation material²¹. The most common cases of iCJD were due to treatment with cadaveric pituitary growth hormone and implantation of dura mater grafts from infected humans whilst the less common iCJD occurrences were due to transmission of iCJD via corneal transplantation and implantation of contaminated EEG electrode^{22, 23}. Kuru and vCJD are also acquired forms of the disease. Kuru was the first human epidemic of prion disease, which occurred through a dietary medium in the Fore linguistic group as part of a ritual cannibalistic mortuary feast in the Eastern Highlands of Papua New Guinea²⁴. Progressive cerebellar ataxia was the main clinical manifestation, in addition to psychiatric and behavioural changes with incubation periods in some individuals exceeding 50 years²⁵.

The arrival of vCJD was identified as a result of BSE exposure to humans^{10, 26}. Clinical features of the disease include psychiatric and behavioural changes as well as cerebellar ataxia, affecting patients that are mostly young^{3, 27, 28}. The median age of onset is 26 years in sharp contrast to the late onset of sporadic CJD, where the median age at death is 68 years²⁹. The transmission of BSE from contaminated cattle to humans by widespread dietary consumption raised serious public health concerns at the time, due to its transmissibility across species^{1, 3, 29}.

1.1.2 Aberrant conversion of PrP^C to PrP^{Sc}

The prion phenomenon revolves around the hypothesis that aberrant conformational conversion of normal cellular PrP^C to PrP^{Sc} is the chief cause underlying all prion conditions^{6, 30-33}. In 1967 Griffith first suggested that the infectious agent was solely protein, which was later supported by Prusiner's work in 1982, where the infectious fraction was enriched from brain homogenates in which the major element was a protease resistant glycoprotein^{6, 34}. The protein was termed a prion, which he described as "small proteinaceous infectious particle which is resistant to inactivation by most procedures that modify nucleic acids"⁶. The basis of this hypothesis states that prion propagation is the result of PrP^{Sc} replication by it serving as a template to encourage the conformational conversion of wild type PrP^C to the disease causing PrP^{Sc}. Both PrP^C and PrP^{Sc} forms have the same primary sequence but differ in their tertiary conformation⁵. This has been lent support by PrP knockout mouse models in which challenge of *PrP^{0/0}* mice with mouse scrapie prions resulted in healthy mice that survived without pathology for their natural life span comparable to controls that died under 6 months³⁵. Pathogenic PrP^{Sc} was absent in brains of these mice following inoculation, indicating that PrP is necessary for prion propagation and that pathology is not the result of loss of PrP function but rather a toxic gain of function from PrP^{Sc}³⁵⁻³⁷. Furthermore, Mallucci and co-workers found that conditional PrP knockout mice were resistant to prion disease; their work showed that neuronal knockout of PrP is protective and that non-neuronal PrP^{Sc} is not pathogenic³⁸. Thus mice devoid of the prion protein fail to propagate infectivity in the absence of PrP^C and thus show resistance to prion infection, indicating that PrP^C is essential for PrP^{Sc} replication³⁵. In addition, mice hemizygous for one PrP^C allele present an enhanced

resistance to prion replication compared to mice with two copies of *Prnp*, shown by a prolonged incubation period³⁵. However, when PrP transgenes were engineered into *PrP^{0/0}* mice, subsequent inoculation with prions led to prion propagation and pathology³⁹. Furthermore, neural grafting of PrP^C-overexpressing tissues into mouse brains devoid of PrP, showed PrP^{Sc} propagation and infectivity accompanied by pathology characteristic of scrapie in the graft following challenge with scrapie prions. However, host PrP^C-deficient tissue showed no histopathological changes although an accumulation of PrP^{Sc}, derived from the grafts, was observed^{40, 41}.

Models that describe the mechanism through which replication may occur, in line with the protein only hypothesis, have been proposed as template-directed refolding and the seeded nucleation hypothesis^{2, 42}. The template-directed refolding mechanism suggests that PrP^{Sc} interaction with PrP^C, promotes conversion of wild type molecules to PrP^{Sc} to form aggregated amyloid. Dissociation of PrP^{Sc}-PrP^{Sc} complexes generate the free pathogenic prion to act on further PrP^C molecules. The seeded nucleation theory postulates that PrP^C exists in dynamic equilibrium with PrP^{Sc}, whereby an infectious seed is formed slowly from PrP^{Sc} molecules and when this is formed, a fast recruitment of monomeric PrP^{Sc} molecules to the seed generates amyloid aggregates. These aggregates can fragment, thereby liberating seeded nuclei to which further PrP^{Sc} monomers may be added to, thus propagating infectivity^{2, 42}.

Both of these models suggest that self-replication of prions gives rise to neurotoxicity, however, a further model postulates an alternative mechanism; an intermediate, PrP^L for lethal, is generated as either a side product or an intermediate in the process of PrP^{Sc} replication³¹. Whether PrP^L is produced as a template intermediate leading to the toxic pathway or as a side product from PrP^{Sc} acting as a surface template, thereby propagating the toxic pathway, it may be that neurotoxicity is the result of accumulation of PrP^L that exceeds a threshold that cannot be tolerated, marking the end of the incubation period, rather than PrP^{Sc} as the toxic agent³¹. This theory has been lent support by a recent study by Sandberg *et al.*, where they uncoupled neurotoxicity from infectivity by showing that prion replication occurs exponentially until saturation is achieved⁴³. The authors suggest that the neurotoxic species is then catalysed from PrP^{Sc} or within that route, which in turn

activates the toxic pathway⁴³. Although these models differ in their kinetics and the species that causes toxicity, they are unified in that prion propagation remains the essence of pathogenesis.

1.1.3 Characterisation of the prion protein

The prion protein was first identified as the protein product of a cellular gene in 1985 by Oesch *et al.*, after which it was mapped to human chromosome 20 and mouse chromosome 2^{44, 45}. The *PRNP* gene that encodes the prion protein is ubiquitously expressed although an abundance of the protein is present in neurons and glial cells, suggesting an essential function that is of particular relevance in the CNS³. Structurally, PrP^C has an N-terminal flexible region containing 5 octarepeats and a C-terminal globular domain, representing the structured region⁴⁶. PrP^C is composed of 40% α -helical structure and virtually no β -sheet (3%), whereas the disease-associated form, PrP^{Sc} has a 30% makeup of α -helix and a high β -sheet content (43%)³³. This β -sheet conformation is thus a central feature in the conversion of normal PrP^C to the pathogenic PrP^{Sc} isoform. β -sheets have a high propensity to aggregate, which is supported by the presence of amyloid plaques of PrP^{Sc} aggregates in some prion diseases³. Three alpha helices and two beta sheets comprise the C-terminal domain, (Figure 1.2), and a conserved disulfide bond with cysteine residues at codon 179 and 214 forms a bridge between alpha helix 2 and 3⁴⁷. A hydrophobic domain features at residues 91-120 and an N terminal octapeptide repeat from residues 60-91⁶.

PrP^C is highly conserved across species and in humans it forms a 253 residue protein⁴⁸. The protein is targeted to the secretory pathway by a 22 residue signal peptide located at the N-terminus, and it is *N*-glycosylated at Asn180 and Asn196 (Figure 1.2)⁴⁸. PrP^C is a membrane bound protein that is attached to the outer cell surface or lipid rafts on plasma membranes by a GPI anchor, attachment of which is mediated by a 23 residue signal sequence⁴⁸. PrP^C undergoes biosynthesis at the ER and is trafficked to the cell surface through the Golgi, after which recycling may occur via endocytic mechanisms by internalization of PrP into clathrin coated pits⁴⁸. Such endocytic internalisation of PrP^C is

of biological interest as the endosomal pathway has been associated with being a site of PrP^{Sc} conversion⁴⁸.

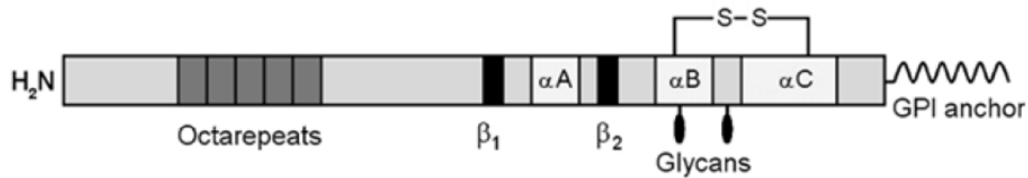


Figure 1.2 Prion protein structure. The secondary structure is comprised of an N-terminal flexible region housing 5 octarepeats and the C-terminal domain forms a globular structured region comprised of three alpha helices (αA , αB , αC) and two beta strands, β_1 and β_2 . The glycans represent *N*-glycosylation at residues Asn180 and Asn196, whilst the disulfide bridge is formed between residues 179 and 214. The GPI moiety is attached at the C-terminus for anchoring to the membrane. *Adapted from Didonna et al., 2013.*

Despite its wide expression profile, the precise physiological function of the prion protein remains elusive. A powerful strategy to unravel its role is to knockout the mouse orthologue of the gene in order to assess its effects in a physiological setting. Several knockout mouse models of PrP exist; *PrP*^{0/0} and *PrP*^{-/-} both describe mice ablated for the prion protein gene^{37, 49}. These knockout mice show modified circadian patterns and rhythm, which results in altered sleep regulation. The authors suggest that the prion protein may serve a function that is relevant to fatal familial insomnia, in which there is profound sleep disturbance^{50, 51}.

Further work has involved targeting PrP gene ablation to neuronal cells of adult mice, which has shown that it does not result in neurodegeneration⁵². However, neurophysiology was altered in these mice, for which the authors suggest a role for the prion protein in neuronal excitability regulation⁵². Depleting neuronal PrP in mice following disease initiation resulted in reversal of early spongiform change and preservation of neurons, although PrP^{Sc} accumulated in glia. The authors found that PrP-depleted neurons confer resistance to infection from surrounding cells³⁸. Furthermore, Collinge *et al.*, showed that PrP is associated with a role in synaptic function⁵³. The authors analysed brain hippocampal slices of PrP null mice and showed that synaptic inhibition was impaired giving rise to speculation that the epileptic-like phenotype seen in CJD patients may be due to dysfunctional synaptic inhibition⁵³.

A cytoprotective activity has been attributed to PrP^C, which has been demonstrated by Bax induction of the apoptotic pathway in a cellular system. When the pro-apoptotic protein, Bax, was overexpressed in human fetal neurons, the majority of the neurons underwent apoptosis, whilst co-expression of PrP and Bax showed that the level of apoptotic cells had decreased to ~10%^{54, 55}. However, the precise function of PrP still remains elusive as this cytoprotective activity seemed to only apply to Bax-mediated apoptosis⁵⁵.

PrP^C has also been implicated as a protective agent against oxidative stress. Brown *et al.*, showed that neurons from *Prnp*^{0/0} mice develop abnormalities in their response to oxidative stress, resulting in cells that are highly susceptible to stress inducing agents relative to wild type neurons^{55, 56}. The authors describe a decline in the Cu²⁺/Zn²⁺-dependent SOD-1 activity, suggesting that loss of PrP is linked to the decline observed in SOD1 activity⁵⁶. This is supported by research where increased levels of oxidative stress markers were found in the brains of *PrP*^{0/0} mice⁵⁷. Some mechanisms of SOD1 activity have been postulated to include a role for PrP^C in directly detoxifying reactive oxygen species or indirectly by upregulating proteins that act to detoxify these agents. These data are in line with the process of neurodegeneration to which increased oxidative stress and neuronal excitability may contribute, placing PrP^C in a neuroprotective role against toxic stressors⁵². However, reports that PrP possesses copper-dependent SOD activity⁵⁸ were followed up by Jackson *et al.*, who identified that the prion protein does not have SOD-1 activity⁵⁹.

PrP^C has been functionally associated with signal transduction in various pathways by virtue of its localisation on cell surfaces and lipid rafts^{48, 60}. Evidence for PrP^C-dependent signaling was provided by Mouillet-Richard *et al.*, who showed that PrP^C is coupled to cytosolic tyrosine kinase Fyn in a caveolin-1 dependent manner, activation of which is facilitated by recruitment of NCAM to lipid rafts by PrP^C^{61, 62, 63}. Such signal transduction has been further substantiated by recent work in which Strittmater *et al.*, found that the deleterious neuronal impairment observed in Alzheimer's brains was linked to amyloid-beta interaction with post-synaptic PrP, which in effect leads to the activation of Fyn to phosphorylate NMDA receptors followed by their subsequent loss^{64, 65}. However, an

effect on incubation time or PrP accumulation is not observed in mice deficient in NCAM or Fyn suggesting that these pathways may not underlie prion pathology.

PrP^C has also been implicated in the PI3K/AKT pathway, which regulates a number of fundamental processes such as cell growth, migration, survival, metabolism and cancer progression⁴⁸. An emerging role in neuroprotection has also been reported by a number of groups, including work by Roffe *et al.*, who showed that PrP^C interaction with stress-inducible protein 1 modulates correct neuronal function through the PI3K/Akt/mTOR and ERK1/2 pathways⁶⁶. PrP^{Sc} neurotoxicity has been investigated using PrP₁₀₆₋₁₂₆ as a model, as this peptide possesses physicochemical and pathological properties like PrP^{Sc} with respect to its partial protease resistance, amyloid forming potential and neurotoxic activity⁶⁷. The PI3K/Akt pathway has been shown to be disrupted following exposure to PrP₁₀₆₋₁₂₆ peptide in a neuronal cell line and its neuroprotective involvement has also been observed following oxidative stress^{68, 69}.

1.1.4 Prion strains

Distinct heterogeneity of PrP^{Sc} has been observed whereby different prion strains can be derived from pathogenic isolates⁷⁰. These strains can be passaged into inbred mice and differ by their distinct patterns of neuropathology and incubation periods^{11, 70-72}. Strains are thus infectious isolates that have heritable properties manifesting as distinct disease phenotypes⁷⁰. These may be propagated in a defined inbred mouse line to produce strain-specific phenotypes²⁹⁻³¹. Although this appears to oppose the protein only hypothesis in that a single protein cannot possibly be the cause of effect of different phenotypes, the diversity of strains have been described as conformational variations of PrP^{Sc}². Conformational variants have the capacity to propagate via conversion of host PrP into one that resembles the variant^{2, 31, 73}. The specificity of strains was lent credibility by work where distinct transmissible mink encephalopathy (TME) prion strains, denoted hyper (HY) and drowsy (DY), which originated from the same PrP sequence, were serially propagated in Syrian hamsters⁷⁴. TME caused by HY propagation presents with hyperexcitability, ataxia and tremors whilst DY manifests as progressive lethargy^{75, 76}. The paradigm of prion strains was further described by the Telling group where they

transmitted isolates from the brains of patients with FFI, sporadic and inherited prion disease to transgenic mice expressing humanised PrP⁷⁷. Challenge with these isolates resulted in the propagation of PrP^{Sc} that retained the biochemical properties of the original inocula. They suggested that strains are enciphered in the conformation of PrP^{Sc}, which serves as a template for the direction of nascent PrP^{Sc} molecules⁷⁷. A number of groups have proposed that prions are an ensemble of PrP^{Sc} molecules that consist of major and minor species which are selectively maintained in a host dependent manner^{30, 31, 78}. The minor subcomponent thus may show dominance in a new host or tissue, preferentially propagating due to factors that are permissive and favour that species, a phenomenon known as strain shifting or mutation that potentially produces a new phenotype, uncharacteristic of the original strain⁷⁸. This was demonstrated by findings that the sheep scrapie 22A prion strain was stable on serial mouse passage under standard conditions, however upon passage into mice with a different genotype, gradual changes in the incubation periods were observed^{79, 80}. Following further subsequent passages, stabilisation occurred in the form of a new strain, 22F⁸⁰.

Prion strains thus showed heritability in their physicochemical properties as observed by distinct prion accumulation in affected brains and different susceptibilities to proteinase K digestion in addition to their different cleavage products upon digestion^{75, 76}. Four major types of human PrP^{Sc} have been defined, according to *Hill et al.*, although classification using an universal nomenclature is yet to be established⁹. These relate to the fragment size and glycoform ratio following protease digestion corresponding to un-, mono or diglycosylated PrP^{Sc}. Types 1-3 correlate with classical CJD (sporadic or iatrogenic) whilst vCJD is associated with PrP^{Sc} forms of type 4 (Figure 1.3). Polymorphism at codon 129, encoding either methionine or valine, is known to have a strong modifying effect to disease susceptibility⁸¹ (discussed in detail in Section 1.1.6) and thus the strain types shown in Figure 1.3 also indicate the codon 129 genotype for a given strain. Types 1 and 4 have only been associated with homozygosity at codon 129 of *PRNP*, type 3 being observed with a valine at one allele and type 2 has been observed for all genotypes of *PRNP* at this polymorphic residue^{9, 71, 82}. Kuru prions were found to have a PrP^{Sc} type that was in line with types 2 and 3, with valine or methionine homozygosity at codon 129⁸³. Although polymorphisms at codon 129 facilitate homotypic interactions,

differences in primary structure alone cannot account for the existence of strains as they can be propagated in mice with identical PrP primary coding sequence^{30, 31}. Furthermore, strains may be isolated from mice following passage in a different species, wherein they retain their biochemical properties. The basis of strain diversity requires that a given isolate imprints its properties on a host PrP. It is thought that these strains account for the clinical and neuropathological heterogeneity seen in patients^{31, 71, 72, 77}. Strains thus serve an important role in determining the ease with which an isolate can propagate in a new species, or the transmission barrier.

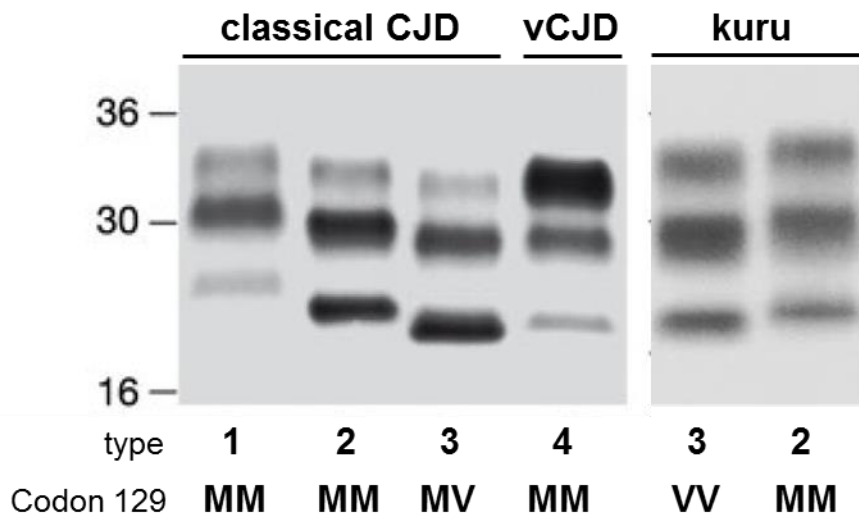


Figure 1.3 Distinct pattern of bands showing types of prion strains for classical CJD, a novel type describing vCJD and kuru. Analysis of proteinase K digested sCJD, iCJD, vCJD and BSE infected brain extracts on an immunoblot show a characteristic type of banding representing diglycosylated, monoglycosylated and unglycosylated forms of PrP^{Sc}. Types 1-3 rare seen in sporadic or iatrogenic CJD brains whilst type 4 is observed in vCJD and both types 2 and 3 in kuru. Analysed using monoclonal antibody 3F4. *Adapted from Wadsworth et al., 2011; Wadsworth et al., 2008.*

1.1.5 Transmission barrier

Prions are transmissible between species but the efficiency with which they can propagate from one species to another is limited by a transmission barrier⁸⁴. Within the same species, propagation may be highly efficient but across species a large barrier may be observed which translates as a prolonged incubation period³⁰. Transmission reflects a stochastic process whereby only a few animals may propagate prions showing prolonged and variable incubation periods whereas subsequent transmissions into the same species permit adaptation and thus present incubation times that are characteristic of that species³⁰. These barriers can be quantified by measuring the difference between first and subsequent passage where a drop in incubation time occurs³⁰. The difference in transmission efficiency between the first passage of a prion into a particular species and the subsequent passages is thought to lie within differences in primary structure of the host and donor prion protein and the permissible conformational variants available, the prion strain type and the co-factors within the environment in which propagation occurs^{28, 73, 85}. The work by Prusiner *et al.* found that when transgenic mice expressing the hamster prion protein were inoculated with hamster prions, synthesis of hamster prions were identified rather than mouse prions whilst transgenic mice for the mouse prion protein produced mouse prions and not hamster prions⁷³. This work contributed to current thinking in that homotypic PrP interactions permit efficient prion propagation and contribute a role in the efficiency of transmission^{2, 73}. Transmission barriers were analysed when hamster scrapie Sc237 prions were inoculated into mice, which did not show any clinical sign 735 days post-inoculation, however following transmission of this prion into mice transgenic for hamster prion protein, short incubation periods were observed^{73, 86}. Sequence differences between hamster and mouse PrP show that they differ at 16 residues, indicating that non-homologous PrP interactions translate as prolonged incubation times^{6, 13}.

Thus transmission barriers reflect the degree of overlap between host and donor PrP, which is shown by the ease with which a strain may propagate in a species or the ability of a given strain to propagate prions in a new host from a limited set of conformations that can be assumed by PrP^{Sc}³⁰. However, the measure of transmission barriers by

determination of clinical end point may be misleading as it has been shown that prions are able to replicate although as a subclinical form of infection as the barrier to disease may be large^{85, 87}. Hill *et al.*, found that hamster prions that were historically thought to be non-pathogenic in mice, were able to replicate in mice, despite the barrier in causing clinical disease⁸⁵. Failure to generate the neurodegenerative syndrome in subclinical animals may be associated with prion kinetics in terms of inefficient propagation, providing further support to this notion³⁰. This results in a lack of the toxic species being able to surpass the threshold for neurotoxicity⁴³. This was further supported by Beringue *et al.*, who showed that prions infect the lymphoreticular system at a subclinical level⁸⁸. They found that following CWD prion infection in mice expressing ovine PrP the transmission barrier to lymphoid tissue was more permissive than in brain⁸⁸. These authors challenged mice expressing human PrP with BSE prions for which they found prion infection in the spleen but less than 10% of animals were found to have presence of prions in the brain following prolonged incubation periods⁸⁸. Together, these findings relate the risk of zoonotic potential of prions despite the large barrier to clinical disease^{30, 88}.

1.1.6 Genetic susceptibility to prion diseases

Polymorphic variation within the *PRNP* gene has a major influence in determining susceptibility to disease for both animals and humans. These polymorphisms are known to have a modifying effect, in particular, codon 129 of the prion protein, which serves as a major risk factor for disease susceptibility. At this location, a methionine or valine residue may alternate which is observed at a frequency of 38% for methionine homozygotes, 11% for valine homozygosity and heterozygotes at 51% in the UK population¹⁹. Homozygosity has been associated with an increased risk to acquired and sporadic cases of CJD. The majority of sporadic cases show methionine homozygosity at codon 129, and all cases of vCJD have methionine homozygosity at this *PRNP* locus^{81, 89, 90}. A crystal structure of human prion protein has shown that interactions with neighbouring prion proteins are mediated by homotypic contacts between residues that

surround codon 129; this shows the importance of this region in determining disease susceptibility⁹¹.

Heterozygosity has however, been shown to confer partial resistance. Patients with iatrogenic CJD and codon 129 heterozygosity have a later age of disease onset⁹². Heterozygosity in familial CJD is also linked to a later age of onset, however, codon 129V in patients with the D178N mutation can predispose individuals to CJD⁹³. Longer incubation times may reflect mechanisms of prion biology due to non-homologous interaction between prion proteins. As a result, the efficiency with which transmission can occur may decrease as the infective seed, PrP^{Sc}, struggles to propagate due to the restrictive conformation posed by the strain³¹. These findings concur with analyses of elderly survivors of kuru that had multiple exposures but were healthy and were heterozygous at codon 129. Heterozygotes were over 30 years of age at onset, whereas homozygotes of either allele were ~19 years of age at onset⁹⁴. The survival advantage conferred by heterozygosity has thus driven a strong balancing selection pressure for codon 129 heterozygosity in the Fore region²⁴.

A protective polymorphism that showed a pronounced effect on kuru susceptibility was identified in the Fore region of Papua New Guinea as G127V, where heterozygosity confers kuru resistance⁹⁵. This polymorphic variant was not found in patients with kuru and occurs at a frequency of 8% in the south Fore region although geographical distribution studies have found that this polymorphism is not seen elsewhere⁹⁵.

In the Japanese population, the E219K polymorphism has been identified with a 6% frequency as susceptibility factor for sporadic CJD¹⁹. Codon 129 is not polymorphic in the Japanese population, however heterozygosity at codon 219 appears to confer resistance to sporadic CJD.

Although polymorphic variation within the *PRNP* gene is the major genetic determinant, there are other genes that may modulate disease susceptibility. To identify genes modulating genetic susceptibility to prion diseases, genome wide association studies (GWAS) and mouse models have proven to be key genetic tools to capture genetic variation between sample cases and normal controls.

1.2 Genetic modifiers of prion disease incubation time in mice

1.2.1 Incubation time

Prion diseases feature a prolonged, clinically silent incubation period. In animal transmission studies, this period is defined as the time between inoculation with prions and the onset of clinical symptoms. The mouse is ideal for modelling prion disease as it closely recapitulates the key features, including incubation time, a trait chosen for further investigation by many research groups⁹⁶⁻¹⁰⁰.

In experimental transmission studies, under standard conditions, infection of inbred lines of mice with the same prion strain demonstrated large differences in incubation times that are well defined and reproducible¹⁰¹⁻¹⁰⁴. The findings from these studies identified these striking variations, ranging in incubation times from 108 ± 1 days for mice with a NZW/OlaHsd background to 313 ± 3 days for Ju/FaCT mice. Incubation times are categorised as short and long incubation periods, where the former is assigned to those that present incubations ~100-200 days long and the latter for those that exceed 255 days¹⁰².

It has been shown that mice hemizygous for *Prnp*, *Prnp*^{0/+}, showed an incubation time that was 125 days longer than that of wild-type mice, *Prnp*^{+/+}³⁵. This reflects an enhanced resistance to scrapie infection, providing evidence of an inverse relationship between incubation time and the level of PrP^C³⁵. This was further supported by transgenic mice studies where overexpression of PrP^C maintains this inverse relationship, which has resulted in incubation times as short as 62 ± 4 days^{35, 73, 105, 106}. Prion strain also plays a role in influencing incubation time^{28, 71, 75}. Following transmission of mouse adapted BSE and scrapie strains into C57BL mouse strains, mean incubation times of 207 ± 3 and 164 ± 4 days were observed respectively, showing the effect exerted by prion strains²⁸. Differences in incubation time can also be attributed to the presence of a species barrier^{28, 107, 108}. This is demonstrated clearly by the incubation times that are obtained upon primary passage in VM mice inoculated with BSE and scrapie, which show incubation times of 471 ± 8 and 769 ± 16 days but following subsequent mouse-mouse passage, 116 ± 3 and 308 ± 15 days, respectively²⁸. The route through which a prion strain is inoculated

presents variations in incubation times. It was shown that intracerebral transmission of Chandler/RML scrapie in C57BL mice had a mean incubation of 138 ± 3 days whilst intraperitoneal inoculation had a prolonged period of 184 ± 5 days, explained by the provision of faster access to the CNS, permitting rapid prion propagation and thus shorter incubation times¹⁰⁹. The inoculum dose is also important in determining these incubation times as dose response curves have shown an inverse relationship between the inoculum titre and incubation time¹¹⁰.

Research by Dickinson and MacKay, found that control of incubation time could also be determined by host genotype. The authors described an exceptionally long incubation time of 280 days in the VM/Dk mouse strain relative to the shorter incubation times between 140 and 180 days of eight other strains upon infection with the ME7 scrapie strain under standard conditions⁹⁷. Further observations of characteristic incubation periods of different mouse strains following infection with a defined prion strain were reported^{98, 102, 111, 112}, highlighting a genetic influence of mouse background on incubation time. Attempts to delineate these genes involved mouse crosses between the RIII and VM/Dk mouse strains representing short and long incubation times respectively. As a result of this work, a discovery of the incubation time regulator, *sinc*, was made, which had short and long incubation time alleles, *s7* and *p7*¹¹¹. Similar segregation in incubation time was observed in crossing a *sinc s7* mouse strain, NZW/LacJ, with a *sinc p7* strain, I/LnJ, producing an incubation time that was intermediate of these two extremes¹⁰¹. Backcrossing of these F1 generation to NZW/LacJ resulted in progeny that segregated into two groups with defined incubation periods, leading to the identification of a single locus *Prni*, considered to be the same locus as *Sinc*. This locus was found to modulate incubation time with its short and long alleles, *N* and *I* and was closely linked to *Prnp*^{101, 102}. These alleles were then re-designated as *Prnp^a* and *Prnp^b* respectively, following the discovery that *Prnp* was expressed as two variants in mice⁹⁸. These variants arise from polymorphisms at codon 108 and 189, where a dimorphism encoding leucine and threonine at position 108 and 189, respectively, gives *Prnp^a* whereas phenylalanine and valine at these codons express as *Prnp^b*. These alleles segregate with incubation time, indicative of *Prnp* dimorphic control of incubation time. This was proven by a gene targeting strategy whereby *Prnp^a* mice were engineered to express the *Prnp^b* variant

endogenously¹¹³. The authors generated a 129/Ola mouse line that expressed PrPB in place of its wild-type PrPA. Upon infection with mouse adapted BSE, 301V, wild-type 129/Ola PrP A/A mice that carry the *Prnp^a* allele show an incubation of 244 ± 2 days in contrast to the 133 ± 0.2 days shown by gene targeted $a^{[108F189V]}/a^{[108F189V]}$ 129/Ola mice that express variant PrPB. This is comparable to wild type VM/Dk PrP B/B mice that have the *Prnp^b* allele, expressing PrPB, which have an incubation of 119 ± 2.1 days following challenge with 301V. This was the first demonstration in mouse that confirmed the congruency of *Prnp* and *Sinc/Prni*, thereby confirming the role of *Prnp* variation in the control of incubation time¹¹³. The difference in incubation times between the gene targeted *Prnp^a[108F189V]* mice and wild-type *Prnp^b* mice can be explained by their different genetic background suggesting that other genetic loci may also modify incubation time. The dimorphisms related here were further analysed separately through gene targeting *Prnp^a* mice¹¹⁴. This work identified that both of these polymorphisms control incubation time and that each of these play a different role. The authors suggest that codon 189 reflects initial binding of the donor PrP with host PrP whilst codon 108 may control the efficiency with which PrP^C is converted to pathogenic PrP^{Sc}¹¹⁴.

Interestingly, a novel allele, *Prnp^c*, was later discovered in MAI/Pas mice, which presented an incubation time greater than that shown by *Prnp^b* alleles. This expanded the categorisation from *Prnp^a* or *Prnp^b* mice as this new variant carried an allele that encodes phenylalanine and threonine at positions 108 and 189 respectively¹⁰⁴. Further work in generating a *Prnp^c* congenic line that expresses this allele on a *Prnp^a* C57BL/6JOLAHsd background found that upon challenge with Chandler/RML, an incubation time of 255 ± 12 days was seen relative to 360 ± 11 days of wild type MAI/Pas mice. This suggests that *Prnp^c* is associated with a long incubation time and is also indicative of a PrP independent control of incubation time, pointing at other genetic loci that may modulate this effect¹⁰⁴.

1.2.2 Incubation time quantitative trait loci

The range of incubation times produced for a given *Prnp* allele with a particular prion inoculum under standard experimental conditions suggests that other genes may also have a modifying effect. This is apparent in *Prnp^a* mice challenged with Chandler/RML scrapie, which produce incubation periods ranging from 108±1 days to 221±5 days^{100, 101, 104, 113}. As incubation time is measured in days it can be used as a quantitative trait for the identification of loci that are linked to this phenotype. The common method by which these quantitative trait loci (QTL) may be identified is through the crossing of two mouse strains bearing the same *Prnp* allele but with distinct incubation times; these may either be intercrossed or backcrossed. In this way, 21 loci were collectively identified across 8 chromosomes through intracerebral inoculations of four combinations of crossing with Chandler/RML scrapie, mouse adapted BSE, BSE and ME7 scrapie; CAST X NZW F2 intercross^{100, 115}, CAST x SJL F2 intercross⁹⁹, C57 X RIII backcross and an intercross^{116, 117}.

These crosses have the benefit of using large progeny numbers with only two different alleles that segregate, making analyses less complicated. However, they carry the limitation that two parental mice strains will not bear all the possibilities of alleles that influence incubation time. In order to maximize the number of QTL detected, experimental parameters may be modified such as route of inoculation or varying the prion strain used. The resulting incubation periods may be influenced by QTLs that might have gone undetected in the absence of prion strain variation or a particular route of prion infection⁸.

The detectable loci that modulate incubation times span regions that encompass several genes covering many megabases, therefore the effect observed cannot be attributed to a single gene. Most of these genes remain undetected because the regions are so large, thus alternative strategies have been employed to fine map and identify candidate genes. One such method is through the use of heterogeneous stocks of mice such as the Northport heterogeneous stock¹¹⁸. Heterogeneous stocks of mice model an outbred population but have the advantage of starting with a defined number of parental alleles, which provide a high level of recombination¹¹⁹. These mice have been used to identify candidate genes, described below in Section 1.2.3, through size reduction of a QTL.

1.2.3 Candidate genes

Much research has been dedicated to identifying some of these genes that modify incubation time through mouse genetics complemented by human genome wide association studies (GWAS) or through an individual candidate gene approach based on genes in pathways implicated in prion disease. By using the Northport heterogeneous stock of mice, Lloyd *et al.*, carried out high resolution fine mapping of *Mmu19* from which emerged several genes. Of these, *Hectd2* was the most significantly associated with prion disease incubation time¹²⁰. *Hectd2* expression in prion-infected brains, from mice at the end stage of disease, was compared to controls and it was found that expression was five times greater in C57BL/6 mice relative to normal, uninfected mice. The authors also performed a human association study, where samples from patients with vCJD (n = 117), and sporadic CJD (n = 452) were analysed in parallel to a UK control population (n = 601). An intronic SNP, *rs12249854*, was linked to an increased risk to vCJD ($p = 0.0049$) and sporadic CJD ($p = 0.012$) although this risk allele was not found to modify human disease phenotypes. However, recent work by Jeong and others have found that this polymorphism is not associated with sporadic CJD¹²¹. Further analyses of *HECTD2* found that in the UK population there exists three *HECTD2* haplotypes, termed 1-3. One of these, haplotype 2, tagged by *rs12249854A*, was linked to an increased risk to vCJD, possessing a statistical significance of $p = 0.006$. Samples from kuru patients were analysed in comparison to elderly female survivors from Papua New Guinea that have had multiple exposures to this prion strain. The Papua New Guinea population possessed four haplotypes, termed 1, 2, 4 and 5, where one of these population specific haplotypes, 4, is associated with kuru. This haplotype showed a strong association with kuru ($p = 9 \times 10^{-4}$). The expression of *HECTD2* was also analysed in human lymphocytes, where heterozygotes for the genotype tagged by *rs12249854*, were shown to express 2.3 times greater than homozygotes, thereby suggesting that increased *HECTD2* is associated with vCJD susceptibility. These data taken together, present *Hectd2* as a strong candidate modifier for prion disease incubation time¹²⁰. However, no functional analyses to link this gene to prion pathology have been found.

Lloyd *et al.*, performed a microarray gene expression analysis on brains of wild type adult mice that manifest different incubation times¹²². Five genes were identified as having differential expression that correlates with incubation time, namely, *Hspa13*, *Fkbp9*, *Cbx1*, *Gpr19* and *AK013823*. The authors further investigated *Hspa13*, encoding the protein Hspa13 (Stch), by generating an *Hspa13* overexpressing transgenic mouse line, Tg222. By challenging Tg222 mice with three different prion strains, the authors were able to determine that the overexpression of *Hspa13* leads to a pronounced reduction in incubation time. Precisely, 16, 15 and 7 % decreases in incubation time relative to wild type mice were observed following inoculation with Chandler/RML, ME7 or MRC2 prions and this was not associated with an upregulation of PrP^C. These results were substantiated using a cell based model of prion disease, wherein siRNA knockdown of *Hspa13* in chronically infected N2a cells was performed to test for correlation of *Hspa13* expression to prion propagation. A curing effect was observed in *Hspa13* knockdown N2a cells relative to the non-targeting control¹²². Hspa13 is a member of the Hsp70 family of molecular chaperones, thus implicating it in the correct folding of proteins¹²³. Furthermore its functional activity has been extended to cell survival by regulation of tumour-necrosis-factor-related apoptosis-inducing ligand (TRAIL)-dependent apoptosis¹²⁴. TRAIL is a cytokine that has been reported in brains of Alzheimer's patients in mediating amyloid-beta induced apoptosis¹²⁵.

Cpne8 is a further candidate quantitative trait gene successfully identified using the Northport heterogeneous stock of mice from *Mmu15*¹²⁶. Comprehensive sequencing of the region linked to incubation time found *Cpne8* as a promising candidate ($p = 0.0002$). The authors found that this copine family member had an upregulated mRNA expression at the terminal stage of prion disease. Copine proteins are calcium dependent phospholipid binding proteins that have been implicated in membrane trafficking; this role may tie in with the regulated trafficking of PrP, suggesting that *Cpne8* may serve to modulate this¹²⁶.

The largest screen performed to date based on an individual candidate approach was by Tamguney *et al.*, who screened 20 genes implicated in prion pathogenesis, by testing knockout or overexpressing transgenic mouse models for each. The authors found that only three of the candidates showed an effect, *SOD1*, *App* and *Il1r1*¹²⁷. Overexpression

of human *SOD1* increased incubation time by 19% whilst knockout models of *Il1r1* and *App* increased survival by 13 and 16%¹²⁷. Superoxide dismutase, *SOD1*, is a ubiquitously expressed metalloenzyme that catalyses superoxide free radicals to hydrogen peroxide to prevent oxidative stress¹²⁸. Mutations in this gene have been causally linked to a subset of familial Amyotrophic Lateral Sclerosis (ALS) cases¹²⁸. It has also been implicated in Alzheimer's disease wherein *SOD1* knockout mice enhance amyloid- β oligomerisation and memory loss, supported by studies in which cerebral endothelial dysfunction that results from APP overexpression is rescued by SOD1^{129, 130}. The cellular oxidative stress response is thus involved in the pathology of a number of neurodegenerative diseases^{131, 132}. Amyloid- β (A4) precursor protein, *App*, was tested due to the similarities between prion and Alzheimer's diseases in terms of neuropathological hallmarks and also due to its co-localisation with PrP^C in mouse¹²⁷. The post-translational product of *App*, amyloid- β (40-42 residues) has been reported to interact with PrP, which mediates amyloid- β induced synaptic plasticity impairment that may be prevented by targeting PrP^{64, 133}. Interleukin-1 receptor, type 1 gene, *Il1r1*, was also tested to follow up studies that detected increased levels of its ligands, IL-1 α and IL-1 β in prion-infected mice and CJD patients¹³⁴. The authors reported a delay in accumulation of PrP^{Sc} in *Il1r1*^{-/-} mice and prolonged incubation time suggesting that suppression of the anti-inflammatory response perhaps by delayed astrocytic gliosis increases survival^{127, 135}.

Lloyd *et al.*, extended these analyses by using the Northport heterogeneous stock of mice to determine whether natural variation in *Sod1*, *App* and *Il1r1* was associated with incubation time through an association study¹³⁶. Although they did not find any association with *App*, a *Sod1* SNP from intron 3 and a non-synonymous *Il1r1* SNP from exon 3 were linked to incubation time ($p < 0.0001$, $p = 0.02$, respectively). The authors challenged *Sod1*^{-/-} mice with RML and ME7, representing mouse adapted scrapie strains and MRC2, a mouse adapted BSE strain. *Sod1*^{-/-} mice all showed reductions in incubation time irrespective of strain used, where RML, ME7 and MRC2 isolates led to decreases of 20, 13 and 24% respectively, relative to wild type. These data support the association of *Sod1* with prion disease incubation time¹³⁶.

Knockout mouse models for a number of pro- and anti- inflammatory cytokines were tested in a bid to determine the role of such cytokines in prion pathology¹³⁷. Interleukin 10, *Il-10*, was found to be linked to incubation time following challenge with RML or ME7 mouse-adapted scrapie strains¹³⁷. *Il-10*^{-/-} mice showed shortened incubation times relative to wild type and an earlier expression of tumour necrosis factor-alpha, TNF-alpha. The authors suggest that this early expression of TNF-alpha sensitises mice to prion pathogenesis, thus placing *Il-10* as a candidate gene that may be important for longer survival¹³⁷.

Genome wide association studies have also been used to detect alleles that are associated with human prion disease. In a human genome wide association study by Mead *et al.*, *STMN2* and *RARB* were identified as genetic risk factors for vCJD¹³⁸. A SNP, *rs1460163*, upstream of *STMN2*, which maps to chromosome 8, was associated with vCJD ($p = 5.6 \times 10^{-5}$) which was also associated with resistance to kuru ($p = 2.5 \times 10^{-4}$)¹³⁸. They also found that *Stmn2* expression was downregulated 30-fold in a cellular model of mouse prion disease¹³⁸. This is supported by previous work by Greenwood *et al.*, who investigated the expression profiles of prion infected neuronal cells and found a downregulation of *Stmn2* expression¹³⁹. *Stmn2* was further investigated by Lloyd *et al.*, who used a stock of ~1000 Northport heterogeneous stock of mice that were inoculated with Chandler/RML prions after which the incubation times were observed¹²². They found a small effect ($p = 0.04$) that associates the gene to incubation time. However, these authors found that *Stmn2* expression in prion-infected brains, from mice at the end stage of disease, was upregulated relative to controls. They suggest that this may be due to the variation in prion propagation that exists in an *in vitro* situation compared to the *in vivo* environment at the end stage of disease and the pathological differences that lie in these two circumstances¹²².

The product of *Stmn2*, SCG10, is a neuronally expressed protein with a high level of expression in the growth cones^{140, 141}. SCG10 is highly expressed in the developing nervous system and the adult brain sustains it in regions of synaptic plasticity¹⁴²⁻¹⁴⁴. *Stmn2* is a key regulator of microtubule stability, which in turn modulates neurite outgrowth and

its subsequent elongation and branching^{145, 146}. Overexpression of SCG10 has been shown to improve neurite outgrowth, substantiating its role in microtubule assembly¹⁴⁶.

Mead *et al.*, found that the *rs6794719* SNP, upstream of *RARB* and maps to chromosome 3, was found to associate with vCJD ($p = 1.96 \times 10^{-7}$), in addition to iatrogenic CJD patients ($p = 0.03$)¹³⁸. This work was followed up by Lloyd *et al.*, who showed a highly significant association of *Rarb* with prion disease incubation time in mice¹⁴⁷. However, the authors also found that this SNP maps within 0.5Mb of the *THRβ* gene locus. In mice the *Rarb-Thrb* locus was linked to incubation time but the observed effect could not be directed towards a single gene as it is the effect of the region that is detectable¹⁴⁷. Although *Rarb* expression in hypothalamic neuronal cells showed no difference upon prion infection, its level in prion-infected brains, at the end stage of disease, was upregulated in comparison to controls^{138, 147}.

RARB encodes the protein retinoic acid receptor beta and is a member of the retinoic acid/thyroid hormone receptor family¹⁴⁸. It has also been demonstrated that retinoic acid regulates the expression of the prion protein through its downregulation. The authors suggest that a therapeutic approach to slowing down prion pathogenesis may benefit from investigating retinoids to prolong incubation time¹⁴⁹.

Mead *et al.*, performed a further genome wide association study across vCJD, sporadic CJD, iatrogenic CJD, inherited prion diseases and kuru in UK and German patients¹⁵⁰. Although their findings supported current knowledge that *Prnp* is the major genetic determinant for all human prion disease cases, certain SNPs were however associated with particular prion diseases. SNPs at the *ZBTB38* locus were linked to CJD in the UK but not sporadic CJD in German cases or Kuru. A SNP in the *CHN2* gene was also found to be associated with vCJD but not in sporadic UK or German cases or kuru. *Zbtb38* is involved in the regulation of apoptosis in murine cells. *Zbtb38* is a zinc finger protein that is highly expressed in the brain and can bind methylated DNA, implicating it in transcriptional repression¹⁵¹.

In an European GWAS study of vCJD cases, an intronic SNP in *MTMR7*, *rs4921542*, was associated with risk to vCJD, ($p = 1.6 \times 10^{-8}$)¹⁵². The protein product of *MTMR7*,

(myotubularin related protein 7 gene) is a CNS-specific phosphatase that targets phosphatidylinositol 3-phosphate and inositol 1,3-bisphosphate, suggestive of a role for the phosphatidylinositol pathway in susceptibility to vCJD¹⁵². MTMR7 interacts with MTMR9, a protein that is implicated in autophagy^{153, 154}. The authors also found a SNP, *rs7565981*, in the intergenic region of *NPAS2*, (neuronal PAS (per-ARNT-sim) domain-containing protein 2). *NPAS2* is a transcription factor that is expressed in the brain and peripheral tissues¹⁵⁵. *NPAS2* serves a role in regulating circadian behaviour and mice deficient in *NPAS2* show impaired contextual memory^{156, 157}.

1.3 HECTD2 is a prion disease modifier linked to incubation time

1.3.1 E3 ubiquitin ligases

Hectd2 is the first candidate gene that has been linked to prion disease incubation time in mice that also influences susceptibility to the human diseases, vCJD and kuru, making it a very promising candidate¹²⁰. Limited information is available for *Hectd2* and thus the characterisation of this gene is important in understanding the molecular basis of incubation times and risk to disease.

By homology, *Hectd2* is an E3 ligase, representing one of a cascade of ubiquitously expressed enzymes that modify proteins at the post-transcriptional level by ubiquitination¹⁵⁸. Ubiquitination is a highly ordered process that regulates a myriad of cellular processes including and not exhaustive of protein quality control by proteasomal or autophagic pathways, cell cycle, transcription, DNA repair, apoptosis, endocytosis and trafficking of transmembrane proteins by serving as a recognition element for downstream effectors to direct its fate¹⁵⁹⁻¹⁶⁶. The multi-step ATP-dependent reaction involves the sequential transfer of 76 amino acid ubiquitin from E1 ubiquitin activating enzyme, where it forms a high energy thiol ester bond, to an ubiquitin conjugating enzyme, E2, via another thiol ester link. The ubiquitin moiety is then transferred to a high energy thiol intermediate on an E3 ligase that catalyses the covalent attachment of the ubiquitin moiety to an NH₂-group of a bound substrate^{160, 167, 168}. This ubiquitination is governed by an evolutionary conserved catalytic cysteine residue harboured within the ~350 residue C-

terminal HECT domain that forms the thioester intermediate with ubiquitin prior to transfer to a given substrate^{160, 169}.

The human genome has been estimated to encode 2 potential E1s, ~30 E2s and over 600 E3 ligases¹⁶². This large number of E3s accounts for the specificity of the ubiquitination system to regulate a myriad of cellular processes. There are two main types of E3s, the HECTs (Homologous to E6-AP Carboxyl Terminus), of which there are 28 and RING (Really Interesting New Gene) ligases which comprise ~95% of E3 ligases¹⁶². These differ in their mechanism of ubiquitin conjugation to their substrates, where HECT E3s use the approach described above by catalysing direct substrate ubiquitination, depicted in Figure 1.4. In contrast, RING E3 ligases, lack the catalytic site and thus serve as scaffolds by which E2 enzymes are brought into close proximity to the target substrate (Figure 1.4)^{162, 170, 171}.

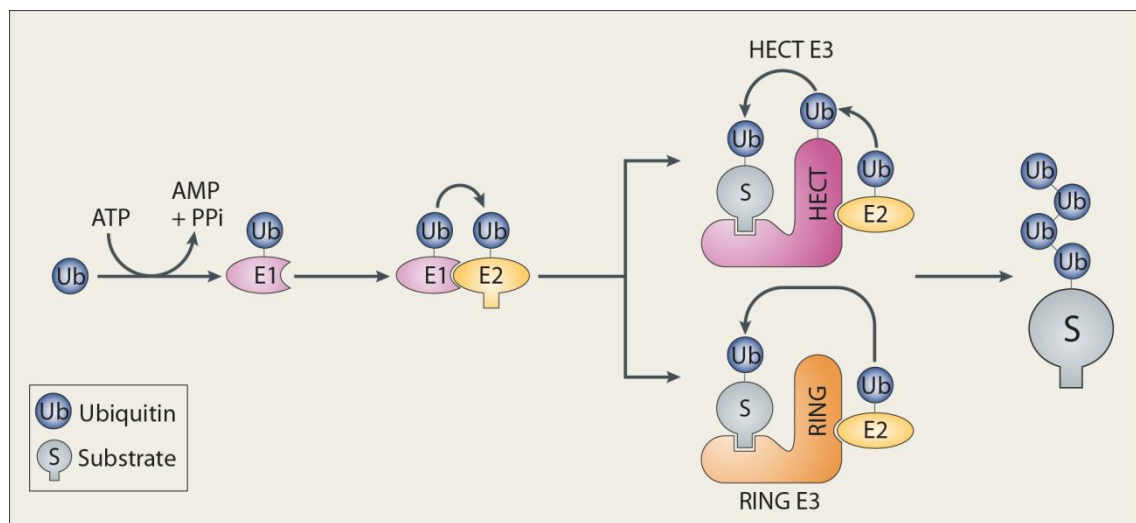


Figure 1.4 Mechanism of substrate ubiquitination by the two main types of ligases, HECT and RING E3s. Ubiquitination is initiated in an ATP-dependent process by E1 activating and E2 conjugating enzymes. HECT ligases can catalyse ubiquitin transfer to the substrate directly whilst RING ligases serve as a scaffold for conjugation of the ubiquitin moiety onto a substrate by E2. *Adapted from Rotin et al, 2009.*

Although poorly characterised, conservation of the catalytic cysteine site indicates that HECT E3 ligases convey the ubiquitination activity¹⁷². The HECT domain is bi-lobal and comprises an N-terminal lobe to which E2 interacts with, and a C-terminal lobe housing the catalytic cysteine that forms the thioester bond with ubiquitin, which are connected by

a flexible hinge region that facilitates ubiquitin transfer through conformational changes^{173, 174}. The N-terminal extension of HECT E3s is thought to be the substrate determinant that dictates the specificity of the ubiquitination system and is variable in length and sequence thus accommodating the diversity of substrates it binds^{162, 172}. This variability in the putative substrate binding region defines the grouping of human E3s into three subfamilies, the HERCS, NEDD4s and other HECTS, based on the domains that they carry in addition to HECT (Figure 1.5). The HERCs, totalling six, possess a regulator of chromosome condensation 1(RCCL)-like domain, (RLD), and the nine NEDD4 group members harbour an N-terminal C2 domain that binds phospholipids and two to four WW domains that contain two conserved tryptophan residues that impart a role in protein-protein interactions^{162, 172}. Other HECTs represent the final subfamily, which lack an archetypal domain architecture, where characterisation of some members of this group has identified a myriad of known domains within the N-terminal region and a number without any known domains¹⁶². Hectd2, falls into the latter category, where its N-terminal extension presents a region to which structural information is yet to be determined¹⁶², and thus extrapolation of potential binding substrates has not yet been possible owing to the absence of known protein-protein interaction domains.

common¹⁶¹. It has been long hypothesised that ubiquitination through K48 of the preceding ubiquitin moiety targets substrates for proteasomal degradation while non-K48 linkages direct non-proteolytic fates¹⁷⁹. K63-mediated ubiquitination has been reported to target substrates for autophagic degradation in addition to other cellular processes such as vesicular sorting and endocytosis, while K11 linkage to substrates implicates them in the endoplasmic reticulum associated degradation, ERAD, pathway^{165, 180}. However, these canonical signals have been challenged as it has emerged that ubiquitination through all residues may target substrates for proteasomal degradation, and further to this, non-lysine ubiquitination of substrates may also occur thus adding complexity to the system¹⁶¹. Thus the multiplicity of the different structures of ubiquitination allows fine tuning of the signaling between a substrate and its effector, allowing the regulation of the numerous processes that it governs, with proteasomal degradation serving a predominant channel for protein fates.

The literature outlined in the following sections highlights the roles of two of the key pathways through which ubiquitination may act as a signaling device in prion disease, the ubiquitin proteasome system (UPS) and autophagy. These cellular mechanisms have shown prominence as emerging themes in neurodegenerative diseases, from which a greater understanding of pathogenesis may be derived, in addition to serving as a possible therapeutic avenue.

1.3.2 Ubiquitin proteasome system-mediated clearance in prion pathology

The major protein turnover system at the cell's disposal for homeostasis maintenance and regulation of a diversity of cellular processes and localisation is the ubiquitin proteasome pathway^{181, 182}. In coordination with the ubiquitin conjugating machinery, this multi-functioning cytosolic complex serves as a quality control mechanism in the degradation of unwanted, misfolded or missense proteins, or for the regulation of short lived proteins^{182, 183}. This may be of particular importance when proteins are toxic or have a propensity to aggregate¹⁸². The degradative capacity of the UPS is governed by its proteolytic core, which harbours caspase-like, trypsin-like and chymotrypsin-like enzymatic activities¹⁸².

With the UPS being implicated in a myriad of cellular processes, dysfunction of components of its machinery have been linked to disease pathogenesis and in particular, prion diseases^{182, 184}. The first evidence of a connection between prions and the UPS was demonstrated by the identification of the GSS-linked prion protein mutant, Y145Stop and wild type prion protein that were degraded by the proteasomal pathway via endoplasmic reticulum-associated degradation (ERAD)¹⁸⁵; ERAD is a process whereby misfolded proteins within the endoplasmic reticulum (ER) are subjected to degradation by the proteasome¹⁸⁶. Incorrectly folded proteins in the ER are retrotranslocated into the cytosol, for proteasomal-mediated degradation^{186, 187}. It was also found that by blocking the proteasome with inhibitors, an accumulation of the mutant protein could be observed – suggestive of an important role for the proteasome^{188, 189}. A further GSS associated prion mutant Q217R, following binding to the chaperone protein BiP, was also targeted for proteasomal degradation¹⁹⁰.

Later studies confirmed that wild type PrP also undergoes ERAD, by means of retrograde transport into the cytosol and subsequent ubiquitination^{188, 189}. It was shown that UPS impairment can thus encourage the conformational conversion of wild type PrP^C to a PrP^{Sc}-like form since a defective degradative ability may increase the propensity for the aberrant conformer to initiate the conversion process^{191, 192}. These authors found that inhibiting the proteasome leads to the accumulation of cytosolic prion aggregates that reflect the pathogenic properties of prions such as self-replication in addition to partial protease resistance. Elimination of the proteasome inhibitors does not demonstrate a reversal of the process since conversion of just one wild type molecule results in a seed for self-perpetuation, leaving the UPS with little power to overcome it^{191, 192}.

Ongoing research in this field suggests a strong relationship between UPS malfunction and prion pathogenesis. Kang *et al.*, , reported that following challenge with the ME7 prion strain in mouse brains, ubiquitin protein conjugates accumulated in parallel to the protease resistant species, coinciding with the first clinical signs and decreased proteasomal activity¹⁸⁴. Subsequent analyses determined that these PrP^{Sc} species were ubiquitinated at the terminal stage of the disease¹⁸⁴. It was observed that the chymotrypsin like and caspase-like peptidase activities of the proteasome were diminished in these scrapie

infected brains¹⁸⁴. Such evidence firmly implicates UPS impairment in prion aetiology and may suggest that the proteasome is inhibited by PrP^{Sc} protein aggregates, which would be consistent with data published by Bence *et al.*, who showed that two different aggregated proteins could inhibit proteasomal function¹⁹³.

Later work by Kristiansen *et al.*, verified these data, by showing that mild infection of two neuronal cell lines that sustain prion infectivity showed a reduction of the caspase-like and chymotrypsin catalytic functions of the proteasome¹⁹⁴. This was substantiated by the finding that RML infected mouse brain also displayed the same decline in the proteasomal catalytic activities. The authors also found that by expressing a fluorescent GFP-tagged proteasome reporter substrate in live cells, the proteasome function could be quantified¹⁹⁵. Upon prion infection, the levels of the fluorescent reporter were significantly increased but a reversal of the effect was seen on curing of the prion-infected cells, suggesting prion-related UPS dysfunction. The mechanism by which prions are thought to cause proteasome dysfunction remains elusive although it is speculated that PrP^{Sc} species act directly by inhibiting gate opening of the 20S chamber, in turn leading to neuronal death^{194, 196}.

These experiments were extended to determine a possible mechanism through which inhibition of the proteasome is achieved. This has been described by Deriziotis *et al.*, where they postulate that misfolded PrP inhibits the proteasome through an antagonistic mechanism, whereby it binds to the outer lateral surface of the proteasome, stabilising the closed- gated conformation^{182, 194, 197}. Although pathologically, the nature of the misfolded PrP species conformation that results in inhibition of substrate entry remains unclear, it has been reported that proteasomal activity is decreased upon exposure to beta-sheet rich PrP oligomers¹⁹⁴, however, the degree to which this affects the neurodegenerative process is yet to be elucidated.

Together these data point towards a role for the UPS in prion disease, and the key role that this system plays in proteostasis makes such a mechanism of neurodegeneration plausible, placing the proteasome or its cognate ubiquitinating machinery as possible therapeutic targets. It is thus clear that a strong relationship between the UPS and prion-mediated toxicity exists although the specific mechanisms underlying pathology remain

unknown. Whether prions themselves are a direct cause of UPS impairment or a secondary effect of deteriorating function is yet to be determined.

1.3.4 Autophagy mediated clearance in prion pathology

Autophagy is another major intracellular quality control pathway that functions in parallel to the UPS as a bulk degradative mechanism to which components bound for destruction may be targeted^{183, 198}. Homeostasis is achieved through this highly conserved system via degradation of cytosolic proteins, organelles and pathogens by lysosomal digestion^{183, 198}. While basal autophagy occurs to target dysfunctional cellular components for degradation in the absence of stimuli, the process can be selective by induction through a number of conditions such as starvation, oxidative stress or toxic insult¹⁹⁸. Autophagy can be defined by the mechanism through which targeted cargo is digested by lysozymes, described as macroautophagy, microautophagy and chaperone-mediate autophagy¹⁹⁸. Macroautophagy is the most common form and is otherwise referred to as autophagy. Unwanted cargo is sequestered within a double membraned vesicle, termed an autophagosome or autophagic vacuole that undergoes maturation by recruitment of specific proteins prior to fusing with endosomes to form amphisomes. The autophagosomes are then transported to fuse with lysosomes for hydrolase-mediated degradation¹⁹⁸. Microautophagy, involves the internalisation of cytosolic material directly into the lysosome via invagination of its membrane¹⁹⁸. Chaperone mediated autophagy facilitates the targeting of cytosolic proteins bearing the KFERQ motif to the lysosome by Hsc70¹⁹⁸. Although these defined mechanisms of autophagy are important in the regulation of degradation, protein synthesis and recycling of resources, macroautophagy has been the most intensively studied owing to its link to neurodegeneration and some forms of cancer^{198, 199}.

Autophagy was first implicated in prion disease following the observation of autophagosomes in the neurons of scrapie infected mice²⁰⁰. Increased presence of these autophagosomes is indicative of defective autophagy²⁰⁰. Furthermore, the accumulation of autophagosomes was also described in scrapie-infected hamster brains, which

correlated with incubation time, suggestive of defective autophagic mechanisms in prion disease²⁰¹. These autophagic vacuoles were localised in neuronal perikarya and processes, gradually accumulating across entire neurites²⁰¹. Autophagy has been linked to neuritic dystrophy and this may be extended to the neurite pathology observed in prion diseases, which may subsequently affect neuronal function²⁰²⁻²⁰⁴.

A protective effect of autophagy in PrP clearance has been substantiated by studies in which the induction of autophagy using small molecules enhanced the degradation of PrP^{Sc} in chronically infected neuronal cells²⁰⁵⁻²⁰⁹. Inhibition of autophagy counteracted PrP^{Sc} clearance indicative of an autophagy-mediated mechanism of degradation^{205, 209}. Furthermore, prion-infected mice treated with an inducer of autophagy, rapamycin, showed longer incubation times relative to mock-treated control mice, suggesting autophagic mechanisms can prolong lifespan^{208, 209}. It has been reported that mice lacking genes essential for autophagy develop neuronal ubiquitin aggregates and selective degeneration of cerebral and cerebellar cortical neurons, in turn leading to neurodegeneration^{210, 211}. This is lent support by studies in which induction of autophagy has been reported to ameliorate protein aggregation that may lead to disease progression^{206, 212-214}.

Autophagy has also been implicated in mitochondrial homeostasis as demonstrated by a neuronal cell model in which Sirt1 activates autophagy to protect against PrP-induced mitochondrial dysfunction^{206, 215}. The authors found that the PrP₁₀₆₋₁₂₆ peptide causes a decrease in the mitochondrial membrane potential and that Sirt1 overexpression can attenuate Bax translocation to mitochondria and cytochrome c release into the cytosol, signals that initiate apoptosis^{206, 215}.

A key feature identified by many proteasomal inhibition studies is the formation of aggresomes - cytosolic structures that accumulate PrP^{Sc} species and proteasomal components²¹⁶. It is thought that formation of aggresomes reflects a cytoprotective response to misfolded and aggregated protein^{201, 217, 218}. Aggresomes have thus been proposed as a cellular response to misfolded proteins that are then targeted to the autophagic-lysosomal pathway for degradation²¹⁸. These findings have been corroborated by studies in neuroblastoma cells, where prion protein mutants linked to familial forms of

the disease were found to convert into a PrP^{Sc}-like form and accumulated in aggresomes following impairment of the UPS²¹⁹. In addition prion-infected neuronal CAD cells show aggresomal sequestration of PrP^{Sc} following proteasome inhibition²²⁰. Substrates may be targeted to aggresomes by ubiquitination, linking the UPS machinery to autophagic mechanisms, however evidence also suggests misfolded proteins may be sequestered by ubiquitin-independent signalling^{221, 222}. This accumulation in aggresomes may serve as a cytoprotective role in response to toxic insult that cannot be degraded by the proteasome perhaps due to prion infection or age related decline²¹⁶. Convergence with the autophagolysosomal pathway thus may ameliorate or may mediate neurotoxicity, as this is yet to be determined²²³.

It is yet unclear as to how UPS and autophagy are orchestrated in the cell for specific degradation of aberrant or unwanted material but substrates that are aggregated and thus exceed the capacity of the proteasome may necessitate activation of the autophagic pathway to facilitate clearance^{182, 223}. However, the evidence points towards a neuroprotective role for both of these systems although the interplay between the two in disease conditions may underlie the neuropathology observed in neurodegeneration and thus the molecular players involved are key to defining the precise mechanism.

1.3.5 E3 ubiquitin ligases in neurodegenerative diseases

The only E3 ligase that has been functionally associated with pathology reminiscent of prion disease is the RING E3 Mahogunin, Mgrn, albeit with conflicting results. Chakrabarti *et al.*, found that Ctm-PrP or cytosolic PrP interacts with Mgrn, resulting in its sequestration and thus functional depletion²²⁴. Loss of this ubiquitin ligase results in spongiform neurodegeneration and a mahoganoid coat colour phenotype in mice suggesting that disruption of Mgrn may contribute to spongiform pathology²²⁵. This interaction between cytosolically exposed prion proteins and Mgrn, lead to sequestration of the ligase, thus depletion of functional Mgrn and aberrant endo-lysosomal trafficking that was rescued by its overexpression²²⁴⁻²²⁶. However, recent work has found that loss of Mgrn, or its overexpression in mice challenged with RML prions does not influence

the onset or pathology of disease²²⁶. The experiments performed by Chakrabarti et al., used transgenic mice and cultured cells expressing cytosolically exposed PrP, and as PrP is not normally cytosolic, this might provide an explanation as to why *Mgrn*-deficient or overexpressing mice challenged with RML show no observable effects.

Miyazaki *et al.*, identified a HECT E3 ligase, NEDL1, that selectively targeted mutant SOD1 but not wild type, for ubiquitination to signal proteasomal-mediated degradation²²⁷. Mutant SOD1 being its substrate implicates this E3 ligase in the pathogenesis of ALS as mutations within *SOD1* are reported to account for 20% of familial ALS cases^{128, 228}. This progressive paralytic disease is characterised by degeneration of motor neurons in the brain stem, cerebral cortex and spinal cord although the mechanism by which this selective neuronal death occurs is yet to be elucidated. NEDL1 is neuronally expressed and has been detected in the Lewy-body like hyaline inclusions that are apparent in the remaining motor neurons of familial ALS patients and transgenic mice expressing mutant SOD1²²⁷. Furthermore, transgenic mice overexpressing human NEDL1 were found to be associated with muscle atrophy and motor neuron degeneration and microglial activation²²⁹. NEDL1 has been shown to ubiquitinate DVL1, which also interacts with mutant SOD1, suggesting an interplay between these proteins that may underlie the selective neuronal degeneration²²⁷. The ability of NEDL1 to distinguish between mutant and wild type forms of SOD1 thus substantiates its position as a quality control E3 ligase, suggestive of a role in neuroprotection.

The RING-finger type E3, Dorfin, has also been identified in Lewy-body like hyaline inclusions in the spinal cord of ALS patients and in mice transgenic for mutant SOD1^{230, 231}. Dorfin ubiquitinates mutant SOD1 associated with familial ALS and enhances its proteasomal degradation and reduces mutant SOD1 inclusions, in turn protecting neural cells from mutant-SOD1 mediated neurotoxicity²³¹. These data were lent support by a mutant SOD1 transgenic mouse model of familial ALS in which overexpression of Dorfin ameliorated motor neuron degeneration and the disease phenotype whilst increasing the clearance of mutant SOD1 in the spinal cord²³², lending E3s as a possible mechanism through which pathogenesis may be mediated. Interestingly, Dorfin is also localised in

the Lewy body neuronal inclusions that characterise patients of Parkinson's disease^{232, 233}. This movement disorder is characterised by selective degeneration of dopaminergic neurons of the substantia nigra accompanied by Lewy bodies or Lewy neurites that are composed of aggregated proteins²³⁴. Parkinson's disease and ALS thus may share a common biochemical pathway via Dorfin that generates the ubiquitinated inclusions and whether this ligase is involved in the degeneration of the specific populations of neurons observed in these diseases is yet to be determined.

Another substrate of Dorfin is Synphilin-1, which forms a major component of Lewy Bodies and has been shown to interact with alpha-synuclein, a protein in which mutations cause autosomal dominant form of PD that also aggregates in these inclusions^{233, 235}. This demonstrates that the interactome of a given ligase may have profound effects regardless of whether that particular ligase itself is directly causative in pathogenesis. The ring finger, cytosolic E3 ligase, Parkin is an example of a ligase that is directly linked to disease as mutations within the gene cause autosomal recessive Parkinson's Disease²³⁶. Physiologically, Parkin has been attributed a role in mitochondrial homeostasis in concert with PINK1, a kinase that recruits Parkin to dysfunctional or depolarised mitochondria to mediate their selective degradation by autophagy²³⁷. Impairment of this process, otherwise known as mitophagy, has been reported to recapitulate a number of hallmark traits such as the neuronal accumulation of proteinaceous aggregates and defective motor coordination and tremor^{210, 237}. Parkin ubiquitinates FAF1 directly and the relevance of this effector protein was investigated using a mouse model in which FAF1 levels were diminished²³⁸. These mutant mice were treated with MPTP, which recapitulates the dopaminergic neuronal loss observed in Parkinson's disease. This model showed that MPTP-induced dopaminergic neuronal loss was attenuated relative to wild type mice and that deficiency of FAF1 averted Parkinson's disease events such as ROS generation, caspase activation and cell death²³⁸. These data provide evidence that relates the importance of downstream targets of E3 ligases and the effects they may culminate in disease.

Recent work has shown that Parkin also plays a role in Alzheimer's disease, where it was found that it co-localises with intraneuronal amyloid- β (1-42) in the cortex and

hippocampus of patients with the disease²³⁹. The authors investigated the role of Parkin in autophagy by using transgenic mice expressing amyloid- β in the presence and absence of Parkin. Defective autophagy was observed by means of autophagosome accumulation following expression of amyloid- β that resulted in hyperphosphorylated tau. Clearance of amyloid- β and hyperphosphorylated tau through the lysosomal pathway was promoted by Parkin via autophagy-mediated degradation²³⁹.

The F-box family of proteins form the substrate recognition component of a multisubunit family of E3 ligases known as the SCF (Skp1, Cullins, F-box proteins) ligases. FBXW7, a member of the F-box family has been implicated in Alzheimer's disease. FBXW7 has been found to interact with the protein product of *Presenilin 1*, a gene in which mutations have been associated with autosomal dominant Alzheimer's disease^{240, 241}. This interaction has been reported to facilitate ubiquitination of Presenilin 1 resulting in modified amyloid-beta peptide generation²⁴⁰. Furthermore, FBXO7, a different member of the F-box family has been associated with PARK15 parkinsonism^{242, 243}. FBXO7 is involved in ubiquitin-dependent proteasomal degradation as well as non-proteasomal functions, although the molecular mechanisms by which mutations in this gene cause its associated parkinsonian syndrome is yet to be determined^{243, 244}. Furthermore, SKP1A, a component of SCF ligase complexes was found to be downregulated in the substantia nigra of sporadic parkinsonian patients^{245, 246}. The authors suggest that this could stipulate defective or altered function in the repertoire of its substrate proteins.

CHIP (Co-chaperone carboxyl terminus of Hsp70-interacting protein) is a bi-functional E3 ligase and co-chaperone that ubiquitinates a number of substrates implicated in neurodegenerative diseases^{247, 248}. In Alzheimer's disease, phosphorylated tau, a pathological hallmark, has been reported to be ubiquitinated by CHIP for targeted degradation²⁴⁹. Furthermore CHIP also ubiquitinates misfolded proteins in Huntington's and hereditary ataxias working in concert with molecular chaperones, thus promoting cell survival^{248, 250, 251}. Although these examples provide evidence of directly selective degradation by ubiquitination of misfolded proteins, CHIP has also been reported to enhance proteasome-mediated degradation of mutant SOD1 via ubiquitination of the chaperone Hsp70²⁴⁷. Interestingly, CHIP has been implicated in Parkinson's disease

where it orchestrates α -synuclein degradation through either proteasomal or autophagy-lysosomal mediated targeting. The authors found that overexpression of this ligase promotes degradation of α -synuclein and alleviates aggregation²⁵², further substantiating a positive regulatory role for E3 ligases.

Together these data provide evidence that E3 ligases serve to orchestrate proper cellular function by calling the fate of their substrates and may thus be viewed as neuroprotective components in the pathogenesis of disease. However, it is feasible that in disease conditions altered cellular metabolism of its substrates or the ligase itself, modifies the cellular response to toxic insult, mediating neurotoxicity. The interactome of a given E3 ligase may be involved in the activation of pathways that may underlie pathogenesis. The connection between neurodegenerative diseases and E3 ligases is thus apparent, although the mechanisms by which neurodegenerative processes transpire are enigmatic. The discovery that Hectd2 is linked to prion disease incubation time corroborates the emerging importance of E3 ligases in the nervous system and calls for further investigation into its functional activity in order to elucidate the downstream processes that it governs.

1.4 Project Outline

The discovery of *Hectd2* as a potential modifier of prion disease incubation time and its association with the human prion diseases, vCJD and kuru shows its promise as an excellent candidate gene for modulating prion susceptibility. The aims of this project were to characterise *Hectd2* in order to elucidate its functional role in pathogenesis. The objective was to identify proteins that interact with *Hectd2* so that its functional pathway(s) could be determined. The downstream effectors of these pathways are anticipated to underlie the mechanisms by which incubation time and disease susceptibility may be modulated. To address this, yeast two-hybrid screening was used to map the interactome of *Hectd2* from a library of universal mouse proteins covering mouse genes that are expressed in all tissues. Interactions identified from the screen were verified independently in yeast and subsequently by co-immunoprecipitation in mammalian cells. *Hectd2* and each of the candidate interactors were tested for a modulatory role in the susceptibility of cells to prion propagation and clearance of prions by using a cell-based model of prion disease. This model, the Scrapie Cell Assay (SCA)²⁵³, allows one to measure the number of cells infected with PrP^{Sc} over time where candidate gene expression is manipulated. Modifications stipulated by a candidate gene in the SCA can allow us to delineate the pathways that are implicated in prion pathology by virtue of the molecular networks that they are placed in.

Genes and pathways identified in mice are anticipated to serve a similar role in human prion diseases. To test the effect of *Hectd2* on incubation time, *Hectd2* knockout and overexpressing transgenic mouse models were generated. These models were challenged with three strains of mouse adapted prions to search for an association with incubation time. Together, it is hoped that this functional characterisation of *Hectd2* will shed light on the molecular basis of incubation time and the mechanisms by which disease susceptibility may be modified.

2 Materials and Methods

2.1 Materials

2.1.1 Chemicals and reagents

Ethanol (Absolute)	Fisher Scientific
Ampicillin	Sigma Aldrich
Aureobasidin A	Clontech Takara Bio Europe
<i>Bgl</i> II	NEB
Better Buffer	Microzone
β – glycerophosphate	Sigma Aldrich
<i>Bgl</i> II	NEB
Big Dye	Applied Biosystems
Bromophenol blue	Sigma
dNTPs	Promega
UltraPure Agarose	Life Technologies Ltd
Ethidium Bromide	Sigma Aldrich
EGTA	Sigma Aldrich
Glass beads	Sigma
Glycerol	Sigma Aldrich
<i>Hind</i> III	NEB
HEPES	Sigma Aldrich
Hyperladder I	Bioline
Hyperladder IV	Bioline
Kanamycin	Sigma Aldrich
Luria Base Agar, Miller	Sigma Aldrich
Luria Broth	Sigma Aldrich

MegaMix Blue	Microzone
MicroCLEAN	Microzone
MgCl ₂	Sigma Aldrich
Oligonucleotides	Sigma Aldrich/Eurofins
<i>Pfu</i>	Promega
Phenylmethylsulfonide	Sigma
<i>PstI</i>	NEB
Puromycin	Sigma
Phosphate Buffered Saline 10X	VWR
NaCl	Sigma Aldrich
<i>NcoI</i>	NEB
N,N-Dimethylformamide	Sigma Aldrich
Dimethylsulfoxide	Sigma Aldrich
Phenylmethanesulfonyl Oxide	Sigma Aldrich
<i>SalI</i>	NEB
SeeBlue Plus II	Life Technologies Ltd
YPDA Broth and Agar	Clontech Takara Bio Europe
SD/-Trp Broth and Agar	Clontech Takara Bio Europe
SD/-Trp Broth and Agar	Clontech Takara Bio Europe
SD/-Leu Broth and Agar	Clontech Takara Bio Europe
SD/-Trp/-Leu Broth and Agar	Clontech Takara Bio Europe
SD/-Trp/-Leu/-Ade/-His Broth and Agar	Clontech Takara Bio Europe
<i>SfiI</i>	NEB
Shrimp Alkaline Phosphatase	Roche
Shrimp Alkaline Phosphatase Buffer 10X	Roche

TaqMan [®] Gene Expression Assay 20X	Life Technologies Ltd
TaqMan [®] Gene Expression Master mix 2X	Life Technologies Ltd
TaqMan [®] Mouse GAPDH Assay 20X	Life Technologies Ltd
T4 DNA Ligase	NEB
T4 DNA Ligase Buffer 10X	NEB
TRIS/Glycine/SDS 10X	VWR
TRIS/Glycine 10X	VWR
Triton-x 100	Sigma Aldrich
TBE 10X	VWR
X- α -Gal	Clontech Takara Bio Europe

2.1.2 Commercial kits

Matchmaker Gold Yeast-Two-Hybrid System	Clontech Takara Bio Europe
Matchmaker Yeast Transformation System	Clontech Takara Bio Europe
Matchmaker Insert Check PCR Mix 2	Clontech Takara Bio Europe
Matchmaker Easy Yeast Plasmid Isolation kit	Clontech Takara Bio Europe
MinElute Gel Extraction Kit	QIAGEN
QIAprep Spin Miniprep Kit	QIAGEN
Endotoxin Free Plasmid Maxi Kit	QIAGEN
ZeroBlunt TOPO PCR Cloning Kit	Life Technologies Ltd
Taqman [®] Gene Expression Cells to CT [™]	Life Technologies Ltd

2.1.3 Equipment

BioRad Thermal Cycler PTC-225	Applied Biosystems
LI-COR Odyssey Imaging System	Biosciences
Molecular Imager Gel Doc XR System	BioRad
3730XL DNA Analyzer	Applied Biosystems
ABI Prism 7700 Sequence Detection System	Applied Biosystems
XCell <i>SureLock</i> ® Mini-Cell system	Life Technologies Ltd
XCell <i>SureLock</i> ® Blot Module	Life Technologies Ltd
Eppendorf Microcentrifuge 5424 R	Eppendorf
Allegra™ 25R Centrifuge	Beckman Coulter
Heracell 150i CO ₂ incubator (cell culture)	Thermo Scientific
Innova® 42 incubator (bacteria/yeast culture)	Eppendorf
V-639 Spectrophotometer	Jasco Inc.
Beckman Coulter Z1 Particle Counter	Beckman Coulter
Zeiss KS ELISPOT system	Carl Zeiss

2.1.4 Software

SeqMan Pro version 7.2.1	DNA Star Lasergene
Odyssey 2.1 Infrared Imaging System	LI-COR Biosciences
Primer 3 Version 0.4.0	Rozen and Skaletsky 2000
GraphPad Prism 6	GraphPad Software, USA

2.1.5 Websites

http://www.ncbi.nlm.nih.gov/	NCBI
http://blast.ncbi.nlm.nih.gov/Blast.cgi	BLAST
http://expasy.org/cgi-bin/dna_aa	Expasy Proteomics Server
http://frodo.wi.mit.edu/primer3/	Primer 3
docs.appliedbiosystems.com/pebi docs/04331468.pdf	3730XL DNA Analyser User Guide
http://www.dharmacon.com/designcenter/	siRNA Design Center

2.2 Methods

2.2.1 Cloning

2.2.1.1 Oligonucleotide primer design

Primers were designed either manually for cloning specific DNA inserts (Table 2.2.1), for amplifying a cloned insert (Table 2.2.2) or by utilising the Primer 3 version 0.4.0 software for sequencing primers²⁵⁴. The following parameters were considered in the primer design: a primer length of 18-30 nucleotides to ensure specificity; a melting temperature in the region 55-78°C with primer pairs having a difference of less than 5°C, calculated using the following formula: 2[no. of A/T nucleotides] + 4[no. of G/C nucleotides]; a GC content of 40-60%; avoidance of primer dimers between primer pairs and avoidance of secondary structure within the primer for maximum availability for PCR amplification; avoidance of stretches of the same nucleotide to prevent mispriming. Primers for cloning of *Hectd2*/fragments and candidate genes into pGBKT7, pCMV-MYC/pCMV-HA or pCRII-Blunt-TOPO expression vectors are listed below (Table 2.2.1). These were sourced from Sigma Aldrich or Eurofins in a freeze-dried form, resuspended to a final concentration of 100µM in 10mM TE, pH 8.0. A working stock concentration of 10µM was made by diluting in 10mM TE, pH 8.0 for storage at -20°C.

Table 2.2.1. Primers for cloning into pGBKT7, pCMV-MYC or pCMV-HA

Primer	Sequence	Vector
Hect414NcoI-F*	5' ggCCATGGagatgagtgaggcgggctcgggatctc	pGBKT7
Hect414Pst-R	3' cgCTGCAGttaaataacatattcatatcaggtct	
Hect330Pst-R	3' cgCTGCAGttaagggtgaaccaaattggtggcagt	
Hect180Pst-R	3' cgCTGCAGttagtcctcaatagttatataatgaggc	
Hect414-F	5' atGTCGACcatgagtgaggcgggctcgggatctc	pCMV-MYC
Hect414-R	3' atGTCGACttaaataacatattcatatcaggtct	
Hectd2-F	5' atGTCGACcatgagtgaggcgggctcgggatctc	
Hectd2-R	3' atGTCGACttattcaagtccaaaaccttctgaatt	

tcSh3glb1-F	5' atGGCCATGGAGGCCgaagaaaagcttggccaggcag	pCMV-HA
tcSh3glb1-R	3' atGGCCTCCATGGCCttacttgcccttttgatttcctctc	
Sh3glb1-F	5' atGGCCATGGAGGCCatgaacatcatggatttcaacgtga	
Sh3glb1-R	3' atGGCCTCCATGGCCttaattgagaagttctaagtaggtaat	
Stmn2-F	5' atGGCCATGGAGGCCatggctaaaacagcaatggccta	
Stmn2-R	3' atGGCCTCCATGGCCtcagccagacagttcaacctgc	
tcPacsin2-F	5' atGGCCATGGAGGCCaagaactggcagaaggaagcctt	
tcPacsin2-R	3' atGGCCTCCATGGCCttactcaaactgtggccagttcat	
Pacsin2-F	5' atGGCCATGGAGGCCatgtctgtcacctacgatgactc	
Pacsin2-R	3' atGGCCTCCATGGCCtcactggatagcctcgacatagt	
tcStambp-F	5' atGGCCATGGAGGCCtatgagcagtataaagagcgaaag	
tcStambp-R	3' atGGCCTCCATGGCCttatcgaaggtctgtgatcgta	
Stambp-F	5' atGGCCATGGAGGCCatgtctgaccatggggatgtga	
Stambp-R	3' atGGCCTCCATGGCCttatcgaaggtctgtgatcgta	
tcSept7-F	5' atGGCCATGGAGGCCaacaacaagaacaaagggcagct	
tcSept7-R	3' atGGCCTCCATGGCCttaaaagatcttgccctttcttctt	
Sept7-F	5' atGGCCATGGAGGCCatgtcggtcagtgcgagatcc	
Sept7-R	3' atGGCCTCCATGGCCttaaaagatcttgccctttcttctt	

*Nco*I, *Pst*I, *Sal*I or *Sfi*I restriction site sequence | base pair insertions to maintain frame | linker region| inserted stop codon. Primers were designed to clone *Hectd2* sequences or candidate gene sequences into their appropriate vector as detailed in the table. The suffixes F and R succeeding primer names denote forward or reverse primers for amplification of the 5' or 3' ends, respectively. *Hect414*Nco*I-F was used to prime the 5' end of Hect414, Hect330 and Hect180 sequences.

2.2.1.2 PCR amplification of inserts for cloning

PCR amplification of DNA was carried out in a 96-well PCR plate (Thermo Scientific) using a DNA plasmid template concentration of 20 ng in a total reaction volume of 25 µl. A mix of 0.5 µl of proof reading, *Pfu* DNA Polymerase, (3 U/µl; Promega), 2.5 µl of *Pfu* DNA Polymerase Buffer (10X; Promega), 1 µl of 10 µM forward primer, 1 µl of 10 µM

reverse primer, 0.5 µl of dNTPs (200 µM; Promega) was added to the DNA and constituted to 25 µl with ddH₂O. A non-template control reaction using H₂O in place of DNA was carried out in parallel and the plate sealed using a Thermocycler PCR lid (ABI) prior to mixing of the reactions by flicking the wells. Following a pulse-spin at 4000 *x g*, the plate was transferred to the Biorad PCR ThermoCycler version PTC-225. Typically, the cycling conditions were as follows: 95°C, 2 minutes for initial denaturation, 95°C, 1 minute for template denaturation, 55°C-65°C gradient cycling for 30 seconds to determine the optimal primer annealing temperature and 73°C, 3 minutes for extension. These steps were repeated for an additional 39 cycles followed by a final extension step at 73°C, 5 minutes to conclude the PCR reaction. However extension times were determined empirically based on amplicon size, where 1.0 kb/per minute is extended. The PCR products were visualised by agarose gel electrophoresis as described in Section 2.2.4.2.

2.2.1.3 Small-scale purification of plasmid DNA

To isolate plasmids from bacterial culture the QIAGEN QIAprep Spin Miniprep kit was used. Plasmid isolation was carried out according to manufacturer's instructions.

Plasmid DNA was extracted from yeast cells using the Clontech Easy Yeast Plasmid Isolation Kit. Plasmid isolation was carried out according to manufacturer's instructions.

2.2.1.4 Large-scale purification of plasmid DNA

To prepare high quality and yield of plasmids, the Endotoxin-Free QIAGEN Plasmid Maxi kit was used. Plasmid isolation was carried out according to the manufacturer's instructions.

2.2.1.5 Vector preparation

Vectors were linearised for cloning by digestion of 20 µg of vector DNA in a 150 µl volume according to Section 2.2.4.3. Digests were cleaned of buffers and enzymes by addition of one volume of MicroCLEAN (Microzone) to one volume of digested DNA

and mixed by brief vortexing. The sample was incubated for 5 minutes at room temperature for binding of DNA to the purifying reagent prior to a spin at 14,000 $\times g$ for 7 minutes. Removal of the supernatant was followed by a further spin at 14,000 $\times g$ for 1 minute to discard residual supernatant. This step was repeated for a final spin after which the cleaned DNA was resuspended in 200 μl of ddH₂O.

Phosphates were removed from the ends of 80 μl of linearised vector (approximately 1 μg) by addition of 10 μl of Shrimp Alkaline Phosphatase (500 U/ μl ; Roche) diluted in 10 μl of Shrimp Alkaline Phosphatase Buffer (10X; Roche). The reaction was incubated for 15 minutes at 37°C followed by 15 minutes at 65°C to inactivate the phosphatase. The DNA was cleaned with microCLEAN as described above and resuspended in 100 μl of ddH₂O.

2.2.1.6 Ligation

For the blunt end ligation of PCR products into pCRII-Blunt-TOPO vector, the Zero Blunt[®] TOPO[®] PCR Cloning kit was used according to the manufacturer's instructions. 4 μl of PCR product, of an approximate concentration of 100 ng, was mixed with 1 μl of Salt Solution and 1 μl of pCRII-Blunt-TOPO vector. The reaction was incubated at room temperature for 30 minutes prior to transformation into *E. coli* as described in Section 2.2.3.1.

For ligation via overhanging ends, restriction digestion according to Section 2.2.4.3 was performed to generate insert and vector with the complementary overhanging ends. Inserts and vectors were prepared according to Sections 2.2.1.5 and 2.2.4.3. An insert:vector molar ratio of 6:1 was mixed with 1 μl of T4 DNA Ligase Reaction Buffer (10X; NEB) and 1 μl of T4 DNA Ligase (400,000 cohesive end units/ml; NEB). The ligation was incubated at 16°C for 24 hours prior to transformation into *E. coli* as described in Section 2.2.3.1.

2.2.1.7 shRNA design and construct generation

shRNAs were designed using the siDesign Center algorithm on Dharmacon RNAi Technologies, (<http://www.dharmacon.com/designcenter/designcenterpage.aspx>), which employs an algorithm to identify functional siRNAs²⁵⁵. Four 19-mer shRNAs generated by the algorithm were selected based on the following parameters; A/U at position 1, no more than 2 T bases at the 3' end, avoiding stretches of 3 A/U and runs of 4 of any base and at least one shRNA in the untranslated region, all with a GC content ranging from 30-64%. 5' *Bgl*II/3' *Hind*III restriction sites were incorporated onto the shRNA oligo preceding the N-19 sequence in the sense and antisense orientation, separated by a 9 nucleotide spacer sequence. The 3' end of this forward oligonucleotide includes a run of 5 thymidines that denotes the termination signal. shRNAs and their duplex sequences were reconstituted to a concentration of 100 pM in 10mM TE, pH 8.0, of which 1 µl of each shRNA and its complementary oligonucleotide were mixed with 43 µl of annealing buffer (10 mM Tris-HCl, pH 7.5, 1 mM EDTA, 50 mM NaCl; 10X) in a PCR reaction tube (ABI) containing 5 µl of ddH₂O. Denaturation at 95°C on a heat block was followed by transfer of the heat block rack onto a room-temperature worktop for cooling. Forward and reverse oligonucleotides are listed in Table 2.2.2. Once at room temperature the annealed oligonucleotides were ligated to linearised pSUPER.retro.puro expression vector in an equimolar ratio and ligated according to Section 2.2.1.6.

Table 2.2.2 shRNA oligonucleotides for cloning into pSUPER.retro.puro

shRNA	Sequence
Sh3glb1-1F	5' GATCCCCACACATGGGCAGTGAGGAA TTCAAGAGA TTCTCACTGCCCATGTGTTTTTTA
Sh3glb1-1R	5' AGCTT AAAAAACACATGGGCAGTGAGGAA TCTCTTGA ATTCCTCACTGCCCATGTGTGGG
Sh3glb1-2F	5' GATCCCCACGTAAAGGCCCAAGGAAA TTCAAGAGA TTCTCTGGGCCTTACGTTTTTTA
Sh3glb1-2R	5' AGCTT AAAAAACGTAAAGGCCCAAGGAAA TCTCTTGA ATTCCTTGGGCCTTACGTGGG
Sh3glb1-3F	5' GATCCCATTAAATGAGTGGAGGGTAC TTCAAGAGA GTACCCTCCACTCATTAATTTTTTA
Sh3glb1-3R	5' AGCTT AAAAAATTAATGAGTGGAGGGTAC TCTCTTGA AGTACCCTCCACTCATTAATGGG
Sh3glb1-4F	5' GATCCCAGACAGAAGTGGACGCTCA TTCAAGAGA TGAGCGTCCAGTTCTGTCTTTTTTA
Sh3glb1-4R	5' AGCTT AAAAAAGACAGAAGTGGACGCTCA TCTCTTGA ATGAGCGTCCAGTTCTGTCTGGG

Stambp-1F	5' GATC CCCAGACAGAGCTCTTGAGAAG TTCAAGAGA CTTCTCAAGAGCTCTGTCTTTTTTA
Stambp-1R	5' AGCTT AAAAAAGACAGAGCTCTTGAGAAG TCTCTTGA ACTTCTCAAGAGCTCTGTCTGGG
Stambp4A	5' GATC CCCGAGATGGATCACTGGGTAA TTCAAGAGA TTACCCAGTGATCCATCTCTTTTTTA
Stambp4B	5' AGCTT AAAAAGAGATGGATCACTGGGTAA TCTCTTGA ATTACCCAGTGATCCATCTCGGG
Pacsin2-1F	5' GATC CCCTGACCAAGATAGAGGATGA TTCAAGAGA TCATCCTCTATCTTGGTCATTTTTTA
Pacsin2-1R	5' AGCTT AAAAATGACCAAGATAGAGGATGA TCTCTTGA ATCATCCTCTATCTTGGTCAGGG
Pacsin2-2F	5' GATC CCCAGATATAGACACAGGAAGA TTCAAGAGA TCTTCCTGTGTCTATATCTTTTTTA
Pacsin2-2R	5' AGCTT AAAAAAGATATAGACACAGGAAGA TCTCTTGA ATCTTCCTGTGTCTATATCTGGG
Pacsin2-3F	5' GATC CCCAGATAGAGGATGAAGATGA TTCAAGAGA TCATCTTCATCCTCTATCTTTTTTA
Pacsin2-3R	5' AGCTT AAAAAAGATAGAGGATGAAGATGA TCTCTTGA ATCATCTTCATCCTCTATCTGGG
Pacsin2-4F	5' GATC CCCAGGTCAATGAGCAGACTTA TTCAAGAGA TAAGTCTGCTCATTGACCTTTTTTA
Pacsin2-4R	5' AGCTT AAAAAAGGTCAATGAGCAGACTTA TCTCTTGA ATAAGTCTGCTCATTGACCTGGG
Sept7-1F	5' GATC CCCTGAAGAAGATGGAGATGGA TTCAAGAGA TCCATCTCCATCTTCTTCATTTTTTA
Sept7-1R	5' AGCTT AAAAATGAAGAAGATGGAGATGGA TCTCTTGA ATCCATCTCCATCTTCTTCAGGG
Sept7-2F	5' GATC CCCACAATGGAGTGGATAACAA TTCAAGAGA TTGTTATCCACTCCATTGTTTTTTA
Sept7-2R	5' AGCTT AAAAACAATGGAGTGGATAACAA TCTCTTGA ATTGTTATCCACTCCATTGTGGG
Sept7-3F	5' GATC CCCTTGGAGATGCAGTGGATAA TTCAAGAGA TTATCCACTGCATCTCCAATTTTTTA
Sept7-3R	5' AGCTT AAAAATTGGAGATGCAGTGGATAA TCTCTTGA ATTATCCACTGCATCTCCAAGGG
Sept7-4F	5' GATC CCCGATGCAGCCTATACAATAA TTCAAGAGA TTATTGTATAGGCTGCATCTTTTTTA
Sept7-4R	5' AGCTT AAAAAGATGCAGCCTATACAATAA TCTCTTGA ATTATTGTATAGGCTGCATCGGG

*Bgl*II or *Hind*III restriction site sequence | spacer nucleotides | The suffixes F and R succeeding oligo names denote forward and reverse shRNAs corresponding to the 5' or 3' ends, respectively that are subsequently annealed. For example, oligos Sh3glb1-1F and Sh3glb1-1R are annealed together prior to cloning and represent one shRNA targeting construct for *Sh3glb1*.

2.2.2 RNA manipulation and analysis

2.2.2.1 RNA recovery from cultured cells

The Taqman[®] Gene Expression Cells to CT[™] kit was used to recover RNA from cultured PK1/2 cells in which shRNA gene targeting was carried out. PK1/2 cell lines were seeded at a density of 10^4 cells in a 96-well tissue culture plate (Nunc), inclusive of two biological replicates for each knockdown line and control lines after which they were incubated for 24 hours at 37°C/5% CO₂. Cells were washed with 1X PBS (Life Technologies Ltd) to remove inhibiting FCS and then lysed for 5 minutes with a 50 µl solution of Cell Lysis Buffer (Ambion) with DNaseI at a 1:100 ratio to degrade genomic DNA. The Cell Lysis Buffer contains inhibitors of endogenous RNases to preserve RNA integrity. 5 µl of Stop Solution was mixed with the lysates for 2 minutes to inactivate the lysis components as a preventative measure from potential inhibition of subsequent reverse transcription or qPCR reactions. RNA lysates were used immediately or stored at -70°C.

2.2.2.2 Reverse transcription

10% of the cell lysate (from Section 2.2.2.1) was used to reverse transcribe the RNA present in the lysates in a 96-well PCR plate (ABI). First strand cDNA was synthesized using a combination of 2.5 µl of 20X Reverse Transcriptase Enzyme Mix and 25 µl of 2X Reverse Transcriptase Buffer (Ambion), which includes a pre-mix of oligo(dT). The reaction was made up to 50 µl with nuclease free ddH₂O, mixed gently and pulse centrifuged. The reaction was subjected to thermal cycling on the BioRad Thermal Cycler using the following parameters; 37°C for 60 minutes for reverse transcription, primed by oligo(dT) that hybridizes to the poly(A) tail of mRNA, 95°C for 5 minutes to inactivate the reverse transcription reaction, completed with a hold at 4°C to cool. Assembled reverse transcription reactions were stored at -20°C until ready for use.

2.2.2.3 Real time quantitative PCR

Real time quantitative PCR, (qPCR), was used to detect and quantify mRNA using target gene-specific primers and probes by means of the 5' nuclease activity of Taq DNA polymerase. Commercially available, TaqMan[®] Gene Expression primer and probe sets were purchased from Life Technologies Ltd as pre-validated assays. The target specific probes were fluorogenic and dual labelled with a reporter FAM[™] dye and a nonfluorescent quencher linked to the 5' and 3' ends, respectively. A reaction totaling 16 µl in volume was comprised from 4 µl of target cDNA (Section 2.2.2.2) with 1 µl of gene-specific 20X TaqMan[®] Gene Expression Assay and 1 µl of 2X TaqMan[®] Gene Expression Master mix. This TaqMan[®] Gene Expression Master Mix contains a pre-mix of Taq DNA Polymerase, buffer and ROX[™] passive reference dye for normalising fluorescence fluctuations independent of the PCR. Samples were duplexed with an endogenous GAPDH control (20X TaqMan[®] Mouse GAPDH Assay, Life Technologies Ltd), harbouring a VIC[™] reporter dye. The ABI Prism 7700 Sequence Detection System was used to perform the following cycling parameters; 95°C for 10 minutes to activate *Taq* Polymerase followed by PCR amplification at 95°C for 15 minutes for 40 cycles and 60°C for 1 minute. Quantitation was determined by a comparative Ct method in which C_T values represent the cycle number where the fluorescence signal for a given accumulated amplicon crosses the threshold set at the exponential phase of the amplification curve. Relative values for target expression, normalised to endogenous GAPDH, relative to control PK1/2 cells expressing non-targeting GFP-sh2 were given by $2^{-\Delta\Delta C_T}$, where $\Delta\Delta C_T$ is defined by the difference in ΔC_T of the sample and the reference PK1/2 cells expressing non-targeting GFP-sh2 ($\Delta\Delta C_T = C_{T \text{ target}} - C_{T \text{ reference:GFP-sh2}}$).

2.2.3 Transformation

2.2.3.1 DH5α *E.coli* cells

All procedures handling bacteria were performed using sterile aseptic techniques. Chemically competent bacterial cells (NEB5 DH5α or One Shot TOPO DH5α; NEB; Life Technologies Ltd) were thawed on ice for 10 minutes prior to incubation with 10ng of

plasmid DNA or ligation mix for 30 minutes. The cells were heat shocked at 42°C for 30 seconds followed by a 5 minute recovery period on ice. 950 µl or 250 µl of SOC (Sigma), prewarmed to 37°C, was added to NEB5 or One Shot TOPO cells and incubated at 37°C/225 rpm for 1 hour. One Shot TOPO cells required a lower volume of SOC according to the volume of cells. Transformants were concentrated by a 30 second spin at 14,000 x g and resuspended in 100 µl of SOC prior to plating out on appropriate selective LB agar plates supplemented with 100µg/ ml ampicillin or 50µg/ ml kanamycin (Appendix I). Plates were incubated at 37°C for 16-20 hours, faced upside down to prevent condensation that builds up on the inside of the plate lids from contaminating any colonies.

2.2.3.2 Y2HGold yeast cells

All procedures handling yeast were performed using sterile aseptic techniques. Competent Y2HGold cells were prepared and transformed using the Clontech Matchmaker Transformation System 2 kit following the manufacturer's instructions. A 2mm Y2HGold colony was inoculated into 3 ml of YPDA broth in a 15 ml culture tube, (Falcon), and incubated at 30°C/250 rpm for 9 hours. 5 µl of the culture was transferred into 50 ml of YPDA broth in a 250 ml flask. This was shaken at 30°C/250 rpm for 16 hours until cells had reached the phase of accelerating growth at an OD₆₀₀ of 0.15 – 0.3, measured using the Jasco V-639 Spectrophotometer. The culture was pelleted at 700 x g for 5 minutes at room temperature and the cell pellet resuspended in 100 ml of fresh YPDA broth and the culture incubated 30°C/250 rpm for 2-5 hours. The OD₆₀₀ was measured hourly until the phase of exponential growth had been reached at 0.4 - 0.5 in order that the greatest number of cells were made competent. The culture was then divided between two 50 ml tubes, (Falcon), and spun at 700 x g for 5 minutes at room temperature prior to resuspension in 30 ml sterile dddH₂O. The cells were spun at 700 x g for 5 minutes and each pellet resuspended in 1.5 ml of 1.1X TE/Lithium Acetate solution (detailed in Appendix 1) in separate microfuge tubes. The cell suspensions were spun for 15 seconds at 14,000 x g, with the supernatant discarded and resuspension of the pellet in 600 µl of 1.1X

TE/Lithium Acetate solution. The competent cells were placed on ice and transformed immediately to avoid loss in efficiency.

In a pre-chilled microfuge tube, 100 ng of high quality DNA was added to 5 μ l of Yeastmaker Carrier DNA (10 μ g/ μ l; Clontech Takara Bio Europe) that was cooled on ice following pre-denaturation at 95°C. 50 μ l of competent Y2HGold cells were combined with the DNA and gently mixed. 500 μ l of PEG/LiAc was added to the cell/DNA suspension, gently mixed and incubated at 30°C for 30 minutes during which the cells were tapped to mix in 10 minute intervals. Cell walls were made permeable by addition of 20 μ l of DMSO (Sigma) prior to a 15 minute heat shock at 42°C, during which the tube was tapped at 5 minute intervals. The cells were spun at 14,000 \times g for 15 seconds and the supernatant discarded and the pellets resuspended in 1 ml of YPD Plus Medium. Transformants were incubated at 30°C/250 rpm for 90 minutes after which they were spun at 14,000 \times g for 15 seconds for a final resuspension in 0.9% (w/v) NaCl solution (Sigma). 100 μ l of 1:10 and 1:100 dilutions in YPDA broth were spread onto the appropriate selective media plates and incubated at 30°C for 5 days.

For co-transformation into Y2HGold, Section 2.2.3.2 was followed, differing only in that 500ng/ μ l of each plasmid was combined with the 50 μ l aliquot of cells and a 1:2 dilution was spread onto the appropriate selective plates (Appendix 1).

2.2.4 Screening of clones

2.2.4.1 Bacterial/yeast colony PCR

To screen DNA constructs, bacterial or yeast colonies were touched lightly with a pipette tip and dispersed in 100 μ l or 12.5 μ l of ddH₂O, respectively, in a 96 well PCR plate (ABI). 1 μ l of bacterial suspension was transferred to 0.5 μ l each of 10 μ M forward and 10 μ M reverse primers (Table 2.2.3), (Sigma; Eurofins) and 8 μ l of MegaMix Blue (Microzone), which contains a pre-mix of DNA polymerase, buffer and dNTPs. For yeast colonies, 12.5 μ l of 2X Matchmaker™ Insert Check PCR Mix 2, a pre-mix of primers (Table 2.2.3), DNA polymerase, dNTPs and buffer, was transferred to 12.5 μ l of the yeast suspension. The plates were sealed with a thermocycler PCR lid (ABI) and the reactions

mixed by flicking the wells prior to a spin at 4000 x g for 1 minute. Thermal cycling parameters were applied; for bacterial reactions: 94°C, 10 minutes for 1 cycle, 94°C, 30 seconds, 55°C, 30 seconds, 72°C for a variable time length, where 1 minute extends 1 kb, for 39 cycles followed by a final extension step at 73°C for 5 minutes, unless otherwise stated; for yeast reactions: 94°C, 1 minute for 1 cycle, 98°C, 10 minutes, 68°C, 3 minutes for 30 cycles. The PCR products were analysed according to Section 2.2.4.2.

Table 2.2.3 PCR screening primers

Primer	Sequence	Vector
M13 Uni (-20)	5' TGTA AACGACGGCCAGT	pCRII-Blunt-TOPO
M13 Reverse	5' CAGGAAACAGCTATGACC	pCRII-Blunt-TOPO
HA Forward	5' ATGTACCCATACGATGTTCCAGA	pCMV-HA
MYC Forward	5' ATGGCATCAATGCAGAAGCTGAT	pCMV-MYC
CMV Reverse	5' GCGGCCGCGGTACCTCGA	pCMV-HA/pCMV-MYC
ADLD Forward	5' CTATTTCGATGATGAAGATACCCCA	pGADT7-recAB
ADLD Reverse	5' AGTGAACCTGCGGGGTTTTTCAGT	pGADT7-recAB

2.2.4.2 Agarose gel electrophoresis

Analytical size separation of DNA fragments was carried out on a 1% or 2% (w/v) agarose gel, where the former was used for resolving products >1.0 kb and the latter <1.0kb. Gels were made by constituting UltraPure™ agarose in 1X TBE and melting at $\geq 90^\circ\text{C}$ for 2 minutes. The agarose solution was cooled to hand temperature prior to addition of 0.2 $\mu\text{g/ml}$ ethidium bromide solution (Sigma) and poured into a casting tray. Once set, the gel was transferred to an electrophoresis tank and 10 μl of DNA/1X gel loading dye (0.25% Orange G, 18% glycerol in 10mM TE, pH 8.0; 6X) were loaded alongside 5 μl of Hyperladder I or IV (Promega) to resolve products >1.0 kb or <1.0 kb, respectively. Electrophoresis in 1X TBE was carried out at 100V for 30 minutes - 1 ½ hours, depending

on the resolution required. Ethidium bromide-stained DNA was visualised on a UV Trans-Illuminator Gel Doc imaging system (Biorad).

2.2.4.3 Restriction digestion

DNA inserts were verified by digesting 800 ng of plasmid DNA with 3 µl of 10X buffer of the appropriate enzyme and 1 µl of restriction endonuclease (40 U/µl). ddH₂O was added to a final volume of 30 µl after which the reaction was mixed by flicking and pulse-spun prior to incubation for 1 hour at 50°C for *Sfi*I and at 37°C for all other restriction endonucleases used. For direct cloning of insert, the reaction volume was scaled up to 150 µl with the reagents appropriately scaled up. The digests were screened according to Section 2.2.4.2.

2.2.4.4 Gel excision and purification

For subcloning purified inserts/vectors, the QIAGEN MinElute Gel extraction kit was used to purify gel excised fragments according to the manufacturer's instructions.

2.2.5 Bacterial/yeast culture

2.2.5.1 Bacterial growth

DH5α *E.coli* cells were cultured at 37°C in LB broth (25g/L; Sigma) or LB agar base (30g/L; Sigma) with the appropriate selective antibiotics, 100µg/ml ampicillin or 50µg/ml kanamycin, for 16-20 hours and at 225 rpm for broth. Solution formulations for these are detailed in Appendix 1. Glycerol stocks were made with 1 ml of bacterial culture/200 µl of glycerol (99.9%; Sigma) and frozen at -70°C. Stocks were recovered by streaking onto the appropriate selective LB agar plates and incubated at 37°C for 16-20 hours.

2.2.5.2 Yeast growth

Yeast strains were cultured at 30°C in YPDA or the appropriate selective broth or agar medium as described in Appendix 1 and grown for 5 days on agar or 16-20 hours/250 rpm in broth unless otherwise stated. Glycerol stocks were made with a single colony resuspended into 500 µl of YPDA/25% (v/v) glycerol and frozen at -70°C. Stocks were recovered by streaking onto YPDA or appropriate selective media plates and incubated for 5 days.

2.2.6 Sequencing

300ng of plasmid DNA or PCR product that was cleaned using the microCLEAN method in Section 2.2.1.5, was diluted in ddH₂O to a final volume of 8.5 µl in a 96-well, non-skirted, sequencing plate, (ABI). These were sequenced using the BigDye® Terminator v1.1 Cycle Sequencing Kit (Applied Biosystems). 0.5 µl of the appropriate primer (10 µM; Sigma/Eurofins) and 5 µl of Better Buffer (Applied Biosystems) were transferred to the DNA dilution prior to addition of 1 µl of Big Dye Terminator v1.1. The reaction was mixed by flicking of the well and the plate sealed with a Thermocycler PCR lid (ABI). The plate was transferred to the Biorad PCR ThermoCycler, (Applied Biosystems) using the following thermal cycling parameters: 96°C for 1 minute, 96°C for 10 seconds, 50°C for 5 seconds, 60°C for 4 minutes with the cycling conditions repeated for an additional 24 cycles. Post-sequencing precipitation followed by addition of 1 µl EDTA (0.125 µM; Sigma), 1 µl sodium acetate (0.3M, pH 5.2; Sigma) and 55 µl of absolute ethanol (Fisher). The solutions were mixed by vortexing and incubated at room temperature for 5 minutes followed by a spin at 4°C/4000 *x g* for 45 minutes. The plate was inverted to discard the supernatant and then spun inverted onto tissue paper at 4°C/100 *x g* for 1 minute. The resulting pellet was washed in 155 µl of 70% ethanol prior to a spin at 4°C/4000 *x g* for 10 minutes. The ethanol was discarded by plate inversion onto tissue paper and an additional spin at 4°C/100 *x g* for 1 minute. The DNA pellet was then resuspended in 10 µl of hi-di-formamide (Life Technologies Ltd) by vortexing. Following a spin at 4°C/4000 *x g* for 1 minute, the DNA was denatured at 96°C, cooled rapidly at 4°C and loaded onto a 3730XL DNA Analyzer platform (Applied Biosystems). Sequencing parameters were

set according to those recommended in the ABI 3730XL user guide, using electrokinetic capillary injection times of 5, 15 and 60 seconds, (user guide referenced in Section 2.1.5).

2.2.7 Yeast two-hybrid screen

Interacting proteins of Hectd2 were identified using yeast two-hybrid screening against a library of unknown proteins, Mate & Plate™ Universal Normalised Mouse Library strain (Clontech product 630483, pre-transformed into Y187, detailed in Section 3.5). The Clontech Matchmaker™ Gold Yeast-Two-Hybrid User Kit and Manual was followed according to the manufacturer's instructions and growth media was prepared according to Appendix 1. A concentrated culture of the bait strain, GAL4 DNA BD-Hect414 was prepared by inoculating 3-5 colonies, ~1mm in size, into 50 ml of SD/-Trp broth. The culture was incubated at 30°C/270 rpm until the peak of the exponential growth phase had been reached at an OD₆₀₀ of 0.8. The culture was spun at 1000 *x g* for 5 minutes prior to cell pellet resuspension in 4 ml of SD/-Trp broth, giving an estimated density of >1 x 10⁸ cells. 1 ml of Mate & Plate™ Universal Normalised Mouse Library strain was thawed and combined with the bait strain into 45 ml of 2X YPDA/50µg/ml of kanamycin in a 2L flask. Following 24 hours incubation at 30°C/45 rpm, the culture was spun at 1000 *x g* for 10 minutes whilst the flask was rinsed twice with 50 ml of 0.5X YPDA broth after which it was used to resuspend the pelleted cells. A final spin at 1000 *x g* for 10 minutes was followed by removal of the supernatant broth and resuspension into fresh 10 ml of 0.5X YPDA/50µg/ml kanamycin, giving a total volume of 11.5 ml. 100 µl of a 1:10, 1:100, 1:1000 and 1:10000 dilutions were spread onto SD/-Trp, SD/-Leu and SD/-Trp/-Leu 10cm agar plates. The remaining culture was spread across 50-55, SD/-Trp/-Leu, 15cm agar plates. The plates were incubated at 30°C for 5 days.

2.2.8 Mammalian cell culture

All tissue culture and preparation of solutions were performed in a Class II laminar flow hood. All materials were sterilised with 70% ethanol or bought pre-sterilised and media/solutions warmed to 37°C prior to use.

2.2.8.1 Maintenance of COS-7, ϕ -NX Eco and N2aPK1/2 cells

COS-7 cells, Phoenix Ecotropic (ϕ -NX Eco) cells and N2aPK1/2 cells were gifted by Emma Quarterman and Dr Craig Brown, MRC Prion Unit, London. COS-7 and ϕ -NX Eco cells were maintained in Complete Dulbecco's Modified Eagle Medium (DMEM) (Life Technologies Ltd) supplemented with 10% (v/v) Heat Inactivated FBS (Life Technologies Ltd) and 1% (v/v) PenStrep, (100U/ ml penicillin, 100ug/ ml streptomycin; Life Technologies Ltd). N2aPK1/2 cells were maintained in OPTIMEM supplemented with 10% (v/v) Heat Inactivated FBS (Life Technologies Ltd) and 1% (v/v) PenStrep, (100U/ ml penicillin, 100ug/ ml streptomycin; Life Technologies Ltd). All cell types were sub-cultured at 90% confluence and only ϕ -NX Eco and N2aPK1/2 cells were resuspended immediately into the fresh media detailed as above, respectively. COS-7 cells are adherent cells and required to be trypsinised and so were washed with 1X PBS, (pH 7.0 Life Technologies Ltd) prior to incubation at 37°C with 3 mls of 0.05% trypsin-EDTA (Life Technologies Ltd) to dislodge the cell monolayer. The trypsin was inactivated after 5 minutes with 10 ml of complete medium. COS-7 cells were harvested by spinning at 300 x g for 5 minutes, media removed and the cell pellet resuspended in complete medium. Cells were plated out at a sub-cultivation ratio of 1:8 and media was renewed 2-3 times a week or cells were counted with haemocytometer and a defined number of cells plated out, typically at a standard density of 1×10^6 cells in a 10 cm dish (Nunc). All cell types were grown in a humidified incubator at 37°C and 5% CO₂ atmosphere until confluent.

2.2.8.2 Cryopreservation of COS-7, ϕ -NX Eco and N2aPK1/2 cells

Following trypsinisation, of COS-7 cells (Section 2.2.8.1), confluent cells from a 10 cm dish were spun for $125 \times g$ for 7 minutes and resuspended in 750 μ l of freezing medium (90% FBS and 10% v/v DMSO). This was transferred to a cryovial (Nunc) and placed in a Nalgene freezing container (Thermo Scientific) to achieve a $-1^{\circ}\text{C}/\text{minute}$ cooling rate in a -70°C freezer. 24 hours later, the cryovials were transferred to the liquid nitrogen vapour phase for long term storage.

2.2.8.3 Recovery of COS-7, ϕ -NX Eco and N2aPK1/2 cells

Frozen cryovials were thawed in a 37°C water bath for 1 minute after which the cells were resuspended in 10 ml of complete growth media (detailed in Section 2.2.8.1) in a 15 ml tube (Falcon). The cells were spun at $300 \times g$ for 5 minutes and the DMSO-containing medium was discarded. The cell pellet was resuspended in 10 ml of complete growth media and transferred to a 10 cm dish (Nunc) and subcultured as in Section 2.2.8.1.

2.2.8.4 Transfections

Cells were seeded at density of 1.2×10^6 or 1.4×10^6 cells into 10 cm culture dishes (Nunc), 24 hours prior to transfection. On the day of transfection, cells underwent media change to un-supplemented DMEM and incubated at $37^{\circ}\text{C}/5\% \text{CO}_2$ for 1 hour. To 1 ml of un-supplemented DMEM was added 5 μ g or 10 μ g of plasmid DNA and mixed by vortexing. A ratio of 1:5 Lipofectamine 2000 Transfection Reagent (Life Technologies Ltd):DNA was used where the appropriate volume of lipofectamine was diluted in 500 μ l of DMEM, pulse vortexed and incubated at room temperature for 5 minutes. The lipofectamine dilution was added to the DNA/DMEM mixture and left to form DNA/lipofectamine complexes by incubating at room temperature for 30 minutes. The complex mixture was added to cells drop-wise and incubated at $37^{\circ}\text{C}/5\% \text{CO}_2$ for 5 hours after which the media was changed to complete growth medium and cells grown for 24 or 48 hours.

2.2.9 Protein expression

2.2.9.1 Preparation of yeast cell protein extract

A 5 ml and 10 ml overnight culture in the appropriate selective media were prepared for extraction of total protein of transformed and untransformed yeast strains respectively. The cultures were pulse vortexed prior to inoculation into 50 ml of YPDA broth and incubated at 30°C/250 rpm for 4-8 hours until an OD₆₀₀ of 0.4 - 0.6 was attained. Upon reaching this log phase peak, the total number of OD₆₀₀ units was calculated by multiplying the OD₆₀₀ of a 1 ml sample by the total culture volume, 55 or 60 ml. The cultures were transferred into a pre-chilled 175 ml centrifuge tube, (Falcon), half filled with ice prior to spinning at 1000 *x g* for 5 minutes at 4°C. The supernatant was discarded and the cell pellet resuspended in 50 ml of ice-cold H₂O and spun at 1000 *x g* for 5 minutes at 4°C. The supernatant was discarded and the pellet snap frozen in dry ice and stored at -70°C until ready for extraction.

Yeast pellets were thawed by resuspending in complete cracking buffer (detailed in Appendix 1) prewarmed at 60°C in a volume of 100 µl/7.5 OD₆₀₀ units of cells, topping up with 1X PMSF at 1 µl/100 µl of cracking buffer every 7 minutes due to the degradative properties of PMSF. The cell/cracking buffer suspension was transferred to microfuge tubes filled with glass beads (425 µm in size; Sigma) at a ratio of 80 µl/7.5 OD₆₀₀ units of cells. Samples were heated to liberate membrane associated proteins at 70°C for 10 minutes followed by vigorous vortexing. Cell debris and any unbroken cells were pelleted at 14,000 *x g* for 5 minutes at 4°C, the supernatant of which was transferred to a fresh microfuge tube and placed on ice. The pellets were boiled at 100°C for 5 minutes and vortexed vigorously prior to spinning at 14,000 *x g* for 5 minutes at 4°C. The residual supernatant was transferred to the microfuge tube containing the first supernatant and run out using SDS PAGE (Section 2.2.9.3).

2.2.9.2 Preparation of mammalian cell protein extract

10 cm plates of cells were washed with 8 ml of 1X PBS twice following media removal. 1 ml of cell lysis buffer (25mM HEPES, 1mM EGTA, 5% glycerol, 1mM MgCl₂, 20mM

β -glycerophosphate, 0.5% triton x-100; pH 7.5; Sigma) with 1X Complete Protease Inhibitor Cocktail tablet (Roche) and 1X PhosStop Phosphatase Inhibitors (for Sh3glb1 and Stmn2 only; Roche) were added to each cell plate and incubated at 4°C for 30 minutes. The lysed cells were scraped off using a 16 cm cell scraper (VWR) and transferred to a microfuge tube. The lysates were spun at 20, 000 \times g for 20 minutes at 4°C after which the cell debris pellet was discarded and the lysate aliquotted as appropriate for subsequent testing prior to storage at -70°C.

2.2.9.3 Sodium dodecyl sulphate polyacrylamide gel electrophoresis (SDS PAGE)

Novex® Tris-Glycine SDS sample buffer, (2X; Life Technologies Ltd) and β -mercaptoethanol, (1:20; Sigma) were added to mammalian cell samples and boiled at 100°C for 10 minutes. Samples were pulse-spun and 50 μ l loaded onto a 16% or 12% Novex® Tris-Glycine 1.5 mm mini-gel (Life Technologies Ltd) and electrophoresed in the XCell *SureLock*® Mini-Cell system (Life Technologies Ltd) at 125V for 2 hours in 1X Tris-Glycine buffer (Appendix I). SeeBlue® Plus2 Pre-Stained Standard was used as the molecular weight marker (Life Technologies Ltd).

2.2.9.4 Western Blotting

SDS PAGE separation of proteins was followed by electrophoretic transfer to a nitrocellulose membrane (BioTrace™; Pall Corporation) using the XCell II™ Blot Module (Life Technologies Ltd). The Blot Module was loaded from the anode with the following components that were pre-soaked in 1X Tris/Glycine/methanol electroblotting buffer (Fisher Scientific, detailed in Appendix I): blotting pad, filter paper, gel, membrane, filter paper and five blotting pads. For the transfer of two gels, the same arrangement follows, except that one blotting pad is placed after the last filter paper onto which filter paper/second gel/filter paper were transferred. The Blot Module was then packed to the cathode with 4 additional blotting pads. The Blot Module was inserted into the XCell *SureLock*® Mini-Cell and the proteins were transferred at 35V for 2½ hours in

1X Tris/Glycine/methanol electroblotting buffer (Appendix I). The transfer was kept cool by the loading of water surrounding the Blot Module.

The membrane was incubated for 1 hour in 5% w/v skimmed milk powder (Marvel) constituted in 1X PBS + 0.0005% v/v Tween-20 (Sigma), (PBST). Following a brief rinse of the membrane with PBST, the membrane was incubated overnight with the appropriate primary antibody (Section 2.2.9.5) diluted in 1% BSA w/v constituted in PBST. The membrane was washed 3X for 15 minutes each with PBST. The membrane was incubated in the dark with IRDye680 (red) conjugated goat anti-mouse IgG or IRDye800 CW (green) conjugated goat anti-rabbit IgG (LI-COR), diluted in 1% BSA in PBST for 1 hour. Following 3 x washes for 15 minutes each, the membrane was scanned using the LI-COR Odyssey infra-red imaging immunofluorescence system using the appropriate 800 nm or 700 nm channel to detect fluorophores in the infrared region.

2.2.9.5 Antibodies used

Table 2.5 Antibodies

Antibody	Concentration	Source
Anti-c-MYC mouse monoclonal	2 µg/ml	Clontech Takara BioEurope
Anti-HA rabbit polyclonal	1 µg/ml	Clontech Takara BioEurope
IRDye680 (red) conjugated goat anti-mouse IgG	0.1 µg/ml	LI-COR
IRDye800 CW (green) conjugated goat anti-rabbit IgG	0.1 µg/ml	LI-COR
Anti-PrP monoclonal antibody, ICSM18*	0.6 µg/ml	D-Gen, Ltd.
Alkaline phosphatase-conjugated anti-mouse IgG1	0.2 µg/ml	Southern Biotechnology Associates

*ICSM18 used in ELISPOT for Scrapie Cell Assay. All other antibodies used for Western blots.

2.2.10 Co-immunoprecipitation

Goat polyclonal anti-HA tag agarose antibody (Abcam) was washed 3 times with 1X PBS (Life Technologies Ltd) plus 1X Complete Protease Inhibitor Cocktail (Roche) with a volume equivalent to the bead slurry taken. Agarose bead-antibodies/PBS mixture was spun at $13,000 \times g$ for 30 seconds between each wash and finally resuspended in a volume of 1X PBS equivalent to initial bead slurry. Cell lysates were thawed and transferred to ice. 50 μ l of anti-HA tag antibody beads were added to each vial of lysate, mixed by inversion and placed on a roller for agitation at 4°C for 24 hours. The samples were spun at $1000 \times g$, 1 minute at 4°C, and the lysate discarded, leaving the beads undisturbed. 1 ml of cell lysis buffer (25mM HEPES, 1mM EGTA, 5% glycerol, 1mM MgCl₂, 20mM β -glycerophosphate, 0.5% Triton x-100; Sigma; pH 7.5), was added to the beads, mixed by inversion and placed on a roller for agitation at 4°C for 10 minutes. The samples were spun as before and the lysis buffer washes repeated 8 or 9 times. The samples were given a final wash 1x or 2x with RIPA buffer (150mM NaCl, 10mM HEPES, pH 7.5, 1% Triton x-100, 0.1% SDS, 1% sodium deoxycholate; Sigma; pH7.5). The samples were spun as before and the remaining beads were resuspended into 50 μ l of SDS sample buffer. Samples were boiled at 100°C for 10 minutes and analysed by SDS-PAGE and immunoblotted with anti-c-MYC monoclonal antibody and detected with IRDye680 (red) conjugated goat anti-mouse IgG secondary antibody (Sections 2.2.9.3 and 2.2.9.4).

2.2.11 Knockdown stable cell lines

2.2.11.1 Virus generation

Phoenix Ecotropic, ϕ -NX Eco, packaging cell line was selected to generate retroviral supernatant²⁵⁶. A transfection mix for each shRNA construct was diluted in 300 μ l serum free OPTIMEM media using a 1 μ g: 3 μ l ratio of DNA to Fugene[®]. Following pulse vortexing, 1×10^6 ϕ -NX Eco cells that were seeded 24 hours earlier, were transfected for a given shRNA construct. Media was changed 24 hours post-transfection after which the cells were incubated for a further 24 hours, a period of time that generates the highest viral titer. Transfection efficiency was visualised by GFP expression in the pRS-GFP

control ϕ -NX Eco plate, which showed ≥ 50 % expression of GFP. Retroviral supernatants were filtered to remove any cells or cell debris using a 0.45 μm filter and syringe assembly (Millipore) and used immediately or stored at -70°C until ready for transduction.

2.2.11.2 Transduction

N2aPK1/2 cells were seeded at a density of 5×10^5 into 10 cm culture dishes, (Nunc), 24 hours prior to transduction. 5 ml of filtered retroviral supernatant was added to N2aPK1/2 cells that were replenished with a fresh 5 ml of OPTIMEM supplemented with 10% (v/v) Heat Inactivated FBS (Life Technologies Ltd) and 1% (v/v) PenStrep, (100U/ ml penicillin, 100ug/ ml streptomycin; Life Technologies Ltd). Polybrene, (Sigma), was added to the cells at a concentration of 8 $\mu\text{g}/\text{ml}$, which is a cationic polymer that enhances retroviral adsorption to the cell surface²⁵⁷. After 6 hours incubation at $37^{\circ}\text{C}/5\%$ CO_2 with retroviral supernatant, the media was changed to fresh OPTIMEM/10% FBS/1% PenStrep, as detailed above, and incubated again for 48 hours. Transductions were performed in parallel with a plate of uninfected N2aPK1/2 cells to serve as a control for subsequent drug selection of transduced cells.

2.2.11.3 Drug selection of shRNA-expressing cells

The pSUPER.retro.puro construct harbours a puromycin resistance cassette that was selected for in transduced N2aPK1/2 cells by adding 4 $\mu\text{g}/\text{ml}$ puromycin (Life Technologies Ltd), a concentration determined by dose-response curve analysis (Dr Craig Brown, MRC Prion Unit). Media change with puromycin-supplemented OPTIMEM/10% OFCS/1% PenStrep media was carried out every 48 hours. Successfully transduced cells survived whilst uninfected negative control cells were dead within 3 days. Cells were maintained on puromycin selection for two weeks after which mRNA expression was measured by real time quantitative PCR (Section 2.2.2.3).

2.2.12 Scrapie Cell Assay

Scrapie Cell Assays were performed by Dr Craig Brown, MRC Prion Unit, London. N2aPK1/2 cells were exposed to a 1×10^{-5} dilution of RML Mouse Scrapie for three days and propagated to confluence for three splits in order to dilute out the original RML Scrapie inoculum²⁵³. 25,000 cells of the RML infected lines were filtered onto the membranes of an ELISPOT plate in 10 replicates in parallel to two non-infected replicates to control for the signals recorded. These cells were subjected to lysis and subsequent proteinase K digestion and denaturation with guanidinium thiocyanate to eliminate PrP^C, in order that only PrP^{Sc} particles remain. Incubation with 0.6 µg/ml monoclonal PrP antibody, ICSM18 was followed by alkaline phosphatase-linked anti-mouse IgG1 antiserum detection of IgG1, thus allowing visualisation of PrP^{Sc}-positive cells upon reaction of the reporter alkaline phosphatase with alkaline phosphatase conjugate substrate (BioRad). These PrP^{Sc} positive cells were counted using the automated Zeiss KS ELISPOT system, which can readily resolve up to 3000 cells per well. The Scrapie Cell Assay was repeated three times to ensure reproducibility.

3 Identification of Hectd2 candidate substrates

3.1 The Yeast-Two-Hybrid Principle

The yeast-two-hybrid assay is a genetic technique, conceived by Fields and Song in 1989, to search for novel interactors to a protein of interest²⁵⁸. The concept was developed as an alternative approach to existing co-immunoprecipitation, co-fractionation and crosslinking methods to determine interactions but with the added advantage of immediate access to the cloned genes of the interacting proteins^{258, 259}. The Clontech Matchmaker™ Gold Yeast Two-Hybrid version of the assay was selected for screening, which utilises the modular property of the yeast transcriptional activator GAL4. The GAL4 transcription factor is a key regulator of galactose metabolism. GAL4 is comprised of an N-terminal DNA binding domain (BD) that is sufficient for nuclear localisation and recognises a specific upstream activating DNA sequence (UAS) and a C-terminal acidic domain, the activation domain (AD), which activates transcription of the downstream reporter genes by recruitment of RNA polymerase II^{258, 260}. The two components of this transcription factor are biologically functional without covalent linkage as proximity is sufficient to effectively activate GAL4 responsive genes²⁵⁸. This feature can be exploited to identify interactors of a known protein by expressing it in yeast as a hybrid to the GAL4 BD, whilst the unknown proteins that it may bind to are expressed as a second hybrid to the GAL4 AD. When proteins of the GAL4 AD hybrid bind to the known protein, the GAL4 transcription factor is reconstituted by bringing the two domains into close proximity by virtue of the protein-protein interaction. This activates four downstream reporter genes regulated by the GAL4 specific UAS (Figure 3.1.1). These are a combination of nutritional reporters, *HIS3* and *ADE2*, that permit growth in media auxotrophic for histidine and adenine, a drug reporter *AURI-C*, which confers resistance to the toxic drug aureobasidin A and a *MEL1* reporter which produces a blue colony phenotype in the presence the chromogenic substrate X- α -gal. Yeast harbouring these interactions are identified by this blue colony phenotype, permitting their isolation and subsequent sequence analyses to determine the identity of the interacting prey proteins.

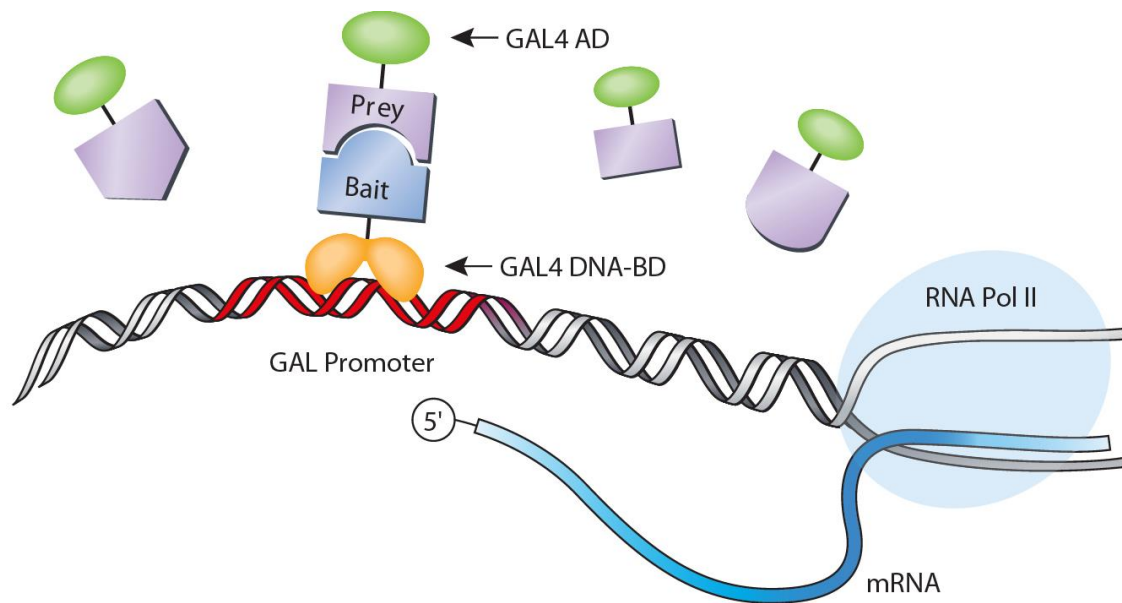


Figure 3.1.1 Principle of yeast-two-hybrid assay. A protein/domain of interest is expressed as a GAL4 DNA BD fusion protein that is screened against a library of unknown prey proteins, expressed as GAL4 AD fusions. When the bait protein interacts with a prey, the GAL4 BD and AD are brought into close proximity, sufficient for it to act as a functional transcription factor that activates the downstream reporter genes, indicating a two hybrid interaction. *Adapted from Clontech Matchmaker Yeast-Two-Hybrid manual*

3.2 Selection of bait constructs

Based on the existing knowledge of mammalian E3 ligases, the C-terminal domain bears the conserved HECT domain, and the N-terminal region is thought to contain the substrate binding domain¹⁶². This region has been identified as the primary determinant of substrate specificity for all known E3 ligases although other regions or specific residues of the protein cannot be ruled out as contact points in protein interactions^{162, 172}. Thus to delineate interactors of Hectd2, using the protein in its entirety would shed light on its *in vivo* binding partners. However a caveat to this is that the HECT domain is functionally distinct in executing the ligase catalytic activity, hence interactions defined through this region are anticipated as substrate non-specific. This may lead to detection of a large number of interactions that would make for labour and cost intensive downstream analyses. Thus to filter out HECT domain binding partners, it is necessary to confine substrate searching to a region of Hectd2 that excludes this domain. A sequence alignment search of the Hectd2 protein sequence (Appendix 3) using the NCBI Basic Local

Alignment Tool (BLAST), (<http://blast.ncbi.nlm.nih.gov/Blast.cgi>), allows a comparison to existing biological protein sequences in the non-redundant protein sequences mouse database. Analysis of the protein sequence located the HECT domain at the C-terminal at residues 415 - 774 (Figure 3.2.1 a). The N-terminal region containing the preceding 414 amino acids represents the region within which the putative substrate binding domain lies, which is referred to as Hect414 henceforth. To avert capture of proteins that bind the HECT domain rather than the putative substrate binding domain, the HECT domain was omitted from Hectd2. Thus, the Hect414 region was selected for yeast two-hybrid screening to ensure that only proteins that bind to the substrate specific region of Hectd2 are drawn from the screen.

The yeast two-hybrid system was exploited to further characterise Hectd2 in an attempt to map the region within the N-terminal sequence to which substrates bind. This binding region may span the entire length of the N-terminal domain or a section of sequence that is sufficient for binding. A series of C-terminal deletion mutants were selected using a systematic approach via BLAST search analysis to identify unique regions that showed no or low homology to other proteins. Such regions may be indicative of unique domain(s) or contact points specific to Hectd2 substrate binding. BLAST search of Hectd2 against the NCBI mouse protein database identified a number of matches of which a subset are depicted schematically in Figure 3.2.1 a. The matches were to a number of other E3 ubiquitin ligases that also contained the HECT domain. This homology alignment revealed distinct regions to which there appeared to be no homologous matches (Figure 3.2.1 a). These regions span 180 residues and 330 residues from the N-terminus (Figure 3.2.1 a, b), and may determine the specificity of Hectd2 for its substrates. These regions were termed Hect180 and Hect330, respectively and were used to screen the candidate pool generated from library screening with Hect414. In this way it may be possible to determine the point at which interaction is abrogated, thus mapping the region of Hectd2 that is important in binding its substrates.

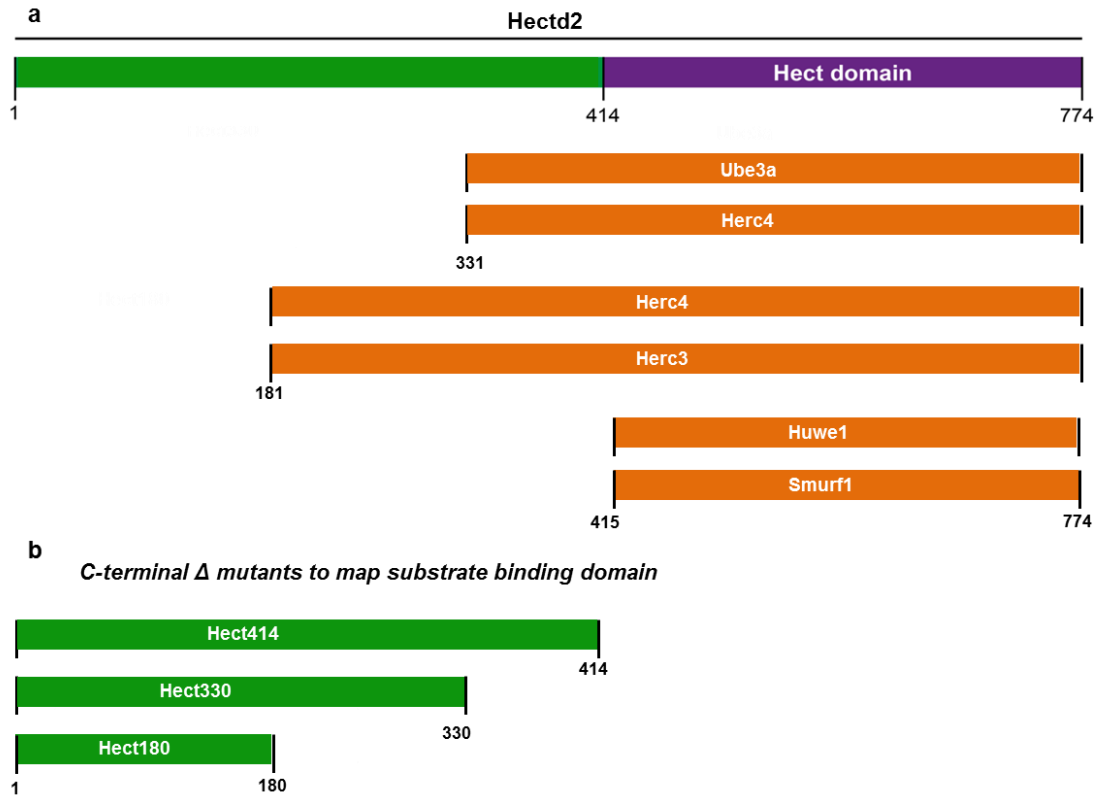


Figure 3.2.1 Sequence analysis of Hectd2. a) BLAST search analysis against the NCBI non-redundant mouse protein database identified the C-terminal HECT domain from residue 415 to 774 and the N-terminal putative substrate binding domain, 414 amino acids in length. A subset of the hits to which homology was identified are shown. Residues 1-180 from the N-terminus were not found to have sequence homology to any known proteins and residues 180-330 showed some homology to known proteins. b) This suggests that Hect180 and Hect330 may represent regions in which there are unique domains for substrate binding. Thus Hect180 and Hect330 regions were selected as deletion mutants to map Hectd2 substrate binding.

3.3 Designing the Hectd2 bait constructs

The pGBKT7 vector was selected for constructing hybrid proteins as it can express the protein of interest as a C-terminal fusion to amino acids 1-147 of the GAL4 DNA BD. The cloning strategy used consisted of a series of steps, depicted in Figure 3.3.1. This was initiated by PCR amplification of the Hect414, Hect330 and Hect180 sequences onto which unique restriction sites were incorporated into the primers to facilitate cloning into the destination vector, pGBKT7. Choice of restriction site was made according to those that were available in the multiple cloning site, (MCS) of pGBKT7 (Appendix 2).

Absence of the restriction site from the insert sequence and vector sequences outside the MCS were required to avert digestion with the appropriate enzyme in subsequent steps.

PCR amplification of each insert sequence was performed using a pre-existing cDNA clone of *Hectd2* as a template (*Hectd2*-TOPO, in the pCR[®]-Blunt II-TOPO vector). *NcoI* sites were engineered in at the 5' ends of *Hect414*, -330 and -180 sequences using oligonucleotide primers that were designed to prime the insert sequence from the 5' end where the primer is preceded by an *NcoI* site (Section 2). The 3' ends of the insert sequences had *PstI* sites engineered in using primers that were complementary to the end of each sequence, succeeded by a *PstI* site. The 3' primers were inclusive of a stop codon to mark the end of each insert sequence to ensure that only fragments of the required sizes are translated precisely. Base pair insertions were made where necessary to maintain the sequences in frame with the GAL4 BD tag and thus the translational integrity of the fusion protein, as depicted in Figure 3.3.2.

These modified PCR products were cloned initially into the shuttle vector, pCR[®]-Blunt II-TOPO, in order to generate a high yield of good quality insert sequences harbouring the correct restriction ends. The insert sequences were then digested from the TOPO vectors prior to transfer to the pGBKT7 destination vector via ligation of overhanging ends generated by *NcoI/PstI* digestion. The resultant clones were screened by PCR using primers complementary to the 5' and 3' ends of the pGBKT7 backbone flanking the DNA insert and inclusive of a 126 and 167 bp region of the vector either side of the MCS, respectively (Section 2). Size resolution of the PCR products by agarose gel electrophoresis identified positives for *Hect414*, -330, and -180, consistent with the appropriate size (Table 3.3.1). The corresponding clones were cultured and purified according to Section 2. Restriction digestion with *NcoI* and *PstI*, confirmed insert sizes reflecting *Hect414*, -330 and -180 (Figure 3.3.3). These constructs were verified by sequencing for accuracy and integrity of the GAL4 BD fusion junction.

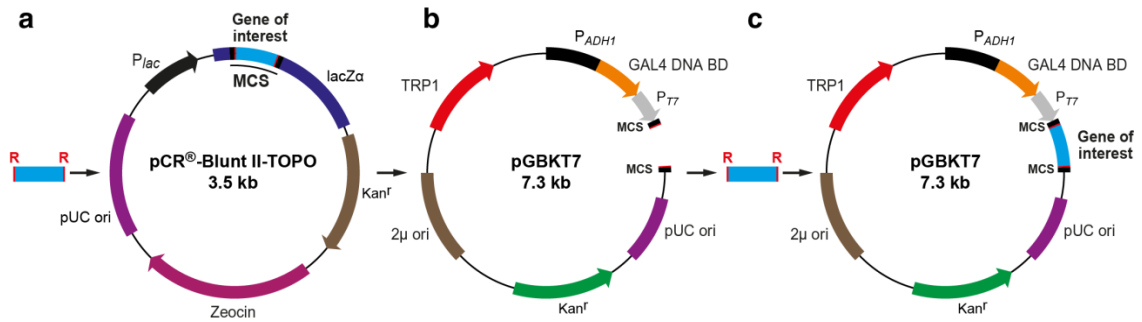


Figure 3.3.1 Cloning strategy for construction of bait plasmids. a) Hect414, Hect330 and Hect180 sequences were PCR amplified using primers designed to span the required region and engineer in restriction sites, which were blunt cloned into the pCRII-Blunt-TOPO vector. b) The destination vector, pGBKT7, was linearised using the cognate restriction enzymes and dephosphorylated to prevent re-ligation. The DNA inserts were prepared from the TOPO plasmids for subsequent ligation into linearised pGBKT7 (c).

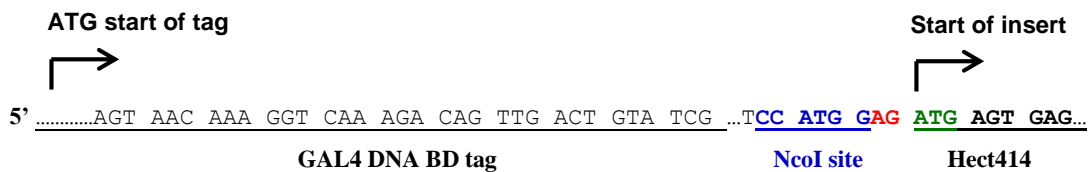


Figure 3.3.2 Construction of the GAL4 BD tagged fusion proteins. The translation frame of the fusion construct for the cloning of Hect414, -330 or -180 into pGBKT7. Hect414, -330 or -180 insert sequences with their ATG site were maintained in frame with the GAL4 BD by PCR amplification using primers that engineer in a 2 base pair insertion indicated in red, preceded by an *NcoI* site, for transfer between vectors.

Table 3.3.1 Molecular weight of Hectd2 fragments

Gene	Hectd2 DNA insert (bp)	Hectd2/GAL4 BD fusion (kDa)
Hect414	1232	67
Hect330	990	57
Hect180	540	40

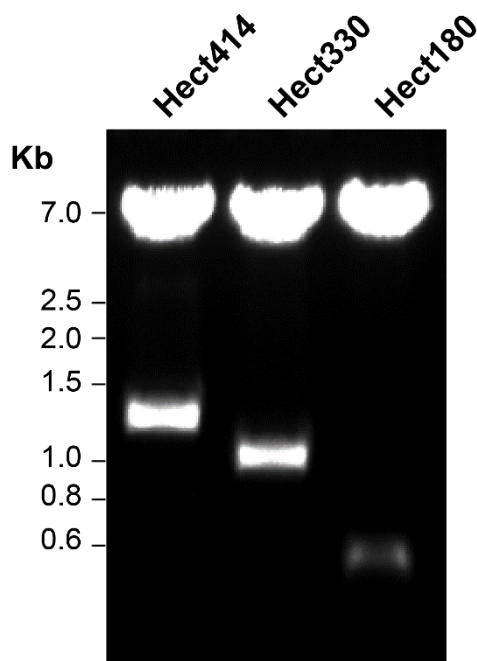


Figure 3.3.3 Insert release from GAL4 BD fusion constructs. To verify that the bait plasmids contain the appropriate inserts, restriction digestion was performed with *NcoI* and *PstI* for pGBKT7·Hect414, pGBKT7·Hect330 and pGBKT7·Hect180. The expected insert sizes of 1.2 kb, 990 bp and 540 bp were observed in addition to the liberated pGBKT7 at 7.3 kb.

3.4 Pre-screening preparation of Hectd2 fusion constructs

Expression in yeast

Prior to use, it is important to ascertain that pGBKT7·Hect414, pGBKT7·Hect330 and pGBKT7·Hect180 constructs are expressed as fusion proteins to the GAL4 BD in yeast. The *S. cerevisiae* strain, Y2HGold, was used to express each BD·bait protein by transforming each clone independently in parallel to a negative control, untransformed Y2HGold. Protein extracts for the fusions to be tested and control were generated by yeast lysis methods (Section 2). Size resolution by SDS PAGE/Western blotting is shown in Figure 3.4.1, where bands of the expected molecular weights were observed for BD·Hect414, BD·Hect330 and BD·Hect180. The band for BD·Hect414 runs slightly lower than the 67 kDa predicted for it, which may be accounted for by the differences that

lie between calculated molecular weights and the actual migration profile. Furthermore, pre-stained molecular weight markers may migrate slightly differently to those that are predicted because proteins used in the marker have covalently attached dye molecules. Thus pre-stained standards determine the approximate molecular weight of a protein but are by no means an accurate prediction of the molecular weight. BD·Hect330 and BD·Hect180 show expression correlating to their expected sizes of 57 and 40 kDa. The untransformed Y2HGold showed no bands as anticipated, indicating that the bands observed for the fusion proteins reflect that of Hect414, -330 and -180.

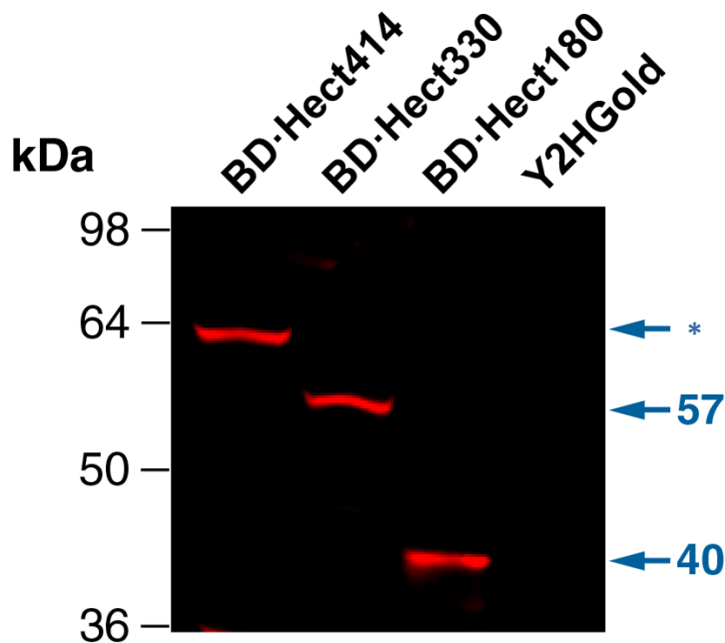


Figure 3.4.1 Expression of Hectd2 bait proteins. Western blot analysis of Y2HGold protein extracts of GAL4 BD fusions to Hect414, Hect330 and Hect180, electrophoresed on a 10% polyacrylamide gel. Fusion proteins were detected using anti-c-MYC mouse monoclonal antibody which binds to the MYC tag that is expressed in frame with the GAL BD. BD·Hect414, BD·Hect330 and BD·Hect180 expressed at their expected molecular weights while untransformed Y2HGold shows an absence of these bands. The asterisk represents the band for BD·Hect414, which shows a migration profile that is slightly lower than its predicted molecular weight of 67 kDa.

Toxicity testing

It is possible that the bait fusion proteins may be toxic to the yeast cells precluding any downstream analyses. If expression of the fusion proteins produces toxic effects in yeast, then impaired growth of solid and liquid cultures may be observed by the number of colonies and their sizes, which would be fewer and/or appear distinctly smaller relative to those formed for control colonies. pGBKT7·Hect414, pGBKT7·Hect330 and pGBKT7·Hect180 were transformed into Y2HGold cells under standard conditions in parallel to the transformation of pGBKT7 vector only control, (Section 2). The transformants were plated onto SD/-Trp media, which selects for the pGBKT7 plasmid by virtue of its *TRP* gene, permissive of growth on media auxotrophic for tryptophan. Following a three day growth period, 418 colonies of an average of ~2 mm in size emerged for the empty vector, pGBKT7, which expresses the BD only. Colonies expressing BD·Hect414, BD·Hect330 or BD·Hect180 formed 412, 253 and 389 colonies respectively, grown to a size circa 2 mm (Figure 3.4.2). It is possible that the BD·Hect330 or BD·Hect180 fusions may be inhibiting growth, however they appear to grow well and thus this does not preclude their use in downstream analyses (Figure 3.4.2).

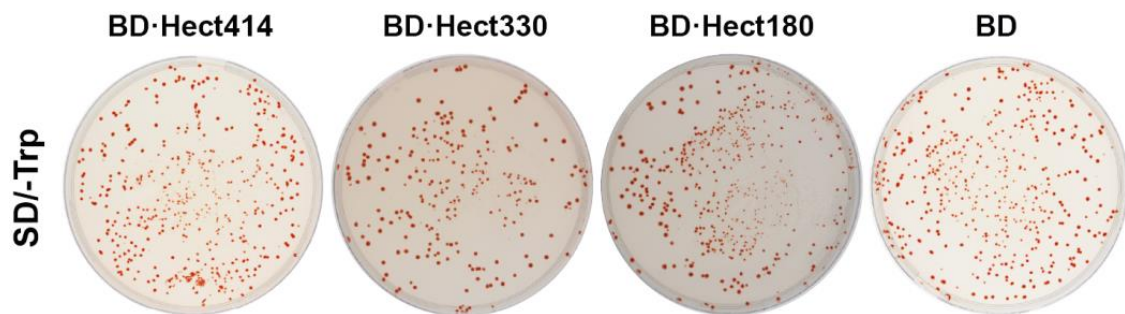


Figure 3.4.2 Toxicity testing of bait proteins. Hect414, Hect330 and Hect180 fusion proteins to the BD were expressed in Y2Hgold cells and plated onto SD/-Trp media that selects for the bait plasmids. The resulting colony sizes were compared to those formed from transformation of an empty bait plasmid, pGBKT7, which expresses the BD only. Y2HGold colonies were ~2mm in size for those expressing the BD only control and also for BD·Hect414, BD·Hect330 or BD·Hect180. The red pigmentation of some colonies reflects the accumulation of a purine precursor that results from low concentrations of adenine in the medium.

Investigating the autoactivity of bait proteins

In order for the yeast-two-hybrid screen to be valid, the bait fusion proteins must not autonomously transactivate the downstream reporter genes. Such an event would hinder the possibility of finding candidate interactors because the downstream reporter genes would always be activated in the presence of only the bait protein. The GAL4 BD·bait constructs were transformed into Y2Hgold cells and plated onto SD/-Trp, SD/-Trp/X and SD/-Trp/X/A selection media. X and A are abbreviations for X- α -gal and aureobasidin A, which are selective for yeast that can activate the *MEL1* and *AURI-C* reporter genes, respectively. *MEL1* encodes α -galactosidase which confers the blue colony phenotype in the presence of the chromogenic substrate X- α -gal. The *AURI-C* gene encodes a dominant mutant form of inositol phosphoryl ceramide synthase that is expressed upon two-hybrid interaction of a bait and prey. This in turn confers resistance to media containing the toxic antibiotic aureobasidin A, permitting growth of yeast that harbour bait-prey interactions. Thus SD/-Trp selects for the bait plasmid, indicative of successful transformation, SD/-Trp/X selects for the bait plasmid and for activation of the *MEL1* reporter and SD/-Trp/X/A selects for the bait plasmid in addition to activation of the GAL4 controlled reporter genes, *MEL1* and *AURI-C*. BD·Hect414, BD·Hect330 and BD·Hect180 fusion proteins did not autoactivate reporter gene expression suggesting that the bait-prey hybrid is necessary for reporter gene activation (Figure 3.4.3).

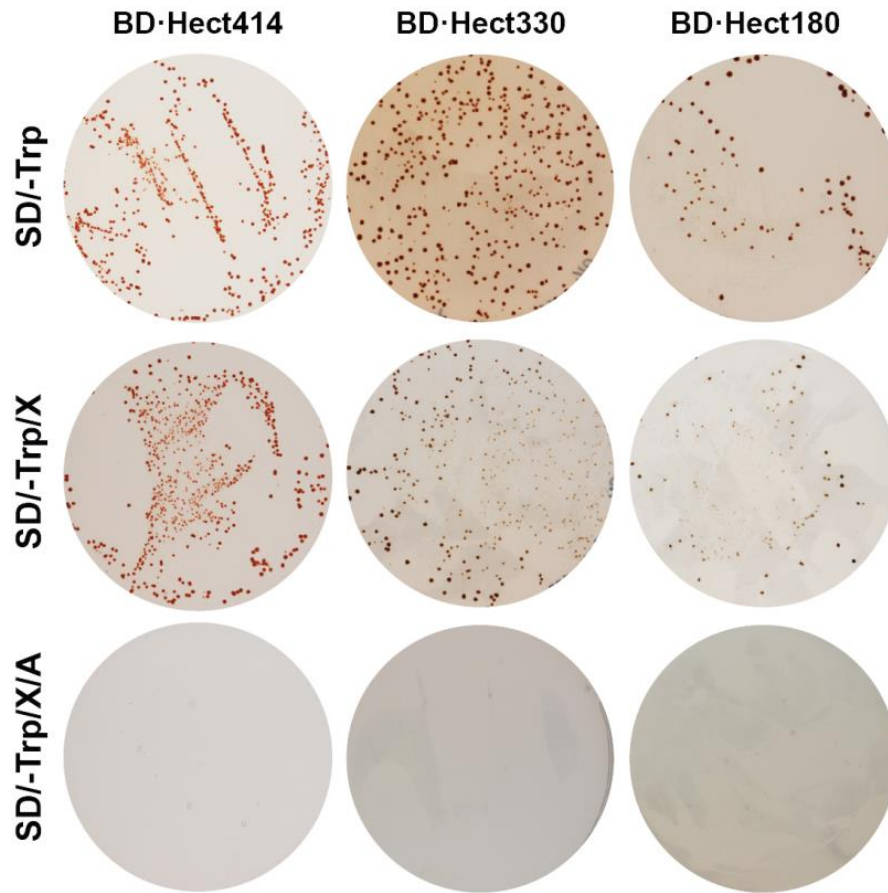


Figure 3.4.3 Testing for autoactivation of Hectd2 bait proteins. Y2HGold cells were transformed with pGBKT7·Hect414, pGBKT7·Hect330 and pGBKT7·Hect180 and plated onto SD/-Trp, SD/-Trp/X and SD/-Trp/X/A. Y2HGold expressing each of these constructs grew on SD/-Trp and SD/-Trp/X plates, which select for the tryptophan biosynthesis gene carried on the bait plasmids. Colonies that grew on SD/-Trp/X were not blue indicating that the bait fusion proteins do not autoactivate the *MEL1* gene. SD/-Trp/X/A selects for two-hybrid interactions, growth on which is indicative of autonomous activation of reporter genes. BD·Hect414, BD·Hect330 and BD·Hect180 fusion proteins do not autoactivate the downstream reporter genes in the absence of the GAL4 AD.

3.5 The library screen using the yeast two-hybrid system

The library of unknown proteins

In order to fish for possible prey interactors that bind to the bait, the Clontech Normalised Universal mouse library was used (Section 2). This is composed of pre-transformed prey plasmids, constructed from fragments of cDNA inserts fused to the GAL4 activation domain of pGADT7-recAB plasmid so that a functional fusion protein is expressed. These prey plasmids were pre-transformed in the haploid Y187 strain such that the prey library can be readily mated to the haploid Y2HGold strain in which the bait proteins are expressed.

The library screen

A concentrated culture of the bait strain, Y2HGold expressing BD·Hect414, was prepared in SD/-Trp broth (Figure 3.5.1, Section 2). This was grown to an OD₆₀₀ of 0.8, a marker of concentrated growth, wherein high level expression of the bait protein is anticipated by virtue of the *ADHI* promoter having its highest activity in the exponential phase of the yeast growth curve²⁶¹. The bait culture was combined with the Clontech Mouse Normalised Universal library which was pre-transformed in the Y187 strain and allowed to mate. The library titre was ascertained by plating onto SD/-Leu agar, which selects for the pGADT7-recAB plasmids into which the library was cloned, by virtue of its *LEU* gene, permissive of growth on media auxotrophic for leucine. The titre was determined by calculating the number of colonies as a function of the dilution factor and the volume plated (Section 2). This amounted to $>2 \times 10^7$ cfu/ml, where cfu represents the number of colony forming units, which is an estimate of the number of Y187 cells containing prey plasmids. The greater the number of cells there are, the greater the number of potential matings between bait- and prey-containing haploids, thereby increasing the possibility of identifying two-hybrid interactions.

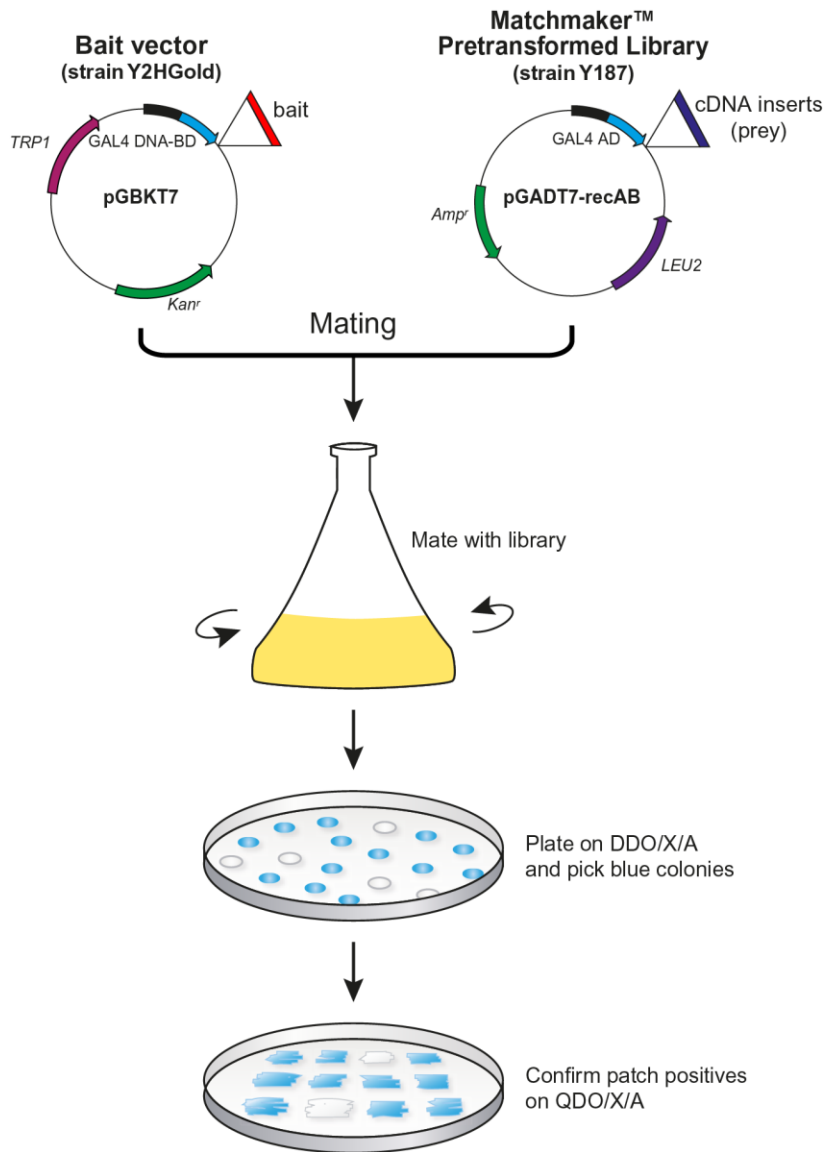


Figure 3.5.1 Library screening workflow. Following transformation of bait plasmid into Y2HGold, a concentrated culture of the bait strain was prepared by shaking at 30°C overnight. This is mated to the prey library strain, overnight by shaking at 45 rpm at 30°C. The clone pool was plated onto low stringency double dropout media auxotrophic for tryptophan and leucine and supplemented with X- α -gal and aureobasidin A (abbreviated to DDO/X/A). This allows detection of all possible interactions prior to high stringency confirmation on quadruple dropout media, (QDO/X/A), which is the same as DDO/X/A media except that it is additionally auxotrophic for histidine and adenine. This confers growth selection of two hybrid interactions that activate all four reporter genes, which are detected by virtue by the blue colony phenotype upon activation of the *MEL1* reporter *Adapted from Clontech Matchmaker™ Yeast-Two-Hybrid manual*

Mating of the haploid strains of yeast results in the budding of diploid daughter cells in which it is expected that the bait and a prey plasmid have been propagated (Section 2). The resultant clone pool was plated onto the low stringency SD/-Trp/-Leu/X/A agar, (termed DDO/X/A, where DDO is double dropout), deficient in the essential amino acids tryptophan and leucine. This double dropout media was supplemented with X- α -Gal and aureobasidin A in order to capture as many interactions as possible. Yeast expressing both the bait and prey plasmids were selected for by means of their tryptophan or leucine biosynthesis genes harboured by the bait or prey plasmids respectively. Two-hybrid interactions were detected by selective activation of these genes as well as *MEL1/AURI-C* reporter expression.

To ensure that the cells containing bait and prey proteins were growing on the media and for subsequent calculation of the number of colonies screened, the culture was also plated onto SD/-Trp, SD/-Leu and SD/-Trp/-Leu agar plates for selection of the bait or prey or both bait and prey plasmids, respectively. The mating efficiency was determined by calculating the viability of diploids as a function of the viability of the rate limiting partner, which was the prey library. Viabilities were measured by the number of cfu/ml of diploids, of the bait or the prey on the appropriate selective media, i.e. SD/-Trp, SD/-Leu, or SD/-Trp/-Leu, respectively. This totalled to 17%, indicating that the mating occurred at a low frequency, thereby reducing the number of viable diploids that can be screened. The number of screened clones was calculated from the product of the number of colony forming units/ml on DDO plates and the volume that the diploids were suspended in, where 32 colonies grew after plating 100 μ l of a 1/1000 dilution of an 11.5 ml suspension of the mated culture. This amounted to 3.68×10^6 independent clones, thus surpassing the threshold for that which provides a representative pool of diploids, that are each likely to harbour a bait and prey plasmid i.e. 1×10^6 (Clontech Matchmaker™ Gold Yeast Two-Hybrid System User Manual). Of these clones, there were 36 true blue colonies and 94 colonies of a paler blue form that could represent potential interactions. All of these colonies were picked and subject to verification by further analyses.

High stringency confirmation of positives

The positives identified from the library screen were subjected to a higher stringency selection screen by transferring the 130 colonies from DDO/X/A selection to a quadruple dropout media formulation that has additional levels of discrimination (Appendix 1, Figure 3.5.2). These high stringency plates (QDO/X/A) are so called as they additionally select for the activation of *HIS3* and *ADE2* reporter genes in addition to *MEL1* and *AUR1-C*. Each of the blue positive colonies were picked from the DDO/X/A plates and patched onto QDO/X/A plates for growth over three days, shown in Figure 3.5.2 for a subset of the library positives. This transferral to QDO/X/A sustained the 36 true blue positives but the 94 colonies with a pale blue phenotype were observed as white colonies, thus eliminating them from subsequent analyses (Figure 3.5.2).

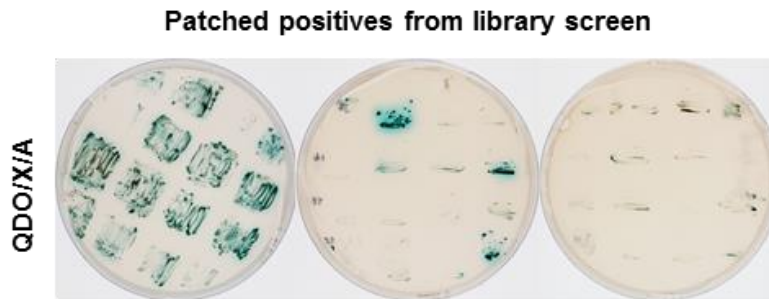


Figure 3.5.2 High stringency selection of library positives. The N-terminal domain of Hectd2, Hect414, was used to screen a Universal Mouse Normalised Library for binding proteins. 36 true blue colonies and 94 pale blue colonies were patched onto high stringency QDO/X/A plates, shown here for a representative group of the library positives. QDO/X/A plates are auxotrophic for histidine, adenine, leucine and tryptophan, supplemented with X- α -Gal and aureobasidin A, to select for all four reporter genes. 36 positives conferred growth on transfer to QDO/X/A, shown here for a subset, whilst the 94 pale blue colonies failed to sustain growth on this high stringency screen.

Yeast have the capacity to uptake multiple plasmids, which introduces a level of uncertainty as to whether the blue positive colonies contain more than one prey. It is thus necessary to isolate each clone in order to capture the prey plasmid that is responsible for a given two-hybrid interaction and to separate it from any mixed colony populations.

Attempts to delineate each of the library positives by serial single streaking of each colony resulted in a mixture of blue and white colonies. This, in effect, segregated the interactors from the non-interacting prey proteins by means of their ability to activate the reporter genes on QDO/X/A media. From these, one prey candidate was not sustained on the high stringency media, leaving 35 prey candidates to be carried forward.

Positive interactions that confer growth on QDO/X/A may represent the same interactor although the normalisation of the library prey proteins significantly reduces this possibility. Putative duplicate clones were eliminated by performing a yeast colony PCR using the Matchmaker Insert Check PCR Mix 2, which allows the specific amplification of the prey insert (Section 2). PCR amplification showed that all 35 of the potential positives harboured cDNA inserts of varying sizes with some inserts showing PCR products of similar size, suggestive that 8 of the clones may be duplicates (Figure 3.5.3). The amplified cDNA inserts were end-sequenced from which partial sequences for each clone were obtained. It was apparent that there were indeed 5 duplicates; clone 12 is a duplicate of clone 2, clones 13 and 23 are duplicates of clone 4 and clones 24 and 29 are duplicates of clone 21. Such identification of multiple copies of a cDNA insert strengthens the likelihood that these clones are true positives. This elimination of duplicates resulted in 30 unique clones that were taken forward for prey plasmid isolation.

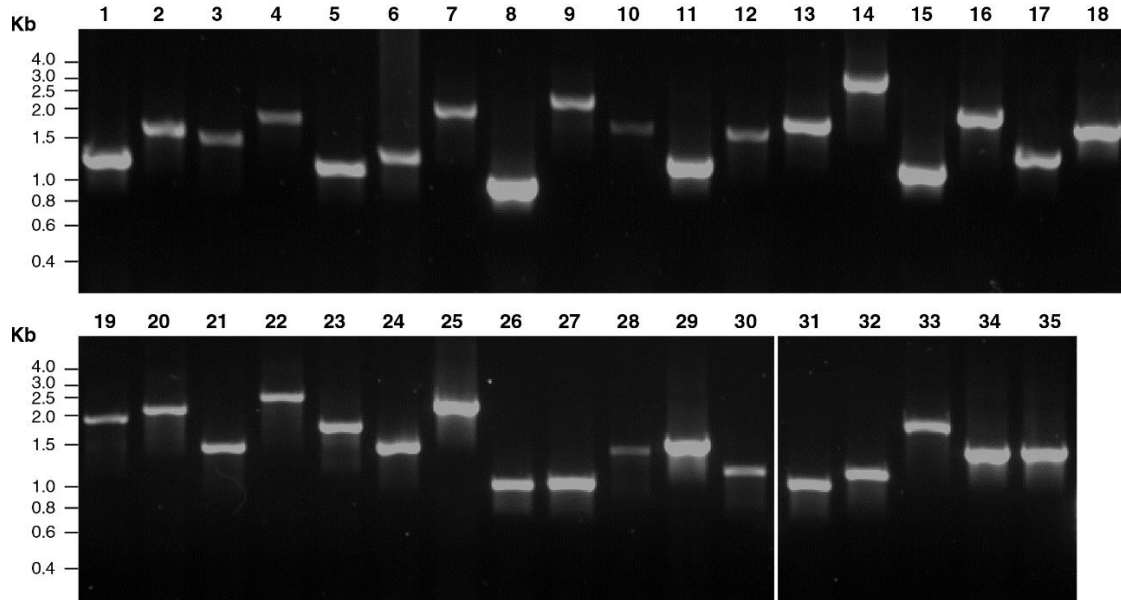


Figure 3.5.3 Prey plasmids insert screening. Inserts of pGADT7 plasmids were amplified using yeast colony PCR and size resolved by electrophoresis on a 1% agarose gel. All 35 positives that grew on high stringency QDO/X/A showed single inserts, indicating each pGADT7 contained one prey insert, although this does not eliminate the possibility of two prey inserts of the same size within the same cell. Similar sized bands may represent duplicate clones, which can be verified by sequence analyses.

Thirty prey plasmids were rescued from their respective yeast colonies using the Easy Yeast Plasmid Isolation Kit, which generates a DNA preparation of both bait and cognate prey plasmids for a given clone (Section 2). To retrieve only the prey plasmid, each clone was transformed into *E. coli* and plated onto ampicillin-containing media, which specifically selects for transformants bearing the prey and not the bait plasmid, by virtue of its ampicillin resistance gene. Four of these clones were cultured and purified for each prey in order to establish whether the prey inserts for a given clone were the same (Section 2). The cDNA inserts were PCR screened using primers complementary to the 5' and 3' ends of the vector backbone flanking the MCS into which the inserts were cloned (Section 2). Size resolution of the PCR products by agarose gel electrophoresis identified that each set of four clones harboured an insert of equal size. This indicates the identical nature of each prey plasmid, suggesting that one prey plasmid per clone have been captured, in concurrence with the sizes identified in the initial yeast colony PCR (Figure 3.5.3).

3.6 Candidate interactors

For each prey plasmid, one clone was selected from the set of four for sequencing. Full length sequence was obtained for all the prey inserts using a primer walking strategy to sequentially sequence the entire length of each insert (Appendix 3). The sequence generated was analysed at the GAL4 AD-insert junction to ensure that the prey cDNA is expressed in frame with the GAL4 AD tag. This confirms that activation of reporter genes are the result of two-hybrid interactions between a correctly expressed GAL4 AD-prey fusion and BD-bait fusion. A BLAST search was performed against the NCBI mouse genomic and transcript database to identify the interactors by sequence similarity (Table 3.6.1). As the prey plasmids were generated from fragments of cDNA of a given gene, the proportion of the expressed full length protein is given to indicate the size of the prey protein expressed from the pGADT7 plasmids (Table 3.6.1). However for one candidate, *Nt5dc3*, the cDNA was a match to the 3' UTR rather than the coding section. This candidate was later found to be a false positive, described in Section 3.7, thereby providing confidence in the screening methods applied. The cDNA sequence for one candidate, *Nrp1*, was not in frame with the GAL4 AD and thus expressing a spurious protein. BLAST search analysis of this spurious protein did not identify any matches to any known proteins in the NCBI mouse protein database. For one of the candidates, the prey cDNA was identified as a match to the genomic region on chromosome 15, position 832157 – 832830 as an mRNA transcript is not available. This resulted in a total of 27 novel candidate binding partners of Hectd2 (Table 3.6.1).

Table 3.6.1 Candidate genes and proportional match to full length protein

Candidate gene by homology	% of full length protein	Reporter gene activation
<i>Klhdc2</i> (Kelch domain containing 2)	73	✓
<i>Sh3glb1</i> (SH3-domain GRB2-like B1 (endophilin))	89	✓
<i>Pbld</i> (Phenazine biosynthesis-like protein domain containing),	80	✓
<i>Cpe</i> (Carboxypeptidase E)	61	autoactivates
<i>Pacsin2</i> (Protein kinase C and casein kinase substrate in neurons 2)	39	✓
<i>Crtac1</i> (Cartilage acidic protein 1)	22	✓
<i>Stambp</i> (Stam binding protein)	72	✓
<i>Zbed4</i> (Zinc finger, BED domain containing 4)	16	✓
<i>Pcca</i> (Propionyl-Coenzyme A carboxylase, alpha polypeptide)	48	autoactivates
<i>Catsperb</i> (Catsper channel auxiliary subunit beta)	22	autoactivates
<i>Vps13d</i> (Vacuolar protein sorting 13 D)	11	autoactivates
<i>Cop9</i> (Constitutive photomorphogenic) homolog, subunit 4)	100	✓
<i>Pcnx14</i> (Pecanex-like 4)	12	✓
<i>Sept7</i> (Septin 7)	26	✓
<i>Stmn2</i> (Stathmin-like 2)	100	✓
<i>Gvin1</i> (GTPase, very large interferon inducible 1)	11	✓
<i>Ppp2ca</i> (Protein phosphatase 2 catalytic subunit alpha isoform)	62	✓
<i>Stk16</i> (Serine/threonine kinase 16)	67	✓
<i>Rbm39</i> (RNA binding motif protein 39)	67	autoactivates
<i>Sh3yl1</i> (Sh3 domain YSC-like 1)	67	✓
<i>Mfsd6</i> (Major facilitator superfamily domain containing 6)	17	✓
<i>Strn3</i> (Striatin, calmodulin binding protein 3)	31	✓
<i>LOC100046859</i>	20	✓
<i>HtrA2</i> (Serine peptidase 2)	26	autoactivates
<i>Ces3</i> (Carboxylesterase 3)	40	✓
<i>Gbl</i> (G protein beta subunit-like)	89	✓
<i>Atp6v1h</i> (ATPase, H ⁺ transporting, lysosomal V1 subunit H)	51	autoactivates

3.7 Co-transformational confirmation of interactions in yeast

Although the incidence of false positives have been reduced by the high stringency screen, it remains a possibility that a prey protein may not interact with the BD·Hect414 in a direct interaction assay or it might be that what appears to be an interaction may be autonomous activation of reporter genes by the prey. This was addressed by independently co-transforming each prey plasmid with pGBKT7·Hect414 or the empty vector, pGBKT7 into competent Y2HGold cells (Section 2). The transformants were plated onto QDO/X/A and DDO/X agar, the former to select for two hybrid interactions and the latter to serve as a control for successful co-transformations. This is important to ensure that detection of two-hybrid interactions are not limited by the number of yeast cells expressing the bait and prey plasmids.

True interactions between bait and a prey are expected to show growth on both low stringency selection, DDO/X, and on high stringency QDO/X/A but no growth when the prey/empty vector combinations are plated onto QDO/X/A. If prey/empty vector combinations show growth on QDO/X/A plates, this would indicate that the prey activates the reporter genes in the absence of the BD·Hect414. All colonies harbouring prey/bait or prey/empty-vector combinations showed growth on DDO/X media, as expected, but only 20 of the prey/bait combinations showed growth on QDO/X/A media, supported by an absence of growth for the equivalent prey/empty-vector combination on this higher stringency selection (Table 3.6.1, Figure 3.7.1). This indicates that the presence of BD·Hect414 is necessary and definitive for a two-hybrid interaction, as reporter gene expression is abrogated in its absence. 7 of the prey proteins were identified as autoactivators of the downstream reporter genes as both prey/bait and prey/empty-vector co-transformations resulted in colony growth on QDO/X/A. The growth discrepancy observed between DDO/X and QDO/X/A media is expected owing to the stress imposed on Y2HGold by the toxicity of aureobasidin A (Clontech Matchmaker™ Gold Yeast Two-Hybrid System User Manual). Figure 3.7.1 shows a representative set of co-transformations, which shows that candidates Sh3glb1, Stmn2, Pacsin2, Stambp and Sept7 bind to Hect414. An example of an autoactivating prey is shown, where Htra2-

expressing yeast activate reporter gene expression in the absence of BD·Hect414 (Figure 3.7.1).

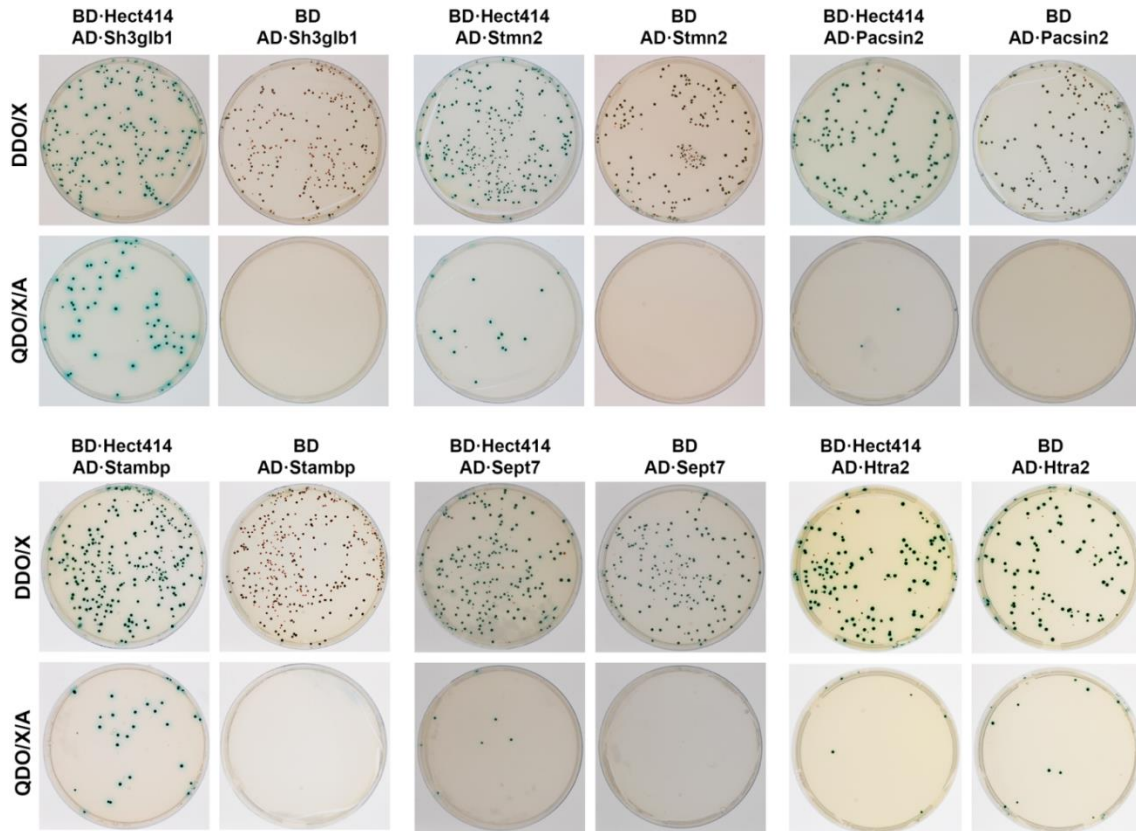


Figure 3.7.1 Representative set of Hect414/prey interactions confirmed in yeast. Positives were confirmed by co-transformation of the Hect414 bait and each of the 27 prey interactors in yeast independently. Cultures were plated out onto high stringency QDO/X/A plates, which selects for all 4 markers representative of a two-hybrid interaction and also on DDO/X plates that select for the presence of both bait and prey plasmids and activation of the *MEL1* reporter gene. Prey plasmids were also tested for autoactivity to check that downstream reporter genes were not activated in the absence of the bait. This was done by co-transforming each prey plasmid with the empty vector, pGBKT7. Successful interacting proteins included Sh3glb1, Pacsin2, Stamp, Sept7 and Stmn2, which only activate in the presence of BD·Hect414 and not BD on its own. In contrast, Htra2 is an autoactivator, whereby growth is seen on QDO/X/A in both the presence and absence of BD·Hect414.

3.8 Mapping the region of Hectd2-substrate binding

Protein interactions are mediated by points of contact with specific amino acid residues that form binding pockets and it is these regions that are important in understanding the molecular mechanism by which a given protein performs its functions. The yeast two-hybrid system was manipulated to provide an insight into mapping the location of Hectd2 substrate binding by using two C-terminal deletion mutants that overlap within the N terminal putative substrate binding region (Figure 3.2.1). Mapping of Hectd2 binding was investigated by testing whether the deletion mutants, Hect330 and Hect180 maintain interaction with the prey proteins that were identified as interactors of Hect414. If each of the prey proteins retained interaction with either Hect330 and/or Hect180, this would highlight the region of the Hectd2 sequence that is important for substrate binding (Figure 3.2.1.).

The Hect330 deletion mutant was co-transformed with each of the 20 positives and plated onto DDO/X and QDO/X/A plates. Only 4 prey clones conferred growth on the high stringency QDO/X/A plates, indicative of a positive interaction with Hect330. This suggests that Hect330 contains a component of the substrate binding domain that is sufficient for the binding of some substrates. (Figure 3.8.1, Figure 3.8.2, Table 3.8.1). These positive interactors were Sh3glb1, Zbed4, Sh3yl1 and LOC100046859. The screen was then repeated for the Hect180 deletion mutant for which there appeared to be no growth on the QDO/X/A plates with any clones (Table 3.8.1). This indicates that the interaction is abrogated with the Hect180 construct, suggesting that the 234 residues upstream of Hect180 are important for the binding of substrates (Figure 3.8.2). Taken together, the data suggests that residues 331-414 of Hect414/N-terminal domain are critical for the binding of the majority of Hectd2 substrates although this region is dispensable for interaction with Sh3glb1, Zbed4, Sh3yl1 and LOC100046859 (Figure 3.8.1, Figure 3.8.2). It is postulated that residues 181-414 forms an integral component of the Hectd2 substrate binding domain (Figure 3.8.2). This region may comprise of multiple binding domains that are substrate-specific or contains key contact points that form binding pockets that are sufficient for protein interactions.

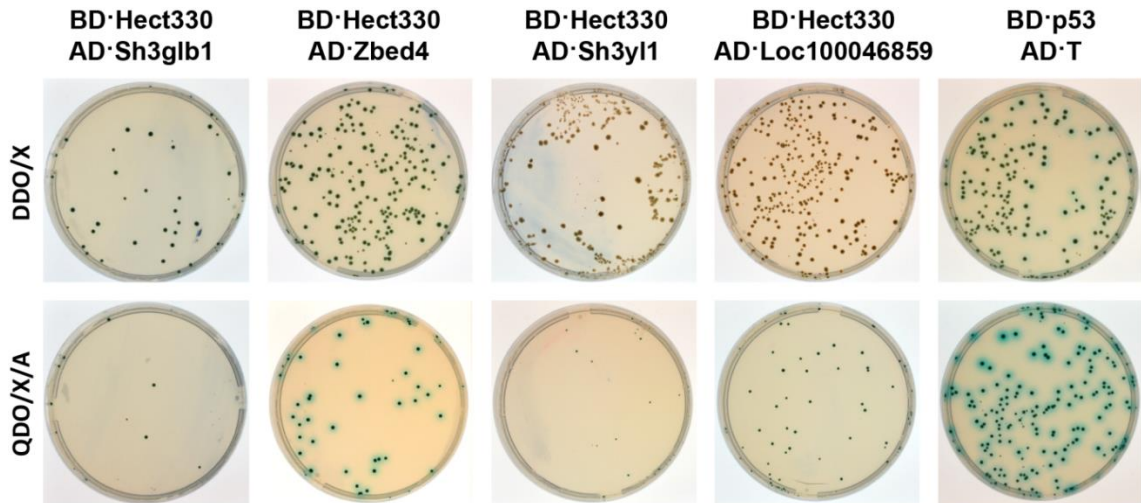


Figure 3.8.1 Locating the region of Hectd2-prey interaction. Each prey plasmid was co-transformed with Hect330 and Hect180 bait plasmids independently into yeast. Only four potential interactors showed binding to Hect330 and none showed binding to Hect180. This suggests that residues 331-414 of Hectd2 serve an indispensable role in forming the contact points for interaction of many of the prey binding partners, although Hect330 is sufficient for binding Sh3glb1, Zbed4, Sh3yl1 and Loc100046859. p53 was co-transformed with large T antigen for positive control testing which conferred the growth of blue colonies across DDO/X and QDO/X/A plates, indicative of successful co-transformations and appropriate activation of the reporter genes.

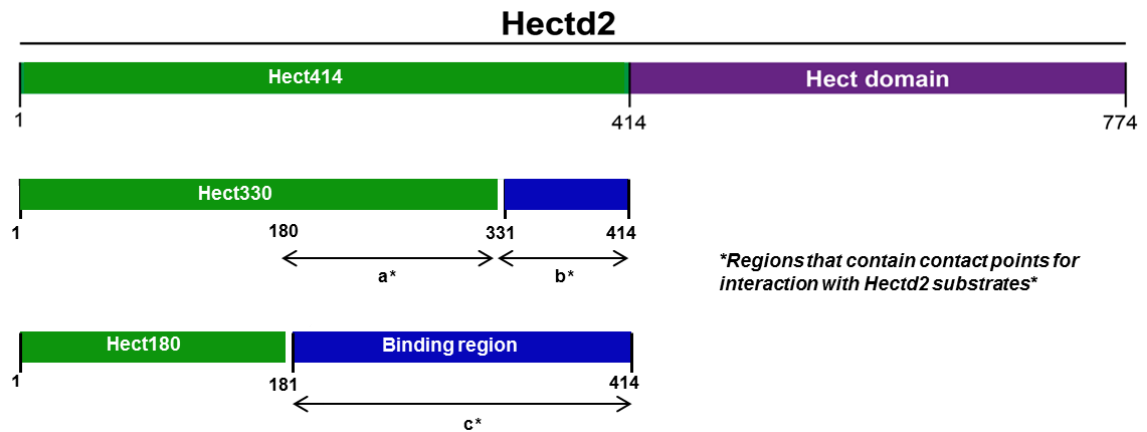


Figure 3.8.2 Putative binding region. The region of Hectd2 substrate binding may be substrate specific and may compose of multiple domains. a) Represents the region that binds Sh3glb1, Zbed4, Sh3yl1 and Loc10004685, and is thus necessary for binding some substrates but not sufficient for binding of all other substrates. b) Denotes the region containing the contact points for interaction of Hectd2 with all other identified candidates listed in Table 3.8.1. c) The region from amino acid 181 – 414 is thus important for binding Hectd2 substrates and may contain multiple domains.

Table 3.8.1 Locating the region of binding to Hectd2 via co-transformation of bait with prey

Candidate gene	Activation of reporter genes	
	Hect330	Hect180
<i>Klhdc2</i>	✗	✗
<i>Sh3glb1</i>	✓	✗
<i>Pbl</i>	✗	✗
<i>Pacsin2</i>	✗	✗
<i>Crtac1</i>	✗	✗
<i>Stambp</i>	✗	✗
<i>Zbed4</i>	✓	✗
<i>Cop9</i>	✗	✗
<i>Pcnx14</i>	✗	✗
<i>Sept7</i>	✗	✗
<i>Stmn2</i>	✗	✗
<i>Gvin1</i>	✗	✗
<i>Ppp2ca</i>	✗	✗
<i>Stk16</i>	✗	✗
<i>Sh3yl1</i>	✓	✗
<i>Mfsd6</i>	✗	✗
<i>Strn3</i>	✗	✗
<i>LOC100046859</i>	✓	✗
<i>Ces3</i>	✗	✗
<i>Gbl</i>	✗	✗

Results summary

Yeast two-hybrid screening was employed in search of Hectd2 binding partners, for which no interactors exist to date. 27 candidates were identified from the screen and subjected to follow up analyses by independent two-hybrid interaction assays in yeast for each putative candidate. 20 of these were confirmed as binding partners of Hectd2 in yeast. The yeast two-hybrid system was further exploited in an endeavor to map the region of Hectd2 to which the candidate interactors bind. By using C-terminal deletion mutants, it has been possible to determine that residues 181-414 of Hectd2 contain the region in which substrates make contact with Hectd2. These findings indicate that the prey interactors do not all bind Hectd2 at the same location as some substrates require different regions, which may be suggestive of multiple binding domains.

4 Validation of interactions in a mammalian cell system

4.1 Candidate gene selection for co-immunoprecipitation assays

Protein-protein interactions are integral to a myriad of cellular mechanisms and can alter the kinetic properties of enzymes, the specificity of a protein for its substrate or serve regulatory roles to refine signalling²⁶². Elucidation of these interactions can thus provide information on protein crosstalk within a pathway and thus functional implications in a given process. To date, Hectd2 remains a protein for which there are no known interactors, such that it has not been possible to place this E3 ubiquitin ligase within any protein network. Yeast-two-hybrid screening identified 20 binding partners of Hectd2, however, interactions in yeast do not necessarily reflect the binding characteristics of a given protein in mammalian cells. Yeast cells may not facilitate the correct folding of a protein into its quaternary conformation, which may require machinery specific to mammalian cells. In addition cellular targeting or location of a given protein may define the interactions that it makes and those identified in yeast may not be biologically relevant. Mammalian cells have the capacity to perform complex post-translational modifications that may adapt a protein for correct structure or render it active or localise it to a specific cellular component²⁶³. Thus the importance of validating such interactions in a mammalian cell line is apparent. The COS-7 cell line was selected to characterise interactions captured in the yeast-two-hybrid screen. COS-7 cells are fibroblast-like kidney cells originating from the African green monkey and represent an adherent line commonly used as a transfection host²⁶⁴.

Of the 20 candidates that emerged from the co-transformations in yeast, 5 were selected for further analyses. The basis for their selection was that of a putative functional or topographical significance that may link the candidates with disease pathology and thus Sh3glb1, Stmn2, Pacsin2, Stambp and Sept7 were chosen for co-immunoprecipitation analyses. Endophilin B1 (Sh3glb1) has a neuronal function in regulating NGF/TrkA, a neurotrophin and its receptor which modulates neuronal survival and differentiation²⁶⁵.²⁶⁶ Endophilin B1 has been associated with neuronal loss and induced autophagy in Parkinson's disease models²⁶⁷ and has been reported as an interactor of Huntingtin²⁶⁸.

Stamp, a deubiquitination enzyme involved in endosomal sorting of a number of cell surface molecules, is required to degrade ubiquitinated proteins in the CNS²⁶⁹ and mice deficient in Stamp show loss of neurons in the hippocampus and cerebral cortex²⁷⁰. Stmn2 is a microtubule destabilizing protein and has been identified as a risk factor for vCJD in a human genome wide association study¹³⁸. Pacsin2 is also a regulator of microtubule stability and plays a key role in membrane curvature and is implicated in endocytosis²⁷¹⁻²⁷⁴. Microtubule stability is of particular interest owing to PrP mediated tubulation that disrupts microtubular cytoskeleton by inducing tubulin oligomerisation²⁷⁵. Sept7 is a cytoskeletal GTPase that is required for normal organisation of the actin cytoskeleton^{276, 277}. Its implication in trafficking²⁷⁸, a function shared by Pacsin2²⁷⁹, Sh3glb1^{266, 280} and Stamp^{281, 282}, may indicate a common molecular pathway. Sept7 has also been reported to interact with Sept2, which is one of three septins found in neurofibrillary tangles in Alzheimer's disease^{283, 284}.

Co-immunoprecipitation assays were performed to capture Hect414, the N-terminal region in which the putative binding domain lies or Hectd2 in complex with its native interactions, described in detail below, (Section 4.3). It was important to test full length Hectd2 in parallel to Hect414 to confirm the interactions identified in the yeast system in addition to providing evidence of biological relevance by demonstrating that the full length proteins also bind. Absence of validated antibodies for Hectd2 and probable binding partners required tagging of the proteins of interest to epitopes for which high affinity antibodies were available. The pCMV-MYC/pCMV-HA vector set (Clontech) was selected to transiently express interacting proteins as either MYC or HA tagged fusions, for which Hectd2/Hect414 and the candidate interactors were chosen to express with the MYC or HA epitopes, respectively.

4.2 Design and construction of c-MYC/HA tagged fusion proteins

The pCMV-MYC/HA tag vector set allows the design of constructs that have MYC/HA tags that are N-terminally expressed (Appendix 2). MYC/HA tagged fusion proteins are thought to have minimal interference with the functional activity of the protein fused to it

owing to their small molecular weight (Appendix 2). The Hect414/Hectd2 sequences were cloned in frame with the MYC tag in pCMV-MYC using the strategy depicted in Section 3.3, Figure 3.3.1. The cDNA clones of the candidate genes isolated from yeast represent a partial sequence of the full length protein except for *Stmn2*, for which the cDNA clone was already in its full length form (Table 3.6.1). The candidate genes, in both their partial and full length sequences were cloned in frame with the HA tag in pCMV-HA. Full length cDNA clones of *Sh3glb1* (IRAVp968D0874D), *Pacsin2* (IRAVp968C0763D), *Stambp* (IRAVp968B0179D) and *Sept7* (IRAVp968C04100D) were purchased from Source Bioscience in the pCMV-SPORT6 vector. Cloning was carried out by PCR amplification of each insert sequence from the templates described above and a pre-existing Hectd2-TOPO clone for amplification of Hectd2/Hect414 (Section 2), through which restriction sites were incorporated at the 5' and 3' ends. This was achieved by using oligonucleotide primers that were designed to prime the insert sequence from its 5' and 3' ends, each preceded by a *SalI* or *SfiI* site for Hectd2/Hect414 or the candidate genes, respectively. These sites were selected based on their absence in the translated region of Hect414/Hectd2 or the candidate genes, thus preventing cutting of the sequence following digestion with *SalI* or *SfiI* respectively (Appendix 2). Base pair insertions were made where necessary to keep the sequences in frame with the tags and thus to retain the translational integrity of the fusion proteins, as depicted in Figure 4.2.1. This was only required for Hect414 and Hectd2 to maintain its frame with the MYC tag.

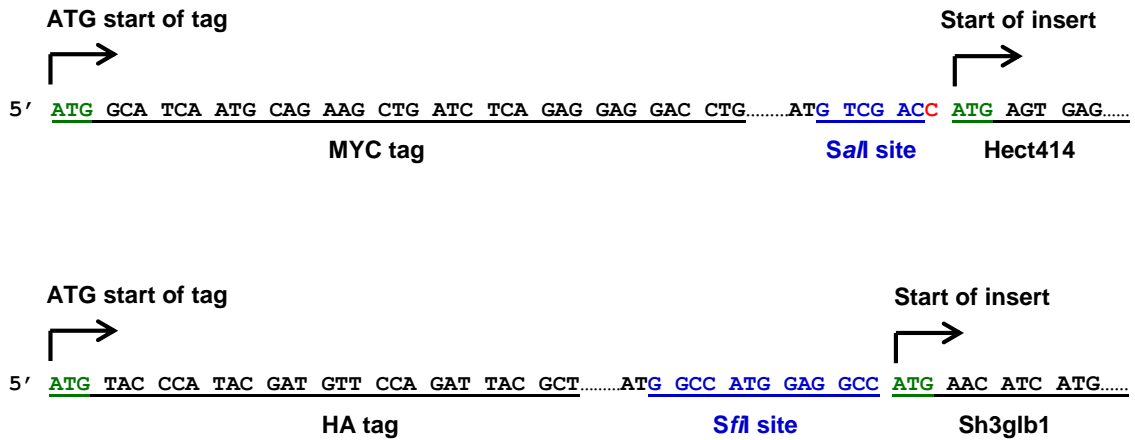


Figure 4.2.1 Construction of the tagged fusion proteins. The translation frame of the fusion construct for the cloning of *Hect414* into pCMV-MYC and *Sh3glb1* into pCMV-HA are shown as examples. Sequences of *Hect414* and *Sh3glb1* were maintained in frame with the N-terminal MYC or HA tags with their respective ATG start codons (green). Restriction sites were incorporated into PCR primers to amplify each gene sequence with either a *SalI* or *SfiI* site for *Hect414/Hectd2* or *Sh3glb1*, respectively. Base pair insertions were made where necessary, indicated in red, to retain the open reading frame.

PCR products were cloned into the TOPO shuttle vector prior to transfer to the pCMV-MYC/HA destination vector via ligation of overhanging ends generated by restriction digestion with *SalI* or *SfiI*, respectively (Section 2). The resultant clones were screened by PCR amplification using primers complementary to the 5' and 3' regions of the pCMV-MYC or pCMV-HA vector flanking the MCS, inclusive of 200 base pairs of the vector backbone flanking the MCS (Section 2). Size resolution of the amplified PCR products by agarose gel electrophoresis identified positives of each cloned gene consistent with the appropriate size (Table 4.2.1). The corresponding positive clone was cultured and purified according to Section 2. Restriction digestion with *SalI* or *SfiI* confirmed their insert sizes, Figure 4.2.2, which was verified by comprehensive sequence analyses for accuracy and integrity of the MYC or HA fusion junction.

Table 4.2.1 Molecular weight of candidate genes and Hectd2/Hect414

Gene	DNA insert size (bp)	Fusion protein predicted molecular weight (kDa)
Hectd2	2322	90
Hect414	1242	49
tcSh3glb1	987	39
Sh3glb1	1098	43
Stmn2	540	22
tcPacsin2	570	26
Pacsin2	1461	58
tcStambp	924	37
Stambp	1275	50
tcSept7	345	19
Sept7	1311	52

The prefix tc represents the truncated form of a candidate gene as identified in the yeast two-hybrid screen.

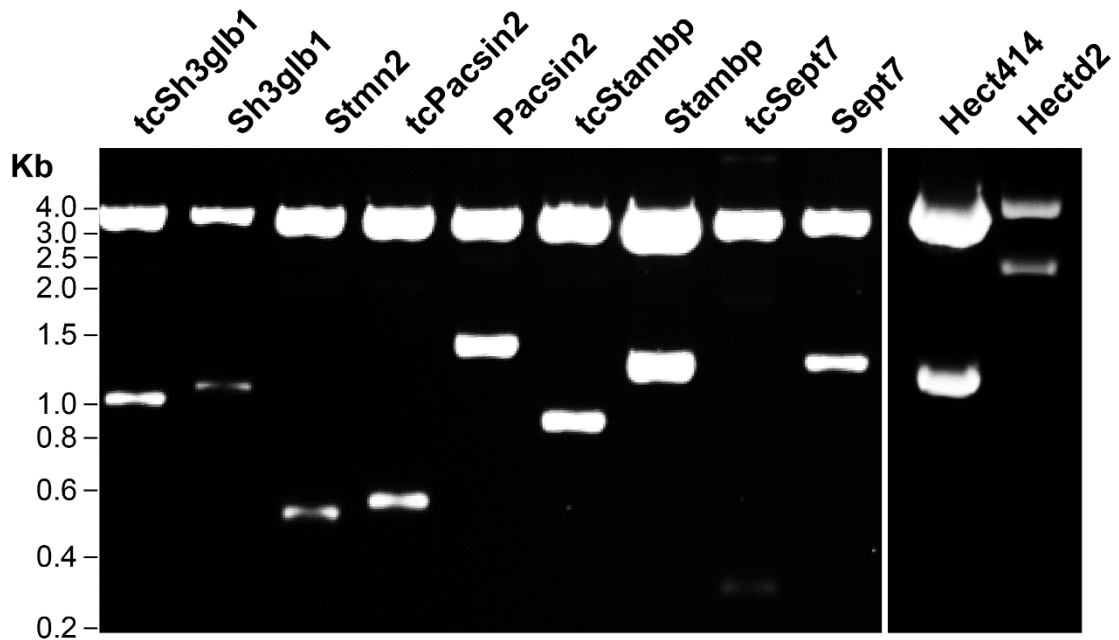


Figure 4.2.2 Insert release from MYC/HA fusion constructs. The truncated (tc) and full length forms of the candidate genes cloned into pCMV-HA were restriction digested with *Sfi*I and Hect414/Hectd2 in pCMV-MYC with *Sal*I. The cleaved inserts corresponded to sizes that were consistent with those that were expected for each gene in base pairs, detailed in Table 4.2.1.

4.3 Co-expression and co-immunoprecipitation of interacting complexes

Characterisation of protein-protein interactions using co-immunoprecipitation is a common method that has been successfully applied to dissect the biological activities of a multitude of proteins²⁶². The underlying principle of the method relies on the stable physiological interaction of proteins that can be captured by immunoprecipitating one of the interactants and thus co-precipitating its binding partner. This is facilitated by use of an antibody linked to a beaded support that detects one of the proteins in an interaction, by which the complex can be ‘pulled down’ from the lysate. The complex is isolated and denatured, from which the binding proteins can be identified by Western blotting with an antibody to specific to the interacting partner.

The putative substrate binding domain, Hect414 and its full length sequence, Hectd2 were co-expressed with each candidate by transfecting the respective fusion constructs in COS-7 cells, an overview of which is depicted in Figure 4.3.1. Whole cell lysates were harvested post-transfection and expression of MYC-tagged Hect414/Hectd2 or HA-tagged candidates were detected from 5% of a 1 ml total lysate using anti-c-MYC mouse monoclonal or anti-HA tag rabbit polyclonal on a Western blot (Section 2). The remaining 95% of the cell lysate was incubated with a Goat anti-HA tag immunoprecipitating antibody (Abcam), immobilised to an agarose bead support. The antibody binds specifically to the HA tag, forming a complex with the candidate interactor-Hectd2/Hect414. Following serial washing and centrifugation steps to eliminate non-specific binding proteins, the immunoprecipitants were eluted in denaturing SDS buffer. The proteins bound to the HA-tagged candidates were detected by Western blotting using anti-c-MYC antibody. Antibody combinations were selected based on the species they were raised in, in order to avoid cross-reactivity between the co-eluted antibody light and heavy chains in the precipitated complex and the secondary antibody used to detect the proteins within that complex. Thus anti-c-MYC mouse monoclonal antibody was used to detect MYC tagged Hectd2/Hect414 that was bound to the interactant, which was immunoprecipitated with Goat anti-HA tag antibody.

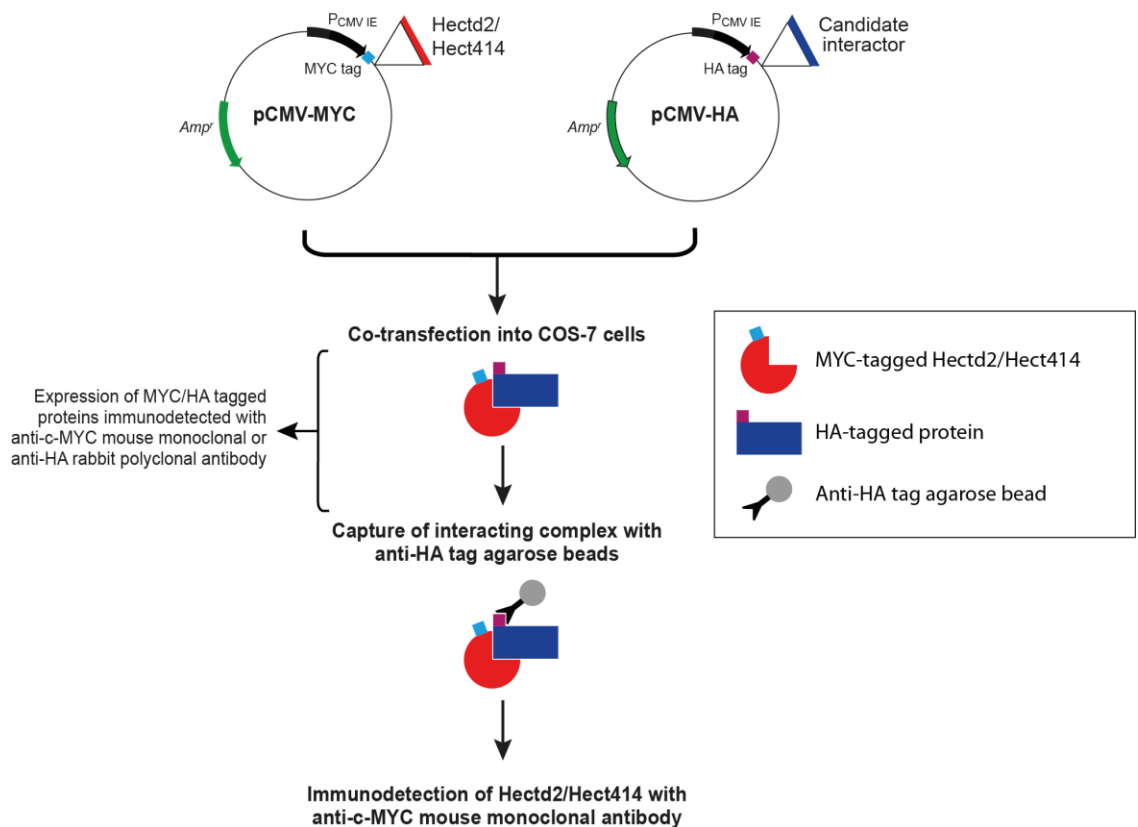


Figure 4.3.1 Overview of co-immunoprecipitation assay. Constructs were designed to express Hect414 or Hectd2 as MYC-tagged fusions and the candidate interactors as HA-tagged proteins. Whole COS-7 cell lysates were harvested post-transfection and expression of the tagged proteins detected by SDS PAGE/Western blotting using anti-c-MYC mouse monoclonal or anti-HA tag rabbit polyclonal antibodies. Goat anti-HA tag agarose beads were incubated with crude cell lysates and the interacting-HA-tagged fusions are captured, co-precipitating the bound protein. The complex is eluted in denaturing sample buffer and followed by SDS PAGE/Western blotting to detect MYC-tagged Hect414/Hectd2 using anti-c-MYC mouse monoclonal antibody.

To authenticate the co-immunoprecipitation experiments several criteria need to be met. Firstly, the immunoprecipitated protein must be recognised by the surface bound antibody and conversely the co-precipitated protein must not. Secondly, the interaction must require both proteins so as to ensure that the interaction is specific. To account for this, a combination of constructs were co-transfected into COS-7 cells as outlined in Table 4.3.1. To standardise the nomenclature, the truncated form of a protein obtained from the yeast-two-hybrid screen is denoted with a 'tc' preceding its name, otherwise an implicit

assumption should be made that the full length protein has been expressed. Plasmids are described as pCMV-MYC·Hect414/Hectd2 or pCMV-HA·Interactor, which represent the MYC or HA plasmids from which Hect414/Hectd2 or the interacting protein are expressed. Their protein counterparts are denoted by MYC·Hect414/Hectd2 or HA·Interactor, respectively. All co-immunoprecipitations were repeated to ensure reproducibility.

Table 4.3.1 Construct combinations for co-immunoprecipitations

Construct combinations for co-immunoprecipitation controls		
pCMV-MYC·Hect414/Hectd2	+	pCMV-HA·Candidate*
pCMV-MYC·Hect414/Hectd2	+	pCMV-HA
pCMV-MYC	+	pCMV-HA·Candidate*
pCMV-MYC	+	pCMV-HA

* Candidate represents Sh3glb1, Stmn2, Pacsin2, Stambp or Sept7 in truncated or full length forms

Hectd2 binds to Sh3glb1

MYC·Hect414, putative substrate binding domain or MYC·Hectd2 co-immunoprecipitated with truncated or full length forms of Sh3glb1 in COS-7 cells in which they were both expressed (Figure 4.3.2 c, f). MYC·Hect414 and MYC·Hectd2 were observed as ~49 or 90 kDa bands, respectively, and were absent in control samples (Figure 4.3.2 a, d). Immunoprecipitants were undetectable in samples where HA·tcSh3glb1 or HA·Sh3glb1 were co-expressed with MYC tag empty vector (Figure 4.3.2 c, f). The Sh3glb1 fusions migrate at ~39 or 43 kDa respectively, while the co-expressed tags on their own are not observed owing to their low molecular weight of 1.4 kDa (Figure 4.3.2 b, e). Co-expression of both empty vectors failed to precipitate any proteins confirming that non-specific MYC- or HA-tagged proteins were not falsely detected. Together, these data indicate a Hect414/Hectd2 dependent co-immunoprecipitation with Sh3glb1.

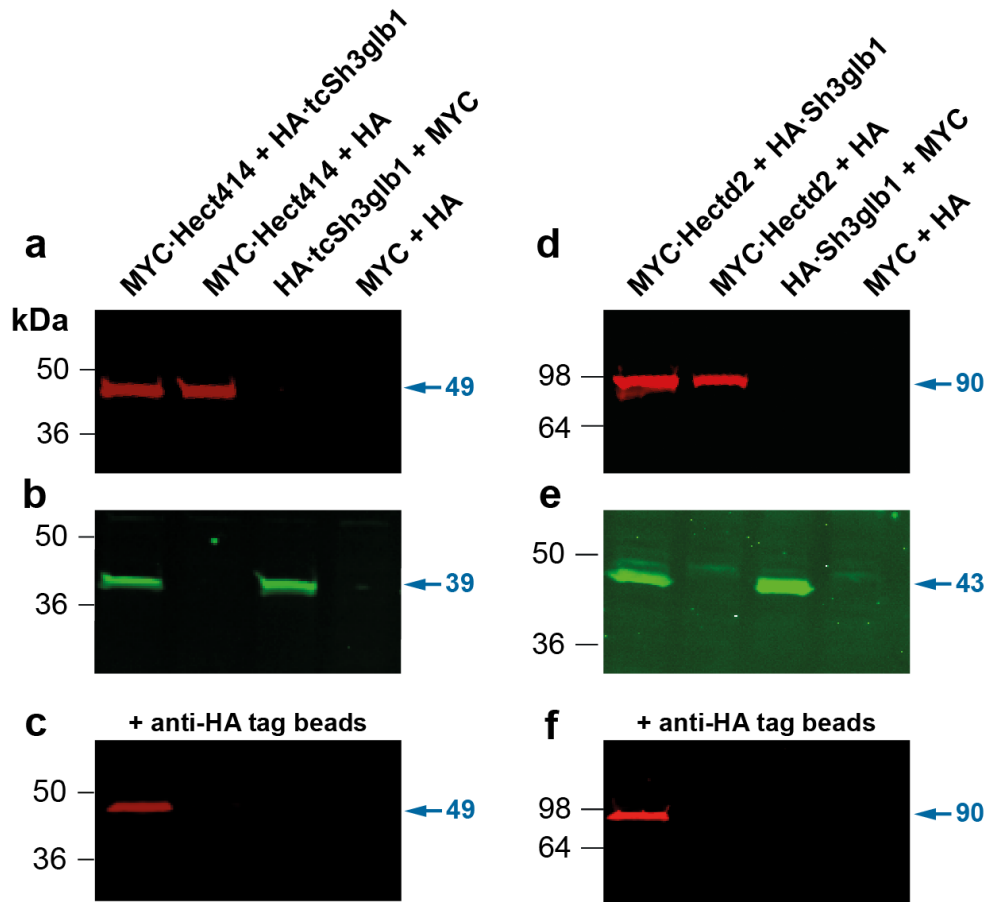


Figure 4.3.2 Sh3glb1 co-immunoprecipitates with Hectd2 in COS-7 cells. 50 μ l of cell lysate containing MYC-tagged Hect414 or Hectd2 and HA-tagged Sh3glb1 in both truncated (tc) and full length forms were electrophoresed on 16 and 12% gels respectively (panels a-c and d-f). Western blotting was followed by detection of MYC or HA epitopes using anti-c-MYC mouse monoclonal antibody (a, c, d and f) or anti-HA tag rabbit polyclonal antibody (b and e). Signals were detected with secondary IRDye680 (red) conjugated goat anti-mouse IgG or IRDye800 CW (green) conjugated goat anti-rabbit IgG using an Odyssey infra-red imaging immunofluorescence system (Li-Cor). MYC-Hect414 (a-c) or MYC-Hectd2 (d-f) were co-expressed with tcSh3glb1 (a-c) or Sh3glb1 (d-f) or with their respective vector only controls (a-f). Both tcSh3glb1 and Sh3glb1 show interaction with Hect414 or Hectd2 when both proteins are present in the lysate but not when Sh3glb1 forms were absent (c and f).

Hectd2 binds to Stmn2

Expression of HA·Stmn2, was observed as a band running at a molecular weight slightly higher than the 22 kDa size expected for the Stmn2 fusion, Figure 4.3.3 b, e. This may be attributed to the discrepancies that sometimes occur in the migration profile of a protein and its calculated molecular weight or perhaps due to post-translational modifications, such as phosphorylation, which is a known alteration for Stmn2²⁸⁵. Co-expression with MYC·Hect414 or MYC·Hectd2 in COS-7 cells identified that Stmn2 co-immunoprecipitated with both MYC·Hect414 and MYC·Hectd2 (Figure 4.3.3 a-f). This is supported by an absence of the MYC·Hect414/Hectd2 proteins in control samples where MYC·Hect414/Hectd2 was expressed with the HA tag empty vector (Figure 4.3.2 c, f). Furthermore, presence of HA·Stmn2 solely with the MYC tag is not sufficient to immunoprecipitate the ~49 or 90 kDa bands observed in Figure 4.3.3 c, f. Co-expression of the MYC and HA tags alone fails to precipitate any proteins suggesting that the interactions between Hect414/Hectd2 and Stmn2 are specific.

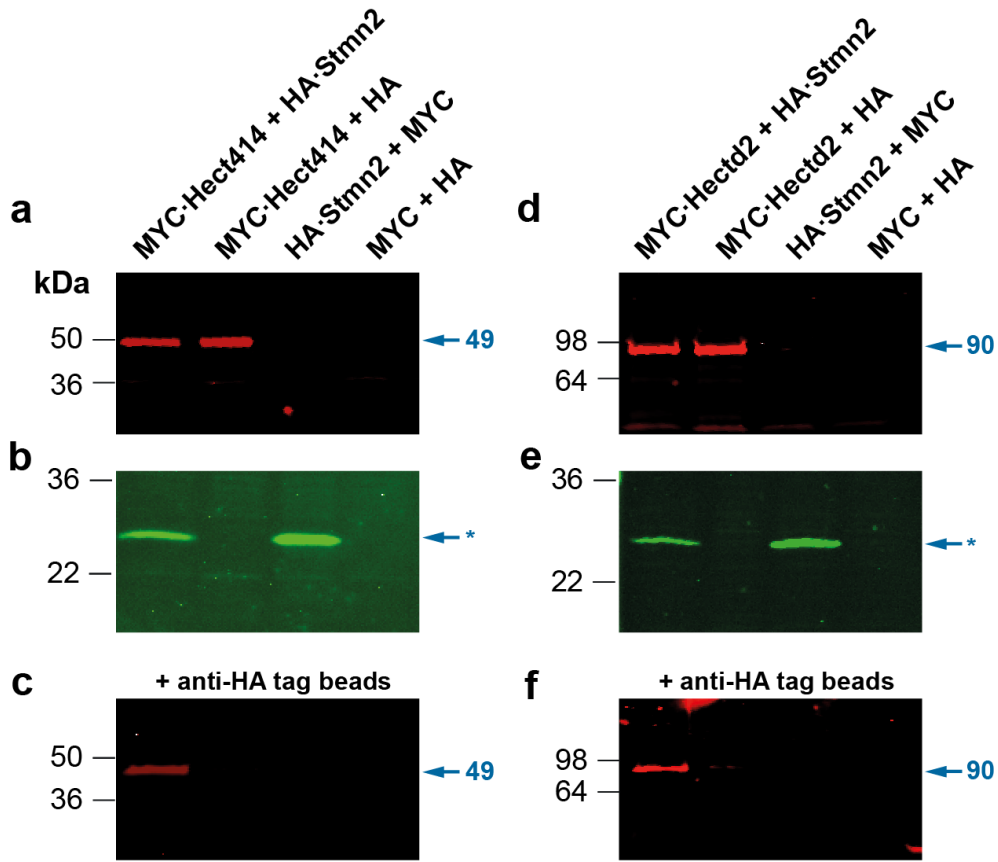


Figure 4.3.3 Stmn2 co-immunoprecipitates with Hectd2 in COS-7 cells. 50 μ l of cell lysate containing MYC-tagged Hect414 or Hectd2 and HA-tagged Stmn2 were electrophoresed on 16 and 12% gels respectively (panels a-c and d-f). Samples were immunoblotted with anti-c-MYC mouse monoclonal antibody (a, c, d, f) or anti-HA tag rabbit polyclonal antibody (b and e) and secondary IRDye680 (red) conjugated goat anti-mouse IgG or IRDye800 CW (green) conjugated goat anti-rabbit IgG using an Odyssey infra-red imager (Li-Cor). Stmn2 was co-expressed with MYC·Hect414 (a-c) or MYC·Hectd2 (d-f) with their respective vector only controls (a-f). The band corresponding to HA·Stmn2 is represented by an asterisk to denote the difference in migration profile and its predicted molecular weight of 22 kDa (b and e). Stmn2 shows interaction with Hect414 and Hectd2 only when co-expressed but not when Stmn2 was absent from the lysate (c and f).

Hectd2 binds to Pacsin2

MYC·Hect414 or MYC·Hectd2 were found to co-immunoprecipitate with HA·Pacsin2 in its truncated or full length forms when co-expressed (Figure 4.3.4 c, f). The truncated form of HA·Pacsin2 runs at a molecular weight of 26 kDa while its full length counterpart runs at a molecular weight of 58 kDa (Figure 4.3.4 b, e). However, when Hect414 or Hectd2 are expressed with the HA tag only, in the absence of the Pacsin2 proteins, Hect414 and Hectd2 both fail to co-immunoprecipitate, indicative of Pacsin2-dependent precipitation (Figure 4.3.4 a-f). Conversely, this was also true when HA·tcPacsin2 or HA·Pacsin2 were co-expressed with the MYC tag only, such that immunoprecipitation of the proteins fails to detect the binding protein (Figure 4.3.4 a-f). The vector only control, supports these findings whereby co-immunoprecipitation is abrogated in the absence of interacting Pacsin2 and Hectd2 (Figure 4.3.4 c, f).

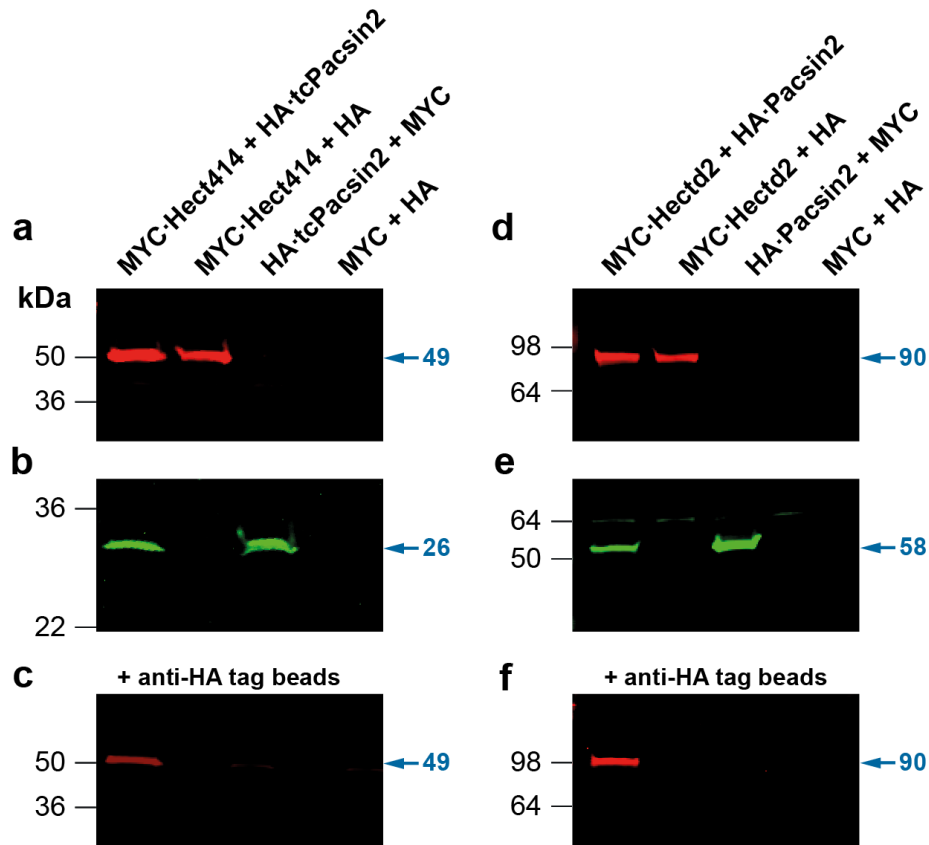


Figure 4.3.4 Pacsin2 co-immunoprecipitates with Hectd2 in COS-7 cells. 50 μ l of cell lysate containing MYC-tagged Hect414 or -Hectd2 and HA-tagged Pacsin2 in both truncated (tc) and full length forms were electrophoresed on 16 and 12% gels respectively (panels a-c and d-f). Samples were immunoblotted with anti-c-MYC mouse monoclonal antibody (a, c, d, f) or anti-HA tag rabbit polyclonal antibody (b and e) and secondary IRDye680 (red) conjugated goat anti-mouse IgG or IRDye800 CW (green) conjugated goat anti-rabbit IgG using an Odyssey infra-red imager (Li-Cor). Panels a, b, d and e show that Pacsin2 in its truncated or full length complement were co-expressed with Hect414 or Hectd2 or with the MYC or HA empty vectors. tcPacsin2 or its full length protein show interaction with Hect414 or Hectd2, respectively, when co-expressed but not when Pacsin2 proteins were absent from the lysate (c and f).

Hectd2 binds to Stambp

HA·tcStambp migrates as a ~37 kDa band and HA·Stambp shows a molecular weight that is slightly higher than the predicted ~50 kDa, (Figure 4.3.5 b, e). Immunoprecipitation of HA·tcStambp or HA·Stambp co-precipitated Hect414 or Hectd2, respectively, in samples where both proteins were present, (Figure 4.3.5 a-c and d-f). However in the absence of one or the other putative interacting protein, where they were expressed with their respective MYC or HA tags only, MYC·Hect414 or MYC·Hectd2 failed to be detected as co-precipitating proteins (Figure 4.3.5 c, f). The vector only control sample in which the MYC and HA tags are co-expressed support these data in that the presence of both Stambp and Hectd2 are required to co-immunoprecipitate Hectd2 (Figure 4.3.5 c, f).

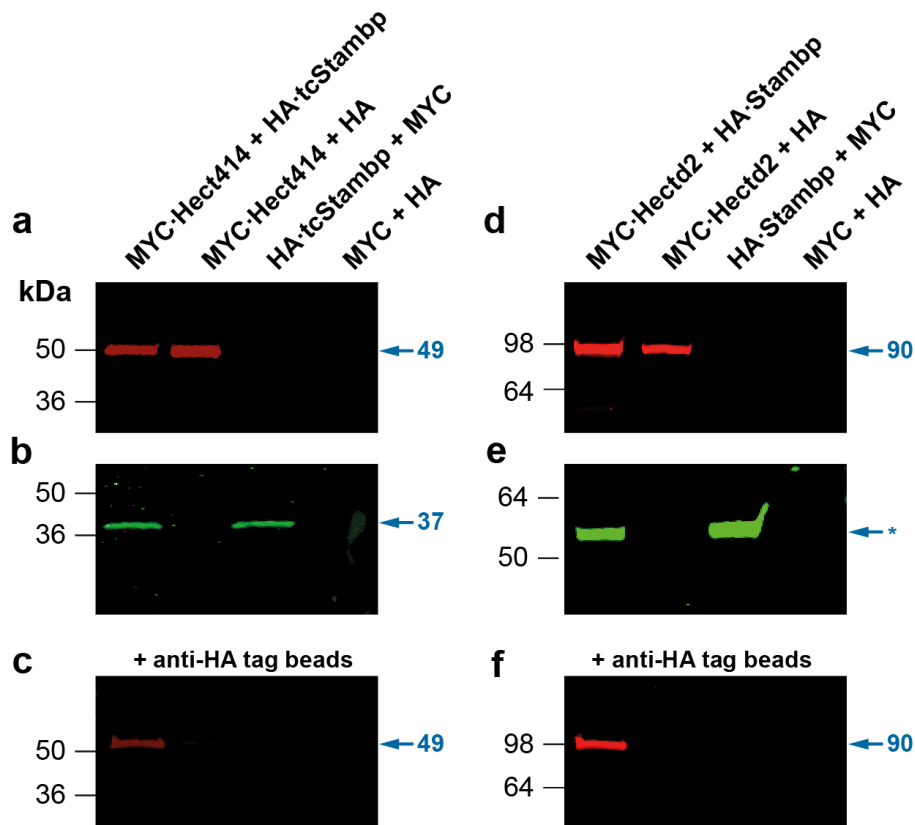


Figure 4.3.5 Stambp co-immunoprecipitates with Hectd2 in COS-7 cells. 50 μ l of cell lysate containing MYC-tagged Hect414 or Hectd2 and HA-tagged Stambp in both truncated (tc) and full length forms were electrophoresed on 16 and 12% gels respectively (panels a-c and d-f). Western blotting was followed by detection of MYC or HA epitopes using anti-c-MYC mouse monoclonal antibody (a, c, d and f) or anti-HA tag rabbit polyclonal antibody (b and e). Signals were detected with secondary IRDye680 (red) conjugated

goat anti-mouse IgG or IRDye800 CW (green) conjugated goat anti-rabbit IgG using an Odyssey infra-red imaging immunofluorescence system (Li-Cor). Truncated Stambp or full length proteins were co-expressed with MYC·Hect414 or MYC·Hectd2 or their complementary empty vector (a-f). The band corresponding to HA·Stambp (e) is represented by an asterisk to denote the difference in migration profile and its predicted molecular weight of 50 kDa. tcStambp or its full length protein show interaction with Hect414 or Hectd2, respectively, when co-expressed but not when Stambp forms were absent from the lysate (c and f).

Hect414 binds to Sept7

When MYC·Hect414 was co-expressed with HA·tcSept7, a protein that runs at ~19 kDa, MYC·Hect414 was found to co-immunoprecipitate with HA·tcSept7 (Figure 4.3.6 a-c). Samples in which MYC·Hect414 was expressed with the HA tag only, failed to detect Hect414 as a co-precipitant, suggesting that HA·tcSept7 is required for interaction with MYC·Hect414 (Figure 4.3.6 a, c). Furthermore, an interaction with Hect414 is not detected in the absence of MYC·Hect414, where HA·tcSept7 is co-expressed with the MYC tag only (Figure 4.3.6 a-c). The vector only control supports these data, which shows no detectable protein, suggesting that interaction between Hect414 and tcSept7 is necessary for co-immunoprecipitation (Figure 4.3.6 c).

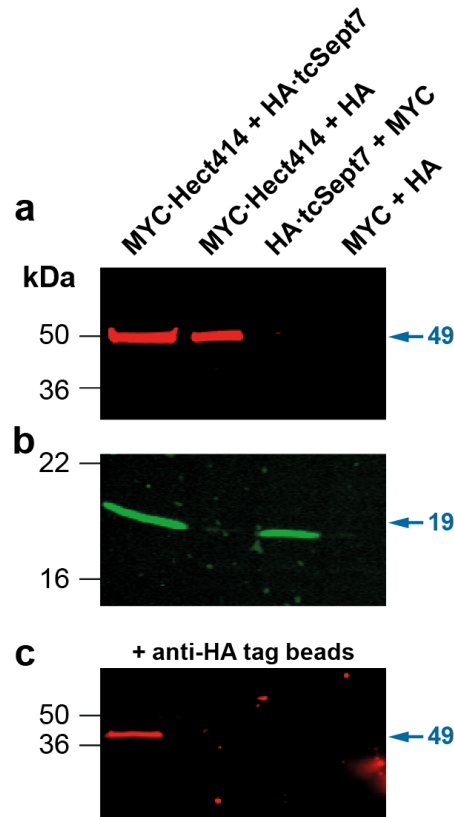


Figure 4.3.6 Sept7 co-immunoprecipitates with Hect414 in COS-7 cells. 50 μ l of cell lysate containing MYC-tagged Hect414 and HA-tagged Sept7 were electrophoresed on 16% gels (panels a-c) Western blotting was followed by detection of MYC or HA epitopes using anti-c-MYC mouse monoclonal antibody (a and c) or anti-HA tag rabbit polyclonal antibody (b). Signals were detected with secondary IRDye680 (red) conjugated goat anti-mouse IgG or IRDye800 CW (green) conjugated goat anti-rabbit IgG using an Odyssey infra-red imaging immunofluorescence system (Li-Cor). Truncated Sept7 was co-expressed with MYC-Hect414 or with the complementary MYC or HA vectors (a-c). tcSept7 was found to interact with Hect414 when co-expressed, but not when tcSept7 proteins were absent from the lysate (c).

Results summary

We selected five candidates from the yeast-two-hybrid screen for confirmation of their interaction in a mammalian cell system. By tagging Sh3glb1, Stmn2, Pacsin2, Stambp and Sept7 to the HA epitope and co-expressing with MYC-tagged Hect414 and full length Hectd2 in COS-7 cells, it has been possible to establish that each of these candidates binds Hectd2.

5 Effect on cell susceptibility to prion infection

5.1 shRNA gene knockdown in N2aPK1/2 cells

The standard method to test the effects of a candidate gene in prion disease is through the use of mouse models that are transgenic or knockout for the gene of interest. A phenotype can be measured by challenging such mice with prions after which a quantitative trait such as incubation time can be measured that can be followed by histopathological assessment relative to control mice. However, functional validation of candidate genes that modulate incubation time by generating mouse models is costly and labour intensive. Cell based assays are therefore often sought to identify phenotypic perturbations that define gene function. One such method is the Scrapie Cell Assay (SCA), developed by Klöhn *et al.*, which is an alternative *in vitro* assay for the quantification of prion infectivity²⁵³. The underlying principle of this method relies on the high susceptibility of the neuroblastoma N2a derivative, N2aPK1/2 cell line, (PK1/2) to RML mouse scrapie prions. Transmission of the infectious species to cells can be measured by automated counting of PrP^{Sc} positive cells following exposure to prions. Application of this approach can be exploited by measuring the susceptibility of cells to prion infection following manipulation of a given candidate gene by knockdown or overexpression. This may shed light on the role of a candidate gene with respect to its propensity to propagate prion infection and its ability to clear prions.

The Hctd2 binding partners, Sh3glb1, Pacsin2, Sept7 and Stambp were selected for functional validation using the Scrapie Cell Assay. Expression of these genes in PK1/2 cells was previously determined by a microarray study (unpublished data, MRC Prion Unit, London) and thus we chose to knockdown each gene independently. The knockdown technology selected for gene silencing was by short hairpin RNA (shRNA) that would be stably expressed to suppress expression of the candidate gene. Stable rather than transient expression was the preferred method to achieve sustainable gene knockdown over the duration of the assay (Section 2). This allows the measurement of cell susceptibility to prion infection over time. Stable cell lines for each candidate gene

were generated and quantified to ascertain knockdown levels prior to screening with the Scrapie Cell Assay.

5.2 Construction of the pSUPER.retro.puro recombinant plasmid

The pSUPER.retro.puro vector was selected to clone target-specific shRNAs as it can direct stable intracellular expression of the shRNA, to facilitate knockdown of the target mRNA transcript when stably maintained within a cell^{256, 286} (Figure 5.2.1) . To mediate transcript silencing of the target gene, custom made 60-nucleotide forward and reverse oligonucleotides including a 19 nucleotide sequence, N-19, derived from the target mRNA, were designed (Section 2). The N-19 target sequences were generated using the siDESIGN Center, an algorithm developed by Dharmacon, to identify functional siRNA sequences (Section 2). This tool was used to generate four shRNAs for each candidate gene to ensure that downstream results are supported by at least two shRNA knockdown lines per gene to provide confidence that a given phenotype is not an artifact. Furthermore, the algorithm generates the shRNA as a prediction of what may serve as a functional siRNA, thus there is a possibility that an shRNA may not silence the target transcript. Cloning of the N-19 oligonucleotide into the pSUPER.retro.puro vector (OligoEngine) was facilitated by use of the *Bgl*III and *Hind*III sites to position the oligonucleotide downstream of the H1 promoter's TATA Box. The forward oligonucleotide was engineered to contain a 5' *Bgl*III restriction site preceding the N-19 sequence in the sense and antisense orientation, separated by a 9 nucleotide spacer sequence that would in turn form the hairpin structure (Figure 5.2.1.) The 3' end of this forward oligonucleotide includes a run of 5 thymidines that denotes the termination signal and includes *Hind*III specific nucleotides (Section 2).

The forward and reverse complement oligonucleotides were annealed to form double stranded units (Section 2). Their *Bgl*III and *Hind*III overhanging ends were thus available for ligation to *Bgl*III/*Hind*III-digested pSUPER.retro.puro. The shRNA constructs were verified by sequencing. A non-targeting shRNA control construct, pRS-GFP-sh2, and a

marker plasmid control, pRS-GFP, were gifted by Dr Craig Brown (MRC Prion Unit, London). The pRS-GFP-sh2 construct represents an shRNA directed against GFP and was used to control for changes to the cells due to the procedure, particularly the antibiotic selection that was used to achieve stable knockdown. The marker plasmid, pRS-GFP, represents the GFP protein cloned into pSUPER.retro.puro and was used to observe the transfection efficiency of candidate gene-specific shRNA constructs.

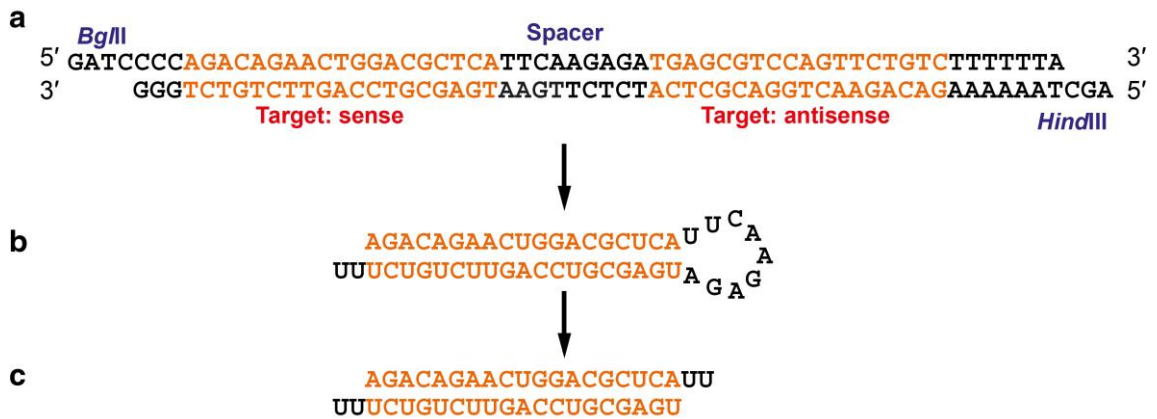


Figure 5.2.1 Transcription of shRNA targeting *Sh3glb1*. a) Oligonucleotides were designed to target a 19 bp region of the cognate mRNA, shown here for *Sh3glb1*, including sense and antisense strands connected by the 9 nucleotide spacer. b) The H1 promoter of pSUPER.retro.puro drives expression of the 60 nucleotide single stranded RNA, which folds to form a hairpin structure. c) This is processed post-transcriptionally into functional si-RNA-like molecules. *Adapted from OligoEngine pSUPER.retro.puro manual.*

5.3 Relative quantitation of target gene shRNA knockdown

To generate stably expressing shRNAs for each gene, retroviral delivery of the constructs was used. The Phoenix Ecotropic, ϕ -NX Eco packaging cell line was selected to produce retroviruses for infection of PK1/2 cells²⁵⁶. Following transduction of PK1/2 cells with retroviruses harbouring each shRNA construct, drug selection with puromycin was performed. Stable cell lines with the relevant integrated constructs were derived following maintenance in puromycin-supplemented media for two weeks (Section 2). These lines

were subject to analysis by measurement of the effect of each shRNA construct on the target mRNA levels. Knockdown shRNA cell lines for *Hectd2* were generated by Dr Craig Brown, MRC Prion Unit, London, using the same procedures.

The mRNA levels of *Sh3glb1*, *Pacsin2*, *Sept7*, *Stambp* and *Hectd2* in their respective PK1/2-shRNA knockdown cell lines were quantified relative to control PK1/2 cells in which the non-targeting construct pRS-GFP-sh2 was expressed. Comparative mRNA quantification in this manner allows the determination of how effective an shRNA is for knockdown of a given target gene. This is expressed as an *n*-fold difference relative to non-targeting control cells (GFP-sh2), which has been normalised to the endogenous reference control, glyceraldehyde-3-phosphate dehydrogenase, (GAPDH), to generate a unit of relative expression.

The Taqman[®] Gene Expression Cells to CT[™] kit was used to recover RNA from PK1/2 cell lysates from which cDNA was transcribed by reverse transcription for analysis by qPCR. Two independent lysates per cell line were used, which have been defined herein as separate lysis reactions and three technical replicates per lysate were made for the PCR reactions described below (Section 2).

The concentration of cDNA for a given gene was quantified by qPCR, which measures real time detection of specific PCR amplification. TaqMan[®] Gene Expression Assays specific for *Sh3glb1*, *Pacsin2*, *Sept7* and *Stambp* were used for relative expression analyses (Section 2). Quantitation was determined by the ΔC_T method which generates relative values for target expression, normalised to endogenous GAPDH, relative to non-targeting control cells, given by the formula $2^{-\Delta\Delta C_T}$ (Section 2). A minimum of 50% difference in target gene expression relative to controls was arbitrarily selected to define sufficient gene knockdown. Thus for each candidate gene, at least two shRNA lines at >50% knockdown were required to provide confidence in the results generated in downstream SCA analyses.

Cells expressing construct Sh3glb1-sh4, which targets the ORF of *Sh3glb1*, had 59 % knockdown, relative to reference PK1/2-GFP-sh2 cells as shown in Figure 5.3.1, Table 5.3.1. However, Sh3glb1-sh1, -sh2 and -sh3 did not show statistically significant differences in knockdown relative to control cells. Targeting of *Pacsin2* showed more promising results as *Pacsin2*-sh2, -sh3 and -sh4 constructs knocked down expression by 57, 86 and 88%, respectively, although *Pacsin2*-sh1 only produced a moderate reduction of 33%. *Sept7* mRNA expression levels demonstrated that shRNAs 1, 2 and 4 targeting *Sept7* reduced expression by 59, 86 and 93%, respectively, relative to PK1/2-GFP-sh2 cells whilst *Sept7*-sh3 did not show significant gene knockdown. Rather, *Sept7*-sh3 appeared to have a 10% increase in *Sept7* mRNA, which may be attributed to natural variation. *Stambp*-sh1, and -sh4 showed knockdown of *Stambp* mRNA by 83 and 90% respectively, relative to the non-targeting control. Table 5.3.1 shows the knockdown cell lines selected for each gene to undergo SCA validation of candidates.

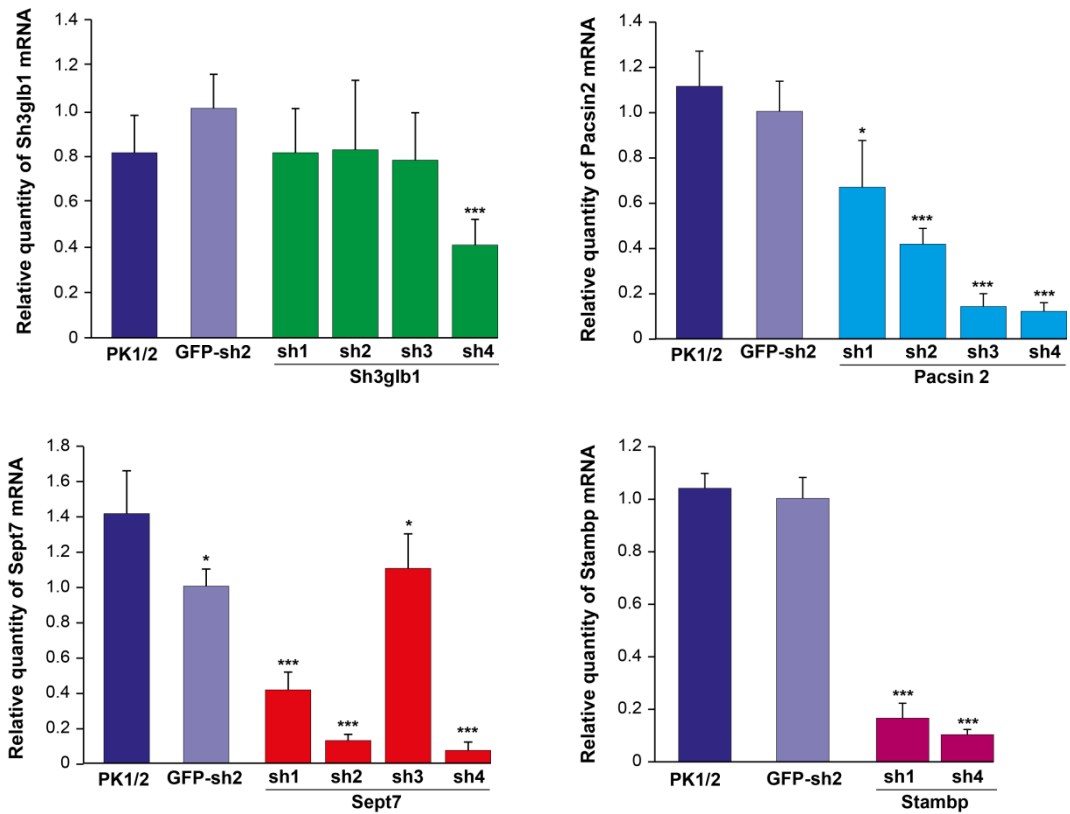


Figure 5.3.1 Relative mRNA expression of candidate genes. Cell lysates from each PK1/2 line expressing gene specific shRNA targeting *Sh3glb1*, *Pacsin2*, *Sept7* and *Stambp* or non-targeting shRNA, GFP-sh2, were used to obtain cDNA by reverse transcription from which their levels were quantified by qPCR using a comparative C_T method. Error bars are SD, * = $p < 0.01$, *** = $p < 0.0001$, t test.

Table 5.3.1 shRNA knockdown lines for Scrapie Cell Assay

Stable shRNA PK1/2 line	Knockdown (%)	SD (\pm %)
Sh3glb1-sh1	19	20
Sh3glb1-sh2	18	31
Sh3glb1-sh3	22	21
Sh3glb1-sh4	59	12
Pacsin2-sh1	33	22
Pacsin2-sh2	57	6
Pacsin2-sh3	86	6
Pacsin2-sh4	88	4
Sept7-sh1	59	10
Sept7-sh2	86	3
Sept7-sh3	*	*
Sept7-sh4	93	5
Stambp-sh1	83	6
Stambp-sh4	90	2
Hectd2-sh1**	96	0.4
Hectd2-sh3**	96	0.4
Hectd2-sh4**	98	0.4

shRNA lines showing >50% knockdown were selected for the SCA

*Sept7-sh3 construct shows no knockdown of *Sept7* expression relative to control GFP-sh2 non-targeting cells **Lines generated by Dr Craig Brown

5.4 Effect of target knockdown on the Scrapie Cell Assay, SCA

The SCA allows the visualisation of proteinase-K (PK) resistant PrP signals, PrP^{Sc}, arising from single cells. Data generated from the assay can be utilised to provide information on the effect of candidate gene knockdown on cell susceptibility to prion infection. The Scrapie Cell Assays described herein were performed by Dr Craig Brown, MRC Prion Unit, London.

The shRNA knockdown cell lines detailed in Table 5.3.1 were infected with RML Scrapie from which a subset of 25,000 cells were filtered onto ELISPOT membranes for which 10 replicates were made (Section 2). PK-digestion eliminated PK-sensitive PrP in order that only PrP^{Sc} is adsorbed to the membranes. PK-resistant PrP positive cells were counted following detection with anti-PrP ICSM18 and alkaline phosphatase linked anti-IgG₁ in the presence of its conjugate substrate (Section 2).

The PK-resistant PrP spot numbers generated from 3 independent assays were normalised to the non-targeting GFP-sh2 controls to calculate the mean of the PrP^{Sc}-positive signals and their standard deviations. In order to have confidence in a modulatory role for a given gene, replication of the result is required in an independent cell line for the same gene knockdown. The results, shown in Figure 5.4.1 a, show that knockdown of *Sh3glb1* in PK1/2 cells expressing *Sh3glb1*-sh4, produces an increase in PK-resistant spot number relative to the non-targeting control, GFP-sh2 and PK1/2 cells. The *p* value corresponding to this difference in signal was 7.8×10^{-22} , calculated by a *t* test, indicating that *Sh3glb1* is an interesting candidate although not confirmed as data for only one cell line was available. *Pacsin2* knockdown showed variation in that cells expressing shRNA construct, *Pacsin2*-sh2 and -sh4, showed no significant difference to the non-targeting control or PK1/2 cells using a *t* test. However, *Pacsin2*-sh3 mediated knockdown resulted in a decrease of spot number, marked by a *p* value of 0.002, using a *Mann-Whitney* test as the data deviate from a Gaussian distribution. Thus it is unlikely that *Pacsin2* modifies prion propagation or clearance, although this cannot be definitively ruled out. PK1/2 cells in which *Sept7* knockdown was targeted by *Sept7*-sh1 or *Sept7*-sh4 showed an increase in the PK-resistant PrP spot signal. This was supported by highly significant *p* values of 7.9×10^{-16} and 1.0×10^{-7} , respectively, using *t* tests. *Sept7*-sh2 conversely appeared to reduce

the spot number, indicative of a possible off-target effect. *Stambp* knockdown by –sh4 resulted in no significant difference relative to controls although targeting by construct *Stambp*-sh1 produced an increase in PK-resistant PrP signal; p value 0.003 (t test), thus confounding the data due to lack of replication as a conclusion cannot be drawn. To account for the effects of multiple testing, a Bonferroni correction was applied to bring a 1% level of significance to $p < 0.001$ for which *Pacsin2*-sh3, *Sept7*-sh2 and *Stambp*-sh1 do not reach significance.

The SCA results for *Hectd2* knockdown cell lines are shown in Figure 5.4.1 b. *Hectd2*-sh1 and *Hectd2*-sh4 mediated silencing of *Hectd2* produced an increase in PK1/2 cell susceptibility to prion propagation relative to the non-targeted control GFP-sh2 cells. Statistical testing found that cells expressing *Hectd2*-sh1 or *Hectd2*-sh4 had p values of 4.1×10^{-6} or 0.0001 in reference to the non-targeting control, (t test). However, one knockdown line, *Hectd2*-sh3, presented a decrease in PrP^{Sc} spot number, with statistical significance at $p = 0.0007$, (t test). Since an increased PrP^{Sc} propagation effect is supported by the two other *Hectd2* knockdown lines, this conflicting data may perhaps be attributable to an off-target effect.

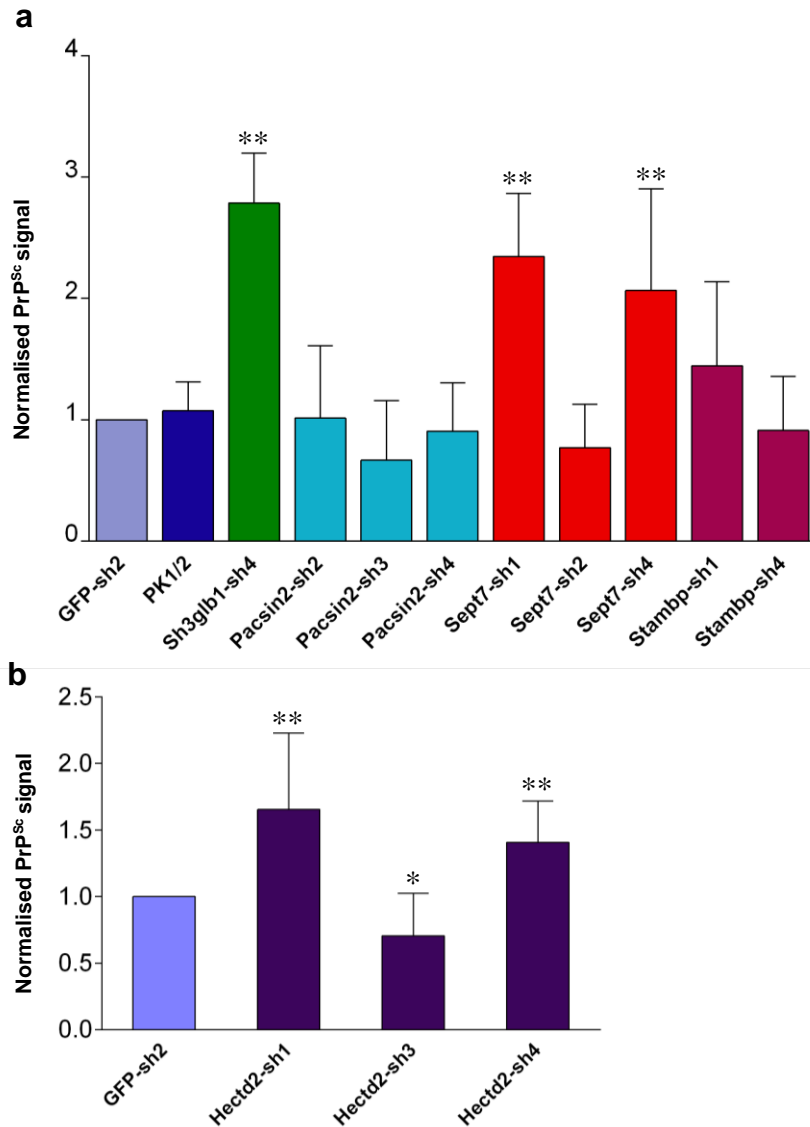


Figure 5.4.1 Effect of candidate gene knockdown in the Scrapie Cell Assay. Knockdown cell lines were exposed to 1×10^{-5} RML/Chandler inocula and the data analysed following the 4th split. PK-resistant PrP-responsive cells were counted using an automated Zeiss KS Elispot system. Error bars are SD, $n=3$, * = $p < 0.001$, ** = $p < 0.0001$ calculated by t test except for Pacsin2-sh3 data that deviate from a Gaussian distribution, calculated using the non-parametric, *Mann-Whitney* test. Panel a) Knockdown of *Sh3glb1* and *Sept7* show modulatory effects in cell susceptibility to prion propagation relative to non-targeting control GFP-sh2. Data for *Pacsin2* and *Stambp* are inconclusive due to lack of replication of the significant differences in propagation, observed only for one cell line each. Panel b) Hectd2-sh1 and -sh4 knockdown lines for Hectd2 show significant increases in the PrP^{Sc} signal. However, Hectd2-sh3 knockdown line presents a decrease in propagation, which may represent an off-target effect as increased propagation is demonstrated by two Hectd2 knockdown lines.

Results summary

From the SCA, it can be inferred that some of the candidate genes affect cell susceptibility by either serving to increase or decrease propagation when knocked down. The significant difference of *Sh3glb1* relative to controls presents it as a promising candidate in prion propagation although this has not been tested in a second cell line. The SCA has shown that *Sept7* may serve as a genetic modifier of cell susceptibility as two knockdown lines for this gene support an increase in prion propagation. *Pacsin2* and *Stambp* are unlikely to modulate prion propagation or clearance following prion infection although there is insufficient evidence to rule these genes out as factors. Thus the candidate genes do not all affect susceptibility to prion propagation in the same manner suggesting different modes of action may apply. The SCA data for *Hectd2* provides convincing evidence for a modulatory role in cell susceptibility to prion infection. Together, these data provide support for *Hectd2* and specific components of its interactome as genetic modifiers of pathology. These interacting proteins and the molecular networks in which they are placed shed light on pathways that have not been previously implicated in the molecular basis of prion propagation and clearance.

6 Supporting work: Hectd2 knockout and transgenic mouse models - role in incubation time

6.1 Mouse models of Hectd2

Hectd2 knockout and transgenic mouse models were developed and experiments carried out by colleagues at the MRC Prion Unit for which I have analysed the data. Mouse models of prion disease are useful in that they can faithfully recapitulate features of prion disease such as neuropathology and biochemical characteristics. Such models can be exploited to measure incubation times of mice challenged with prions following manipulation of a given candidate gene by knockout or overexpression. Incubation time is defined as the time (in days) from inoculation to the point at which clinical diagnosis of prion disease is made following transmission of a given prion strain.

6.2 Generation of the Hectd2 knockout mice

The *Hectd2* knockout mouse model was generated by inGenious Targeting Laboratory, Inc. Exon 2 of *Hectd2* was targeted for deletion by homologous recombination by constructing a targeting vector from a C57BL/6J BAC clone (RPCI23) in which a neomycin cassette was cloned such that it replaces exon 2 (Figure 6.2.1 a). Exon 2 was selected for deletion because it induces a frameshift mutation that results in a stop codon at the start of exon 3. This was expected to result in the translation of a truncated 103 amino acid protein for *Hectd2*^{-/-} mice (Figure 6.2.1 b and Figure 6.2.2 b), whilst wild type mice express the full length protein of 774 residues (Figure 6.2.1 b and Figure 6.2.2 a). The neomycin cassette was flanked at its 5' and 3' ends by short and long arms that extend ~2.3 kb and ~9.4 kb, which are homologous to the genomic locus into which the construct integrates (Figure 6.2.1 a). The targeting construct was inserted into C57BL/6J embryonic stem cells by electroporation prior to injection into blastocysts from Balb/c mice. The resultant chimeric mice were crossed with wild type C57BL/6J mice until germline transmission was achieved. Heterozygote mice were intercrossed to homozygosity. The

resultant *Hectd2*^{-/-} mice were phenotypically normal, fertile and showed a normal life span.

To confirm correct targeting, PCR amplification of the *Hectd2*^{-/-} genomic region was performed with UNI and A1 primers which bind respectively within the neomycin cassette and outside of the homology region used to create the targeting construct, (Figure 6.2.1 a). This PCR amplification was performed in a duplex reaction with primers Hex2F and Hex2R, shown in Figure 6.2.1 a, that flank exon 2 to amplify exon 2. This amplified a ~2.7 kb region of the *Hectd2* gene inclusive of the ~1.8 kb neomycin cassette that replaced exon 2 (Figure 6.2.1 c), indicating that exon 2 has been deleted. Confirmation of exon 2 deletion at the mRNA transcript level was performed by RT-PCR (Figure 6.2.1 d). PCR amplification was performed on cDNA derived from whole brain RNA extracts of *Hectd2*^{-/-} and wild type C575BL/6J mice, (Figure 6.2.1 d). This amplification was carried out using primers that flank exon 2 (HectSL4F and HectSL4R), depicted in the *Hectd2* sequence schematic in Figure 6.2.2. Bands corresponding to 323 bp were observed for *Hectd2*^{-/-} cDNA indicative of exon 2 deletion (Figure 6.2.1 d). Wild type C57BL/6J mice expressed a transcript containing exon 2 as shown by amplification of a 452 bp band (Figure 6.2.1 d). Correct splicing of the exons was confirmed by sequencing. However, knockout at the protein level remains undetermined owing to an absence of specific anti-Hectd2 antibodies for mouse Hectd2.

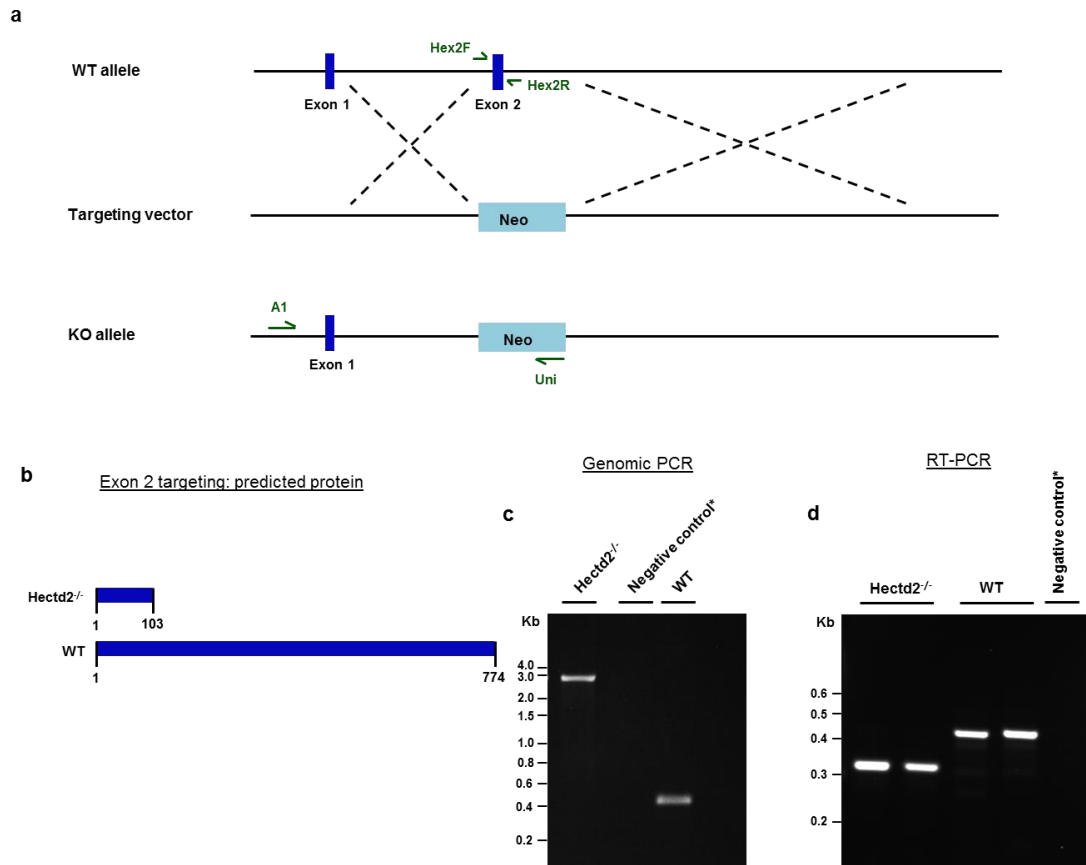


Figure 6.2.1 Construction of targeting allele to generate *Hectd2* knockout mice. a) Exon 2 of *Hectd2* was targeted on a ~15 kb region cloned from C57BL/6J wild type (WT) mice via homologous recombination with the targeting vector pGK-gb2 containing a loxP/FRT-flanked neomycin cassette (~1.8 kb). b) Exon 2 targeting induces a frameshift stop mutation at the start of exon 3 thus translation of the transcript is expected to result in a truncated 103 amino acid protein whilst wild type C57BL/6J mice express the full length 774 residue protein. c) PCR amplification of genomic DNA surrounding exon 2 of *Hectd2* knockout (KO) mice in a duplex reaction using A1/UNI and Hex2F/Hex2R primers, where UNI anneals within the neomycin cassette and A1 anneals 5' to the short homology arm outside the region used to create the targeting construct and Hex2F/Hex2R flank exon 2. The ~2.7 kb band indicates the presence of the neomycin cassette, spanning the region in which exon 2 was deleted. To amplify the region surrounding exon 2 for WT, Hex2F and Hex2R primers were used to amplify a ~480 bp product. *Negative control represents a non-template H₂O control. d) PCR amplification of cDNA derived from *Hectd2* knockout and wild type (C57BL/6J) mouse brains. Lanes 1 and 2 represent separate samples of *Hectd2* knockout mice, for which exons 1, 3 and 4 are amplified (323 bp) while wild type samples show that exons 1, 2, 3 and 4 are amplified (452 bp).

a Wild type C57BL/6J

start
agacatgagtgaggcggctcgggatctctcgcccggagcgcgcgcccggcggtagccgcggccgccccgga
HectSL4F
ggagaggaagggaaagaaccggagcgcgagaagctgccgccatcgtgacggccggcgcagccgcgggc
ttggacagaggaaccaaggccagatttccacctcagcagctttgtctcgactgtcaccagaagaagg
aagctgctgagaacagaagctcgcctaccaccttgctctccctaacaacaggaatgtgagagacctacc
accaatttgtcttgatgtagacaaaaacagcgcgatgtctgtggaagcgttacatctgaagtgaaggtc
ccgccccttcagaaccttctcttcttagccagcccaaaactgtaaagactttgaggaagatttagaaa
aagctgaggccaaggggaattggaagacagtacatgctttttatataacagcatttgattctttcacaga
HectSL4R
actaaactgcatttaag

b *Hectd2*^{-/-}

start
agacatgagtgaggcggctcgggatctctcgcccggagcgcgcgcccggcggtagccgcggccgccccgaggagag
HectSL4F
gaaggggaaagaaccggagcgcgagaagctgccgccatcgtgacggccggcgcagccgcgtgagagacctacca
stop
ccaatttgtcttgatgtagacaaaaacagcgcgatgtctgtggaagcgttacatctgaagtgaaggctccgccc
cttcagaaccttctcttcttagccagcccaaaactgtaaagactttgaggaagatttagaaaaagctgaggcc
acaggggaattggaagacagtacatgctttttatataacagcatttgattctttcacagaactaaactgcattt
HectSL4R
aag

Exon 1|Exon 2|Exon 3|Exon 4

Figure 6.2.2 *Hectd2* mRNA sequence. a) A region of *Hectd2* mRNA sequence is shown with the corresponding coding sections of exons 1-4, with the ‘atg’ start codon highlighted in green. Exon 2 is indicated in red, which was shown to be deleted in cDNA of *Hectd2*^{-/-} mice using the HectSL4F and HectSL4R primers (b). Exon 2 deletion induces a frameshift mutation, creating a ‘tga’ stop codon at the start of exon 3, highlighted in red. Deletion of exon 2 was confirmed by sequencing.

6.3 Transmission of prions to *Hectd2*^{-/-} mice

Hectd2^{-/-} and C57BL/6J control mice were anaesthetised with isoflurane/O₂ and intracerebrally inoculated into the right parietal lobe with three different prion strains. These consisted of two mouse adapted scrapie strains, RML and ME7 and a mouse adapted BSE strain, MRC2^{103, 287}, of which 30 µl of a 1% brain homogenate were inoculated. These strains differ in their glycoform ratios with respect to mono-, di- or unglycosylated PrP^{Sc} following protease digestion. Strain types can be distinguished by Western blot although classically defined by their characteristic incubation times and neuropathological targeting following passage in mice¹⁰³. The RML strain shows an abundance of the mono-glycosylated, low molecular mass glycoform. MRC2 is defined by the presence of predominant di-glycosylated, high molecular mass glycoform and ME7 represents all glycoforms equally^{103, 287}.

The onset of first signs of prion disease and the point at which clinical diagnosis was made i.e. the incubation time, were recorded. Signs of disease onset consisted of piloerection, erect ears, rigid tail, ungroomed appearance, hunched posture or claspings of hind limbs when lifted by the tail. Although these signs are indicative of prion disease, they are not specific to prion disease as they may occur due to alternative reasons such as old age. Diagnostic criteria for clinical prion disease included ataxia, tremor, limb paralysis or loss of righting reflex. Mice were examined daily for the signs of clinical onset and were culled when a definitive diagnosis was made or earlier if mice showed health concerns or signs of distress. Data for male and female mice were obtained and analysed separately as it has been established that sex differences can have a significant effect on incubation time²⁸⁸. Kaplan-Meier survival curves were derived for each group of males and females using GraphPad Prism 6 for which Log-rank (Mantel-Cox) testing was applied. The mean number of days following prion transmission for clinical onset and diagnosis/incubation time data are listed in Table 6.3.1.

Figure 6.3.1 shows the curves for the onset of first signs of clinical symptoms for *Hectd2*^{-/-} and WT mice. RML transmission to *Hectd2*^{-/-} female mice resulted in an 8% reduction in the onset of first signs of clinical symptoms relative to control mice ($p = 0.0001$, log-rank (Mantel-Cox) test, where the mean first signs occur at 138 ± 0 days for *Hectd2*^{-/-} and

150 ± 0 days for WT mice), Figure 6.3.1.a, Table 6.3.1. This difference in the time of onset in *Hectd2*^{-/-} mice relative to WT but not in the time of diagnosis results in an increase in duration of disease until clinical endpoint for *Hectd2*^{-/-} relative to wild type mice (significant at $p = 1.5 \times 10^{-42}$, *t* test, where *Hectd2*^{-/-} had a mean duration of 23 ± 8 days whilst wild type mice showed a duration of 8 ± 2 days). Data for male mice challenged with RML were not available. Table 6.3.1 and Figures 6.3.1 b, c, d and e show the onset times for ME7 and MRC2 transmissions to *Hectd2*^{-/-} and control mice. However, there is a caveat to the MRC2 data because these mice suffered health issues concerning sore skin in the genital area, possibly due to incontinence-related wetness, which may be linked to prion disease. However, as this is not a well characterised sign of prion disease and thus mice could not be definitively diagnosed, these mice were required to be culled early, before a diagnosis of clinical prion disease could be made. Thus we cannot confirm that the onset symptoms were that of prion disease as these animals did not progress to diagnosis because criteria for early signs are not specific for prion disease.

Table 6.3.1 shows that the incubation times for female *Hectd2*^{-/-} and control mice challenged with RML were not statistically significant (Figure 6.3.2 a). ME7 transmission to male or female *Hectd2*^{-/-} and control mice also did not show statistical significance in incubation times (Kaplan-Meier log-rank survival), Figure 6.3.2 b and c.

Table 6.3.1 Mean incubation times for *Hectd2*^{-/-} and WT mice

Prion Strain	Sex	Line (n mice)	Onset of first signs ± SD (days)	p value	Mean incubation time ± SD (days)	p value
RML	Female	<i>Hectd2</i> ^{-/-} (n=17)	138 ± 0	<0.0001	161 ± 8	0.32
		WT (n=17)	150 ± 0		158 ± 2	
	Male	Data not available				
ME7	Female	<i>Hectd2</i> ^{-/-} (n=8)	164 ± 0	0.91	165 ± 1	0.15
		WT (n=13)	164 ± 1		167 ± 4	
	Male	<i>Hectd2</i> ^{-/-} (n=9)	167 ± 2	0.34	175 ± 5	0.21
		WT (n=11)	168 ± 3		175 ± 7	
MRC2	Female	<i>Hectd2</i> ^{-/-} (n=16)*	179 ± 6	0.28*	178 ± 6 [†] (n=4)	n/a [†]
		WT (n=10)*	177 ± 4		186, 175 [†] (n=2)	
	Male	<i>Hectd2</i> ^{-/-} (n=6)*	174 ± 4	0.72*	186 [†] (n=1)	n/a [†]
		WT (n=15)*	173 ± 1		180 ± 4 [†] (n=12)	

Statistical analyses were performed using Kaplan-Meier log-rank (Mantel-Cox) tests (GraphPad Prism 6).

*Group sizes include animals that showed multiple early (non-specific) signs of prion disease but did not progress to a confirmed diagnosis due to intercurrent health problems. †Statistical testing was not performed

for diagnosis times as sample sizes were too small due to culling of animals before a diagnosis could be made, (shown by n/a = not applicable).

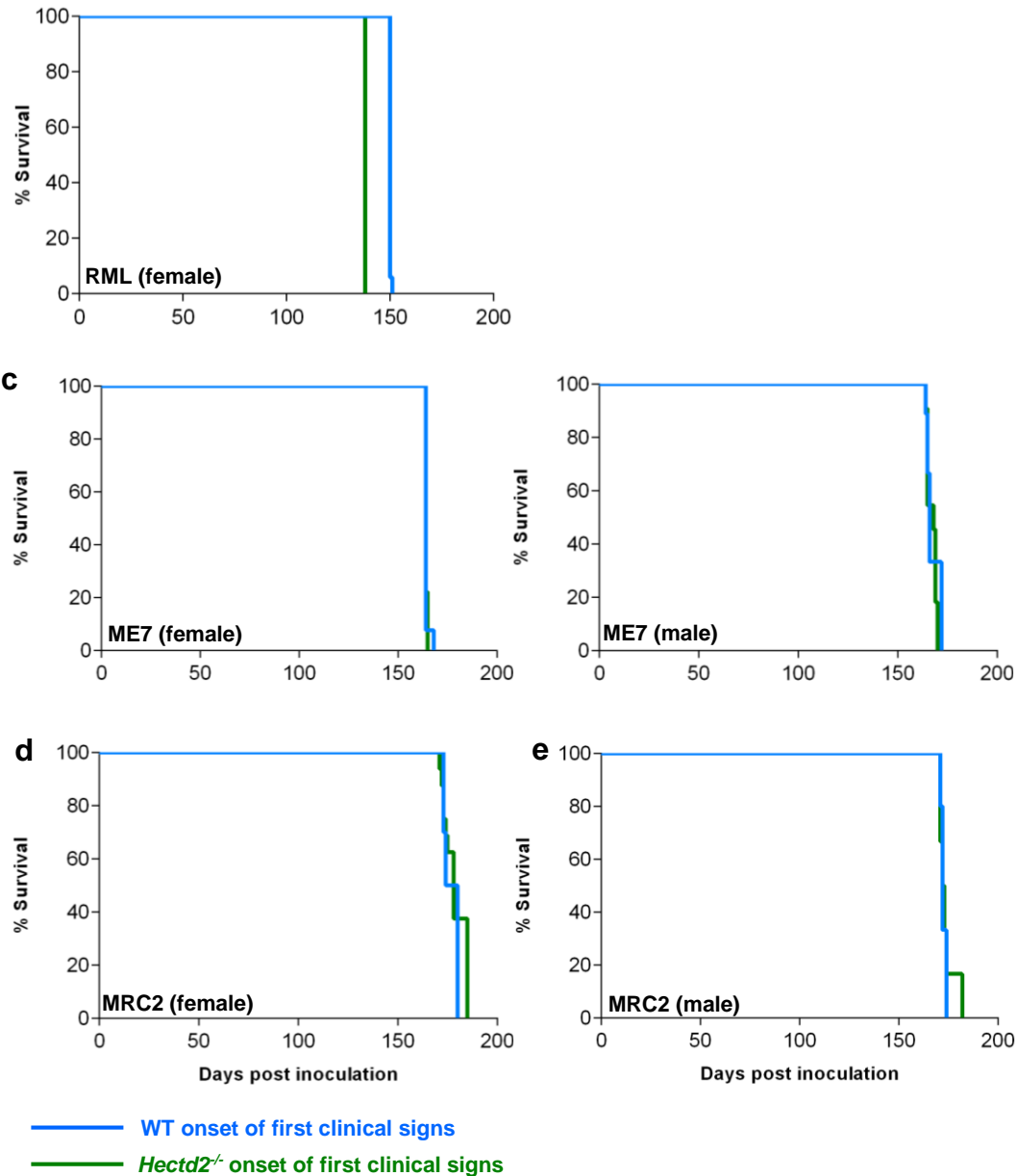


Figure 6.3.1 Kaplan-Meier curves for onset of first clinical signs for *Hectd2* knockout mice. Wild type and *Hectd2*^{-/-} mice were challenged with RML, ME7 and MRC2 prions and the first signs of disease onset plotted as the percentage of surviving animals against the number of days post inoculation. a) Shows the onset times for female *Hectd2*^{-/-} and wild type (WT) following transmission of RML ($p < 0.0001$, Log-rank (Mantel-Cox) test). Data for male mice were unavailable. b) and c) Show the onset times for *Hectd2*^{-/-} and wild type mice following transmission of ME7 prions. d) and e) Show onset times following transmission of MRC2 prions to *Hectd2*^{-/-} and wild type mice. The group size includes animals that showed multiple early (non-specific) signs of prion disease but did not progress to a confirmed diagnosis due to health problems. Only onset data for RML transmission in female mice was statistically significant according to Kaplan-Meier log-rank (Mantel-Cox) test (GraphPad Prism 6).

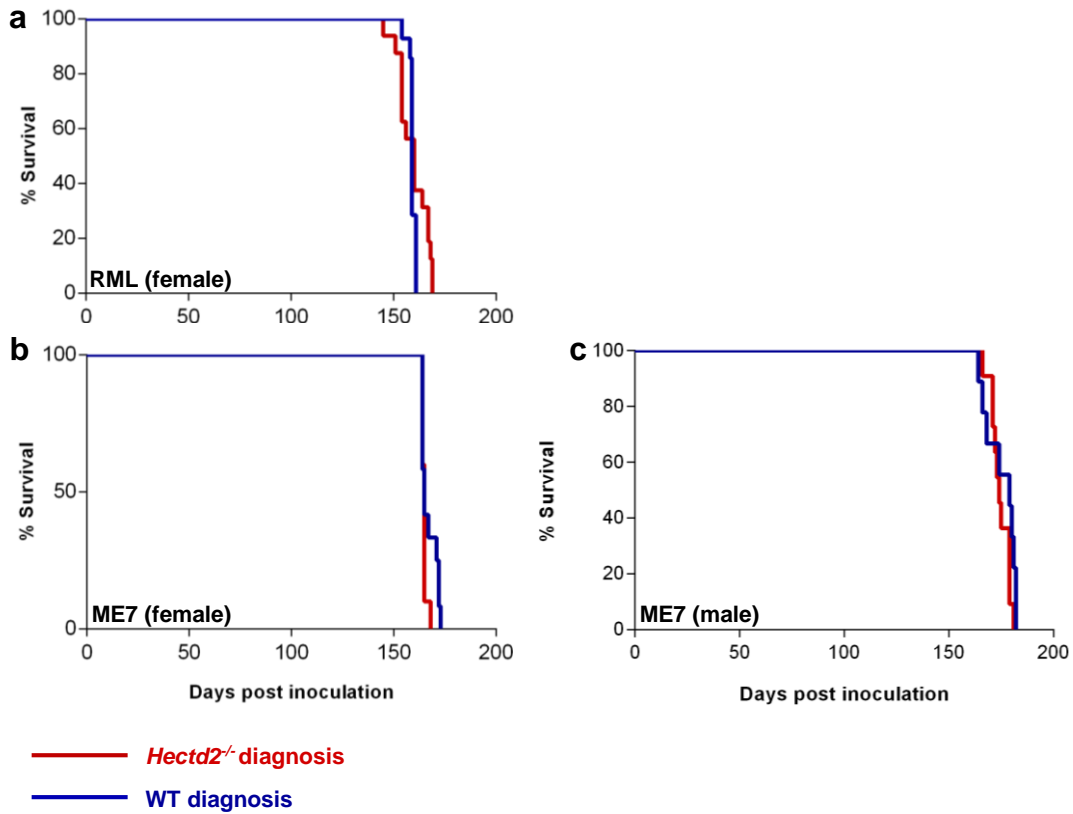


Figure 6.3.2 Kaplan-Meier survival curves for *Hectd2* knockout mice. Wild type and *Hectd2*^{-/-} mice were challenged with RML, ME7 and MRC2 prions and plotted as the percentage of surviving animals against the number of days post inoculation. a) Shows diagnosis of disease for *Hectd2*^{-/-} and wild type (WT) mice defined as the incubation time following transmission of RML. Data for male mice were unavailable. b) and c) show diagnosis of ME7 transmission to *Hectd2*^{-/-} and wild type mice. Incubation time data for MRC2 transmission to *Hectd2*^{-/-} and wild type mice are not shown due to small sample sizes as some mice were culled due to health concerns before a diagnosis of clinical disease could be made (see Table 6.3.1).

6.4 Generation of *Hectd2*-overexpressing mice (*Tg260*^{+/+})

The *Hectd2* ORF was amplified from cDNA derived from brains of C57BL/6J mice, onto which the *SalI* and *XhoI* restriction sites were engineered. This was to facilitate cloning into the cosmid vector SHaCosTt, in which expression is driven by the hamster PrP promoter⁸⁶. The construct was inserted into F2 CBA x C57BL/6J fertilised eggs by pronuclear microinjection and implanted into an F1 CBA x C57BL/6 recipient mother²⁸⁹. One founder was identified by screening genomic DNA extracted from tail biopsies by

PCR. The founder was bred to FVB/NHsd mice to establish the colony from which heterozygotes were generated. Wild type and homozygote mice were produced by intercrossing heterozygotes, which were subsequently distinguished by quantitative PCR. The resultant Tg260 mouse line thus was of a mixed genetic background comprised of CBA, C57BL/6J and FVB. Mixed genetic backgrounds provide less power to detect small differences and thus identification of small changes may be obscured. The level of mRNA expression of *Hectd2* overexpressing mice was determined by real time RT-PCR, for which heterozygotes (Tg260^{+/-}) were found to overexpress *Hectd2* mRNA two fold relative to endogenous levels (Figure 6.4.1). Although Tg260^{+/+} mice were not tested for *Hectd2* expression, by extrapolation it is anticipated that they may overexpress by 4 fold.

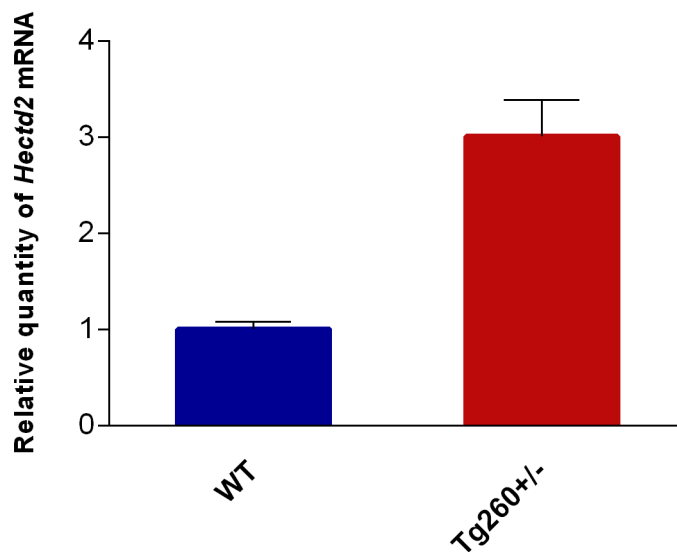


Figure 6.4.1 Relative expression of *Hectd2* overexpressing, Tg260, heterozygous mice. Expression levels of *Hectd2* mRNA derived from the brains of wild type and Tg260^{+/-} mice were measured by quantitative RT-PCR, relative to an endogenous control, *GAPDH*. The quantity of *Hectd2* expressed by heterozygous mice was normalised to that expressed by wild type C57BL/6J mice, showing that Tg260^{+/-} show a 2-fold relative expression of *Hectd2*. Group sizes for Tg260^{+/-} are n=6 and 3 technical replicates for each, WT controls n=4 with 3 technical replicates ($p = 1 \times 10^{-5}$, *t* test).

6.5 Transmission of prions to *Hectd2*-overexpressing transgenic mice

Tg260^{+/+} mice overexpressing *Hectd2* and littermate wild type controls Tg260^{-/-} were challenged with RML and ME7 prions in addition to a mouse adapted BSE strain, MRC2^{103, 287}. Table 6.5.1 details the averages for the first signs of clinical onset and the mean diagnosis/incubation time. Figure 6.5.1 panels a-e show the onset of first signs for female and male Tg260^{+/+} mice and their respective controls to which RML, ME7 or MRC2 prions were transmitted. These mice showed no statistical differences with respect to their onset times relative to those shown by control mice (Kaplan-Meier log-rank (Mantel-Cox) tests).

Figure 6.5.2 a, c and e shows the survival curves for RML, ME7 or MRC2 transmission in female mice, for which there are no significant differences between incubation times (Kaplan-Meier log-rank (Mantel-Cox) test). Similar data were observed for male mice for RML and MRC2 strains. However, transmission of ME7 to male Tg260^{+/+} mice showed a 13% reduction in incubation time (160 ± 11 days relative to wild types, 181 ± 21 days). This incubation time was significant at $p = 0.004$ log-rank (Mantel-Cox) test, Table 6.5.1 and Figure 6.5.2 d. However, to account for the effects of multiple testing, a Bonferroni correction was applied to bring the 5% significance level to $p < 0.003$. This reduction in incubation time for male Tg260^{+/+} mice to which ME7 was transmitted thus does not reach the significance level and may be considered of border line significance.

Table 6.5.1 Mean incubation times for *Hectd2*-overexpressing (Tg260^{+/+}) and WT mice

Prion Strain	Sex	Line (n mice)	Onset of first signs \pm SD (days)	p value	Mean incubation time \pm SD (days)	p value
RML	Female	Tg260 (n=13)	149 \pm 10	0.53	156 \pm 7	0.08
		WT (n=11)	149 \pm 8		165 \pm 14	
	Male	Tg260 (n=9)	149 \pm 10	0.96	164 \pm 15	0.44
		WT (n=12)	151 \pm 10		160 \pm 12	
ME7	Female	Tg260 (n=11)	159 \pm 10	0.36	173 \pm 11	0.11
		WT (n=13)	154 \pm 1		169 \pm 6	
	Male	Tg260 (n=10)	140 \pm 11	0.33	160 \pm 11	0.004
		WT (n=10)	151 \pm 30		181 \pm 21	
MRC2	Female	Tg260 (n=12)	163 \pm 13	0.05	182 \pm 12	0.30
		WT (n=12)	177 \pm 20		188 \pm 15	
	Male	Tg260 (n=8)	146 \pm 32	0.60	182 \pm 10	0.96
		WT (n=12)	155 \pm 9		181 \pm 9	

Statistical analyses were performed using Kaplan-Meier log-rank (Mantel-Cox) tests (GraphPad Prism 6).

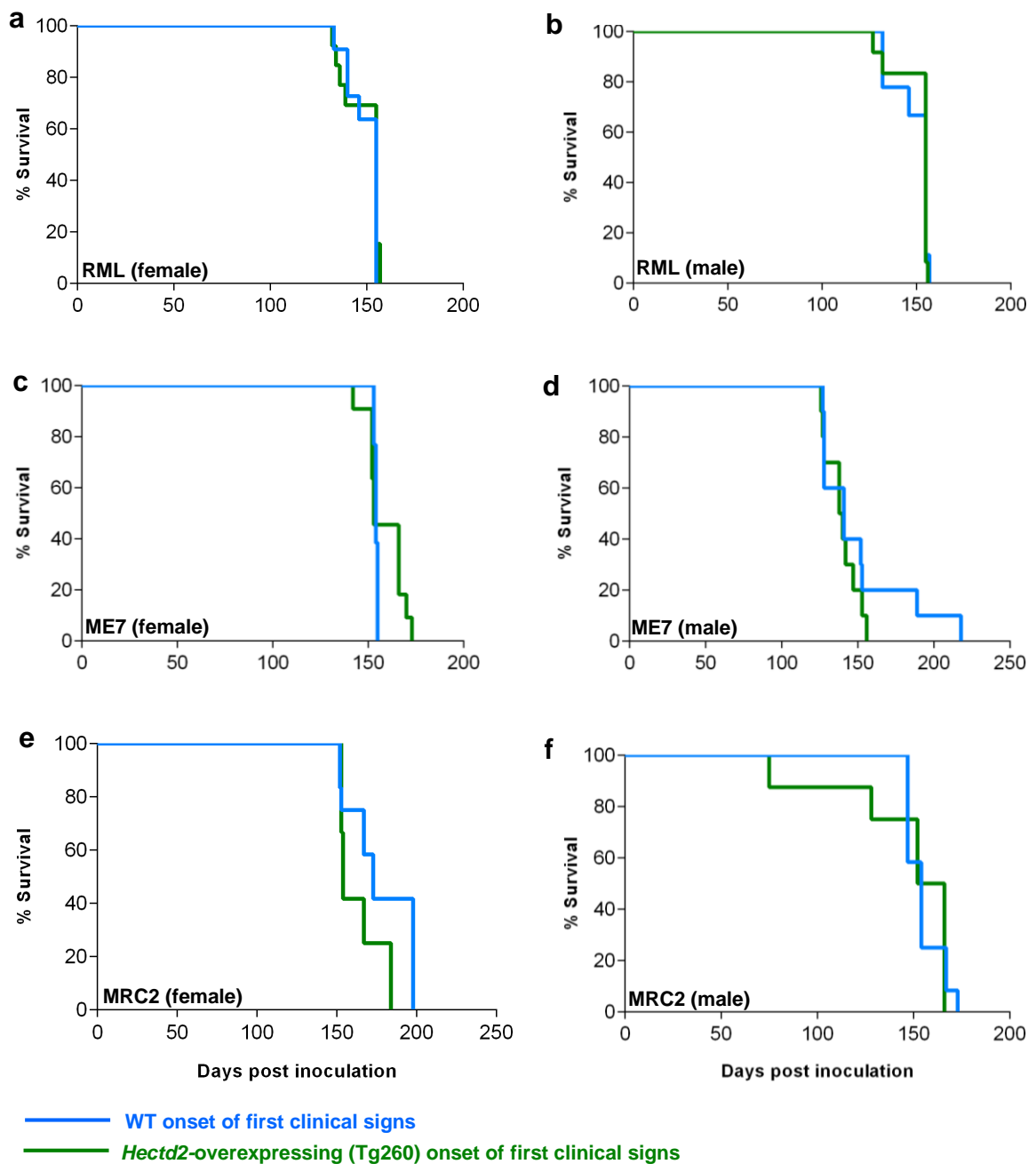


Figure 6.5.1 Kaplan-Meier curves for onset of first clinical signs for Tg260, *Hectd2*-overexpressing mice. Wild type and Tg260^{+/+} mice were challenged with RML, ME7 and MRC2 prions and the first signs of disease onset plotted as the percentage of surviving animals against the number of days post inoculation. a) and b) Show the onset times for female and male Tg260^{+/+} and wild type (WT) mice following transmission of RML. c) and d) Show the onset times for Tg260^{+/+} and wild type mice following transmission of ME7 prions. e) and f) Show onset times for transmission of MRC2 prions to Tg260^{+/+} and wild type mice. Onset times for transmission with any prion strain were not statistically significant according to Kaplan-Meier log-rank (Mantel-Cox) test (GraphPad Prism 6).

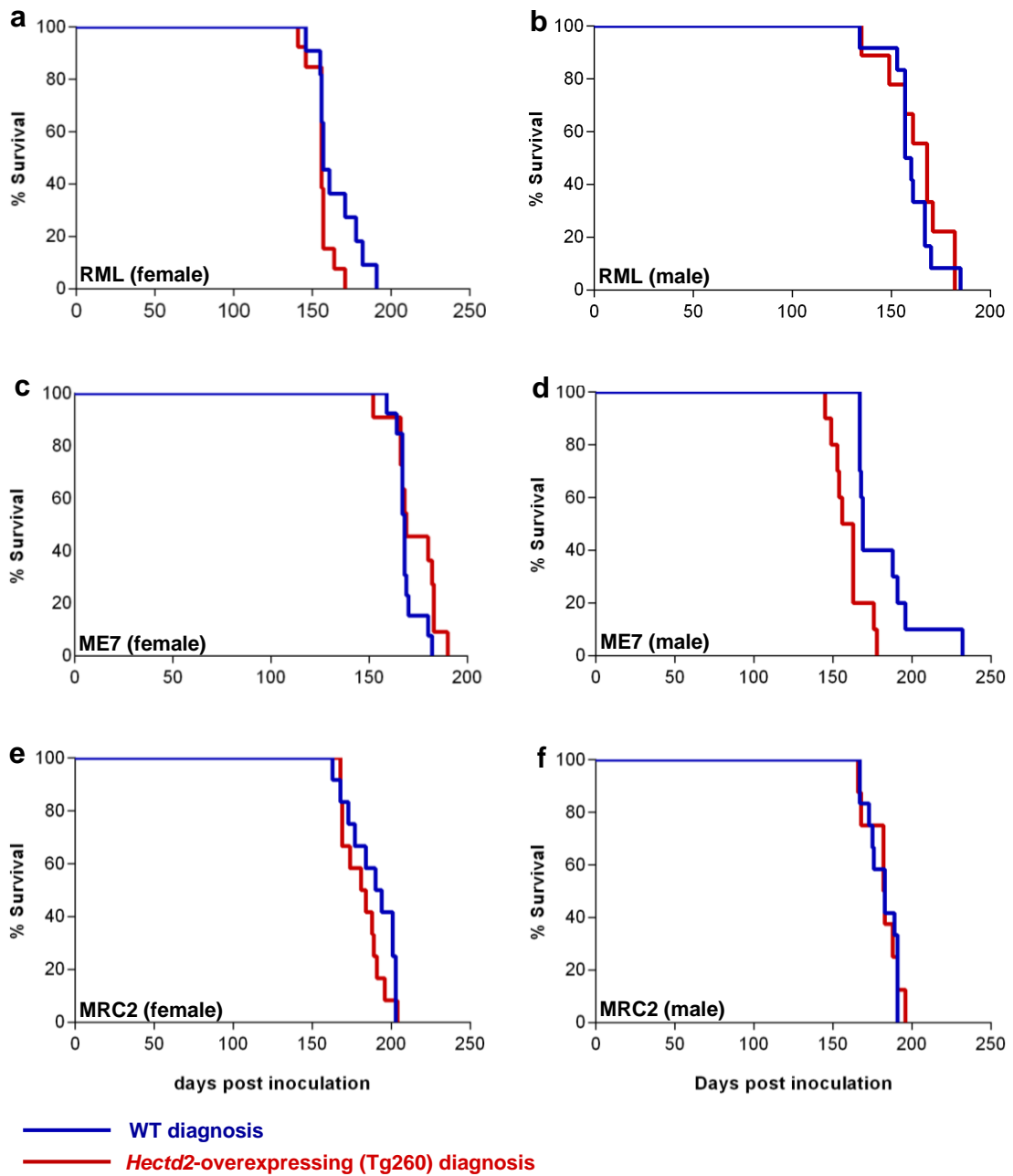


Figure 6.5.2 Kaplan-Meier survival curves for Tg260, *Hectd2*-overexpressing mice. Wild type and Tg260^{+/+} mice were challenged with RML, ME7 or MRC2 prions. Data are plotted as the percentage of surviving animals against the number of days post inoculation. Panels a-f show the incubation times for Tg260^{+/+} and wild type (WT) defined here as the point of diagnosis of disease following transmission of RML for female and male mice. a) and b) show transmission of RML to Tg260^{+/+} and wild types. c) and d) show ME7 transmission for which male Tg260^{+/+} incubation time ($p = 0.004$, log-rank (Mantel-Cox) test), which is borderline significance following Bonferroni correction at the 5% significance level. e) and

f) show transmission of MRC2 prions to Tg260^{+/+} and wild type female and male mice. Data were analysed using the Kaplan-Meier log-rank (Mantel-Cox) test).

6.6 Prion strains in infected mouse brains and histology

In order to check if the modification of *Hectd2* expression affects the strain type and that the prion strains that were inoculated retained their strain properties following propagation, Western blot analyses was performed on brains of infected animals. Figure 6.6.1 shows the strain patterns of PrP^{Sc} for RML, ME7 and MRC2 prions transmitted to *Hectd2*^{-/-} or Tg260^{+/+} mice, left and right panels respectively. Although not quantitative, the ratios appear to show the characteristic strain pattern typical of RML, ME7 and MRC2^{103, 287}. This suggests that the strains did not change PrP^{Sc} type following replication in wild type mice or in the experimental model.

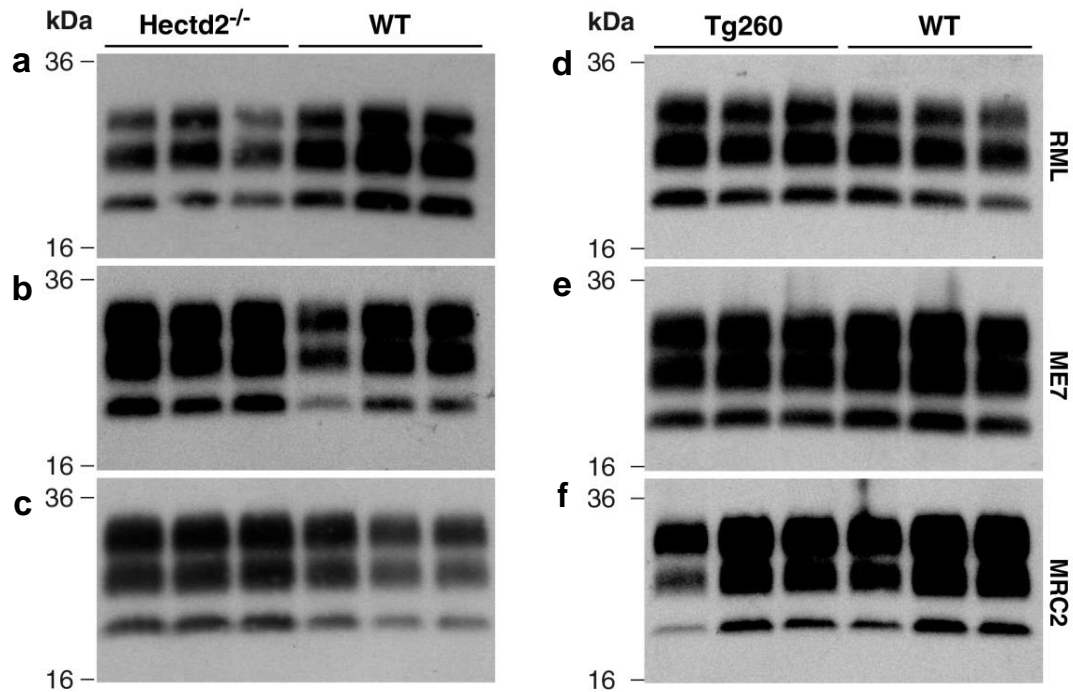


Figure 6.6.1 PrP^{Sc} type determination from infected mouse brains. 10% w/v of *Hectd2*^{-/-} or Tg260^{+/+} (*Hectd2*-overexpressing) brain homogenates (n = 3 for each mouse line) were treated with proteinase K. The digested proteins were immunoblotted with anti-PrP ICSM35. a) Transmission of RML to *Hectd2*^{-/-} and wild type C57BL/6J mice. b) Transmission of ME7 to *Hectd2*^{-/-} and wild type C57BL/6J mice. c) Transmission of MRC2 to *Hectd2*^{-/-} and wild type C57BL/6J mice. d) Transmission of RML to Tg260^{+/+} and wild type mice. e) Transmission of ME7 to Tg260^{+/+} and wild type mice. f) Transmission of MRC2 to Tg260^{+/+} and wild type mice. No differences in prion strains were observed between *Hectd2*^{-/-} or Tg260^{+/+} over-expressors and their respective controls.

Histopathological analyses were performed on brain sections from *Hectd2*^{-/-}, Tg260^{+/+}, and their respective wild type controls for each prion strain transmitted (Figures 6.6.2 – 6.6.7). These sections were derived from brains taken at the end stage of disease. The pattern of PrP^{Sc} deposition, neuronal loss and spongiosis was similar between *Hectd2*^{-/-} and wild type mice for each transmission. Figure 6.6.2 shows the histopathology in *Hectd2*^{-/-} and WT mice challenged with RML, for which mild spongiform degeneration in the thalamus and neuronal loss in the hippocampus were observed, typical of RML transmissions. Figure 6.6.3 shows characteristic ME7 transmission in that mild neuronal loss in the hippocampus and very mild spongiform degeneration in the thalamus were observed in wild type mice and similar changes were seen in *Hectd2*^{-/-} mice also challenged with ME7.

Evaluation of MRC2 transmissions found that in wild type mice, mild spongiform degeneration in the thalamus and moderate neuronal loss in the hippocampus was observed (Figure 6.6.4). *Hectd2*^{-/-} transmission of MRC2 showed similar spongiform changes in the thalamus and similar neuronal loss (Figure 6.6.4). Transmission of RML to Tg260^{+/+} and wild type mice showed mild neuronal loss and mild spongiosis (Figure 6.6.5). Transmission of ME7 to Tg260^{+/+} and wild type mice showed variable neuronal loss and spongiosis (Figure 6.6.6). MRC2 transmissions to Tg260^{+/+} and wild type mice showed severe neuronal loss and variable spongiosis (Figure 6.6.7). However, overall, neuropathologic examination found that there were no clear differences between the two groups of mice for a given prion strain.

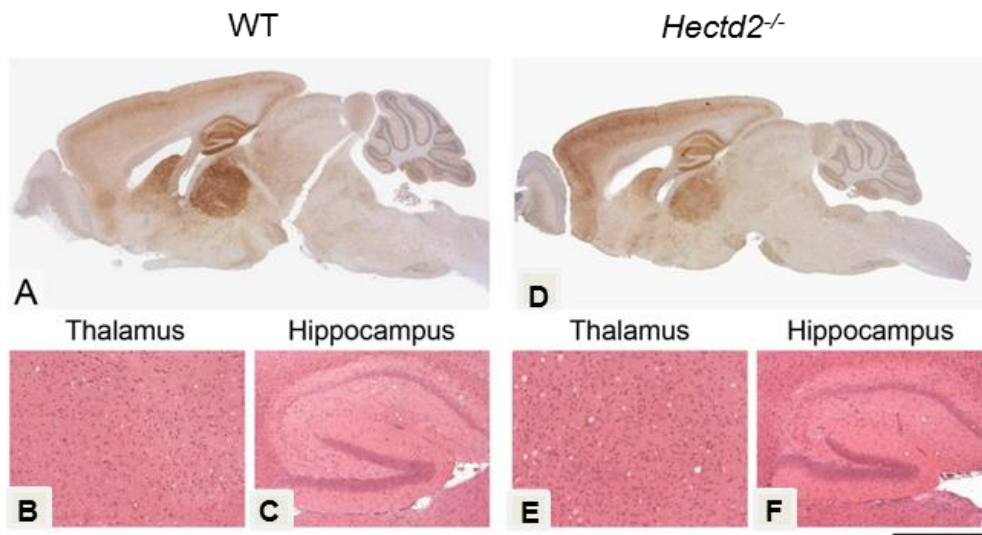


Figure 6.6.2 RML transmission to *Hectd2*^{-/-}: histological analysis. Histological features of RML transmission to wild type C57BL/6J controls (A-C) and *Hectd2*^{-/-} (D-F). Panels A and D show the distribution of PrP^{Sc} using immunohistochemistry with anti-PrP ICSM35 monoclonal antibody. Panels B, C, E and F were stained with haematoxylin and eosin to show spongiform degeneration and neuronal loss in the thalamus and hippocampus. There appears to be no differences in the pattern of PrP distribution and spongiosis between wild type and *Hectd2*^{-/-} mice. Scale bar corresponds to 3 mm (A, D), 330 μ m (B, E) and 660 μ m (C, F).

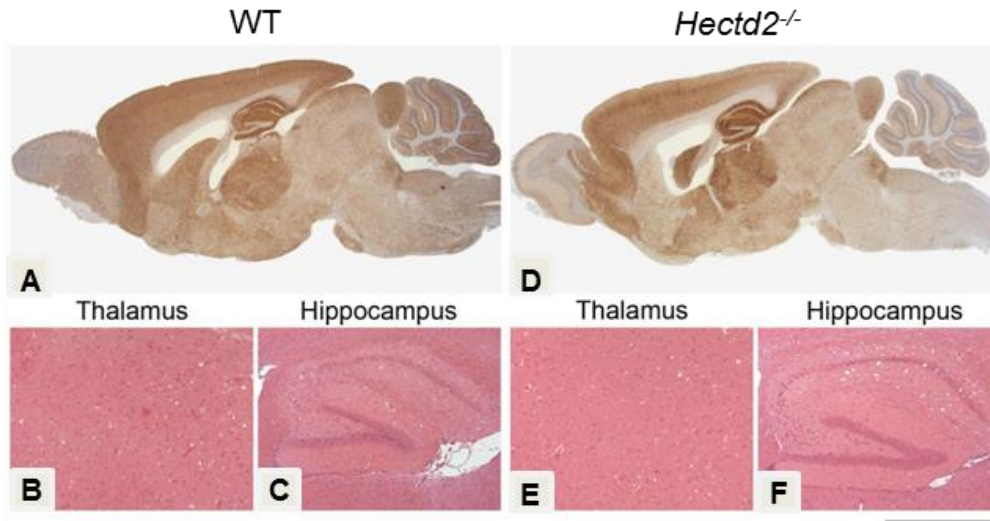


Figure 6.6.3 ME7 transmission to *Hectd2*^{-/-}: histological analysis. Histological features of ME7 transmission to wild type C57BL/6J controls (A-C) and *Hectd2*^{-/-} (D-F). Panels A and D show the distribution of PrP^{Sc} using immunohistochemistry with anti-PrP ICSM35 monoclonal antibody. Panels B, C, E and F were stained with haematoxylin and eosin to show spongiform degeneration and neuronal loss in the thalamus and hippocampus. The pattern of PrP distribution, degree of neuronal loss and spongiosis are similar between wild type and *Hectd2*^{-/-} mice. Scale bar corresponds to 3 mm (A, D), 330 μ m (B, E) and 660 μ m (C, F).

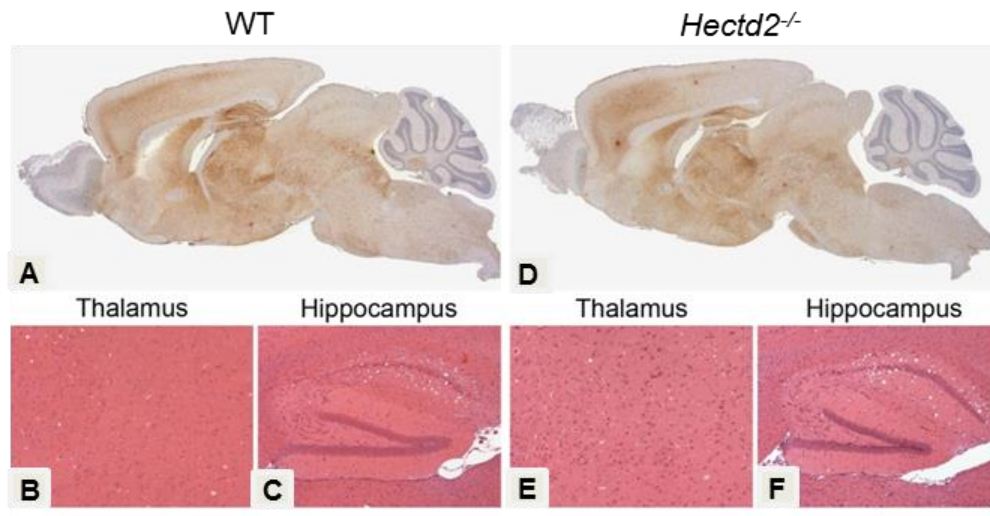


Figure 6.6.4 MRC2 transmission to *Hectd2*^{-/-}: histological analysis. Histological features of MRC2 transmission to wild type C57BL/6J controls (A-C) and *Hectd2*^{-/-} (D-F). Panels A and D show the distribution of PrP^{Sc} using immunohistochemistry with anti-PrP ICSM35 monoclonal antibody. Panels B, C, E and F were stained with haematoxylin and eosin to show spongiform degeneration and neuronal loss in the thalamus and hippocampus. Overall, there are no differences in the pattern of PrP distribution and

spongiosis between wild type and *Hectd2*^{-/-} mice following transmission of MRC2. Scale bar corresponds to 3 mm (A, D), 330 μ m (B, E) and 660 μ m (C, F).

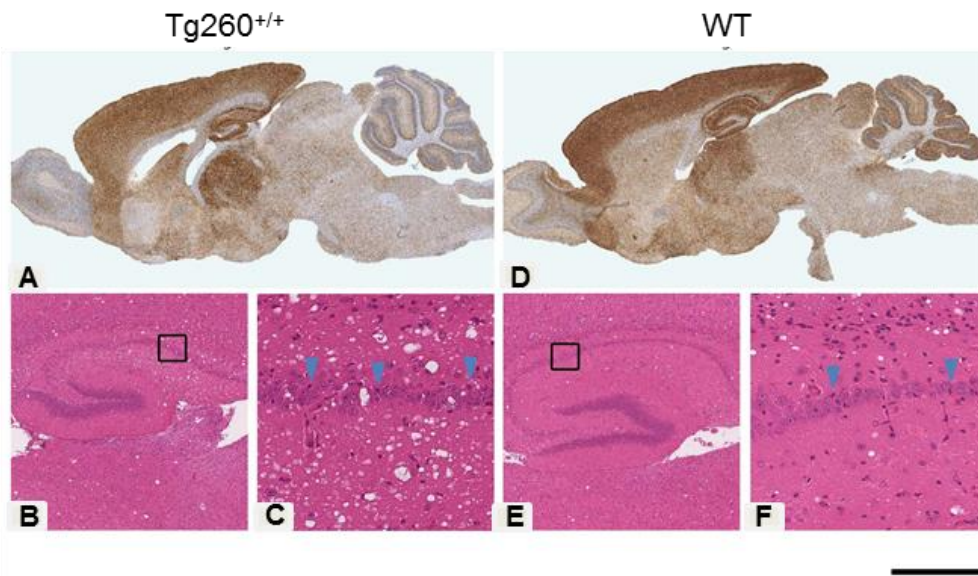


Figure 6.6.5 RML transmission to Tg260^{+/+}: histological analysis. Histological features of RML transmission to Tg260^{+/+} (A-C) and wild type controls (D-F). Panels A and D show the distribution of PrP^{Sc} using immunohistochemistry with anti-PrP ICSM35 monoclonal antibody. Panels B, C, E and F were stained with haematoxylin and eosin to show spongiform degeneration and neuronal loss in the hippocampus. C and F show detail from the hippocampus (inset in B and E, respectively). Arrows indicate apoptotic cells. There appears to be no differences in the pattern of PrP distribution and spongiosis between wild type and Tg260^{+/+} mice. Scale bar corresponds to 2 mm (A, D), 400 μ m (B, E) and inset (C, F) is 100 μ m.

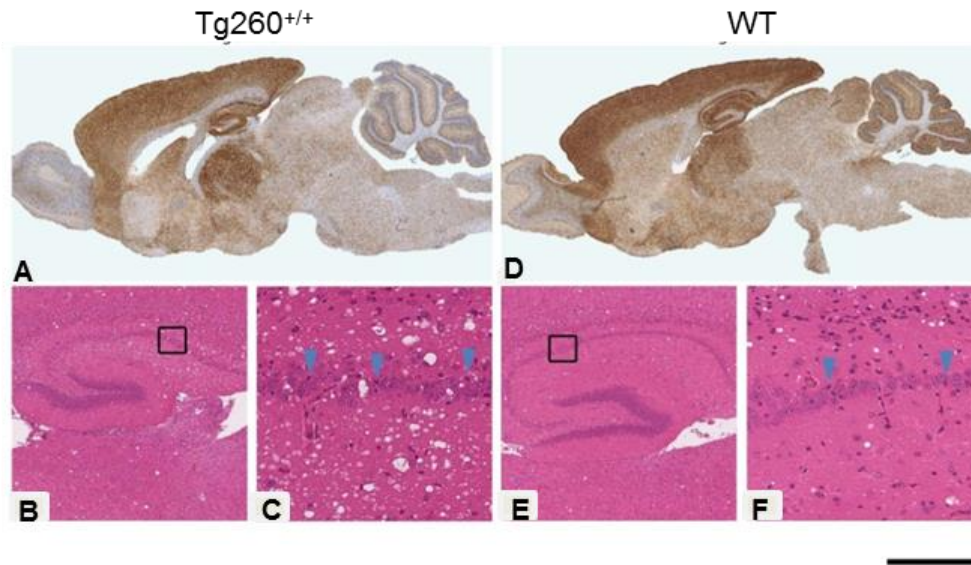


Figure 6.6.6 ME7 transmission to Tg260^{+/+}: histological analysis. Histological features of ME7 transmission to Tg260^{+/+} (A-C) and wild type controls (D-F). Panels A and D show the distribution of PrP^{Sc} using immunohistochemistry with anti-PrP ICSM35 monoclonal antibody. Panels B, C, E and F were stained with haematoxylin and eosin to show spongiform degeneration and neuronal loss in the hippocampus. C and F show detail from the hippocampus (inset in B and E, respectively). Arrows indicate apoptotic cells. There appears to be no differences in the pattern of PrP distribution and spongiosis between wild type and Tg260^{+/+} mice. Scale bar corresponds to 2 mm (A, D), 400 μ m (B, E) and inset (C, E) is 100 μ m.

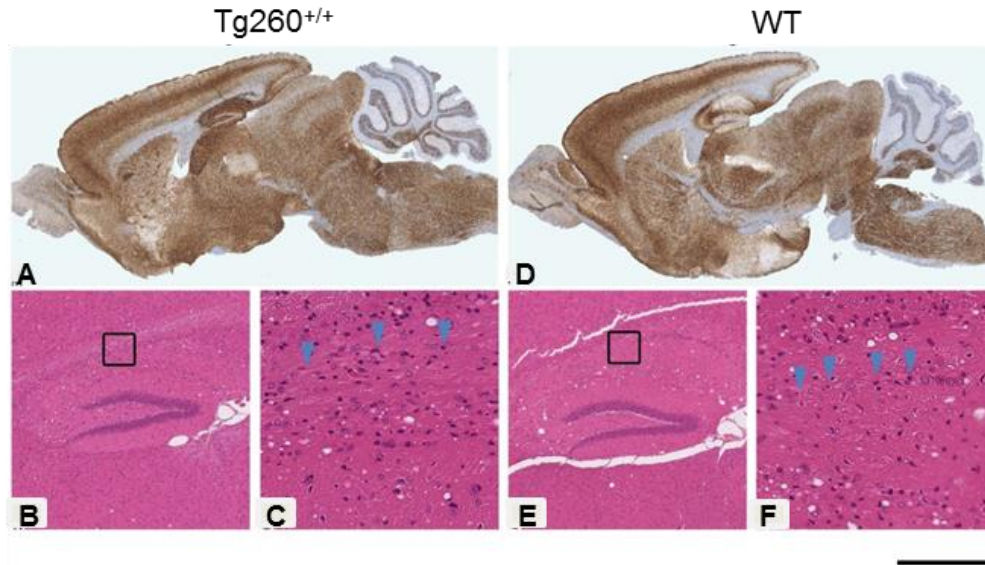


Figure 6.6.7 MRC2 transmission to $Tg260^{+/+}$: histological analysis. Histological features of MRC2 transmission to $Tg260^{+/+}$ (A-C) and wild type controls (D-F). Panels A and D show the distribution of PrP^{Sc} using immunohistochemistry with anti- PrP ICSM35 monoclonal antibody. Panels B, C, E and F were stained with haematoxylin and eosin to show spongiform degeneration and neuronal loss in the hippocampus. C and F show detail from the hippocampus (inset in B and E, respectively). Arrows indicate apoptotic cells. There appears to be no differences in the pattern of PrP distribution and spongiosis between wild type and $Tg260$ mice. Scale bar corresponds to 2 mm (A, D), 400 μ m (B, E) and inset (C, F) is 100 μ m.

Results summary

The data show that incubation times were not modified by *Hectd2* deficient mice, although the duration of disease and the first signs of clinical symptoms differed statistically for RML transmission to female *Hectd2*^{-/-} relative to wild type mice, suggestive of a protective role for *Hectd2*. Transgenic overexpressing *Hectd2* ($Tg260^{+/+}$) mice showed that females did not modify incubation time with any strain of prion. However, male $Tg260^{+/+}$ to which ME7 prions were transmitted, decreased incubation time by 13% relative to wild type mice. However, taking into consideration the effects of multiple testing, this did not reach the significance level required for it be considered a real effect but is suggestive that *Hectd2* may serve a modulating role. This was not replicated for female $Tg260^{+/+}$ mice and nor for any other prion transmissions. Together these data show that *Hectd2* does not modulate genetic susceptibility to incubation time universally but may have an effect in a strain and sex dependent manner.

7 Discussion

7.1 Discovery of novel candidate interactors of Hectd2

Prion diseases are fatal neurodegenerative diseases, characterised by a clinically silent incubation period that can exceed 50 years in humans¹⁹. This variability has been attributed to a number of factors, with genetic composition serving a major role. *Hectd2* was identified as one of these genes using the Northport Heterogeneous stock of mice, by which it was found to be linked to prion disease incubation time¹²⁰. Further analysis showed a significant upregulation of *Hectd2* at the terminal stage of disease in prion-infected mouse brains relative to normal brains, which may be suggestive of a protective role. The authors performed a human association study and identified an association between *HECTD2* haplotypes and susceptibility to the acquired human prion diseases, vCJD and kuru¹²⁰. This was the first demonstration of a mouse incubation time candidate gene that influences susceptibility to human prion diseases. Thus the functional analysis of such genes and the molecular networks in which they lie, may shed light on the underlying mechanism of incubation period and outline new targets for therapy.

The data presented in this thesis have attempted to characterise Hectd2 with respect to its possible roles in prion pathology. By homology to other family members, Hectd2 is an HECT E3 ubiquitin ligase, with no other functional information assigned¹⁶². E3 ubiquitin ligases are enzymes that determine the fate of a protein at the post-translational level by ubiquitination¹⁶⁰. Ubiquitination regulates a plethora of cellular processes including protein quality control via proteasome or autophagy-mediated degradation, cell cycle, transcription, DNA repair, apoptosis, endocytosis and trafficking of transmembrane proteins by serving as a signal for downstream effectors to direct its fate^{160, 162, 165}. E3 ligases have been implicated in the pathogenesis of a number of neurodegenerative diseases, including Parkinson's, Alzheimer's and polyglutamine diseases^{230, 237, 290-292}. Thus E3 ligases in concert with their target substrates are important in orchestrating the downstream pathways that they operate in, deregulation of which may underlie pathogenesis. The discovery of Hectd2 as a candidate gene that modulates prion disease

incubation time substantiates the role of E3 ligases in neurodegeneration. In order to gauge an understanding of the underlying mechanism by which prion pathogenesis is affected, a functional analysis of Hectd2 is required to delineate the downstream processes that it governs.

The yeast two-hybrid system was selected to initiate a screen to search for candidate interactors of Hectd2 as prior knowledge of its binding partners is not required. The use of yeast as a host for screening provides an *in vivo* environment that has a greater relative resemblance to mammalian systems than a bacterial host. The N-terminal region of E3 ligases is thought to dictate the substrate specificity of a given ligase^{162, 172}. Thus for Hectd2, the 414 residues preceding the HECT domain, i.e. the putative substrate binding domain which was termed Hect414, was used to screen for interactors of Hectd2.

The yeast two-hybrid system was successfully applied to yield an initial 130 positive colonies bearing candidate binding partners of Hectd2. Large-scale screening assays typically capture false positive interactors and the yeast two-hybrid system is no exception in this regard²⁹³. Prey proteins that were detected may activate the reporter genes autonomously in the absence of the Hectd2 bait. Furthermore colonies identified as containing a positive interaction may indeed harbour more than one prey protein, where only one prey protein may actually be responsible for the two hybrid interaction with Hectd2. Such false interactors were eliminated by a series of additional screening levels. Transfer of all the positive colonies to a higher stringency selection media sustained only 35 of the 130 colonies. End sequencing of each isolated prey plasmid identified five of these candidates as duplicates. This was followed by comprehensive sequencing, which identified that one candidate, *Nrp1*, was not in frame with the GAL4 AD, thereby producing a spurious non-functional protein. *Nt5dc3*, also did not reach the next level of screening as it was found to be a match to the 3' UTR rather than the coding section, which was subsequently identified as a false positive, when co-expressed with Hect414 independently of the library screen, thereby providing confidence in the screening methods applied. The prey cDNA for another candidate was identified as a match to the genomic region on chromosome 15, position 832157 – 832830 rather than an mRNA

transcript. It is possible that this may represent a new cDNA sequence that is not available in the database or perhaps it may be the result of genomic contamination of the library. Although it may be premature to eliminate this candidate at this stage, the main purpose of the search for Hectd2 substrates is to identify those candidates that are involved in prion disease. Due to the lack of information available for this candidate, the decision was made to not include it in the follow-up analyses as more promising candidates were available for investigation. The remaining 27 candidates were subjected to independent co-transformation experiments to ascertain whether the interactions captured by the library screen were maintained in yeast expressing both the prey and Hectd2. Each candidate was also tested for its potential to autonomously activate the reporter genes, of which 7 autoactivators were found. This generated a final list of 20 novel putative binding partners of Hectd2.

These candidates represent proteins of a number of different molecular pathways and some that may be implicated in related pathways such as autophagy and endocytic trafficking where Sh3glb1 and Stambp serve roles in both of these functions^{266, 267, 280-282}. Pacsin2 and Stmn2 are implicated in the regulation of microtubule stability, however, whether their functions are complementary or redundant is not yet known^{146, 273}. Sept7 is a cytoskeletal GTPase that is required for normal organisation of the actin cytoskeleton^{276, 277, 294}. It is possible that Hectd2 has a predominant role in autophagy and cytoskeletal maintenance as the functions of a number of the interactions identified include those that are implicated in these pathways. For example, G protein beta subunit-like (Gbl) also known as mLST8, is a component of the mTOR complexes 1 and 2 (mTORC1 and mTORC2, respectively), of which autophagy and regulation of the actin cytoskeleton are downstream pathways^{295, 296}. The Hectd2 candidate interactor, Cop9 subunit 4, is a component of the Cop9 signalosome, an evolutionary conserved multi-protein complex for which functions are still being determined. Recent work has identified that the Cop9 signalosome regulates proteasome-mediated degradation as well as autophagy²⁹⁷. Yeast two-hybrid screening also identified the candidates, Ppp2ca and Strn3, which also interact with each other; Strn3 forms a regulatory unit of Ppp2a, which directs the downstream activity of Ppp2ca²⁹⁸. Ppp2ca is a serine/threonine phosphatase that regulates a plethora

of processes including gene transcription, protein translation, cell growth and apoptosis and most interestingly it serves a regulatory role in neuronal autophagy^{299, 300}. However, the majority of the candidate genes do not have clearly defined functions and thus it is difficult to group the remaining candidates into functionally related pathways. Whether Hectd2 interacts with all 20 of these proteins is yet to be determined, but this is plausible because E3 ligases regulate the specificity of a multitude of processes, which are mediated through interaction with their substrates¹⁶². Whilst Hectd2 may have substrates outside of the CNS, it is expected that those interactions that occur within the CNS may be implicated in prion pathology based on disease topography and it is expected that very few of these interactions will show a modulatory role in disease.

It is also of note that the genes listed in Table 3.6.1 may not represent a comprehensive list of Hectd2 interactions formed *in vivo*. This is because the two-hybrid system relies on nuclear targeting of bait and prey proteins to activate the GAL4 responsive reporter genes, which may be challenged if a prey protein harbours a strong non-nuclear or extracellular signal. The candidate prey proteins may only be expressed in a specific cell compartment or interact with Hectd2 in a given subcellular location, which may define the interactions that it makes. It may be that some of these interactors are false positives; if prey proteins that are physiologically expressed in a particular tissue or compartment or at a particular time during development are induced in yeast, we may find that it binds to the bait although such an interaction may not normally occur²⁹³. Thus, the genes identified in this screen may not be representative of all Hectd2 interactions that occur *in vivo*.

A further caveat generated by the candidates from the screen is that the prey proteins are not all full length proteins, but fragments of cDNA. Although the expressed fragment may bind to Hect414, this may be due to the lack of steric hindrances in the folding of the protein for which the HECT domain has been omitted, thus the entire ORF may not replicate the same binding. Of particular importance is the correct folding of proteins into their native structures, which may be challenged in the absence of a mammalian cell line context. Yeast cells may not facilitate the correct folding of a protein into its quaternary conformation, which may require machinery specific to mammalian cells. These issues

were addressed by validating the interactions of selected candidates with both Hect414 and Hectd2 by co-immunoprecipitation in the COS-7 mammalian cell line. These fibroblast-like kidney cells²⁶⁴ are a commonly used transfection host and present an environment that is capable of performing complex post-translational modifications that would be observed physiologically and may more closely represent Hectd2 interactions in humans.

Five candidates were selected for confirmation of their interaction with Hect414 and their full length proteins with Hectd2. Sh3glb1, Stmn2, Pacsin2, Stambp and Sept7 were chosen to be tested based on their possible functional or topographical significance in neurons that may link the candidates with disease pathology. The decision to overexpress the putative interacting proteins with epitope tags was made owing to the absence of validated antibodies for Hectd2 or the binding partners. Through this method, it has been possible to determine that Sh3glb1, Stmn2, Pacsin2 and Stambp bind to both the putative substrate binding domain, Hect414, as well as the full length protein, Hectd2. The binding of Hect414 to truncated Sept7, derived from the cDNA library used in the library screen has also been demonstrated. However, the binding of full length Sept7 to Hectd2 is yet to be determined.

All co-immunoprecipitation assays performed were confirmed by replication of the experiment for each candidate, thereby validating findings from the yeast two-hybrid screening. Overexpressing putative interactors may not represent a real physiological event due to the fold increases in expression relative to the endogenously expressed proteins. It is thus important that these interactions are confirmed with the endogenous proteins. These interactions could also be confirmed in brain tissue as prion pathology specifically affects the brain. However, overexpression of putative binding proteins also runs the risk of detecting interactions for which the proteins may have been mislocalised and thus spuriously interact. This can be addressed by the use of fluorescent tags to antibodies to the endogenous proteins to visualize subcellular localisation by microscopy or by FACS sorting to identify whether two proteins that are thought to interact are expressed in the same vicinity. Yeast two-hybrid screening relies on the direct interaction

between bait and prey proteins and this suggests that it is unlikely that an ancillary protein bridges the interaction between Hectd2 and its putative interactor. However, this can be confirmed by mass spectrometric analyses of the proteins within a co-immunoprecipitated sample. Despite these caveats, this is the first demonstration of interactome mapping for Hectd2, providing an insight into the biological networks of Hectd2.

7.2 Mapping the region of Hectd2 binding

The yeast two-hybrid system was further exploited to map the region to which substrates bind Hectd2. C-terminal deletion mutants of Hect414, spanning 180 (Hect180) or 330 (Hect330) residues from the N-terminus were co-expressed with each candidate for which two-hybrid interactions were determined by detection of reporter gene expression. It was found that Hect180 did not bind to any of the candidates that interacted with Hect414, suggesting that the substrate binding domain is upstream of residue 180 from the N-terminus. The C-terminal mutant, Hect330, retained its interaction with four of the candidates, Sh3glb1, Zbed4, Sh3yl1 and LOC100046859, thus providing an indication of where the contact points for substrate interaction may be harboured. From this data we can conclude that for some substrates, i.e. Sh3glb1, Zbed4, Sh3yl1 and LOC100046859, residues 180-330 of Hectd2 are sufficient for interaction but the majority of candidates require residues 331-414. It has thus been possible to confine an area to which putative substrates bind to Hectd2. It is hypothesised that residues 180-414 residue region may form an integral component of the Hectd2 substrate binding domain (Figure 3.7.2). This could be subject to further investigation by generating an extensive series of deletion mutants across the length of Hect414. The binding chemistry of these mutants can then be analysed using co-immunoprecipitation assays with each candidate interactor in mammalian cells. Combining such approaches with biophysical techniques such as X-ray crystallography to co-crystallise Hectd2 and its substrate may provide insight into the functional mechanism through which it operates.

7.3 Mechanism of action of candidate genes in prion propagation and pathology

7.3.1 Sh3glb1 modulates prion propagation

Knockdown PK1/2 cell lines for 4 candidate genes in their full length forms and Hectd2 were made and tested using the Scrapie Cell Assay (SCA). This assay measures the susceptibility of cells to prion infection by quantifying the level of PrP^{Sc}-infected cells which have been cultured over time. Thus stable rather than transient knockdown was chosen to achieve sustainable gene knockdown over the duration of the assay. The SCA allows the detection of modulatory effects exerted by the manipulation of gene expression with respect to infectivity and by extrapolation, propagation and clearance of prions. The SCA assay is the only available *in vitro* method to delineate a phenotypic function of a gene in prion disease for which the alternative is to generate mouse models, which are costly and time consuming whilst the SCA is an order of magnitude more rapid and less costly²⁵³. The SCA uses a derivative of the N2a neuroblastoma cell line, (PK1/2), and thus of neuronal lineage, which can be used to model characteristics of prion infection following gene manipulation. The advantage of using this assay is that the PK1/2 cells are immortal and thus prion infection over time can be measured. However, this also forms its disadvantage because prion infection cannot be sustained in neurons without ultimately leading to death.

A major limitation of the SCA is that it does not fully model the disease process in the brain and it may not report genes that may be important in pathogenesis and those that function outside of the CNS. Also, the SCA has been highly optimised for the RML strain and for the PK1/2 cell line, which may obscure the detection of genes that do not work in concert with the RML strain in these cells. The changes that are detected in the SCA also do not necessarily correlate with incubation time thus genes that may have a genuine effect on incubation time may not report in the SCA. Thus, the SCA models a narrow phenotype of the disease process but aspects that are considered fundamental, i.e. infection, propagation and clearance. The SCA thus serves as a triage for the identification of genes that show profound effects in the fundamental aspects of disease. The SCA

therefore allows us to follow prion infection in cells that have altered gene expression for the gene of interest for which a proof of principle has been provided in that PrP^C knockdown in the SCA results in no propagation of prions and thus PrP^C is necessary for infection and propagation³⁰¹. The SCA can thus indicate whether a given gene presents a positive or negative role in the modulation of susceptibility to infection.

In *Hectd2* knockdown PK1/2 cells, a significant increase in PrP^{Sc} signal was observed in two independent cell lines. *Sh3glb1* knockdown PK1/2 cells also showed a highly significant increase in PrP^{Sc} signal. This suggests that both *Hectd2* and *Sh3glb1* modulate susceptibility to prion infection and affect prion propagation in the same direction, which may indicate that *Hectd2* and *Sh3glb1* function in the same pathway. Although data for *Sh3glb1* was only demonstrated for the one cell line available, follow up work has confirmed this data with two additional, independent *Sh3glb1*-knockdown PK1/2 cell lines (unpublished data, Dr Craig Brown, MRC Prion Unit, London).

To date, prion diseases of humans or animals have not been linked to *Sh3glb1*, however there is a wealth of data indicative of a modulating role in neurodegenerative disorders. *Sh3glb1* alias Endophilin B1 or Bif-1 (Bax-interacting factor) is a member of the endophilin family of cytosolic proteins and was discovered as the binding partner of the pro-apoptotic protein Bax through yeast-two-hybrid screening^{302, 303}. *Sh3glb1* has been reported to orchestrate apoptosis and mitochondrial morphology with substantial evidence pointing towards a key role in the regulation of autophagy³⁰⁴⁻³⁰⁶. Deregulation of autophagy has been implicated in a number of neurodegenerative diseases and has even been proposed as a possible cause in Parkinson's disease^{183, 198}. Wong and others found that *Sh3glb1* is phosphorylated by the neuronal activator Cdk5 at Thr145 to induce autophagy in models of Parkinson's disease²⁶⁷. Phosphorylation of *Sh3glb1* leads to its interaction with Beclin 1, which in turn regulates the activation of class III PI3 kinase (PI3KIII), to promote the biogenesis of autophagosomes^{267, 307, 308}. The authors observed autophagy-mediated neuronal loss in these models, suggestive of a role of *Sh3glb1* in concert with Cdk5 in the pathology of Parkinson's disease. It is thus plausible that the interplay between Cdk5 and *Sh3glb1* may coordinate autophagic processes in prion

diseases to mediate PrP^{Sc} clearance and that deregulation of the pathway may abrogate the route to clearance of prions, giving way to prion accumulation.

Concurring with the theme of autophagy, Sh3glb1 has also been found to be a regulator of mitophagy, which is the selective autophagic degradation of mitochondria³⁰⁹. Takahashi and others found that loss of Sh3glb1 suppressed mitophagy in Parkin-expressing mouse embryonic fibroblasts following treatment with the mitochondrial uncoupler, carbonylcyanide *m*-chlorophenylhydrazone, (CCCP)³⁰⁹. Mitochondrial dysfunction is an emerging theme in neurodegenerative diseases and has been postulated as a key event underlying pathogenesis in Alzheimer's and Parkinson's diseases³¹⁰, it is thus possible that Sh3glb1 may serve a modulating role. Thus *Sh3glb1* knockdown in PK1/2 cells may impair autophagy/mitophagy, affecting neuronal health and this may be a contributing factor to the increased level of cells that are infected relative to controls.

This evidence provides strength to the notion that Sh3glb1 is important in orchestrating autophagy and mitophagy, and that dysfunction may be associated with pathology in prion disease. Interestingly, Sh3glb1 has been shown to regulate NGF/TrkA endocytic trafficking and is involved in the activation of the ERK module on endosomes to mediate downstream TrkA effectors such as NGF-induced neurite growth^{265,266}. It is thus plausible that Sh3glb1 may also regulate the survival effects of neurotrophins by trafficking of TrkA and possibly other neurotrophic receptors and may promote neuronal survival.

The precise mechanism by which prion propagation is sustained within knockdown *Sh3glb1* cells is yet to be determined, however key evidence shown by other groups point towards a pathway that may involve autophagic processes. It is possible that Hectd2 ubiquitinates Sh3glb1 to promote autophagy induction following neurotoxic stress based on the observations by Wong et al²⁶⁷. These authors found that in the absence of neurotoxic insult, Cdk5-mediated phosphorylation of Sh3glb1 did not trigger autophagy²⁶⁷. Challenge with RML prions in the SCA thus supports this hypothesis as knockdown of *Sh3glb1* may impair induction of autophagy-mediated clearance of PrP^{Sc}, facilitating the accumulation of prions and thus the increase in propagation. I propose that Hectd2 may ubiquitinate Sh3glb1 for proteasomal degradation to regulate basal levels of

Sh3glb1 and that under pathological conditions, this switch is shifted towards enhancing autophagy. This notion is in line with the observed increase in prion infection in *Hectd2* knockdown lines, which may be the result of a failure to ubiquitinate accumulating Sh3glb1. I hypothesise that the sole accumulation of Sh3glb1 may not be sufficient to activate autophagic processes and that this is dependent on ubiquitination by Hectd2. Thus the increase in PrP^{Sc} signal observed in knockdown *Hectd2* PK1/2 lines may be the result of an inability to activate autophagic processes.

7.3.2 *Sept7* modulates prion propagation

Application of the SCA on PK1/2 cells in which *Sept7* was knocked down, showed a significant increase in prion propagation. These results were supported by two independent knockdown lines, providing confidence that *Sept7* modulates prion propagation. However, one knockdown line for *Sept7* showed a reduction in prion propagation. This conflicting result may be due to off-target effects caused by artefactual dysregulation of non-target genes by the shRNA used. This can occur when there are short sequence matches between the shRNA and a non-target gene³¹¹.

Sept7 is a member of the highly conserved septin family of polymerising GTPases, which form homo- and heterologous complexes that organise into filaments^{276, 277}. Septins serve as scaffolds for the recruitment of other proteins and are important for maintaining neuronal integrity^{312, 313} and they have been reported to participate in a myriad of cellular processes from cell division, vesicle trafficking, cytoskeletal organisation, dendrite branching to dendritic spine morphology^{276, 277, 313-317}.

Sept7 localises at presynaptic terminals and dendritic branch points in neurons, suggestive of a role in pre and postsynaptic nerve terminals³¹³. Based on this topography, it may be that reduction in *Sept7* concentrations at synapses might have an effect on its downstream processes. Septins are enriched in the CNS^{283, 313, 318, 319}, where they have been implicated in exocytosis^{278, 313, 320, 321}. *Sept7* in mammalian brains has been observed to co-precipitate with the exocyst, a vesicle tethering complex that also complexes with Sept1, - 4 and -

6²⁷⁷. This septin-exocyst complex has been suggested to be involved in the recruitment of secretory vesicles to the appropriate exocytic targeting site and cellular location, and thus may regulate vesicle trafficking and the delivery of proteins which may affect downstream exocytic processes that may be important in normal functioning of the cell^{278, 313}.

Recent work has identified that Sept7 functions downstream of p35, the neuronal activator of Cdk5, and has been associated with a decreased expression in schizophrenic brains^{322, 323}. The authors found that in a mouse model overexpressing p25, Sept7 levels were upregulated and this was accompanied by an increase in dendritic spine count, which may be accounted for by the increase in Sept7 levels³²². Generation of p25 is mediated by p35 cleavage by calpain and has been regarded as an event that leads to neurotoxicity³²⁴. Thus the finding that Sept7 is upregulated when p25 is overexpressed is suggestive that Sept7 may be neuroprotective. Engmann *et al.*, suggest that the Cdk5 activator p35, regulates the expression of synaptic proteins, such as Sept7³²³. p35 is a known activator of autophagy³²⁵ and thus its cleavage to p25 may well be a regulatory factor that might downregulate autophagy by depleting p35 levels. It has been reported that p25 deregulates Cdk5 activity via constitutive activation, thereby altering its cellular location and substrate specificity which may ultimately lead to neuronal dysfunction³²⁶. It is thus plausible that loss of Sept7 may lead to accumulation of p25, to upregulate Sept7 expression. Generation of p25 may alter Cdk5 induction of autophagic mechanisms, disabling cells from being relieved of their prion burden. If Sept7 does have a protective role in this regard, whether its downstream functions include appropriate activation of autophagy or activation of alternative mechanisms that switch on autophagic processes is yet to be determined. However, such a hypothesis may implicate Sept7 and Sh3glb1 in convergent pathways.

Thus the increase in prion propagation observed in PK1/2 cells knocked down for *Sept7* may be the result of abrogation of normal Sept7 function. Although it is expected that knockdown of *Hectd2* would result in an opposing effect, the increase in propagation observed in *Hectd2* knockdown cells may be accounted for by the accumulating Sept7 that is no longer subject to turnover by Hectd2, abnormal expression of which could also deregulate normal Sept7 function. Whether vesicle trafficking mediated by Sept7 and

other septins converges with endocytic trafficking mediated by Sh3glb1 will be an interesting point of investigation. The effect of Hectd2 knockdown may represent the cumulative effect of deregulated functions of Sept7 and Sh3glb1 and that of any other substrates of Hectd2.

Although it may be intuitive that *Hectd2* knockdown in the SCA results in an opposing effect to that observed by knockdown of its substrates, Sept7 or Sh3glb1, there are explanations that counter this. Sept7 or Sh3glb1 may be reliant on Hectd2-dependent ubiquitination to target each of these substrates to activate their downstream pathways. When Hectd2 is knocked down, Sept7 or Sh3glb1 may not be functionally effective without the ubiquitin signal conferred by Hectd2. It may be that the interaction of Hectd2 with a substrate other than those investigated here, may have an opposing effect to that of Sh3glb1 and/or Sept7. This might mean that knockdown of Hectd2 may accumulate Sh3glb1 and Sept7 but the accumulation of other Hectd2 substrates may pose a stronger effect that is permissive for prion infection. If Sept7 or Sh3glb1 do in fact accumulate, this may be suggestive that the primary function of Hectd2 is to direct these substrates for degradation although it does not rule out the possibility that it can target substrates to activate a particular pathway.

Septin proteins have been implicated in a diversity of neurodegenerative diseases detailed below, positioning Sept7 as a plausible candidate gene for prion disease modulation. Sept7 has been recorded as an interactor of CD2AP, a recently identified susceptibility gene for Alzheimer's disease^{327, 328}. Furthermore, in Alzheimer's disease, Sept4, Sept1 and Sept2 were identified in neurofibrillary tangles²⁸³. Sept9 has been identified as a disease causative gene for hereditary neuralgic amyotrophy³²⁹, suggesting that the septins may serve a key function in the CNS. The septins have also been implicated in Parkinson's disease as Sept4 and Sept5 were identified as substrates for Parkin^{330, 331}. Interestingly, Sept4 deficiency diminishes dopaminergic neurotransmission and enhances alpha synuclein mediated neurotoxicity by exacerbating alpha synuclein aggregation³³⁰, suggesting that the septins may serve a protective role, although the underlying mechanism remain elusive. Whether Sept7 modulates neurotransmission and impacts on

neurotoxicity in prion disease is yet to be determined but data from the SCA indicates a protective role for *Sept7* and it is thus tempting to speculate that *Sept7* may help to protect against prion infection.

To conclude there is insufficient evidence to rule out any of these proposed mechanisms by which neurodegenerative events in prion disease may occur. Genes that operate downstream of *Hectd2* may collectively contribute to the increase in propagation seen in *Hectd2* knockdown cells. It is expected that manipulation of gene expression of *Sept7* or *Sh3glb1* would deregulate the effectors in the pathways that they function, which may result in altered cell metabolism and neuronal health.

7.3.3 Stambp, Pacsin2 and Stmn2: possible candidate genes that modulate prion propagation

The results of the SCA for *Stambp* and *Pacsin2* knockdown cells are inconclusive because although they showed modulatory effects in prion propagation, there was only one cell line for each gene that demonstrated this. PK1/2 cells knocked down for *Stambp*, showed an increase in prion propagation in one out of two independent cell lines. *Pacsin2* knockdown reduced prion propagation in one out of three cell lines, suggesting that *Pacsin2* may not be a promising candidate in the modulation of prion pathology, although this cannot yet be ruled out. These conflicting results may be due to off-target effects caused by sequence complementarity between the shRNA used and non-target genes³¹¹. Although from these preliminary results it seems that *Pacsin2* and *Stambp* may not have modulatory roles, until support is provided for these data by at least a further independent cell line targeted for both of these genes, it is difficult to gauge the direction, if any, in which prion propagation is affected.

Failure to report in the assay does not render these genes irrelevant in prion disease due to the limitations of the SCA that were described earlier. However, as the aims of this project were to identify genes that are important in modulating the fundamental aspects of prion disease, modelled in the SCA, it has thus been possible to triage the candidate

genes, for which *Stambp* and *Pacsin2* may not have an effect as profound as *Sh3glb1* and *Sept7*. Although *Hectd2* may have a number of different substrates, it is likely that very few of these interactions, perhaps one or two, will be important in prion disease. Thus it is unsurprising that all of these candidate genes have not shown an effect in the SCA and that *Sh3glb1* and *Sept7* may be the only candidates that confer a modulatory role.

As *Stambp* and *Pacsin2* remain as possible candidates in prion disease, their functions are thus discussed herein. *Stambp*, also known as AMSH (Associated Molecule with the SH3 domain of STAM) is a deubiquitinating enzyme that associates with ESCRT-I and ESCRT-III complexes, which mediate the sorting and trafficking of ubiquitinated cargoes for lysosomal targeting^{281, 282, 332-334}. It has been reported to have a positive regulatory role in autophagy mediated degradation and is known to specifically deubiquitinate lysine 63-linked ubiquitin chains, which have been reported as targets of the autophagy-lysosomal pathway³³⁵. Recent evidence has linked *Stambp* to a central role in the CNS, where *Stambp* dysfunction leads to missorted ubiquitinated cargoes *in vitro* and severe neurodegeneration *in vivo*, indicative of a key role in the CNS^{269, 270}.

Pacsin2 or protein kinase C and casein kinase substrate in neurons protein 2, is a ubiquitously expressed protein²⁷⁴ for which a role in neuron morphogenesis has been reported. *Pacsin2* is involved in actin cytoskeleton organisation and may regulate vesicular traffic^{272, 274}. *Pacsin2* has also been reported to regulate microtubule growth²⁷³. Interestingly, PrP^C has also been shown to bind tubulin, which inhibits microtubule assembly by inducing tubulin oligomerisation^{275, 336-338}. Thus PrP^C can serve as a microtubule destabilizing factor, mirroring *Pacsin2* in its role in regulating microtubule stability, substantiating the role of microtubule stability in prion pathogenesis^{337, 338}.

The effect of *Stmn2* on prion propagation has not yet been established. However, this candidate gene has been identified as a vCJD risk factor in an independent GWAS study by Mead et al., whilst more recently Lloyd et al, found that it associated with incubation time in mice. *Stmn2* is a microtubule-destabilising factor that impairs the stability of microtubules. Loss of *Stmn2* can result in axonal retraction and neuronal degeneration³³⁹, whilst excessive microtubule stability can impair axonal health and result in

neuropathy^{340, 341}. Deregulated microtubule stability has been implicated in Huntington's disease and hereditary spastic paraplegia³⁴², and may affect axonal health due to impairment in the trafficking of axonal cargo³³⁹. Interestingly Stmn2 is involved in the homeostasis of mitochondrial trafficking³³⁹, strengthening the evidences for mitochondrial involvement in prion pathology.

Phosphorylation by JNK leads to Stmn2 degradation by methods which are yet unknown. It is possible that Hectd2 functions downstream of JNK to target Stmn2 for degradation either basally, or in cells subjected to neuronal stress to orchestrate the balance between microtubule stabilisation and destabilisation. Together the hypotheses outlined in this thesis for how all of these novel candidate genes may function, position Hectd2 as a switch in the regulation of a myriad of processes, making it a promising candidate for prion pathology.

To summarise, interactome mapping of Hectd2 identified 20 potential candidate interactors, of which five were verified. The evidence and literature detailed in this thesis, have shown cross talk between Hectd2 and other proteins that may serve to modulate susceptibility of cells to prion propagation. Although the underlying mechanisms by which these candidates modulate disease is yet to be determined, autophagy and cytoskeletal regulation appear to be emerging themes.

It is anticipated that of the remaining 16 candidates, a proportion of these will represent true Hectd2 binding partners owing to the stringent selection criteria used for the initial pool of positive interactors. These candidates include a range of proteins for which functions have not been clearly defined although some of these show brain-specific expression and some may operate in the same pathway. Characterisation of Hectd2 and its binding partners has thus positioned Hectd2 as a possible regulatory molecule that may govern such interactions by fine tuning their activation or degradation to modulate downstream processes.

7.4 Evidence from mouse models: Is *Hectd2* a genetic modifier of prion disease?

An important aspect of functional testing of a potential candidate implicated in disease is to generate mouse models to correlate phenotypic effects in prion pathology. *Hectd2* knockout and overexpressing transgenic mouse lines were developed to address this question. The data detailed in Chapter 6 indicate that when *Hectd2*^{-/-} female mice were challenged with RML, there was a significant difference in disease onset relative to control mice, where *Hectd2*^{-/-} showed an earlier onset by 12 days. Furthermore, the duration of disease for these RML infected *Hectd2*^{-/-} mice was prolonged relative to controls although there was no significant difference in the time to diagnosis of disease (incubation time). These data therefore suggest a protective role for *Hectd2*, supporting the hypothesis that *Hectd2* deficiency facilitates propagation of prions and deregulated clearance. This is in concurrence with the data obtained for knockdown of *Hectd2* in the SCA, which showed that prion propagation was increased in the absence of *Hectd2*. This data is lent support by previous findings by Lloyd *et al.*, who showed that there was a significant upregulation of *Hectd2* at the end stage of disease in prion-infected mouse brains relative to normal brains, perhaps suggestive of a protective role¹²⁰. Although incubation time in mouse and the SCA are not directly correlative, it is expected that a reduction in incubation time correlates with an increased propagation of prions in the SCA. However all other prion strains tested in knockout mice did not show any differences in onset or incubation time.

Hectd2 overexpressing mice, Tg260^{+/+}, challenged with ME7 prions²⁸⁷ showed a 13% reduction in incubation time in males. However, taking into consideration the effects of multiple testing, the significance level for this reduction in incubation time was borderline. This is suggestive that *Hectd2* may serve a modulating role although the lack of replication in female mice and in those to which RML and MRC2 were transmitted indicates that this data may not be real. It is postulated that the downstream functions of *Hectd2* are neuroprotective and that overexpressing the gene would prolong incubation time and thus this reduction is surprising as it also conflicts with the SCA data for *Hectd2*.

Significant differences in incubation time were not seen for any other prion strain tested in Tg260^{+/+} mice. Overall, for both *Hectd2* knockout and transgenic mice, we did not observe a universal effect shown by all prion strains tested in modulating incubation time. However, the differences outlined above suggest that *Hectd2* modulates disease onset and diagnosis in a strain and sex- specific manner. It is possible that *Hectd2* may have a larger effect than that observed in these models owing to a number of caveats inherent in both of the mouse models. Currently, neither of the lines have been confirmed at the protein level that *Hectd2* is completely knocked out or overexpressed, respectively due to a lack of specific mouse anti-*Hectd2* antibodies. The start codon for *Hectd2* in exon 1 is its predicted initiator ATG but it is possible that an alternative start site is the second methionine in exon 3, which would translate all but 103 residues of *Hectd2*. This would mean that *Hectd2* is still expressed in its most part, hindering the possibility of identifying an association in mice. Of note is that the level of endogenous PrP^C expression was not tested in these mouse models to ensure that there were no differences relative to controls that could account for any changes in incubation time. Furthermore, there is only one transgenic line for overexpressing *Hectd2* thus it is necessary to have more than one mouse line in case of an aberrant transgene integration effect. It should be also noted that the transgenic *Hectd2* overexpressing line is of a mixed genetic background, which could obscure small effects and thus work is underway to address this by backcrossing these mice. However, it could be argued that small effects may not be interesting in terms of identifying genes that profoundly modulate the disease process. Thus it is possible that *Hectd2* may only show modest effects in modulating disease incubation time, however this does not detract from its importance in the disease process as genes that show moderate effects may serve key roles that implicate pathways that underlie pathogenesis.

Together, data from the knockout and overexpressing transgenic mouse models suggest that *Hectd2* may serve as a genetic modulator of prion disease. These findings are corroborated by data obtained from the SCA, which provides convincing evidence that *Hectd2* and its downstream effectors possess roles in neuroprotection with respect to prion infection.

7.5 Continuing research

7.5.1 Does Hectd2 confer E3 ubiquitin ligase activity?

Hectd2 is an E3 ligase by homology and thus its catalytic ligase activity is putative. To assess whether the substrates of Hectd2 are subject to ubiquitination, ubiquitinated forms of the endogenous protein must be identified. An antibody to ubiquitin could be used to distinguish the ubiquitinated form of a given Hectd2 substrate in cells expressing physiological levels of the substrate or when the substrate is knocked down or overexpressed. Furthermore knockdown of *Hectd2*, should result in the accumulation of its potential substrates. Owing to the complexity of the ubiquitination system, substrates are not necessarily targeted for proteasomal degradation (see Section 1.3). To test the hypothesis that Hectd2 substrates are targeted to the proteasome for basal degradation, inhibition of the proteasome with pharmacological inhibitors should result in the accumulation of the putative targets. If Hectd2 is shown to be a functional E3 ubiquitin ligase then residues of the HECT domain may be systematically mutated or its predicted cysteine active site and the effect of these mutations on catalytic activity and binding chemistry may be measured using enzyme assay or co-immunoprecipitation experiments. When a protein has been established as a Hectd2 substrate, peptide mapping by mass spectrometry can be employed to identify sites of post translational modification such as ubiquitination, which may confirm whether a given substrate is indeed ubiquitinated. This may also shed light on the site at which the protein is modified or ubiquitination chain topology, which might provide insight into the fate of a given protein as particular modifications direct specific processes¹⁶¹.

7.5.2 Characterisation of the molecular pathway by which prion clearance is mediated

Lessons can be learnt from the perspectives taken by research in autophagy in neurodegeneration in the wider context as this field is under-recognised in prion disease. It is anticipated that prion clearance is mediated by the autophagy-lysosomal pathway as aggregated prions are beyond the capacity of proteasomal degradation (Section 1.3).

Autophagic flux may be measured in cells in which *Sh3glb1*, *Sept7* or *Hectd2* gene expression has been manipulated. The candidates may be tagged and their distribution visualised to assess whether they colocalise with autophagosomes, which may indicate involvement in the autophagic process. These factors can be investigated in prion-infected cells treated with pharmacological inhibitors and inducers of autophagy to assess whether prions are cleared through the autophagy-lysosomal pathway and whether these candidates are effectors in this pathway.

The role of *Hectd2* could be investigated further by overexpressing this gene in the SCA. It is expected that this would lower PrP^{Sc} levels in cells. This could be investigated further by overexpressing Hect414, which would be expected to bind to its substrates but should not ubiquitinate them. This may result in an effect similar to that of knockdown of *Sh3glb1* or *Sept7*. Overexpression of *Sept7* and *Sh3glb1* may result in decreased PrP^{Sc} as the effectors of their downstream processes may clear PrP^{Sc}. However, if *Sept7* and *Sh3glb1* are dependent on *Hectd2* ubiquitination to activate their downstream processes, a reduction in prion infection may not be observed solely by their overexpression, if endogenous *Hectd2* is not able to ubiquitinate the overexpressed protein effectively. Rather, if *Hectd2* is overexpressed with either *Sh3glb1* or *Sept7*, a reduction in prion infection would be expected.

Extending on the SCA, it would be interesting to assess whether the autophagy response is correlated in terms of PrP^{Sc} signal. PK1/2 cells may be treated with activators or inhibitors of autophagy where candidate gene expression is manipulated. It would be particularly interesting to evaluate whether double knockdown of *Sh3glb1* and *Sept7* in the same cell line produces an additive effect where we might observe a cumulative increase in PrP^{Sc} signal or whether these candidates have opposing effects.

Mitochondrial impairment has been implicated in prion pathology¹³² and recent evidence for *Sh3glb1* and *Stmn2* suggest their involvement in mitochondrial function^{309, 339}. Further investigations could be undertaken to assess the role of mitochondria in the autophagy-lysosomal pathway in prion pathology. Chronically infected cells could be

measured for their ability to clear prions following treatment with a mitochondrial uncoupler such as carbonylcyanide *m*-chlorophenylhydrazone (CCCP), to determine whether dysfunctional mitochondrial metabolism correlates with prion clearance mechanisms.

Sept7 and *Sh3glb1* have shown to be promising candidates in the modulation of prion disease and thus a key step to extrapolating these findings is to generate mouse models for each of these genes in prion disease and search for an association with incubation time. Gene knockdown or overexpression in primary neuronal cultures could also be developed to search for whether *Hectd2*, *Sept7* or *Sh3glb1* confer neuroprotective roles. If these genes are identified as essential to neuronal function, this could provide support for the hypotheses outlined in this thesis in that perturbation of *Hectd2*, *Sept7* and *Sh3glb1* may deregulate normal function and may thus modulate the disease process.

7.6 Concluding comments

This has been the first demonstration of interactome mapping of a genetic modifier of prion disease that also influences susceptibility to human prion diseases. 20 novel binding partners of *Hectd2* were identified of which 5 were verified as putative interactors. A cell based model of prion disease, the SCA, was used to define the phenotype of *Hectd2* and each interactor from which *Sh3glb1* and *Sept7* were confirmed as modulators of cell susceptibility to prion infection. Interestingly, the SCA data for *Hectd2* showed convincing evidence for a modulatory role in the same direction as *Sh3glb1* and *Sept7*, suggesting that these genes may function in the same pathway. These analyses were extended to a mouse model, whereby an association of *Hectd2* with incubation time was investigated from which it was found that *Hectd2* modulates disease onset in a strain and sex- specific manner. Together, these data provide support for *Hectd2* and specific components of its interactome as genetic modifiers of prion disease and has shed light on molecular pathways that have not been previously implicated in prion disease.

Hectd2 is an HECT E3 ubiquitin ligase with no previously associated functional information assigned. Cytoskeletal regulation, autophagy and mitochondrial dysfunction are themes which have emerged from characterising Hectd2 and the pathways in which its substrates lie. These themes are under-recognised in prion disease and it is expected that these findings will lead the way into scrutinising how deregulation of the cytoskeleton, autophagy or mitochondria may affect the pathology of prion disease. The significance of Hectd2, the first E3 ubiquitin ligase linked to human prion diseases, is thus apparent, although the precise role it plays is yet to be determined. However, the identification of these novel targets and the molecular networks in which they are placed may accelerate research in this field and draw us closer to a treatment for this fatal disease.

8 References

1. Collinge, J. Variant Creutzfeldt-Jakob disease. *Lancet* **354**, 317-323 (1999).
2. Prusiner, S.B. Molecular Biology of Prion Diseases. *Science* **252**, 1515-1522 (1991).
3. Collinge, J. Molecular neurology of prion disease. *Journal of Neurology Neurosurgery and Psychiatry* **76**, 906-919 (2005).
4. Prusiner, S.B. & DeArmond, S.J. Molecular Biology and Pathology of Scrapie and the Prion Diseases of Humans. *Brain Pathology* **1**, 297-310 (1991).
5. Weissmann, C. The state of the prion. *Nature Reviews Microbiology* **2**, 861-871 (2004).
6. Prusiner, S.B. Novel proteinaceous infectious particles cause scrapie. *Science* **216**, 136-144 (1982).
7. Prusiner, S.B. Molecular biology of prion diseases. *Science* **252**, 1515-1522 (1991).
8. Lloyd, S. & Collinge, J. Genetic Susceptibility to Prion Diseases in Humans and Mice. *Current Genomics* **6**, 1-11 (2005).
9. Hill AF *et al.* Molecular classification of sporadic Creutzfeldt-Jakob disease. *Brain* **126**, 1333-1346 (2003).
10. Hill AF *et al.* The same prion strain causes vCJD and BSE. *Nature* **389**, 448-450 (1997).
11. Wadsworth, J. & Collinge, J. Molecular pathology of human prion disease. *Acta Neuropathologica* **121**, 69-77 (2011).
12. Wadsworth, J.D. *et al.* Molecular diagnosis of human prion disease. *Methods in Molecular Biology* **459**, 197-227 (2008).
13. Gambetti, P., Kong, Q., Zou, W., Parchi, P., & Chen, S.G. Sporadic and familial CJD: classification and characterisation. *British Medical Bulletin* **66**, 213-239 (2003).
14. Collinge J Human prion diseases and bovine spongiform encephalopathy (BSE). *Human Molecular Genetics* **6**, 1699-1705 (1997).
15. Riek, R. *et al.* Prion protein NMR structure and familial human spongiform encephalopathies. *Proceedings of the National Academy of Sciences USA* **95**, 11667-11672 (1998).
16. Wang, X. *et al.* Familial CJD Associated PrP Mutants within Transmembrane Region Induced Ctm-PrP Retention in ER and Triggered Apoptosis by ER Stress in SH-SY5Y Cells. *PLoS ONE* **6**, e14602 (2011).
17. Hegde, R.S. *et al.* Transmissible and genetic prion diseases share a common pathway of neurodegeneration. *Nature* **402**, 822-826 (1999).

18. Shi,Q. & Dong,X.P. (Ctm) PrP and ER stress: A neurotoxic mechanism of some special PrP mutants. *Prion* **5**, (2011).
19. Lloyd,S., Mead,S., & Collinge,J. Genetics of Prion Disease. *Topics in Current Chemistry* (2011).
20. Medori,R. *et al.* Fatal familial insomnia, a prion disease with a mutation at codon 178 of the prion protein gene. *New England Journal of Medicine* **326**, 444-449 (1992).
21. Brown,P. *et al.* Iatrogenic Creutzfeldt-Jakob disease at the millennium. *Neurology* **55**, 1075-1081 (2000).
22. Yamada,S. *et al.* Creutzfeldt-Jakob disease transmitted by a cadaveric dura mater graft. *Neurosurgery* **34**, 740-744 (1994).
23. Gibbs,C.J.Jr. *et al.* Clinical and pathological features and laboratory confirmation of Creutzfeldt-Jakob disease in a recipient of pituitary-derived human growth hormone. *New England Journal of Medicine* **313**, 734-738 (1985).
24. Mead,S. *et al.* Balancing selection at the prion protein gene consistent with prehistoric kuru-like epidemics. *Science* **300**, 640-643 (2003).
25. Collinge,J. *et al.* Kuru in the 21st century--an acquired human prion disease with very long incubation periods. *Lancet* **367**, 2068-2074 (2006).
26. Bruce,M.E. *et al.* Transmissions to mice indicate that 'new variant' CJD is caused by the BSE agent. *Nature* **389**, 498-501 (1997).
27. Hill,A.F. *et al.* The same prion strain causes vCJD and BSE. *Nature* **389**, 448-50, 526 (1997).
28. Bruce,M. *et al.* Transmission of bovine spongiform encephalopathy and scrapie to mice: Strain variation and the species barrier. *Philosophical Transactions of the Royal Society of London Biological Sciences* **343**, 405-411 (1994).
29. Collinge,J. Prion diseases of humans and animals: their causes and molecular basis. *Annual Review of Neuroscience* **24**, 519-550 (2001).
30. Collinge,J. Cell biology. The risk of prion zoonoses. *Science* **335**, 411-413 (2012).
31. Collinge,J. & Clarke,A. A general model of prion strains and their pathogenicity. *Science* **318**, 930-936 (2007).
32. Prusiner,S.B. Prions. *Proceedings of the National Academy of Sciences USA* **95**, 13363-13383 (1998).
33. Pan,K.M. *et al.* Conversion of α -helices into β -sheets features in the formation of the scrapie prion proteins. *Proceedings of the National Academy of Sciences USA* **90**, 10962-10966 (1993).
34. Griffith,J.S. Self Replication and scrapie. *Nature* **215**, 1043-1044 (1967).

35. Bueler,H. *et al.* Mice devoid of PrP are resistant to scrapie. *Cell* **73**, 1339-1347 (1993).
36. Sailer,A., Bueler,H., Fischer,M., Aguzzi,A., & Weissmann,C. No propagation of prions in mice devoid of PrP. *Cell* **77**, 967-968 (1994).
37. Bueler,H. *et al.* Normal development and behaviour of mice lacking the neuronal cell-surface PrP protein. *Nature* **356**, 577-582 (1992).
38. Mallucci G *et al.* Depleting neuronal PrP in prion infection prevents disease and reverses spongiosis. *Science* **302**, 871-874 (2003).
39. Weissmann,C. *et al.* The use of transgenic mice in the investigation of transmissible spongiform encephalopathies. *Revue scientifique et technique* **17**, 278-290 (1998).
40. Brandner S *et al.* Normal host prion protein necessary for scrapie-induced neurotoxicity. *Nature* **379**, 339-343 (1996).
41. Brandner S *et al.* Normal host prion protein (PrP^C) is required for scrapie spread within the central nervous system. *Proceedings of the National Academy of Sciences USA* **93**, 13148-13151 (1996).
42. Jarrett,J.T. & Lansbury,P.T.J. Seeding "one-dimensional crystallization" of amyloid: a pathogenic mechanism in Alzheimer's disease and scrapie? *Cell* **73**, 1055-1058 (1993).
43. Sandberg,M.K., Al Doujaily,H., Sharps,B., Clarke,A.R., & Collinge,J. Prion propagation and toxicity in vivo occur in two distinct mechanistic phases. *Nature* **470**, 540-542 (2011).
44. Liao,Y.C., Lebo,R.V., Clawson,G.A., & Smuckler,E.A. Human prion protein cDNA: molecular cloning, chromosomal mapping, and biological implications. *Science* **233**, 364-367 (1986).
45. Sparkes,R.S. *et al.* Assignment of the human and mouse prion protein genes to homologous chromosomes. *Proceedings of the National Academy of Sciences USA* **83**, 7358-7362 (1986).
46. Zahn,R. *et al.* NMR solution structure of the human prion protein. *Proceedings of the National Academy of Sciences USA* **97**, 145-150 (2000).
47. Prusiner,S.B., Scott,M.R., DeArmond,S.J., & Cohen,F.E. Prion protein biology. *Cell* **93**, 337-348 (1998).
48. Didonna,A. Prion protein and its role in signal transduction. *Cellular and Molecular Biology Letters* **18**, 209-230 (2013).
49. Manson,J.C. *et al.* 129/Ola mice carrying a null mutation in PrP that abolishes mRNA production are developmentally normal. *Molecular Neurobiology* **8**, 121-127 (1994).
50. Tobler,I. *et al.* Altered circadian activity rhythms and sleep in mice devoid of prion protein. *Nature* **380**, 639-642 (1996).

51. Brown,K. & Mastrianni,J.A. The Prion Diseases. *Journal of Geriatric Psychiatry and Neurology* **23**, 277-298 (2010).
52. Mallucci G *et al.* Post-natal knockout of prion protein alters hippocampal CA1 properties, but does not result in neurodegeneration. *EMBO Journal* **21**, 202-210 (2002).
53. Collinge J *et al.* Prion protein is necessary for normal synaptic function. *Nature* **370**, 295-297 (1994).
54. Bounhar,Y., Zhang,Y., Goodyer,C.G., & LeBlanc,A. Prion protein protects human neurons against Bax-mediated apoptosis. *Journal of Biological Chemistry* **276**, 39145-39149 (2001).
55. Roucou,X., Guo,Q., Zhang,Y., Goodyer,C.G., & LeBlanc,A.C. Cytosolic prion protein is not toxic and protects against Bax-mediated cell death in human primary neurons. *Journal of Biological Chemistry* 40877-40881 (2003).
56. Brown,D.R., Schulz-Schaeffer,W.J., Schmidt,B., & Kretzschmar,H.A. Prion protein-deficient cells show altered response to oxidative stress due to decreased SOD-1 activity. *Experimental Neurology* **146**, 104-112 (1997).
57. Wong,B.S. *et al.* Increased levels of oxidative stress markers detected in the brains of mice devoid of prion protein. *Journal of Neurochemistry* **76**, 565-572 (2001).
58. Brown,D.R. *et al.* Normal prion protein has an activity like that of superoxide dismutase. *Biochemical Journal* **344**, 1-5 (1999).
59. Jones S *et al.* Recombinant prion protein does not possess SOD-1 activity. *Biochemical Journal* **392**, 309-312 (2005).
60. Simons,K. & Toomre,D. Lipid rafts and signal transduction. *Nature Reviews Molecular Cell Biology* **1**, 31-39 (2000).
61. Mouillet-Richard,S. *et al.* Signal transduction through prion protein. *Science* **289**, 1925-1928 (2000).
62. Beggs,H.E., Soriano,P., & Maness,P.F. Ncam-Dependent Neurite Outgrowth Is Inhibited in Neurons from Fyn-Minus Mice. *Journal of Cell Biology* **127**, 825-833 (1994).
63. Santuccione,A., Sytnyk,V., Leshchyns'ka,I., & Schachner,M. Prion protein recruits its neuronal receptor NCAM to lipid rafts to activate p59(fyn) and to enhance neurite outgrowth. *Journal of Cell Biology* **169**, 341-354 (2005).
64. Lauren,J., Gimbel,D.A., Nygaard,H.B., Gilbert,J.W., & Strittmatter,S.M. Cellular prion protein mediates impairment of synaptic plasticity by amyloid-beta oligomers. *Nature* **457**, 1128-1132 (2009).
65. Um,J.W. *et al.* Alzheimer amyloid-beta oligomer bound to postsynaptic prion protein activates Fyn to impair neurons. *Nature Neuroscience* **15**, 1227-1235 (2012).

66. Roffe,M. *et al.* Prion protein interaction with stress-inducible protein 1 enhances neuronal protein synthesis via mTOR. *Proceedings of the National Academy of Sciences USA*, **107**, 13147-13152 (2010).
67. Forloni,G. *et al.* Neurotoxicity of a prion protein fragment. *Nature* **362**, 543-546 (1993).
68. Seo,J.S. *et al.* Hypoxia protects neuronal cells from human prion protein fragment-induced apoptosis. *Journal of Neurochemistry* **112**, 715-722 (2010).
69. Dai,R.L. *et al.* Involvement of PI3K/Akt pathway in the neuroprotective effect of sonic hedgehog on cortical neurons under oxidative stress. *Journal of Huazhong University of Science and Technology-Medical Sciences* **32**, 856-860 (2012).
70. Wadsworth,J.D. & Collinge,J. Molecular pathology of human prion disease. *Acta Neuropathologica* **121**, 69-77 (2010).
71. Collinge,J., Sidle,K.C., Meads,J., Ironside,J., & Hill,A.F. Molecular analysis of prion strain variation and the aetiology of 'new variant' CJD. *Nature* **383**, 685-690 (1996).
72. Parchi,P. *et al.* Molecular Basis of Phenotypic Variability in Sporadic Creutzfeldt-Jakob Disease. *Annals of Neurology* **39**, 669-680 (1996).
73. Prusiner,S.B. *et al.* Transgenic studies implicate interactions between homologous PrP isoforms in scrapie prion replication. *Cell* **63**, 673-686 (1990).
74. Marsh,R.F. & Kimberlin,R.H. Comparison of Scrapie and Transmissible Mink Encephalopathy in Hamsters. II. Clinical Signs, Pathology, and Pathogenesis. *Journal of Infectious Diseases* **131**, 104-110 (1975).
75. Bessen,R.A. & Marsh,R.F. Distinct Prp Properties Suggest the Molecular-Basis of Strain Variation in Transmissible Mink Encephalopathy. *Journal of Virology* **68**, 7859-7868 (1994).
76. Bessen,R.A. & Marsh,R.F. Biochemical and Physical-Properties of the Prion Protein from 2 Strains of the Transmissible Mink Encephalopathy Agent. *Journal of Virology* **66**, 2096-2101 (1992).
77. Telling,G.C. *et al.* Evidence for the conformation of the pathologic isoform of the prion protein enciphering and propagating prion diversity. *Science* **274**, 2079-2082 (1996).
78. Li,J.L., Browning,S., Mahal,S.P., Oelschlegel,A.M., & Weissmann,C. Darwinian Evolution of Prions in Cell Culture. *Science* **327**, 869-872 (2010).
79. Collinge,J. Medicine. Prion strain mutation and selection. *Science* **328**, 1111-1112 (2010).
80. Bruce,M.E. Scrapie strain variation and mutation. *British Medical Bulletin* **49**, 822-838 (1993).
81. Collinge,J., Palmer,M.S., & Dryden,A.J. Genetic predisposition to iatrogenic Creutzfeldt-Jakob disease. *Lancet* **337**, 1441-1442 (1991).

82. Wadsworth,J.D.F., Jackson,G.S., Hill,A.F., & Collinge,J. Molecular biology of prion propagation. *Current Opinion in Genetics & Development* **9**, 338-345 (1999).
83. Wadsworth,J.D.F. *et al.* Kuru prions and sporadic Creutzfeldt-Jakob disease prions have equivalent transmission properties in transgenic and wild-type mice. *Proceedings of the National Academy of Sciences USA* **105**, 3885-3890 (2008).
84. Wadsworth,J.D. Human prion strains and species barriers: Transgenic mouse models and biochemical studies. *Journal of Neurochemistry* **102**, 8 (2007).
85. Hill,A.F. *et al.* Species-barrier-independent prion replication in apparently resistant species. *Proceedings of the National Academy of Science USA* **97**, 10248-10253 (2000).
86. Scott,M. *et al.* Transgenic mice expressing hamster prion protein produce species-specific scrapie infectivity and amyloid plaques. *Cell* **59**, 847-857 (1989).
87. Hill AF & Collinge J Subclinical prion infection in humans and animals. *British Medical Bulletin* **66**, 161-170 (2003).
88. Beringue,V. *et al.* Facilitated Cross-Species Transmission of Prions in Extraneural Tissue. *Science* **335**, 472-475 (2012).
89. Palmer,M.S., Dryden,A.J., Hughes,J.T., & Collinge J Homozygous prion protein genotype predisposes to sporadic Creutzfeldt-Jakob disease. *Nature* **352**, 340-342 (1991).
90. Lee,H.S. *et al.* Increased susceptibility to Kuru of carriers of the *PRNP* 129 methionine/methionine genotype. *Journal of Infectious Diseases* **183**, 192-196 (2001).
91. Lee,S. *et al.* Conformational diversity in prion protein variants influences intermolecular beta-sheet formation. *EMBO Journal* **29**, 251-262 (2010).
92. Huillard d'Aignaux,J. *et al.* Incubation period of Creutzfeldt-Jakob disease in human growth hormone recipients in France. *Neurology* **53**, 1197-1201 (1999).
93. Petersen,R.B., Parchi,P., Richardson,S.L., Urig,C.B., & Gambetti,P. Effect of the D178N mutation and the codon 129 polymorphism on the metabolism of the prion protein. *Journal Biology Chemistry* **271**, 12661-12668 (1996).
94. Cervenakova,L. *et al.* Phenotype-genotype studies in kuru: Implications for new variant Creutzfeldt-Jakob disease. *Proceedings of the National Academy of Sciences USA* **95**, 13239-13241 (1999).
95. Mead,S. *et al.* A Novel Protective Prion Protein Variant that Colocalizes with Kuru Exposure. *New England Journal of Medicine* **361**, 2056-2065 (2009).
96. Carlson,G.A. *et al.* Genetic control of prion incubation period in mice. *Ciba Foundation Symposium* **135**, 84-99 (1988).
97. Dickinson,A.G. & Mackay J.M.W. Genetical control of the incubation period in mice of the neurological disease, scrapie. *Heredity* **19**, 279-288 (1964).

98. Westaway,D. *et al.* Distinct prion proteins in short and long scrapie incubation period mice. *Cell* **51**, 651-662 (1987).
99. Stephenson,D.A. *et al.* Quantitative trait loci affecting prion incubation time in mice. *Genomics* **69**, 47-53 (2000).
100. Lloyd,S. *et al.* Identification of multiple quantitative trait loci linked to prion disease incubation period in mice. *Proceedings of the National Academy of Sciences USA* **98**, 6279-6283 (2001).
101. Carlson,G.A. *et al.* Linkage of prion protein and scrapie incubation time genes. *Cell* **46**, 503-511 (1986).
102. Carlson,G.A. *et al.* Genetics and polymorphism of the mouse prion gene complex: control of scrapie incubation time. *Molecular Cellular Biology* **8**, 5528-5540 (1988).
103. Lloyd,S. *et al.* Characterization of two distinct prion strains derived from bovine spongiform encephalopathy transmissions to inbred mice. *Journal of General Virology* **85**, 2471-2478 (2004).
104. Lloyd,S. *et al.* Identification and characterization of a novel mouse prion gene allele. *Mammalian Genome* **15**, 383-389 (2004).
105. Collinge,J. *et al.* Unaltered susceptibility to BSE in transgenic mice expressing human prion protein. *Nature* **378**, 779-783 (1995).
106. Fischer,M. *et al.* Prion protein (PrP) with amino-proximal deletions restoring susceptibility of PrP knockout mice to scrapie. *EMBO Journal* **15**, 1255-1264 (1996).
107. Dickinson,A.G. Scrapie in sheep and goats. *Frontiers in Biology* **44**, 209-241 (1976).
108. Kimberlin,R.H., Cole,S., & Walker,C.A. Temporary and permanent modifications to a single strain of mouse scrapie on transmission to rats and hamsters. *Journal of General Virology* **68**, 1875-1881 (1987).
109. Kimberlin,R.H. & Walker,C.A. Evidence that the Transmission of One Source of Scrapie Agent to Hamsters Involves Separation of Agent Strains from a Mixture. *Journal of General Virology* **39**, 487-496 (1978).
110. Kimberlin,R.H. & Walker,C.A. Pathogenesis of Mouse Scrapie - Effect of Route of Inoculation on Infectivity Titers and Dose-Response Curves. *Journal of Comparative Pathology* **88**, 39-47 (1978).
111. Dickinson,A.G., Meikle,V.M.H., & Fraser,H. Identification of a gene which controls the incubation period of some strains of scrapie agent in mice. *Journal of Comparative Pathology* **78**, 293-299 (1968).
112. Kingsbury,D.T. *et al.* Genetic control of scrapie and Creutzfeldt-Jakob disease in mice. *The Journal of Immunology* **131**, 491-496 (1983).

113. Moore,R.C. *et al.* Mice with gene targeted prion protein alterations show that *Prnp*, *Sinc* and *Prni* are congruent. *Nature Genetics* **18**, 118-125 (1998).
114. Barron,R.M. *et al.* Polymorphisms at codons 108 and 189 in murine PrP play distinct roles in the control of scrapie incubation time. *Journal of General Virology* **86**, 859-868 (2005).
115. Lloyd,S., Uphill,J.B., Targonski,P.V., Fisher E, & Collinge J Identification of genetic loci affecting mouse-adapted bovine spongiform encephalopathy incubation time in mice. *Neurogenetics* **4**, 77-81 (2002).
116. Moreno,C.R., Lantier,F., Lantier,I., Sarradin,P., & Elsen,J.M. Detection of new quantitative trait loci for susceptibility to transmissible spongiform encephalopathies in mice. *Genetics* **165**, 2085-2091 (2003).
117. Manolakou,K. *et al.* Genetic and environmental factors modify bovine spongiform encephalopathy incubation period in mice. *Proceedings of the National Academy of Science USA* **98**, 7402-7407 (2001).
118. Hitzemann,B., Dains,K., Kanen,S., & Hitzemann,R. Further-Studies on the Relationship Between Dopamine Cell-Density and Haloperidol-Induced Catalepsy. *Journal of Pharmacology and Experimental Therapeutics* **271**, 969-976 (1994).
119. Valdar,W. *et al.* Genome-wide genetic association of complex traits in heterogeneous stock mice. *Nature Genetics* **38**, 879-887 (2006).
120. Lloyd,S.E. *et al.* HECTD2 is associated with susceptibility to mouse and human prion disease. *Plos Genetics* **5**, e1000383 (2009).
121. Jeong,B.H. *et al.* Absence of Association between Two HECTD2 Polymorphisms and Sporadic Creutzfeldt-Jakob Disease. *Dementia and Geriatric Cognitive Disorders* **31**, 146-151 (2011).
122. Grizenkova,J. *et al.* Overexpression of the Hspa13 (Stch) gene reduces prion disease incubation time in mice. *Proceedings of the National Academy of Sciences USA* **109**, 13722-13727 (2012).
123. Otterson,G.A. *et al.* Stch Encodes the Atpase Core of A Microsomal Stress70 Protein. *EMBO Journal* **13**, 1216-1225 (1994).
124. Yamagata,N., Furuno,K., Sonoda,M., Sugimura,H., & Yamamoto,K. Stomach cancer-derived del223V-226L mutation of the STCH gene causes loss of sensitization to TRAIL-mediated apoptosis. *Biochemical and Biophysical Research Communications* **376**, 499-503 (2008).
125. Uberti,D. *et al.* TRAIL is expressed in the brain cells of Alzheimer's disease patients. *Neuroreport* **15**, 579-581 (2004).
126. Lloyd,S.E., Maytham,E.G., Grizenkova,J., Hummerich,H., & Collinge,J. A Copine family member, Cpne8, is a candidate quantitative trait gene for prion disease incubation time in mouse. *Neurogenetics* **11**, 185-191 (2010).

127. Tamguney,G. *et al.* Genes contributing to prion pathogenesis. *Journal of General Virology* **89**, 1777-1788 (2008).
128. Rosen,D.R. *et al.* Mutations in Cu/An superoxide dismutase gene are associated with familial amyotrophic lateral sclerosis. *Nature* **362**, 59-362 (1993).
129. Murakami,K. *et al.* SOD1 (Copper/Zinc Superoxide Dismutase) Deficiency Drives Amyloid beta Protein Oligomerization and Memory Loss in Mouse Model of Alzheimer Disease. *Journal of Biological Chemistry* **286**, 44557-44568 (2011).
130. Iadecola,C. *et al.* SOD1 rescues cerebral endothelial dysfunction in mice overexpressing amyloid precursor protein. *Nature Neuroscience* **2**, 157-161 (1999).
131. Freixes,M., Rodriguez,A., Dalfo,E., & Ferrer,I. Oxidation, glycooxidation, lipoxidation, nitration, and responses to oxidative stress in the cerebral cortex in Creutzfeldt-Jakob disease. *Neurobiology of Aging* **27**, 1807-1815 (2006).
132. Siskova,Z. *et al.* Morphological and Functional Abnormalities in Mitochondria Associated with Synaptic Degeneration in Prion Disease. *American Journal of Pathology* **177**, 1411-1421 (2010).
133. Barry,A.E. *et al.* Alzheimer's Disease Brain-Derived Amyloid-beta-Mediated Inhibition of LTP In Vivo Is Prevented by Immunotargeting Cellular Prion Protein. *Journal of Neuroscience* **31**, 7259-7263 (2011).
134. Sharief,M.K., Green,A., Dick,J.P.R., Gawler,J., & Thompson,E.J. Heightened intrathecal release of proinflammatory cytokines in Creutzfeldt-Jakob disease. *Neurology* **52**, 1289-1291 (1999).
135. Schultz,J. *et al.* Role of interleukin-1 in prion disease-associated astrocyte activation. *American Journal of Pathology* **165**, 671-678 (2004).
136. Akhtar,S. *et al.* Sod1 Deficiency Reduces Incubation Time in Mouse Models of Prion Disease. *PLoS ONE* **8**, e54454 (2013).
137. Thackray,A.M., McKenzie,A.N., Klein,M.A., Lauder,A., & Bujdoso,R. Accelerated prion disease in the absence of interleukin-10. *Journal of Virology* **78**, 13697-13707 (2004).
138. Mead,S. *et al.* Genetic risk factors for variant Creutzfeldt-Jakob disease: a genome-wide association study. *Lancet Neurology* **8**, 57-66 (2009).
139. Greenwood,A.D. *et al.* Cell Line Dependent RNA Expression Profiles of Prion-infected Mouse Neuronal Cells. *Journal of Molecular Biology* **349**, 487-500 (2005).
140. Stein,R., Mori,N., Matthews,K., Lo,L.C., & Anderson,D.J. The Ngf-Inducible Scg10 Messenger-RNA Encodes A Novel Membrane-Bound Protein Present in Growth Cones and Abundant in Developing Neurons. *Neuron* **1**, 463-476 (1988).

141. Stein,R., Orit,S., & Anderson,D.J. The Induction of A Neural-Specific Gene, Scg10, by Nerve Growth-Factor in Pc12 Cells Is Transcriptional, Protein-Synthesis Dependent, and Glucocorticoid Inhibitable. *Developmental Biology* **127**, 316-325 (1988).
142. Himi,T., Okazaki,T., & Mori,N. Scg10 Messenger-Rna Localization in the Hippocampus - Comparison with Other Messenger-Rnas Encoding Neuronal Growth-Associated Proteins (Ngaps). *Brain Research* **655**, 177-185 (1994).
143. Himi,T., Okazaki,T., Wang,H., Mcneill,T.H., & Mori,N. Differential Localization of Scg10 and P19/Stathmin Messenger-Rnas in Adult-Rat Brain Indicates Distinct Roles for These Growth-Associated Proteins. *Neuroscience* **60**, 907-926 (1994).
144. Sugiura,Y. & Mori,N. SCG10 expresses growth-associated manner in developing rat brain, but shows a different pattern to p19 stathmin or GAP-43. *Developmental Brain Research* **90**, 73-91 (1995).
145. Manna,T., Grenningloh,G., Miller,H.P., & Wilson,L. Stathmin family protein SCG10 differentially regulates the plus and minus end dynamics of microtubules at steady state in vitro: Implications for its role in neurite outgrowth. *Biochemistry* **46**, 3543-3552 (2007).
146. Riederer,B.M. *et al.* Regulation of microtubule dynamics by the neuronal growth-associated protein SCG10. *Proceedings of the National Academy of Sciences USA* **94**, 741-745 (1997).
147. Grizenkova,J., Akhtar,S., Collinge,J., & Lloyd,S.E. The retinoic Acid receptor Beta (rarb) region of mmu14 is associated with prion disease incubation time in mouse. *PLoS ONE* **5**, e15019 (2010).
148. Shen,S., Kruyt,F.A., den Hertog,J., van der Saag,P.T., & Kruijer,W. Mouse and human retinoic acid receptor beta 2 promoters: sequence comparison and localization of retinoic acid responsiveness. *DNA Sequence* **2**, 111-119 (1991).
149. Rybner,C., Hillion,J., Sahraoui,T., Lanotte,M., & Botti,J. All-trans retinoic acid down-regulates prion protein expression independently of granulocyte maturation. *Leukemia* **16**, 940-948 (2002).
150. Mead,S. *et al.* Genome-wide association study in multiple human prion diseases suggests genetic risk factors additional to PRNP. *Human Molecular Genetics* **21**, 1897-1906 (2012).
151. Sasai,N., Nakao,M., & Defossez,P.A. Sequence-specific recognition of methylated DNA by human zinc-finger proteins. *Nucleic Acids Research* **38**, 5015-5022 (2010).
152. Sanchez-Juan,P. *et al.* Genome-wide study links MTMR7 gene to variant Creutzfeldt-Jakob risk. *Neurobiology of Aging* **33**, e21 (2012).
153. Mochizuki,Y. & Majerus,P.W. Characterization of myotubularin-related protein 7 and its binding partner, myotubularin-related protein 9. *Proceedings of the National Academy of Sciences USA* **100**, 9768-9773 (2003).

154. Zou, J. *et al.* Myotubularin-related protein (MTMR) 9 determines the enzymatic activity, substrate specificity, and role in autophagy of MTMR8. *Proceedings of the National Academy of Sciences USA* **109**, 9539-9544 (2012).
155. Garcia, J.A. *et al.* Impaired cued and contextual memory in NPAS2-deficient mice. *Science* **288**, 2226-2230 (2000).
156. Dudley, C.A. *et al.* Altered patterns of sleep and behavioral adaptability in NPAS2-deficient mice. *Science* **301**, 379-383 (2003).
157. Wu, X.L., Wiater, M.F., & Ritter, S. NPAS2 deletion impairs responses to restricted feeding but not to metabolic challenges. *Physiology & Behavior* **99**, 466-471 (2010).
158. Hershko, A. & Ciechanover, A. The ubiquitin system. *Annual Review of Biochemistry* **67**, 425-479 (1998).
159. Li, W. *et al.* Genome-Wide and Functional Annotation of Human E3 Ubiquitin Ligases Identifies MULAN, a Mitochondrial E3 that Regulates the Organelle's Dynamics and Signaling. *PLoS ONE* **3**, e1487 (2008).
160. Glickman, M.H. & Ciechanover, A. The ubiquitin-proteasome proteolytic pathway: Destruction for the sake of construction. *Physiological Reviews* **82**, 373-428 (2002).
161. Kravtsova-Ivantsiv, Y., Sommer, T., & Ciechanover, A. The Lysine48-Based Polyubiquitin Chain Proteasomal Signal: Not a Single Child Anymore. *Angewandte Chemie-International Edition* **52**, 192-198 (2013).
162. Rotin, D. & Kumar, S. Physiological functions of the HECT family of ubiquitin ligases. *Nature Reviews Molecular Cell Biology* **10**, 398-409 (2009).
163. Clague, M.J., Liu, H., & Urbe, S. Governance of Endocytic Trafficking and Signaling by Reversible Ubiquitylation. *Developmental Cell* **23**, 457-467 (2012).
164. Hicke, L. Protein regulation by monoubiquitin. *Nature Reviews Molecular Cell Biology* **2**, 195-201 (2001).
165. Tan, J.M.M., Wong, E.S.P., Dawson, V.L., Dawson, T.M., & Lim, K.L. Lysine 63-linked polyubiquitin potentially partners with p62 to promote the clearance of protein inclusions by autophagy. *Autophagy* **4**, 251-253 (2008).
166. Tan, J.M.M. *et al.* Lysine 63-linked ubiquitination promotes the formation and autophagic clearance of protein inclusions associated with neurodegenerative diseases. *Human Molecular Genetics* **17**, 431-439 (2008).
167. Scheffner, M., Nuber, U., & Huibregtse, J.M. Protein Ubiquitination Involving An E1-E2-E3 Enzyme Ubiquitin Thioester Cascade. *Nature* **373**, 81-83 (1995).
168. Huibregtse, J.M., Scheffner, M., Beaudenon, S., & Howley, P.M. A Family of Proteins Structurally and Functionally Related to the E6-Ap Ubiquitin-Protein Ligase. *Proceedings of the National Academy of Sciences USA* **92**, 5249 (1995).

169. Hershko,A. & Ciechanover,A. The Ubiquitin System for Protein-Degradation. *Annual Review of Biochemistry* **61**, 761-807 (1992).
170. Wang,M. & Pickart,C.M. Different HECT domain ubiquitin ligases employ distinct mechanisms of polyubiquitin chain synthesis. *EMBO Journal* **24**, 4324-4333 (2005).
171. Ozkan,E., Yu,H.T., & Deisenhofer,J. Mechanistic insight into the allosteric activation of a ubiquitin-conjugating enzyme by RING-type ubiquitin ligases. *Proceedings of the National Academy of Sciences USA* **102**, 18890-18895 (2005).
172. Scheffner,M. & Staub,O. HECT E3s and human disease. *BMC Biochemistry* **8**, (2007).
173. Huang,L. *et al.* Structure of an E6AP-UbcH7 complex: Insights into ubiquitination by the E2-E3 enzyme cascade. *Science* **286**, 1321-1326 (1999).
174. Metzger,M.B., Hristova,V.A., & Weissman,A.M. HECT and RING finger families of E3 ubiquitin ligases at a glance. *Journal of Cell Science* **125**, 531-537 (2012).
175. Ciechanover,A. Proteolysis: from the lysosome to ubiquitin and the proteasome. *Nature Reviews Molecular Cell Biology* **6**, 79-86 (2005).
176. Shcherbik,N. & Haines,D.S. Ub on the move. *Journal of Cellular Biochemistry* **93**, 11-19 (2004).
177. Haglund,K. & Dikic,I. Ubiquitylation and cell signaling. *EMBO Journal* **24**, 3353-3359 (2005).
178. Haglund,K. & Dikic,I. The role of ubiquitylation in receptor endocytosis and endosomal sorting. *Journal of Cell Science* **125**, 265-275 (2012).
179. Hicke,L. & Dunn,R. Regulation of membrane protein transport by ubiquitin and ubiquitin-binding proteins. *Annual Review of Cell and Developmental Biology* **19**, 141-172 (2003).
180. Kirkin,V., Mcewan,D.G., Novak,I., & Dikic,I. A Role for Ubiquitin in Selective Autophagy. *Molecular Cell* **34**, 259-269 (2009).
181. Goldberg,A.L. Protein degradation and protection against misfolded or damaged proteins. *Nature* **426**, 895-899 (2003).
182. Andre,R. & Tabrizi,S.J. Misfolded PrP and a novel mechanism of proteasome inhibition. *Prion* **6**, 32-36 (2012).
183. Rubinsztein,D.C. The roles of intracellular protein-degradation pathways in neurodegeneration. *Nature* **443**, 780-786 (2006).
184. Kang,S.C. *et al.* Prion protein is ubiquitinated after developing protease resistance in the brains of scrapie-infected mice. *Journal of Pathology* **203**, 603-608 (2004).
185. Zanusso,G. *et al.* Proteasomal degradation and N-terminal protease resistance of the codon 145 mutant prion protein. *Journal of Biological Chemistry* **274**, 23396-23404 (1999).

186. Meusser,B., Hirsch,C., Jarosch,E., & Sommer,T. ERAD: the long road to destruction. *Nature Cell Biology* **7**, 766-772 (2005).
187. Bonifacino,J.S. & Weissman,A.M. Ubiquitin and the control of protein fate in the secretory and endocytic pathways. *Annual Review of Cell and Developmental Biology* **14**, 19-57 (1998).
188. Ma,J.Y. & Lindquist,S. Wild-type PrP and a mutant associated with prion disease are subject to retrograde transport and proteasome degradation. *Proceedings of the National Academy of Sciences USA* **98**, 14955-14960 (2001).
189. Yedidia,Y., Horonchik,L., Tzaban,S., Yanai,A., & Taraboulos,A. Proteasomes and ubiquitin are involved in the turnover of the wild-type prion protein. *EMBO Journal* **20**, 5383-5391 (2001).
190. Jin,T. *et al.* The chaperone protein BiP binds to a mutant prion protein and mediates its degradation by the proteasome. *Journal of Biological Chemistry* **275**, 38699-38704 (2000).
191. Ma,J.Y. & Lindquist,S. Conversion of PrP to a self-perpetuating PrPSc-like conformation in the cytosol. *Science* **298**, 1785-1788 (2002).
192. Hooper,N.M. Could inhibition of the proteasome cause mad cow disease? *Trends in Biotechnology* **21**, 144-145 (2003).
193. Bence,N.F., Sampat,R.M., & Kopito,R.R. Impairment of the ubiquitin-proteasome system by protein aggregation. *Science* **292**, 1552-1555 (2001).
194. Kristiansen,M. *et al.* Disease-associated prion protein oligomers inhibit the 26S proteasome. *Molecular Cell* **26**, 175-188 (2007).
195. Dantuma,N.P., Lindsten,K., Glas,R., Jellne,M., & Masucci,M.G. Short-lived green fluorescent proteins for quantifying ubiquitin/proteasome-dependent proteolysis in living cells. *Nature Biotechnology* **18**, 538-543 (2000).
196. Deriziotis,P. & Tabrizi,S.J. Prions and the proteasome. *Biochimica et Biophysica Acta* (2008).
197. Deriziotis,P. *et al.* Misfolded PrP impairs the UPS by interaction with the 20S proteasome and inhibition of substrate entry. *EMBO Journal* **30**, 3065-3077 (2011).
198. Metcalf,D.J., Garcia-Arencibia,M., Hochfeld,W.E., & Rubinsztein,D.C. Autophagy and misfolded proteins in neurodegeneration. *Experimental Neurology* **238**, 22-28 (2012).
199. Huang,J. & Klionsky,D.J. Autophagy and human disease. *Cell Cycle* **6**, 1837-1849 (2007).
200. Boellaard,J.W., Kao,M., Schlote,W., & Diringer,H. Neuronal autophagy in experimental scrapie. *Acta Neuropathologica* **82**, 225-228 (1991).

201. Sikorska,B., Liberski,P.P., & Brown,P. Neuronal autophagy and aggresomes constitute a consistent part of neurodegeneration in experimental scrapie. *Folia Neuropathologica* **45**, 170-178 (2007).
202. Lee,S., Sato,Y., & Nixon,R.A. Primary lysosomal dysfunction causes cargo-specific deficits of axonal transport leading to Alzheimer-like neuritic dystrophy. *Autophagy* **7**, 1562-1563 (2011).
203. Chu,C.T. *et al.* Autophagy in neurite injury and neurodegeneration: in vitro and in vivo models. *Methods Enzymology* **453**, 217-249 (2009).
204. Migheli,A., Attanasio,A., Vigliani,M.C., & Schiffer,D. Dystrophic neurites around amyloid plaques of human patients with Gerstmann-Straussler-Scheinker disease contain ubiquitinated inclusions. *Neuroscience Letters* **121**, 55-58 (1991).
205. Aguib,Y. *et al.* Autophagy induction by trehalose counteracts cellular prion infection. *Autophagy* **5**, 361-369 (2009).
206. Jeong,J.K., Moon,M.H., Lee,Y.J., Seol,J.W., & Park,S.Y. Autophagy induced by the class III histone deacetylase Sirt1 prevents prion peptide neurotoxicity. *Neurobiology of Aging* (2012).
207. Beranger,F., Crozet,C., Goldsborough,A., & Lehmann,S. Trehalose impairs aggregation of PrP(Sc) molecules and protects prion-infected cells against oxidative damage. *Biochemical and Biophysical Research Communications* (2008).
208. Heiseke,A., Aguib,Y., & Schatzl,H.M. Autophagy, Prion Infection and their Mutual Interactions. *Current Issues in Molecular Biology* **12**, 87-97 (2010).
209. Heiseke,A., Aguib,Y., Riemer,C., Baier,M., & Schatzl,H.M. Lithium induces clearance of protease resistant prion protein in prion-infected cells by induction of autophagy. *Journal of Neurochemistry* (2009).
210. Hara,T. *et al.* Suppression of basal autophagy in neural cells causes neurodegenerative disease in mice. *Nature* **441**, 885-889 (2006).
211. Komatsu,M. *et al.* Homeostatic levels of p62 control cytoplasmic inclusion body formation in autophagy-deficient mice. *Cell* **131**, 1149-1163 (2007).
212. Webb,J.L., Ravikumar,B., Atkins,J., Skepper,J.N., & Rubinsztein,D.C. Alpha-Synuclein is degraded by both autophagy and the proteasome. *Journal of Biological Chemistry* **278**, 25009-25013 (2003).
213. Ravikumar,B. *et al.* Inhibition of mTOR induces autophagy and reduces toxicity of polyglutamine expansions in fly and mouse models of Huntington disease. *Nature Genetics* **36**, 585-595 (2004).
214. Wu,Y.C. *et al.* Resveratrol-Activated AMPK/SIRT1/Autophagy in Cellular Models of Parkinson's Disease. *Neurosignals* **19**, 163-174 (2011).

215. Seo,J.S. *et al.* SIRT1, a histone deacetylase, regulates prion protein-induced neuronal cell death. *Neurobiology of Aging* (2010).
216. Kristiansen,M. *et al.* Disease-related prion protein forms aggresomes in neuronal cells leading to caspase-activation and apoptosis. *Journal of Biological Chemistry* **280**, 38851-38861 (2005).
217. Garcia-Mata,R., Gao,Y.S., & Sztul,E. Hassles with taking out the garbage: aggravating aggresomes. *Traffic*. **3**, 388-396 (2002).
218. Johnston,J.A., Ward,C.L., & Kopito,R.R. Aggresomes: a cellular response to misfolded proteins. *Journal of Cell Biology* **143**, 1883-1898 (1998).
219. Mishra,R.S., Bose,S., Gu,Y., Li,R., & Singh,N. Aggresome formation by mutant prion proteins: The unfolding role of proteasomes in familial prion disorders. *Journal of Alzheimers Disease* **5**, 15-23 (2003).
220. Dron,M., Dandoy-Dron,F., Salamat,M.K., & Laude,H. Proteasome inhibitors promote the sequestration of PrPSc into aggresomes within the cytosol of prion-infected CAD neuronal cells. *Journal of General Virology* (2009).
221. Kawaguchi,Y. *et al.* The deacetylase HDAC6 regulates aggresome formation and cell viability in response to misfolded protein stress. *Cell* **115**, 727-738 (2003).
222. Garcia-Mata,R., Bebok,Z., Sorscher,E.J., & Sztul,E.S. Characterization and dynamics of aggresome formation by a cytosolic GFP-chimera. *Molecular Biology of the Cell* **10**, 1239-1254 (1999).
223. Yao,H., Zhao,D., Khan,S.H., & Yang,L. Role of autophagy in prion protein-induced neurodegenerative diseases. *Acta Biochimica Biophysica Sinica*(2013).
224. Chakrabarti,O. & Hegde,R.S. Functional depletion of mahogunin by cytosolically exposed prion protein contributes to neurodegeneration. *Cell* **137**, 1136-1147 (2009).
225. He,L. *et al.* Spongiform degeneration in mahoganoid mutant mice. *Science* **299**, 710-712 (2003).
226. Silviu,D. *et al.* Levels of the Mahogunin Ring Finger 1 E3 Ubiquitin Ligase Do Not Influence Prion Disease. *PLoS ONE* **8**, e55575 (2013).
227. Miyazaki,K. *et al.* NEDL1, a novel ubiquitin-protein isopeptide ligase for dishevelled-1, targets mutant superoxide dismutase-1. *Journal of Biological Chemistry* **279**, 11327-11335 (2004).
228. Gagliardi,S. *et al.* SOD1 mRNA expression in sporadic amyotrophic lateral sclerosis. *Neurobiology of Disease* **39**, 198-203 (2010).
229. Zhang,L., Haraguchi,S., Koda,T., Hashimoto,K., & Nakagawara,A. Muscle Atrophy and Motor Neuron Degeneration in Human NEDL1 Transgenic Mice. *Journal of Biomedicine and Biotechnology* **2011**, 831092 (2011).

230. Hegde,A.N. & Upadhyya,S.C. Role of ubiquitin-proteasome-mediated proteolysis in nervous system disease. *Biochimica et Biophysica Acta-Gene Regulatory Mechanisms* **1809**, 128-140 (2011).
231. Niwa,J. *et al.* Dornfin ubiquitylates mutant SOD1 and prevents mutant SOD1-mediated neurotoxicity. *Journal of Biological Chemistry* **277**, 36793-36798 (2002).
232. Hishikawa,N. *et al.* Dornfin localizes to the ubiquitylated inclusions in Parkinson's disease, dementia with Lewy bodies, multiple system atrophy, and amyotrophic lateral sclerosis. *American Journal of Pathology* **163**, 609-619 (2003).
233. Ito,T. *et al.* Dornfin localizes to Lewy bodies and ubiquitylates synphilin-1. *Journal of Biological Chemistry* **278**, 29106-29114 (2003).
234. Hardy,J., Lewis,P., Revesz,T., Lees,A., & Paisan-Ruiz,C. The genetics of Parkinson's syndromes: a critical review. *Current Opinion in Genetics & Development* **19**, 254-265 (2009).
235. Mezey,E. *et al.* Alpha synuclein is present in Lewy bodies in sporadic Parkinson's disease. *Molecular Psychiatry* **3**, 493-499 (1998).
236. Kitada,T. *et al.* Mutations in the parkin gene cause autosomal recessive juvenile parkinsonism. *Nature* **392**, 605-608 (1998).
237. Deas,E., Wood,N.W., & Plun-Favreau,H. Mitophagy and Parkinson's disease: The PINK1-parkin link. *Biochimica et Biophysica Acta-Molecular Cell Research* **1813**, 623-633 (2011).
238. Sul,J.W. *et al.* Accumulation of the parkin substrate, FAF1, plays a key role in the dopaminergic neurodegeneration. *Human Molecular Genetics* **22**, 1558-1573 (2013).
239. Lonskaya,I. *et al.* Diminished Parkin Solubility and Co-Localization with Intraneuronal Amyloid-beta are Associated with Autophagic Defects in Alzheimer's Disease. *Journal of Alzheimers Disease* **33**, 231-247 (2013).
240. Li,J.H. *et al.* SEL-10 interacts with presenilin 1, facilitates its ubiquitination, and alters A-beta peptide production. *Journal of Neurochemistry* **82**, 1540-1548 (2002).
241. Schellenberg,G.D. & Montine,T.J. The genetics and neuropathology of Alzheimer's disease. *Acta Neuropathologica* **124**, 305-323 (2012).
242. Shojaee,S. *et al.* Genome-wide linkage analysis of a Parkinsonian-pyramidal syndrome pedigree by 500 KSNP arrays. *American Journal of Human Genetics* **82**, 1375-1384 (2008).
243. Di Fonzo,A. *et al.* FBXO7 mutations cause autosomal recessive, early-onset parkinsonian-pyramidal syndrome. *Neurology* **72**, 240-245 (2009).
244. Ho,M.S., Ou,C., Chan,Y.R., Chien,C.T., & Pi,H. The utility F-box for protein destruction. *Cellular and Molecular Life Sciences* **65**, 1977-2000 (2008).

245. Lewis,P.A. & Cookson,M.R. Gene expression in the Parkinson's disease brain. *Brain Research Bulletin* **88**, 302-312 (2012).
246. Grunblatt,E. *et al.* Gene expression profiling of parkinsonian substantia nigra pars compacta; alterations in ubiquitin-proteasome, heat shock protein, iron and oxidative stress regulated proteins, cell adhesion/cellular matrix and vesicle trafficking genes. *Journal of Neural Transmission* **111**, 1543-1573 (2004).
247. Urushitani,M. *et al.* CHIP promotes proteasomal degradation of familial ALS-linked mutant SOD1 by ubiquitinating Hsp/Hsc70. *Journal of Neurochemistry* **90**, 231-244 (2004).
248. Jana,N.R. *et al.* Co-chaperone CHIP associates with expanded polyglutamine protein and promotes their degradation by proteasomes. *Journal of Biological Chemistry* **280**, 11635-11640 (2005).
249. Petrucelli,L. *et al.* CHIP and Hsp70 regulate tau ubiquitination, degradation and aggregation. *Human Molecular Genetics* **13**, 703-714 (2004).
250. Miller,V.M. *et al.* CHIP suppresses polyglutamine aggregation and toxicity in vitro and in vivo. *Journal of Neuroscience* **25**, 9152-9161 (2005).
251. Sakahira,H., Breuer,P., Hayer-Hartl,M.K., & Hartl,F.U. Molecular chaperones as modulators of polyglutamine protein aggregation and toxicity. *Proceedings of the National Academy of Sciences USA* **99**, 16412-16418 (2002).
252. Shin,Y.G., Klucken,J., Patterson,C., Hyman,B.T., & Mclean,P.J. The co-chaperone carboxyl terminus of Hsp70-interacting protein (CHIP) mediates alpha-synuclein degradation decisions between proteasomal and lysosomal pathways. *Journal of Biological Chemistry* **280**, 23727-23734 (2005).
253. Klohn,P., Stoltze,L., Flechsig,E., Enari,M., & Weissmann,C. A quantitative, highly sensitive cell-based infectivity assay for mouse scrapie prions. *Proceedings of the National Academy of Sciences USA* **100**, 11666-11671 (2003).
254. Rozen,S. & Skaletsky,H. Primer3 on the WWW for general users and for biologist programmers. *Methods in Molecular Biology* **132**, 365-386 (2000).
255. Reynolds,A. *et al.* Rational siRNA design for RNA interference. *Nature Biotechnology* **22**, 326-330 (2004).
256. Brummelkamp,T.R., Bernards,R., & Agami,R. Stable suppression of tumorigenicity by virus-mediated RNA interference. *Cancer Cell* **2**, 243-247 (2002).
257. Davis,H.E., Rosinski,M., Morgan,J.R., & Yarmush,M.L. Charged polymers modulate retrovirus transduction via membrane charge neutralization and virus aggregation. *Biophysical Journal* **86**, 1234-1242 (2004).
258. Fields,S. & Song,O.K. A Novel Genetic System to Detect Protein Protein Interactions. *Nature* **340**, 245-246 (1989).

259. Chien,C.T., Bartel,P.L., Sternglanz,R., & Fields,S. The 2-Hybrid System - A Method to Identify and Clone Genes for Proteins That Interact with A Protein of Interest. *Proceedings of the National Academy of Sciences USA* **88**, 9578-9582 (1991).
260. Silver,P.A., Keegan,L.P., & Ptashne,M. Amino Terminus of the Yeast Gal4 Gene-Product Is Sufficient for Nuclear-Localization. *Proceedings of the National Academy of Sciences USA* **81**, 5951-5955 (1984).
261. Parent,S.A., Fenimore,C.A., Bostian,K.A. Vectors systems for the expression, analysis and cloning of DNA sequences in *S. cerevisiae*. *Yeast* **1**, 83-138 (1985).
262. Phizicky,E.M. & Fields,S. Protein-Protein Interactions - Methods for Detection and Analysis. *Microbiological Reviews* **59**, 94-123 (1995).
263. Fernandez,J., & Hoeffler,J. Gene expression systems: using nature for the art of expression. *Academic Press, San Diego CA*, 1-460 (1999).
264. Gluzman,Y. Sv40-Transformed Simian Cells Support the Replication of Early Sv40 Mutants. *Cell* **23**, 175-182 (1981).
265. Wan,J. *et al.* Endophilin B1 as a novel regulator of nerve growth factor/TrkA trafficking and neurite outgrowth. *Journal of Neuroscience* **28**, 9002-9012 (2008).
266. Cheung ZH,I.NY. Endophilin B1: Guarding the gate to destruction. *Communicative & Integrative Biology* **2**, 130-132 (2009).
267. Wong,A.S.L. *et al.* Cdk5-mediated phosphorylation of endophilin B1 is required for induced autophagy in models of Parkinson's disease. *Nature Cell Biology* **13**, 568-U167 (2011).
268. Modregger,J., Schmidt,A.A., Ritter,B., Huttner,W.B., & Plomann,M. Characterization of endophilin B1b, a brain-specific membrane-associated lysophosphatidic acid acyl transferase with properties distinct from endophilin A1. *Journal of Biological Chemistry* **278**, 4160-4167 (2003).
269. Suzuki,S. *et al.* AMSH is required to degrade ubiquitinated proteins in the central nervous system. *Biochemical and Biophysical Research Communications* **408**, 582-588 (2011).
270. Ishii,N. *et al.* Loss of neurons in the hippocampus and cerebral cortex of AMSH-deficient mice. *Molecular and Cellular Biology* **21**, 8626-8637 (2001).
271. Senju,Y., Itoh,Y., Takano,K., Hamada,S., & Suetsugu,S. Essential role of PACSIN2/syndapin-II in caveolae membrane sculpting. *Journal of Cell Science* **124**, 2032-2040 (2011).
272. Ritter,B., Modregger,J., Paulsson,M., & Plomann,M. PACSIN 2, a novel member of the PACSIN family of cytoplasmic adapter proteins. *FEBS Letters* **454**, 356-362 (1999).

273. Grimm-Gunter,E.M.S., Milbrandt,M., Merkl,B., Paulsson,M., & Plomann,M. PACSIN proteins bind tubulin and promote microtubule assembly. *Experimental Cell Research* **314**, 1991-2003 (2008).
274. Modregger,J., Ritter,B., Witter,B., Paulsson,M., & Plomann,M. All three PACSIN isoforms bind to endocytic proteins and inhibit endocytosis. *Journal of Cell Science* **113**, 4511-4521 (2000).
275. Osiecka,K.M., Nieznanska,H., Skowronek,K.J., Jozwiak,J., & Nieznanski,K. Tau inhibits tubulin oligomerization induced by prion protein. *Biochimica et Biophysica Acta-Molecular Cell Research* **1813**, 1845-1853 (2011).
276. Hall,P.A., Jung,K., Hillan,K.J., & Russell,S.E.H. Expression profiling the human septin gene family. *Journal of Pathology* **206**, 269-278 (2005).
277. Hall,P.A. & Russell,S.E.H. The pathobiology of the septin gene family. *Journal of Pathology* **204**, 489-505 (2004).
278. Hsu,S.C. *et al.* Subunit composition, protein interactions, and structures of the mammalian brain sec6/8 complex and septin filaments. *Neuron* **20**, 1111-1122 (1998).
279. Kessels,M.M. & Qualmann,B. The syndapin protein family: linking membrane trafficking with the cytoskeleton. *Journal of Cell Science* **117**, 3077-3086 (2004).
280. Takahashi,Y. *et al.* Bif-1 regulates Atg9 trafficking by mediating the fission of Golgi membranes during autophagy. *Autophagy* **7**, 61-73 (2011).
281. Sierra,M.I., Wright,M.H., & Nash,P.D. AMSH Interacts with ESCRT-0 to Regulate the Stability and Trafficking of CXCR4. *Journal of Biological Chemistry* **285**, 13990-14004 (2010).
282. Agromayor,M. & Martin-Serrano,J. Interaction of AMSH with ESCRT-III and deubiquitination of endosomal cargo. *Journal of Biological Chemistry* **281**, 23083-23091 (2006).
283. Kinoshita,A. *et al.* Identification of septins in neurofibrillary tangles in Alzheimer's disease. *American Journal of Pathology* **153**, 1551-1560 (1998).
284. Kinoshita,M. Assembly of mammalian septins. *Journal of Biochemistry* **134**, 491-496 (2003).
285. Tararuk,T. *et al.* JNK1 phosphorylation of SCG10 determines microtubule dynamics and axodendritic length. *Journal of Cell Biology* **173**, 265-277 (2006).
286. Brummelkamp,T.R., Bernards,R., & Agami,R. A system for stable expression of short interfering RNAs in mammalian cells. *Science* **296**, 550-553 (2002).
287. Vorberg,I. & Priola,S.A. Molecular basis of scrapie strain glycoform variation. *Journal of Biological Chemistry* **277**, 36775-36781 (2002).

288. Akhtar,S., Wenborn,A., Brandner,S., Collinge,J., & Lloyd,S.E. Sex effects in mouse prion disease incubation time. *PLoS ONE* **6**, e28741 (2011).
289. Hogan,B., Beddington,R., Costantini,F., & Lacy,E. Manipulating the mouse embryo. A laboratory manual. *Cold Spring Harbor Press* 1-497 (1994).
290. Shimura,H. *et al.* Familial Parkinson disease gene product, parkin, is a ubiquitin-protein ligase. *Nature Genetics* **25**, 302-305 (2000).
291. Bhutani,S., Das,A., Maheshwari,M., Lakhotia,S.C., & Jana,N.R. Dysregulation of core components of SCF complex in poly-glutamine disorders. *Cell Death & Disease* **3**, (2012).
292. Cummings,C.J. *et al.* Mutation of the E6-AP ubiquitin ligase reduces nuclear inclusion frequency while accelerating polyglutamine-induced pathology in SCA1 mice. *Neuron* **24**, 879-892 (1999).
293. Bartel,P., Chien,C.T., Sternglanz,R., & Fields,S. Elimination of False Positives That Arise in Using the 2-Hybrid System. *Biotechniques* **14**, 920-924 (1993).
294. Tada,T. *et al.* Role of septin cytoskeleton in spine morphogenesis and dendrite development in neurons. *Current Biology* **17**, 1752-1758 (2007).
295. Nakashima,A. *et al.* Association of CAD, a multifunctional protein involved in pyrimidine synthesis, with mLST8, a component of the mTOR complexes. *Journal of Biomedical Science* **20**, (2013).
296. Jacinto,E. *et al.* Mammalian TOR complex 2 controls the actin cytoskeleton and is rapamycin insensitive. *Nature Cell Biology* **6**, 1122-1130 (2004).
297. Su,H. *et al.* The COP9 Signalosome Is Required for Autophagy, Proteasome-Mediated Proteolysis, and Cardiomyocyte Survival in Adult Mice. *Circulation: Heart Failure* **113**, 1-31 (2013).
298. Ma,H.L. *et al.* The Goldfish SG2NA Gene Encodes Two α -Type Regulatory Subunits for PP-2A and Displays Distinct Developmental Expression Pattern. *Gene Regulation and Systems Biology* **3**, 115-129 (2013).
299. Magnaudeix,A. *et al.* PP2A blockade inhibits autophagy and causes intraneuronal accumulation of ubiquitinated proteins. *Neurobiology of Aging* **34**, 770-790 (2013).
300. Qi,Z.F. *et al.* Loss of PINK1 function decreases PP2A activity and promotes autophagy in dopaminergic cells and a murine model. *Neurochemistry International* **59**, 572-581 (2011).
301. Goold,R. *et al.* Rapid cell-surface prion protein conversion revealed using a novel cell system. *Nature Communications* **2**, (2011).
302. Cuddeback,S.M. *et al.* Molecular cloning and characterization of Bif-1 - A novel Src homology 3 domain-containing protein that associates with Bax. *Journal of Biological Chemistry* **276**, 20559-20565 (2001).

303. Pierrat,B. *et al.* SH3GLB, a new endophilin-related protein family featuring an SH3 domain. *Genomics* **71**, 222-234 (2001).
304. Takahashi,Y., Meyerkord,C.L., & Wang,H.G. BARgaining membranes for autophagosome formation: Regulation of autophagy and tumorigenesis by Bif-1/Endophilin B1. *Autophagy* **4**, 121-124 (2008).
305. Takahashi,Y., Meyerkord,C.L., & Wang,H.G. Bif-1/Endophilin B1: a candidate for crescent driving force in autophagy. *Cell Death and Differentiation* **16**, 947-955 (2009).
306. Karbowski,M., Jeong,S.Y., & Youle,R.J. Endophilin B1 is required for the maintenance of mitochondrial morphology. *Journal of Cell Biology* **166**, 1027-1039 (2004).
307. Takahashi,Y. *et al.* Bif-1 interacts with Beclin 1 through UVRAG and regulates autophagy and tumorigenesis. *Nature Cell Biology* **9**, 1142-1151 (2007).
308. Petiot,A., Ogier-Denis,E., Blommaert,E.F.C., Meijer,A.J., & Codogno,P. Distinct classes of phosphatidylinositol 3'-kinases are involved in signaling pathways that control macroautophagy in HT-29 cells. *Journal of Biological Chemistry* **275**, 992-998 (2000).
309. Takahashi,Y. *et al.* Bif-1 haploinsufficiency promotes chromosomal instability and accelerates Myc-driven lymphomagenesis via suppression of mitophagy. *Blood* **121**, 1622-1632 (2013).
310. McInnes J. Insights on altered mitochondrial function and dynamics in the pathogenesis of neurodegeneration. *Translational Neurodegeneration* **2**, 1-7 (2013).
311. Jackson,A.L. *et al.* Widespread siRNA "off-target" transcript silencing mediated by seed region sequence complementarity. *RNA* **12**, 1179-1187 (2006).
312. Shehadeh,L., Mitsi,G., Adi,N., Bishopric,N., & Papapetropoulos,S. Expression of Lewy Body Protein Septin 4 in Postmortem Brain of Parkinson's Disease and Control Subjects. *Movement Disorders* **24**, 204-210 (2009).
313. Tsang,C.W. *et al.* Characterization of presynaptic septin complexes in mammalian hippocampal neurons. *Biological Chemistry* **392**, 739-749 (2011).
314. Field,C.M. & Kellogg,D. Septins: cytoskeletal polymers or signalling GTPases? *Trends in Cell Biology* **9**, 387-394 (1999).
315. Versele,M. & Thorner,J. Some assembly required: yeast septins provide the instruction manual. *Trends in Cell Biology* **15**, 414-424 (2005).
316. Xie,Y.L. *et al.* The GTP-binding protein septin 7 is critical for dendrite branching and dendritic-spine morphology. *Current Biology* **17**, 1746-1751 (2007).
317. Kinoshita,M. Diversity of septin scaffolds. *Current Opinion in Cell Biology* **18**, 54-60 (2006).

318. Kinoshita,A., Noda,M., & Kinoshita,M. Differential localization of septins in the mouse brain. *Journal of Comparative Neurology* **428**, 223-239 (2000).
319. Kinoshita,M., Field,C.M., Coughlin,M.L., & Mitchison,T.J. The mammalian septin complexes: composition, ultrastructure and interaction. *Molecular Biology of the Cell* **11**, 1111-1122, (2000).
320. Beites,C.L., Xie,H., Bowser,R., & Trimble,W.S. The septin CDCrel-1 binds syntaxin and inhibits exocytosis. *Nature Neuroscience* **2**, 434-439 (1999).
321. Beites,C.L., Campbell,K.A., & Trimble,W.S. The septin Sept5/CDCrel-1 competes with alpha-SNAP for binding to the SNARE complex. *Biochemical Journal* **385**, 347-353 (2005).
322. Engmann,O. *et al.* Cyclin-Dependent Kinase 5 Activator p25 Is Generated During Memory Formation and Is Reduced at an Early Stage in Alzheimer's Disease. *Biological Psychiatry* **70**, 159-168 (2011).
323. Engmann,O. *et al.* Schizophrenia is associated with dysregulation of a Cdk5 activator that regulates synaptic protein expression and cognition. *Brain* **134**, 2408-2421 (2011).
324. Lee,M.S. *et al.* Neurotoxicity induces cleavage of p35 to p25 by calpain. *Nature* **405**, 360-364 (2000).
325. Harada,T., Morooka,T., Ogawa,S., & Nishida,E. ERK induces p35, a neuron-specific activator of Cdk5, through induction of Egr1. *Nature Cell Biology* **3**, 453-459 (2001).
326. Patrick,G.N. *et al.* Conversion of p35 to p25 deregulates Cdk5 activity and promotes neurodegeneration. *Nature* **402**, 615-622 (1999).
327. Naj,A.C. *et al.* Common variants at MS4A4/MS4A6E, CD2AP, CD33 and EPHA1 are associated with late-onset Alzheimer's disease. *Nature Genetics* **43**, 436-441, (2011).
328. Wasik,A.A. *et al.* Septin 7 forms a complex with CD2AP and nephrin and regulates glucose transporter trafficking. *Molecular Biology of the Cell* **23**, 3370-3379 (2012).
329. Kuhlenbaumer,G. *et al.* Mutations in SEPT9 cause hereditary neuralgic amyotrophy. *Nature Genetics* **37**, 1044-1046 (2005).
330. Ihara,M. *et al.* Sept4, a component of presynaptic scaffold and Lewy bodies, is required for the suppression of alpha-synuclein neurotoxicity. *Neuron* **53**, 519-533 (2007).
331. Ihara,M. *et al.* Association of the cytoskeletal GTP-binding protein Sept4/H5 with cytoplasmic inclusions found in Parkinson's disease and other synucleinopathies. *Journal of Biological Chemistry* **278**, 24095-24102 (2003).
332. McCullough,J. *et al.* Activation of the endosome-associated ubiquitin isopeptidase AMSH by STAM, a component of the multivesicular body-sorting machinery. *Current Biology* **16**, 160-165 (2006).

333. Raiborg,C. & Stenmark,H. The ESCRT machinery in endosomal sorting of ubiquitylated membrane proteins. *Nature* **458**, 445-452 (2009).
334. Kim,M.S., Kim,J.A., Song,H.K., & Jeon,H. STAM-AMSH interaction facilitates the deubiquitination activity in the C-terminal AMSH. *Biochemical and Biophysical Research Communications* **351**, 612-618 (2006).
335. McCullough,J., Clague,M.J., & Urbe,S. AMSH is an endosome-associated ubiquitin isopeptidase. *Journal of Cell Biology* **166**, 487-492 (2004).
336. Nieznanski,K., Nieznanska,H., Skowronek,K.J., Osiecka,K.M., & Stepkowski,D. Direct interaction between prion protein and tubulin. *Biochemical and Biophysical Research Communications* **334**, 403-411 (2005).
337. Nieznanski,K., Podlubnaya,Z.A., & Nieznanska,H. Prion protein inhibits microtubule assembly by inducing tubulin oligomerization. *Biochemical and Biophysical Research Communications* **349**, 391-399 (2006).
338. Osiecka,K.M. *et al.* Prion protein region 23-32 interacts with tubulin and inhibits microtubule assembly. *Proteins-Structure Function and Bioinformatics* **77**, 279-296 (2009).
339. Shin,J.E. *et al.* SCG10 is a JNK target in the axonal degeneration pathway. *Proceedings of the National Academy of Sciences USA* **109**, E3696-E3705 (2012).
340. Lipton,R.B. *et al.* Taxol Produces A Predominantly Sensory Neuropathy. *Neurology* **39**, 368-373 (1989).
341. Cortes,J. & Baselga,J. Targeting the microtubules in breast cancer beyond taxanes: The epothilones. *Oncologist* **12**, 271-280 (2007).
342. De Vos,K.J., Grierson,A.J., Ackerley,S., & Miller,C.C.J. Role of axonal transport in neurodegenerative diseases. *Annual Review of Neuroscience* **31**, 151-173 (2008).

9 Appendices

Appendix 1 Solution formulations

1.1 Bacterial selection plates

Media	Antibiotic selection [concentration]
LB agar/broth	Kanamycin, [50 µg/ml], reconstituted in ddH ₂ O
LB agar/broth	Ampicillin, [100 µg/ml], reconstituted in ddH ₂ O

1.2 Yeast selection plates

Ready-to-go yeast media pouches were sourced from Clontech Takara BioEurope and prepared as follows: 500 ml of ddH₂O was mixed with the pouch contents and autoclaved at 121°C for 15 minutes. Agar/broth media were cooled to 50°C prior to addition of supplements; agar was poured into plates and set at room temperature and both media types were stored at 4°C.

YPDA plates are constituted from a mix of yeast extract, peptone and dextrose supplemented with adenine hemisulfate and SD, (minimal synthetically defined) medium is a blend of yeast nitrogen base, glucose and the indicated amino acid dropout supplement. Growth and selection of yeast were carried out using the media listed below.

Agar/broth media	Selection supplement [final concentration]	Strain
YPDA Agar	-	Y2HGold/Y187
YPDA Broth	-	Y2HGold/Y187
SD/-Trp	-	Y2HGold
SD/-Leu	-	Y187
SD/-Trp/-Leu	-	Y2HGold
SD/-Trp/-Leu/X	X- α -Gal [40 µg/ml]	Y2HGold
SD/-Trp/-Leu/X/A	X- α -Gal [40 µg/ml], Aureobasidin A [125 ng/µl]	Y2HGold
SD/-Trp/-Leu/-Ade/-His	-	Y2HGold
SD/-Trp/-Leu/-Ade/-His/X/A	X- α -Gal [40 µg/ml], Aureobasidin A [125 ng/µl]	Y2HGold

Yeast media selection supplements

X- α -Gal (X)	20mg dissolved in 1ml N, N-dimethylformamide
Aureobasidin A (AbA)	1mg dissolved in 2ml absolute ethanol

1.3 Yeast transformation solutions

Yeast transformation solutions

Reagent	Final concentration
TE/Lithium Acetate	1.1 X
PEG/Lithium Acetate	
50% PEG 3350	40% v/v
TE	1X
1M Lithium Acetate	1X
NaCl	0.9% w/v

1.4 Yeast protein extraction solutions and buffers

Protease inhibitor solution

	Final concentration
Pepstatin A	1 mg/ml
Leupeptin	10.5 mM
Benzamidine	200 mM
Aprotinin	2.1 mg/ml

Cracking buffer stock solution	
	<i>Final concentration</i>
Urea	8M
SDS	5% w/v
Tris.HCl	40mM
EDTA	0.1 mM
Bromophenol blue	0.4mg/ml

Complete cracking buffer	
	<i>To prepare 1.13ml</i>
Cracking buffer stock solution	1ml
B-mercaptoethanol	10 µl
Protease inhibitor solution	70 µl
PMSF	50 µl of 100X stock solution

1.5 Mammalian cell lysis buffers

1.5.1 Standard cell lysis buffer*

Reagent	Final concentration
HEPES	25mM
EGTA	1mM
Glycerol	5% v/v
MgCl ₂	1mM
β-glycerophosphate	20mM
Triton x-100	0.5% v/v

1.5.2 RIPA buffer*

Reagent	Final concentration
NaCl	150mM
HEPES	10mM
Triton x-100	1% v/v
Sodium Dodecyl Sulphate	0.1% v/v
Sodium deoxycholate	1% v/v

*Buffers adjusted to pH 7.5 and protease inhibitors added as detailed in Section 2.2.9.2

Appendix 2 Vectors

Vector	Source	Vector map electronic reference
pGBKT7	Clontech	PT3248-5
pGADT7-recAB	Clontech	PT3718-5
pCRII-Blunt-TOPO	Life Technologies Ltd	K2820-20
pCMV-MYC	Clontech	PT3282-5
pCMV-HA	Clontech	PT3283-5
pSUPER.retro.puro	OligoEngine	VEC-PRT-0002

Appendix 3 Sequences

Nucleotide sequences of clones were obtained using the ABI PRISM 3700 DNA Analyzer platform and are presented below. Identities of each sequence were ascertained via a BLAST search using the NCBI mouse transcript database (Section2). Nucleotide positions in reference to the mRNA transcript are provided with the reference sequence accession numbers. Start and stop codons are marked in green or red, respectively, on the full length sequences obtained and if appropriate on the cDNA fragment of the same sequence. The cDNA sequences represent fragments of genes cloned into the pGADT7-recAB plasmid, derived from the yeast two-hybrid screen. Their coverage of the full length counterpart is indicated in Table 3.5.1, Section 3.

Hectd2 / accession number: NM_172637.2

5 **atg**agtgaggcggctcgggatctctcgcccggagcgccgcccggcggtagccgcccggccccggag
gagaggaaggggaaagaaccggagcgcgagaagctgccgccatcgtgacggccggcgcagccgcccggctt
ggacagaggatccaagggccagatctccaccttcagcagctttgtctcgactgtcaccagaagaaggaag
ctgctgagaacagaagctcgcctaccaccttgctctccctaacatcaggaatgtgagagacctaccacca
atctgtcttgatgtagacaaaaacagcgcgatgtctgtggaagcgttaccatctgaagtgaaggtcccgcc
ccttcagaaccttctcttcctagccagcccaaaactgtaaaagactttgaggaagatttagaaaaagctg
aggccacaggggaattggaagacagtacatgctttttatataacagcatttgattctttcacagaactaac
actgcatttaagaaagatgccacggcctcatttaatactattgaggactctgggcttaatgccaatgtgt
gaatgctgtgtttgatgccttacttaatactcctcaagatatccagaagtcagtattgaagggaaatcatta
acagcttgttacaagaatggaaaggtccacgaacaaaagatgatcttagagcatatcttatactgttacag
aatcctcaatttaatatcacatctacatatgtcatctatgctcatttgctacgacagatagctaccttagt
ggaagctgacctcacttctagttcactggcttaaaaaattatcccagaagaaattcaagcaactggtag
agagattgctgcaatttgctttctttacggctgtttccagcaaaacctgaagaattcccgcctctaacgaag
tgtacctgggtggatcccacagccggtaaaagttctggctttgcttaacactgccacaatttggttccacc
tcccctcgttcttactgattttctataattctaccctggatcacattgatctcatggaagagtatcaca
cgtggcagagctttgggaactctcacaggttttcttctgtcagtagccattcgttattttctatagctgca
aaaaaatcattattcaagagactcagaacaacagatgataagcatcgcaaggcaaagtctgggtggataa
agtatctcgaagacaaagacctgatatgaatatgttattttctaaatatgaaagtaaggaggacacatctgg
ttagcgactcacttgatgagtttaaccgggaagagagctgacttgaagaagaagttgaaagttacatttgta
gggtgaagctgggttgatattgggcccgttgactaaagaatgggttcttcttctaattcgccagatcttcca
tccagattatggcatgtttacataaccacaaggattcacactgccattgggttagcagctttaaattgtgata
actattctgaattccgattgggttggaaattctcatgggactagctgtttataacagcatcaccttggatatt
cgttttctcctcctgctgtttacaaaaattactgagccctcctgtcgtaccaagtgatcagagtacaccagt
aggcatctgcagtggttaccattgacgacttgtgccaggttatgcctgaattggcccatggactaaaggaac
ttttatcatatgaaggcaacggttgaagaagattttctattcaacatttcagggtttttcaagaagaatttggg
gtaattaaatcctataacttaaaaccaggggggtgataagattccagttaccaatcagaatagaagagagta
tgtacagctttatactgacttctgttgaacaaatctatctataagcaatttgctgcattttactgtggat
ttcatagtgtgtgtgcttcaaagccctaagtctgcttccgtaagaagtagaaatcctgggtttgtggc
agtctgaactggatgcatgcactgcagaggagcacacagtagcagcggctatgcaagacagacctgac
catacgatacttttgggatgttgtgcttggatctccacttgaacttcagaaaaagctgttacactttacta
caggaagcgacagagtacctgttggagggtgctgatttgaattttaaaatttcaaagaatgaaacttct
actaactgggttacctgtggcacacacttgtttcaatcaactctgccttccccatacaagagcagaaaaga
tctgaaacagaaactgattattggaatttcaaattcagaaggttttggactt**gaa** 2326

Hect414

5 **atg**agtgaggcggctcgggatctctcgcccggagcgccgcccggcggtagccgcccggccccggag
gagaggaaggggaaagaaccggagcgcgagaagctgccgcccatcgtgacggccggcgcagccgcccggctt
ggacagaggatccaagggccagatctccaccttcagcagctttgtctcgactgtcaccagaagaaggaag
ctgctgagaacagaagctcgcctaccaccttgctctccctaacatcaggaatgtgagagacctaccacca
atctgtcttgatgtagacaaaaacagcgcgatgtctgtggaagcgttaccatctgaagtgaaggtcccgcc
ccttcagaaccttctcttcctagccagcccaaaactgtaaaagactttgaggaagatcttagaaaaagctg
aggccacaggggaattggaagacagtacatgctttttatataacagcatttgattctttcacagaactaac
actgcatttaagaaagatgccacggcctcatttaatactattgaggactctgggcttaatgccaatctggg
gaatgctgtgtttgatgccttacttaatactcctcaagatatccagaagtcagtattgaagggaaatcatta
acagcttgttacaagaatggaaaggtccacgaacaaaagatgatcttagagcatatcttatactgttacag
aatcctcaatcttaatatcacatctacatatgtcatctatgctcatttgctacgacagatagctaccttagt
ggaagctgaccatcacttcctagttcactggcttaaaaaattatcccagaagaaattcaagcaactggtag
agagattgctgcaatctgtttctttacggctgtttccagcaaaacctgaagaattcccgcctctaacgaag
tgtacctgggtggatcccacagccggtaaaagttctggctttgcttaacactgccacaatctgggtcacc
tcccctcgttccttacctgatttctataattctacctggatcacattgatctcatggaagagtatcaca
cgtggcagagctttgggaactctcacaggtttctctctgtcagtagccattcggtatcttatagctgca
aaaaaatcattattcaagagactcagaacaacagatgataagcatcgcaaggcaaagtctgggtggataa
agtatctcgaagacaaagacctgatatgaatatgttatct 1246

Sh3glb1 / full length / accession number: NM_019464.2

271 **atg**aacatcatggatctcaacgtgaagaagctggcggccgacgcgggcaccttcctcagccggg
ccgtgcagttcacagaagaaaagcttgccagggcagagaagacagaactggacgctcacctggaaaacctc
cttagcaaaagctgaatgtaccaaaatattggacagaaaagataatgaagcagaccgaagtgtgttgagcc
aaatccaaatgccaggatagaagaatctgtttatgagaaaactggatagaaaagcaccgaagtcgtataaaca
accgggaacttttgggacaatatatgattgatgcaggaactgagtttggcccagggacagcttatggaaat
gcccttattaaatgtggagaaaacacagaagcgaattggaacagctgaccgagagctgattcaaacatcagc
cttaaatttcctcactcctttaagaaactttatagaaggggattacaaaacaatcgcaaaagaaaggaaac
tattacagaataagagactggatttgatgctgcaaaaacaagactaaaaaggcaaaagctgcagaaact
aaaagttcatctgaacaggaattgagaataactcaaagtgaatttgatcgtcagggcagagattaccggact
cctgcttgagggaaatcagcagtagcacacgcccacatctccgctgtctgaatgactttgtagaagcccaga
tgacttactatgcacagtggtaccagtatatgcttagacctacagaagcaactgggaagttttccatccaat
tatctttctaacaacaatcagacctctgggacaccagtgccatattgctttgtcaaattgcaattggctcttc
tgcccaggcttcaacgggtagccttgtaatcacctgtccttctaacctcaatgaccttaagaatccagca
acaacaggaaggctagggctctctatgattatgatgctgcaaatagcactgaaactgtcactcctggccgat
gaggaatcactgtgttcagtgctcgttggaaatggactccgactggctaattgggagagagaggaaatcaaaa
gggcaaggtgccaatcactacttagaacttctcaat**taa** 1368

***Sh3glb1* / cDNA clone from library plasmid pGADT7-recAB**

349 gaagaaaagccttggccaggcagagaagacagaactggacgctcacctggaaaacctccttagca
aagctgaatgtacaaaaatattggacagaaaagataatgaagcagaccgaagtgctggttcagccaaatcca
aatgccaggatagaagaatattgtttatgagaaaactggatagaaaagcaccaagtcgtataaacaacccgga
acttttgggacaatatatgattgatgcaggaactgagtttggcccaggacagcttatggaaatgccctta
ttaaatgtggagaaacacagaagcgaattggaacagctgaccgagagctgattcaaacatcagccttaaat
ttcctcactcctttaagaaactttatagaaggggattacaaaacaatcgcaaaagaaaggaaactattaca
gaataagagactggatttggatgctgcaaaaaacaagactaaaaaaggcaaaagctgcagaaaactaaaagt
catctgaacaggaattgagaataactcaaagtgaatttgcgctcaggcagagattacccgactcctgctt
gagggaatcagcagtacacacgcccacatctcctgctgctgaatgactttgtagaagcccagatgactta
ctatgcacagtgttaccagtatatgctagacctacagaagcaactgggaagttttccatccaattatcttt
ctaacaacaatcagacctctgggacaccagtgccatattgctttgtcaaatgcaattggctccttctgccag
gcttcaacgggtagccttgtaatcacctgtccttctaacctcaatgaccttaagaatccagcaacaacag
gaaggctagggctcctctatgattatgatgctgcaaatagcactgaactgtcactcctggccgatgaggtaa
tcactgtgttcagtgctgttggaatggactccgactggctaattgggagagagaggaaatcaaaagggcaag
1335

***Stambp* / full length / accession number: NM_024239.2**

109 atgctctgaccatggggatgtgagcctcccacccaagaccgggtgaggattctgtcccaacttg
ggagtgcagttgagttaaatgaagacattccaccccgctcgtactaccgctccgggtgttgagatcatccgc
atggcgtccgcttactcggagaaggcaacattgaacatgcctttatcctctacaacaagtacatcacgct
gtttattgaaaaacttccgaaacaccgagactacaaatcagctatcattcctgagaagaaagatgctgtca
agaaattaaagagcgtcgtcttccctaaagcgggaagagctgaagacagagctcttgagaagatacacaaa
gaatatgagcagtataaagagcgaagaaaaaggagaagaggaacttgcccgaatatcgccatccagca
agagttggaaaaagaaaaacagaggggttgcctcagcagaagcagaagcagctagagcaggagcaattccatg
cctttgaggagatgatccagaggcaggagctggaaaaagaacggctgaaaattgttcaagagttcgggaag
gtagaccctggcccctgcgggcctctgctccctgatctggaaaagccttgtgtagatgtggccccagctc
accgttctcggccacgcagactccagactgtaacacaggcatgaggccagctaagccacctgtggtggaca
ggctccctgaaacctggagcgttaagcgtcatagaaaatgttcccaccattgaaggcctgcgccacatcgtg
gtgccccgtaatctgtgctcagaatttctccagcttgccagtgccaataccgccaaggcattgaaacctg
tggagtcctctgtggaaaactgatgagaaatgaattcacaatcacacatgttctcatccccagacaaaatg
gtgggctgattattgccacacggagaatgaagaagaaatcttctttatgcaggatgaccttggaactcctc
actcttggctggatccatactcatccaacccaacggccttctgtccagtgtggatctccacactcactg
ctcctacaaatgatgttaccagagtcctatcgcaatcgtctgttccccaaagttccaggaaactggattct
ttaagctaactgactatggtcttcaagagatttcaacctgccggcagaaaggctttcacccccatggcaga

gaccaccgctgttctgtgactgcagccatgtcactgtcaaggacagaattgtgacgatcacagaccttcg
ataa 1383

Stambp / cDNA clone from library plasmid pGADT7-recAB

460 tatgagcagtataaagagcgaagaaaaaggaagaagaggaacttgcccgaaatatcgccatcc
agcaagagttggaaaaagaaaaacagaggggttgctcagcagaagcagaagcagctagagcaggagcaattc
catgcctttgaggagatgatccagagggcaggagctggaaaaagaacggctgaaaattgttcaagagttcgg
gaaggtagaccctggccccctgcgggcctctgctccctgatctggaaaagccttgtgtagatgtggcccca
gctcacggttctcgcccacgcagactccagactgtaacacaggcatgaggccagctaagccacctgtggtg
gacaggtccctgaaacctggagcgttaagcgtcatagaaaatgttcccaccattgaaggcctgcgccacat
cgtggtgccccgtaatctgtgctcagaatttctccagcttgccagtgccaataccgccaaggcattgaaa
cctgtggagtcctctgtggaaaactgatgagaaatgaattcacaatcacacatgttctcatccccagacaa
aatgggtggcctgattattgccacacggagaatgaagaagaaatcttcttatgcaggatgacctggact
cctcactcttggtggatccatactcatccaacccaaacggccttctgtccagtggtgatctccacactc
actgctcctaccaaataatgatgttaccagagtccatcgcaatcgtctgttccccaaagttccaggaaactgga
ttctttaagctaactgactatggtcttcaagagatttcaacctgccggcagaaaggctttcacccccatgg
cagagaccaccgctgttctgtgactgcagccatgtcactgtcaaggacagaattgtgacgatcacagacc
ttcgaataatctcaaatcatgaaccagggagatggatcactgggtaacagcacttgtcaccaagcccaaca
gcccaggctcagttcttgggaccacatggtagaaggagtgtaccgacattcccccaagttgtcctctaac
ctccacatgtgtgctgtggtatgtgtgttctcacgtgtgtgtgcacatacacacacacgcataatcaatt
aatttaaaaagcgaataaatgtaaattataaaaagagtcttccccctcttaagctgcataatcccgttca
gtttattgccccatggagttgagtaagcttttaagacaggataggaaaggggtcaacactaaggggagact
gttgttgttgttgttgttgttgttgttgttgttcttaatttgaaatcatcttattttttaagacaaa
tgtgaaaatgaccaaatacacaccaagcaactaactcaaaaattaggatgcaagagaaaatacttctctaga
tccaaacactggccttctgttctcttgaaatcttaccctcccaacttgttcatctctgcctttggactaaat
aggggcatctgtgcaaaaactgtagaagccatcttgaaggatgttggctttttattgtttgtggcattaataa
gggagcttaccattctgggtgggatgtgcatgaggcgttcacagccccatacatggatcttgtttaaagtg
tattatttaaaaggtcaggggtgttattttcttctataataaaacagctcacttgtgttgtg 2146

Stmn2 / full length / accession number: NM_025285.2

86 atgggctaaaacagcaatggcctacaaggaaaaaatgaaggagctgtctatgctgtcactgatctg
ctcctgcttctaccggagccgcgcaacatcaacatctacacctacgacgatggaggtgaagcagatca
acaagcgggcctctggccaggcttttgagctgatcttgaagccaccatctccatctcagaagctccacga
actctagcttctccaaagaagaaagacctgtctctggaggagattcagaaaaagctggaggctgcagagga
gccaagaaagtctcaagaggctcaggtgctgaagcagttggcagagaagagggagcagagcgagaggtgc
tccagaaggcgtggaggagaacaacaacttcagcaagatggcggaggagaagctgatcctgaagatggaa

cagattaaggaaaaccgtgaggctaattctagctgctatcattgaacgtctgcaggaaaaggagagggcatgc
tgcagagggttcgcaggaacaaggaactgcagggtgaactgtctggctga 625

Pacsin2 / full length / accession number: NM_011862.3

261 atgtctgtcactacgatgactctgtgggagtggaagtgtccagcgacagcttctgggaggttgga
actacaaacggactgtgaagcggattgacgatggccaccgcctgtgtggtgacctcatgaactgtctgcat
gagcgggacgcatcgagaaggcgtatgcacagcagctcactgagtgggcccagcgtggaggcagctggg
agagaagggaccacagtatgggaccgtggagaaggcctggatagctgtcatgtctgaagcagagaggggtga
gtgaactgcacctggaagtgaaggcatcactgatgaatgaagactttgagaagatcaagaactggcagaag
gaagcctttcacaagcagatgatgggaggcttcaaggagaccaaagaagcagaggatggccttcggaaggc
ccagaagcctgggccaagaagctgaaagaggtggaagcggcaagaaggcgcaccacacagcgtgcaaag
aggagaagctggccatctcccgggaagccaacagcaaggcagatccatccctcaaccctgagcagctgaag
aaactgcaagacaagatagaaaaatgcaaacaggacgcttctaaagaccaaggacaagtatgagaagtcct
gaaggagcttgatcagaccacacccagtacatggagaacatggagcaggtgttcgagcagtgccagcagt
ttgaagagaagcgctgcgcttcttcgggaggttctgctggaggttcagaagcacttgatctgtccaat
gtggctagctataaaaccatctaccgggagctggagcagagcatcaaagcagcagatgctggtagaggacct
gaggtgggttcgggctaaccatgggcccaggtatggctatgaactggccacagtttgaggagtggtctgcag
atctgaatcgaactctcagccggagagagaagaagaaggctgttgacggtgtcaccctaacagggatcaac
cagacaggtgaccagtctggacagaacaagcctggcagcaaccttagtgtcccagcaacccccgccagtc
cacgcagttacagtccagctacaacccttcgaggacgaggacgacacgggcagcagcatcagtgagaagg
aggacattaaggccaaaaatgtcagcagctatgagaagactcagacttacccccactgactggtctgatgat
gagtctaacaaccctttctcctccacggatgccaacggggattcgaaccatttgatgaggacacgacctc
aggaacagaagtgcgagttcgggcccctctatgactatgaggggcaggaacatgatgagctgagcttcaagg
ctggggatgaactgaccaagatagaggatgaagatgaacaggggttggtgcaagggacgtttagacagcggc
caggttgccctataccagccaactatgtcgaggctatccagtgga 1721

Pacsin2 / cDNA clone from library plasmid pGADT7-recAB

597 aagaactggcagaaggaagcctttcacaagcagatgatgggaggttcaaggagaccaaagaag
cagaggatggccttcggaaggcccagaagcctgggccaagaagctgaaagaggtggaagcggcaagaag
gcgaccacacagcgtgcaaagaggagaagctggccatctcccgggaagccaacagcaaggcagatccatc
cctcaaccctgagcagctgaagaaactgcaagacaagatagaaaaatgcaaacaggacgcttctaaagacca
aggacaagtatgagaagtcctgaaggagcttgatcagaccacacccagtacatggagaacatggagcag
gtgttcgagcagtgccagcagtttgaagagaagcgctgcgcttcttcgggaggttctgctggaggttca
gaagcacttgatctgtccaatgtggctagctataaaaccatctaccgggagctggagcagagcatcaaag

cagcagatgCGGTAGAGGACCTGAGGTGGTTCGGGGCTAACCATGGGCCAGGCATGGCTATGAACTGGCCA
cagtttgag 1166

Sept7 / full length / accession number: NM_001205367.1

201 **atg**tCGGTCAGTGCAGATCCGCTGCTGCCGAGGAGAGGAGCGTCAACTGCGGCACCATGGCTC
aaccgaagaaccttgagggctatgtgggctttgccaacctcccaaatcaagtgtacagaaaatccgtgaaa
agaggatttgaattcactcttatggtagtaggtgaatctggactgggaaagtgcacattaatcaactcatt
attcctcacagatttgtattctccagagatccaggaccttctcatagaatcaaaaagactgtacaggtgg
agcaatccaaagttttaatcaagaaggtgggtggttcagttgctgctgacaatagttgatactccaggattt
ggagatgcagtgataatagtaattgctggcagcctgttatcgactacattgatagtaaatttgaagatta
cttaaatgcagaatctcgagtgaacagacgctcagatgcctgataacaggggtgcagtggtgtttatacttca
ttgctccttcaggacatggacttaaacattggacattgagtttatgaaacgtttgcatgaaaaagtgaat
atcatccattaattgccaaagcagacacacttacaccagaggaatgccaaacagtttaaaaagcagataat
gaaagaaattcaagaacataaaattaaaatatatgaatttcagaaacagatgatgaagaagagaataaac
tggttaagaagataaaggaccttacctcttgctgtggttaggtagtaatactatcattgaagttaatggc
aaaagagtcagaggaaggcagtatccttgggggtgtggctgaagttgaaaatggtgaacattgtgatttcac
aattctaagaaatagtgtgataagaacacatatgcaggacttgaaagatgttaccaataacgtacactatg
agaactacagaagcagaaagctagcagcagtgacttacaatggagtggataacaacaagaacaaagggcag
cttaccaagagccctctggcacagatggaagaagaaagaagggaaacatgtagccaaaatgaagaagatgga
gatggagatggaacaggtgtttgagatgaaggtcaaagaaaaagttcaaaaactgaaggactctgaagcag
agctccagcggcgccatgagcaaatgaaaaagaatttagaagcacagcacaagaatttagaggaaaaacgt
cgtcagtttgaagaagaaaaggcaaactgggaagctcaacagcgtattttagagcaacagaactcttcaag
aaccttgaaaagaacaagaagaaggcaagatcttt**taa** 1511

Sept7 / cDNA clone from library plasmid pGADT7-recAB

1167 aacaacaagaacaaagggcagcttaccaagagccctctggcacagatggaagaagaagaagg
gaacatgtagccaaaatgaagaagatggagatggagatggaacaggtgtttgagatgaaggtcaaagaaaa
agttcaaaaactgaaggactctgaagcagagctccagcggcgccatgagcaaatgaaaaagaatttagaag
cacagcacaagaatttagaggaaaaacgtcgtcagtttgaagaagaaaaggcaaactgggaagctcaacag
cgtattttagagcaacagaactcttcaagaaccttggaaaagaacaagaagaaggcaagatcttt**taa**ac
tctattgaccaccagttatgtattagttgccaatatgccagcttggacatcagtgtttgttggatccgttt
gaccaatttgcaccaattttatccataatgatggatttaacagcatgacaaaaattatTTTTTgttgttct
cgaaggagattaagatgccttgaattgtctaggatattgtgtacttagaaattaacagctctaagtacctt
tctacattTTTTTTCTTTTTTTTTaaattaaaagatgtcttcagtttaatgcaagaaaacattttactgt
tgtacaatcatgttctgggtggtttgattgtttacagaatattctaaaataaaaggactctggaaggttttc
attgaggataaattgccataatatgatgcaaacctatgcttctctatgataattataatacagaggttccat
tcgatgcagcctatacaataatgtattttagtctaacacagtgaccctatTTTTTgacacttccattgttt

aaaagtacacatggaaaaacatatatgcttacagtgcacctagagctttttataacagccttttttgttt
gtttgtttgttttggattctttaatatataaatatattattctcatttagtgcccctgtagccagaacct
cattactgcttcatttttgaataacatttaatttagatattttccatatattggccctgctaaaatagaa
tatagcatctttcatatggtaggaaccaacgaggaaactttcctttaactccctttttacactttatggaa
agtagcaggaggagaaatgcattttagatcatttctaggcaaattgtgaagctaacgaccagcctgtttc
ttcctatactcagtcttgttttactagaaatgggaatcatggcctcttgaagagaaaaaagtcaccattct
gcatttagctgtatctatatattgcatacctgtattttttgtttgtattgtaaaaaaattcacataata
aacaatgtttgtgat 2521

Klhdc2 / cDNA clone from library plasmid pGADT7-recAB | NM_027117.3

828 ttgggaacttttgaattttagatgaaacatctttttggaattcaagtcacccaagaggatggaatg
atcatgtccatatttttagacactgaaacatttgcctggagccagcccatcaccactggtaaggcaccttca
cctcgggctgccatgcctgtgcaactgttggaaacaagggctttgtgtttggaggagataccgggatgc
tagagatcttcactatcttaactctggatacgtgggagtggaaatgaactaattccacaaggtgtgtgcctg
ttggcagatcctggcactcactgacaccagtctcttcagaccatctttttctctttggaggatttaccact
gaaaaacagccactaagtgatgcctggacttactgcatcagtaaaaatgaatggattcagtttaaatcatcc
ttatgttgaaaaaccaagattatggcacacagcttgtgagatgatgaaggagaagtcattgttttggtg
gttgtgctaacaatctgctggttcatcacagagctgcacacagtaaatgaagtacttatattttcagttcaa
ccaaaatctctgtacggctaagcttagaagcagtcacatctgctttaagagatgctagccaactcgtggag
ctgccttccaaaacacttacttcacagcgttaaatcagaggtttggtagtaacaacacttctggatca^{taa}
1529

Pbld1 / cDNA clone from library plasmid pGADT7-recAB | NM_026701.2

2 ^{atg}aaagctcccaatcttcatagcagatgcgttactgcgacagctttccggggcaatcctgccgca
gtctgcctcctggagcgcacattggaggaagacgcccatcagcaaattgaggggagatgaacctctcaga
aacggctttcatcaggaaactgcagccgactgacagcttcacacaaagctctcgctttggactgagatgg
ttacgccagtgagtgaagtccccttgtgcgccacgccacactggcctctgaggctgtgctgtttcacaaa
atacagaacaggaacagcaccctgacctttgtcacaatgagcggggagctaaaggccagaagagcagaaga
tgggatagtctggactttcctgtctaccaacctttcccaggacttccatgaagttgaagacttgataa
aggcagccataggtgacacctgggtccaggacatccgggtactctacagataccagaaaactcctgggtccg
ctcagcgattcttatgacaggtcctttctagagagcctgaaggtgaacacagagcctctgcctgcaattga
gaagacaggggaaggtgagaggcctcatcctcactgtcaaaggagagcctggggggcagacggccccgtatg
acttctactccagatacttcgcgccgtgggttggattgtgctgaagaccgggtgacagg 693

Cpe / cDNA clone from library plasmid pGADT7-recAB | NM_013494.3

652 gaaccgtaacttcccagacctggacaggatcgtgtatgttaatgagaaagaaggcggtcctaac
aatcacctgctgaagaatctgaagaaaattgtggacacaaaattcaaagcttgcccccgagaccaaggctgt
cattcactggatcatggacattccatttctgtgctttctgccaatctgcacggaggagaccttgtggctaatt
acccatatgatgagacacggagcggtagctgctcacgaatacagttcctgcccctgatgacgcaattttccaa
agcttggctcgcgcgtactcttctttcaaccagtcacgtctgaccccaatcgacctccctgtcgcaagaa
tgacgatgacagcagctttagatggaacgaccaatggtggtgcatggtacagcgtccccggtggaatgc
aagacttcaattacctgagcagcaactgcttcgagatcactgtggagcttagctgtgagaagtcccaccg
gaagagactctcaaaagctactgggaagataacaaaaactccctcatcagctacctggagcagatacaccg
aggtgttaaagggtttgtccgtgaccttcagggtaacccgattgccaacgcaaccatctctgtggacggga
tagaccatgatgtcacctcggctaaggatggggattactggcgattgcttgctcctggaaactataaactt
acagcctccgctcctggctacctggcaatcacaagaaagtggcagttccttttagccctgctgttgggggt
ggactttgagcttgagtcttctctgaaaggaaggaggaggaaggaagaattgatggagtgggtgaaaa
tgatgtcagaaaactttgaatttt**taa** 1522

Crtac1 / cDNA clone from library plasmid pGADT7-recAB | NM_145123.4

1662 ggaggtgacgtggccagatggcaagatggtgagccgaagtgtggccagcggaggagatgaactc
gggtgttgagatcctctacccccaggatgaggacaaaacttcagaacacagccccactagagtgcggccaag
gattctcccagcaggacaatggccattgcatggacaccaatgaatgcatccagttcccatttgtgtgcct
cgagacaaaaccgtagtgtcaacacctatggaagctacaggtgccggaccaataaaagatgcaatcgggg
ctatgaaccaatgaagacggcacagcctgtgtggctcaagtggccttttttaggtgggtactcatcggtg
ccttttagactctctgagcctctctctcaggcctcgtatctttctctaggcctgggactttgccttcagtta
tatgcactt**taa** 2091

Zbed4 / cDNA clone from library plasmid pGADT7-recAB | NM_181412.3

3534 gtccctgaaggaagccatggcaagccgctgtctgccacactccatgacccccaggtacatctt
tgccacactgctggaccctcgctacaaagcttccctgttcacagaggaggaggcagagcagtagcagggcaag
acttaacagggagctagaaatactgaattctacctcagaggacactgccacctccaatggctgtgactca
gggtccccacttaaagacactggcacagaggagcctgtggctcactcgcaccgataaagagagatcagag
agagaagctacctgaagacatggtgcttgcgtatttggaggaagaggtgctggaacacagctgtgaccac
tcacctactggaacctaaagcggtcacgtggcctgggctgtctaccttagcagttcgatcttctgggatgt
cccccaagtacagctccccctcagaaaagctgttcagcacacccatggatgctggcagctttggccagcccag
gctcatgatggagcattttgaaaagctcatcttttttaaagtgaaatcttctttaaataatgctttcagtat**t**
ga 4095

***Pcca* / cDNA clone from library plasmid pGADT7-recAB | NM_144844.2**

1180 aagcaagaggatattcccatcagtggtggcagttgaatgtcgggtttatgctgaggacccc
tacaagtctttcgggtttaccgtctattgggaggctgtcccagtagcaagagccgatacatctacctggtgt
ccgagttgacagtggtcatccaaccaggaagtgacatcagcatctattatgatcctatgatttcaaagctag
tcacatatgggtctgacagagcagaagccctgaagaggatggaagacgcactggacaattatgtgatccgg
ggtgttacacacaacatcccattgctccgggagggtgataatcaacacacgttttgtgaaaggagacatcag
cactaagtttctctctgatgtgtatcctgatggcttcaaagggcacacgttaacactgagtgagagaaacc
agttattggccattgcatcatctgtattttgtggcatcccagctacgagctcagcgcttccaagaacattca
agagtaccagttattagcctgatgtggctaagtgggagctctcggtaaagttacatgatgaagatcatac
tgtcgtggcatctaacaatgggccggtttaccgtggaagttgatggctcgaaactaaatgtgaccagta
cgtggaacctggcgtcacccttattgtctgtcaacgttgatggcacgcagaggactgtgcagtgcttttct
cgggaagcaggtggaacatgagcatccagtttcttggcacagtgtacaaagtgcacattttaaccaagct
tgctgcagagctgaacaaattcatgcttgaaaagtgcccaaggacaccagcagcactctgtgctccccga
tgcctggagtggtggcgtttctgtcaagcctggagacatggtagcagaaggtcaggaaatctgtgtg
attgaagctatgaaaatgcagaacagtatgacagctgggaaaatgggcaaggtgaaattggtgactgcaa
agctggagacacagttggtgaaggagacctgcttgtggagctggaa **tga** 2214

***Catsperb* / cDNA clone from library plasmid pGADT7-recAB | NM_173023.2**

2708 gcccaaccataaagagcagctgcagttacctcaggactatgcaccacactcctggcagggacat
accacctgaagactggattagcggagttcacaaggacagtcagggtttcaatatgatcaaaactctgccga
taaactacagacctccatcccacatgggaatttctattccactcacagataatTTTTATCATGCAGACCT
agcaaaccataccgagaaatcaatttcacaagtcaaaggaaactggcaatacaaacagtggtgctaagt
taccagtcgggcaatgtgcaactgctcagaacatcaaaagttttccatgctgttgccttctcagattgca
aagaaaaggttcatcgtttcaagtttccagtcacacaataccagttgttttggaaatTTTCAATGAAAGA
gacaaaatctccgcagaacctccgtatttagttaccatgactgaagtgaatatgaggaaaaactggcaact
aaaacacaatgagccagaaaacgtaagaaaatgaagcattacttagagccactgcttaagactccagtg
ataatcctttaggtctcaacctaacatacagggtctgaactgtttcacttcaaggtgtctgtggttct
ggagtcagcttttgtgagttaagtgaagaatttcagatttatgtcgacgaagtcctattgccttttccagg
acatgcactaatagctggtgcaacatctgtagtgttaggagtttaatttttatagcatttgtattccaac
tgcgtaacatccacctgaaggcattgaagaaatctattaggggaaatcctggactcacctcaagtaca
actgttagctca **taa** 3449

***Vps13d* / cDNA clone from library plasmid pGADT7-recAB | NM_001128198.1**

11698 cacctgatggctcacggctcagaggttcacagtacaaattgaggagaaactgctgctcaagct
actaagtttctttggctacgatcaggcagaatcagaggtggaaaagtatgatgaaaacatccatgagaaaa
cagcagagcagggaggaactccaactcgatactactttgagaacctcaagatcagcatccccagatcaag

ctcagtgtgttcacctccaacaagctgccactggaccttaaggctctgaaaagcaccctaggattcccact
gattcgggtttgaagatgctgtgatcaatctggatcccttcactcgggtgcatccctatgagaccaaggagt
tcatcatcaatgacatcctcaagcacttcaggaggaactccttagccaggcagctcggatcctaggatcg
gtagacttccttggcaatcccatgggccttttgaatgatgtatccgaaggggtcactggactgataaagta
tggaaatgtcgggggtctcataagaaatgttaccatggagtgtaaattctgcccgaagtttgaggga
cactatcagatggcctggggaagacgatggacaatcggcaccagtcagagcgagagtacatcagataccat
gctgccaccagtggagagcaccttgtggctggcattcatggattggctcatggatcattgggtggattgac
cagtgttataacatcaacagtggaaggtgtaaaacagaaggaggagtcaaggattcatalctggccttg
gcaagggactcgttggcactgtgaccaagccagtggcaggtgcctggatcttgcacagaaacagctcag
gcagtgagagacacagccacactcagtggtcccaggacccaagcccagaggggttcggaaaccacgttgctg
cactgggtccccaggggtgcttcctcgatattctgagagccaagcagaaggacaggaacagctcttcaagc
taacggacaacatccaggacgagttcttcatagccgtggagaacattgatagctactgctgctcatctcc
tctaaagctgtgtactttctgaagagcggggactacgttagaccgagaggccattttcctcgaggtcaaata
tgatgacctctaccactgtcttgtctcctcacaagaccatgggaaggtgtatgtgcaagtaactaagaaagctg
caaattctagcagtggtgtgtccatcccaggtccatcccaccagaagccaatgggtgcatgtgaaatctgag
gtccttgctgtcaagttatcacaagaaataaactatgcaaagagcctctactatgaacagcaacttatgtt
aagactcagtgagaatcaagagcagttggagctggactcctga 13080

***Pcnxl4* / cDNA clone from library plasmid pGADT7-recAB | NM_026327.3**

3350 aagcaagtttgggtccaatagaagactttaagaactgaccaactgcctcagagagtacgaga
gagactggtacattggcttagtgtctgaagagcagtggaagagagcaattctagaagaaaagccatgcttg
ttctgcctggggtatgagtctagatggtggtttacacctcgaggggtgctgatgcttcaggagatgtcgg
gcacatcgggaagctgaacgctgaggccgttcgaggtcagtgggccaacctctcgtgggaactgctttatg
ccaccaacgatgatgaggaacggtacagcatccaggctcaccactgctgctgaggaacctcactgtacaa
gccgctgacctcccttgggataccaattttctcttcaaacctctccctatacatctgtgttagttcat
tttgacatccaaatgcaggcacatcagaggaggctcactgaaaagtaagagtgtgagtattgtaatttc
actagactttctctttgccccagaatgcctgagagaaaaccatattggtctgcaaagctgtttgtcagccg
ttcaaatgactcagacaacaggtcctctgtgtctaacgtgggtaaaagtagttggccaatatttgtgctgt
atgagttctgattgggttttggtagctagagatatttgtacacgattagatatttttttactgctttgtta
aatgtctgaaaagtggtttgtcttttaaaaagtcaacaggtatgtaattacatagttaaaaagacgttcat
atcagtgtttaataataatgaatctttttgatgttaacataacatgtatatatattttatttgaaatgta
attaatttttagtattttcgaatgtactgttttagcatttaacatgggtgtgggcagttccattcagtgat
ccatgattcatataacttggccttggaaaccgaaaaaacttgaataaaaatctcaccagctaaa 4326

Cop9 / cDNA clone from library plasmid pGADT7-recAB | NM_012001.2

211 tcaagcggctctcataaagatctggcgggcaaatatcgtcagattctggaaaaagccattcagt
tatctgggacagaacaactagaagcattgaaagcttttgtggaagcgatggtgaatgagaatgtcagcctc
gtgatctcacggcaactgctaacagatttctgcacacacctccctaacctgccagacagcacagccaagga
ggtctaccattttcaccttggaagaagatccagcctcgggctcatttctttgaagagcaggttgcttccataa
gacagcatctggcatctatttatgagaaggaggaagactggagaaatgcagcccaagtgttgggtggggatt
cctctggaaacaggacaaaaacagtacaacgtagattataagctggagacttacctgaagattgcaaggct
atacctggaggatgacgatcccgctccaggccgaggcttacataaacgagcgtccttacttcagaacgaat
ccacaaatgaacagttacagatacactataaggtttgctatgcgcgtgtccttgattacagaaggaaattc
attgagggccgcccagaggtacaatgagctctcttacaagacaatagtcctatgaaagtgagagactagagggc
cttaaagcatgcactgcactgcaccatcttagcatcggcaggacagcagcgtctctcggatgctggctactc
tttttaaggatgaaagggtgccagcaactagctgcataatgggatcctagagaagatgtacctagacagaatc
atcagaggggaaccagcttcaagaatttgctgctatgctgatgccacaccaaaaagcaacgacagctgatgg
ttccagcatcttgacagagctgttattgagcataatttgttgtcagcaagcaaattatataacaatatca
cctttgaagaacttgagctcttttagagatccctgcagctaaggcagaaaagatagcatctcagatgata
acggaaggacgcatgaatgggtttattgaccagatcgatggaatagttcattttgaaacacgagaagccct
gccaacatgggacaagcagatccagtcactttgtttccaagtaacaacctcctgggaaaaatttagtcaga
cggccccggagtggacagcacaagccatggaagcgcagatggcccagtgagccctcagcgtgtgvcgact
gcatctttgccacttcgtgcagattgattcactgcccctcaaagcatttgcatcatgaccttagacatctc
agcctcctttgctggatcccacttgaagaagatgctagagcaagaagtgcacgttttaacataatagctc
ccgtgagatctgggtctgtgtattgaaactaactcagacgctttgaaaacttgttctttaagtggaaagtga
agacctgaagtttgggatttgtgatcactttgtagtcatgtaaaacttaagtgctttgtgcctctccacat
gtggttactctaataaacggagcggtgagccaaataaaggcagtagtcttggttttaattaaaaaaaaaaaa
aaaaaa 1771

Gvin1 / cDNA clone from library plasmid pGADT7-recAB | NM_001039160.2

6634 tgttcagaaaaagagagtgaaaaaataaaaacttttttaaacataagcttaggtgacatcaag
aatactatcctgtctgccattcataactccacaaaggtagctaaagctaaaggcagcactgcatctcactg
gctggatttgttctgtgaccacctagggagcaacctgggtcttcccaaggaaagacctggtaagcatagagc
accaggagctaattggatactgagttcctcaaagaagccatgagcaaagctttggatcctgcaatgagggaa
gtagaagaggattgttcaagtaagcacatagatgaaattgttctctgacattgagaaaattctctctgaaca
tctctgtggctgttggaaacagtgctcctttttgtaaggcaatttgtacaaacaccattccccagcatgaag
gagaccacagtggtgccattccaccgtcctcaggctgtcagtggttggcattggcataaaaacagaccagttc
cacattaatgtttgtactagtagttagcaagtaaatatttcttcattttagatggcttccgggaattccc
actcaagaaatatcgagaagcaggaggtgattatgccacatggagcatcaccacagactcatctaccagc
catattggaaatggtttgtctgtcatttcagatcaaacctagaagagaattatggcaaaaaatttacaggg
aaaggtagtcttccagatttatggacccaaatcacaagcaagaagtcctgaatgacttaaaaaaa **taata**
actgccacagacagaacactagatggggccacagaaattttacttcagccaagggagcctaattggagaacac

catgcaggaggatctgcagtagacatcttgagcttcctcgatatggcccactctattgggcaatctctg
agaccaatatgaagttaaactttcataaaataagactgttttagatgaattaatgattttatagaatctg
agttgatttaaatagttttaggcactaggggttaatgatagaaagtttaaggagatggcttaattgttctg
ctaaatagatatgataaagttagaattaagagcagaatgtgacctttcccttgtaggataatgagagctac
ataggtttgaaaaggagtacagtgagctttcatgcattgcaagtatgtgattgtacttggaagaagaaaat
aggcttgggacaagttaatgctcaaaacattcattctaggttgggtctgagttcctggattttgtgatcta
gagacatagtcacaggttttggtgggcaccataaaaaggcaaggtaataaacaaggagtaataaattcgat
tattagtatagaatagagaatagatgattctccagtatagctgaacaagactacaaaaataagatgtaaga
gagattgttccttcgtaaacagattgatcaccatctaagcatatggaaaacttgctactgtagacttgg
cttgcttaaacattgttaatacaatacaaaaaaattatagctttagggttgctatggagaaaaagatgaga
gaacgtagatgagaaatgcttaggtatgagtttcaaagagaaatacacaatcaatgctcctgttgaat
ctcttggtgatgattttattgtcttattgaagaacatgtgttttgattgttttagaaaacttgcaac
ttatggctatgaagtaatcttctgcaaacatagagaactttgtcttagatgggtgtaaaaggctaagagaa
caataaagatgtagagctca 8421

Stk16 / cDNA clone from library plasmid pGADT7-recAB | NM_011494.5

617 aagaaaggtacactgtggaatgagatagaaaggctgaaggaccaaggcagcttcctgactgaag
accagatcctgccgctgttgctgggtatcagcagaggccttgaggctattcatgccaaaggttatgcacac
agggacctgaagcccaccaatattttgcttgggtgatgaggggcagccagtttaatggacttgggttctat
gaatcaagcatgcattcaagtggagggtctcgcaggcactagctcttcaggactgggcagctcagcggg
gcaccatctcctaccgggcacctgaactttttctgtgcaaagccactgtgtcatcgatgagcggactgat
gtctgggtccctaggctgtgtgctttatgccatgatgtttgggaaggcccttacgatatggtgttccagaa
gggtgacagtggtggcccttgctgtgcagaatgaactcagcatcccacaaagcccaggcattcttcagcat
tgcgacagctattgtcttctatgatgactgtggacccccagcagaggcctcacatccctgtcctcctcagt
cagttggaggcattgcagccaccagctcctggccagcacaccacccaaatctgatcaaatcagtggacata
ttgggaagatgacctgaagtggctttcatccctcattggaactccttcattcttcaggatggctctca
cagctagtggaaggatagtggtccttgatattctgccttcttaccccaataacctgggcaaggaaccta
ggg 1393

Ppp2ca / cDNA clone from library plasmid pGADT7-recAB | NM_019411.4

580 gagagcagacagatcacacaggtttatgggttctacgacgagtgtttaaggaaatacggaaatg
caaatgtttgaaataacttcacagacctttttgactatcttcctctcactgccttgggtggatgggcagatc
ttctgtctacacgggtggtctgtcaccatccatagacacactggatcacatccgagcactcgatcgctaca
ggaagttcctcatgagggtccaatgtgtgacttgctgtgggtcagatccagatgaccgtgggtggctggggga
tatctcctcggggagctgggtatacctttggccaagatatttctgagacatttaaatcatgccaatggcctc

acgttgggtgtccagagctcaccagctgggtgatggagggatataactgggtgccatgaccggaacgtagtaac
aattttcagtgctccaaactattgctatcggttggtaaccaagctgcaatcatggaacttgacgacactc
ttaagtattctttcttgagtttgaccagcacctcgtagagggcgagccacatgtcactcgtcgtaccca
gactacttctgt^{taa}tgaaaatgtaaacttgtacagatattgccatgaaccgtatattgacctaattggaat
gggaagagcaacagtaactccaaagtgtcagaaaatagttaacattcaaaaacttgttttcacacggacca
aaagatgtgccatataaaatacaaaagcctcttgtcatcaacagccgtgaccactttagaatgaaccagttc
attgcatgctgacgagcattgttgggtcaagaatccagtttctggcatagcgctattttagttacttttg
ctttcttgagagactgcagatataggattaaacattaacaccctgagtcagttgacttacttagctgt
agcttactcagcatgactgtagatgaggatagcaacaatcattggagcttaatgaacatttttaataag
taccaaggcctcccctcttgttgtgtttctttcagggataaccattaatttaattgtatgatttgtctgcac
tcagtttctccccttctcaaatctcagccccgcttgttctttgttactgtcagaaaacctgggtgagttgt
tttgaacagaactgtttccctcctgtaagatgatgttactgcacaagtcaccgcagtgttttcataataaa
cttgagaactgagaaagtacaggttgaattgtatcagtgggcagcactgggtgctgtttattaacaagataa
atctattgatcaatttcagaatttgtagaatccaggtaaagaaaaataaagatcaaggccactgtgtaac
ctctctggc 1930

Rbm39 / cDNA clone from library plasmid pGADT7-recAB | NM_133242.2

896 ggaaagggttcgagatgtgagaatgatttctgatagaaattcaagacgttccaaaggaattgcat
atgtggaatttgttgatgtcagttcagtgccctctagcaattggattaactggccaacgagtttaggagtg
ccaatcatagttcaggcatcacaggcagaaaaaacagagctgctgcaatggcaaacatttacaaaaggg
aagtgctggacctatgaggctctatgtaggctcattacactttaacataactgaagacatgcttcggggga
tctttgaaccttttggaggattgaaagtattcagctcatgatggatagtgaaactggccgatctaagggga
tatggatttattacatcttctgactcagaatgtgccaaaaaggctttggaacaactgaatggatttgagtt
agctgggagaccaatgaaagtgtgtcagttactgaacgaactgatgcttcgagtgctagttcatttttg
acagtgacgaactagaaaggactggaattgacttgggaacaactggacgtcttcagttaatggcaagactt
gcgagggtaccggttgcagattccacctgccgcacaacaagcattacaaatgagtggtctctctggcatt
tggtgctgtggcagaattctcttttgttatagatttgcaaacacgactttcccaacagaccgaagcctcag
cttttagctgcagctgcgtctgttcaacctcttgcaacacagtgttccaactttctaactgtttaatcct
caaacagaagaagaagttggatgggatacagagattaaagatgatgtcattgaagaatgtaataaacatgg
aggagtcattcatatttatgttgataaaaaattcagctcagggcaatgtgtatgtgaagtgcccatctattg
ctgcggtctattgctgctgtcaatgcattgcatggcagatgggttctgtggtaaaatgataacagcagcgtat
gtacctcttccaacttaccacaacctctttctgattctatgacagcaacacaactactggttccaagtag
acga^{tga}aggaagatacagtccttatgtatatagctttttttctcttgagaattcatcttgagttatct
tttatttagataaaataaagaggcaaggtctactgtcatttgtatacaactcctgttaccttgaaaaata
aaaatgttaacaggaatgcagtggtcattatccctaactagcaaatcctactttatgcaaagctgttct
cttgttctgctgttttaaatgtccatgtagaaaatgacattaaggatctatagaatagctctaggggaaca
aatgtgctttctgtataaaggcagacaggtcacgttttaattgtttcagaaaccttaactttttacacagcag

ttacaattcacattcatgtatTTGGCTCATGGTTCAGCAAAGGTTCCAGAATCCACATTTAGTGTGTGAA
aagtctaagTGGCTGTATGGCTGCTTGGCATTGATCTTGATTATTTGGCAAGAATGGGATTTCAAATAA
tatttctcgatggtaatTTTTTCAATTAATGTCTCTGTAAAAGTTCTTTGTAAATACTGTATGTTTTAGT
gtgtcttgagattccaacaaaatgatccctgcatttctcaaggTGGCTGACGTAACAGATTGAGTAAGC
agtcttgggcaagagatgggaaatgcagaaaaaggTTTTGTCTGGTTGCATATAATCTTTGCTCTTTTAA
gctctgtgagctctgaaatataTTTTTGGGTTACTTCAGTGTGTTGACAAGACAGCTTGATATTTCTATC
aaacaaatgactttcatattgcaacaatctttgtaagaaccactcaaataaaattctctgaaaaaggccac
aa 2807

Sh3yl1 / cDNA clone from library plasmid pGADT7-recAB | NM_013709.4

895 gcctttgcaaagggTGGAAACCTGACCCTGGAGGGAATTTACTGTCTGCAGTTGGGCCCTAG
gcaggaacctggaaggcaacgtgtccctgaggagctccgcagccgtcttcacatactgcaagtccaggggc
ctctttgctggTATCTCCCTGGAAGGAAGCTGTCTGATTGAGAGGAAAGAAACCAATCGGAAATTTACTG
tcaggacattcgagcttacgacatTTTATTTGGAGATGTTCCGCAGCCTGCTCAAGCAGAAGATCTTTATG
aaattcttaattccttcaactgagaaatagaactgaagggcagcgcacatcaatttgaagaaagtagcccg
gagcagaggaaggccaagaattacctccaaaacctcttcaaggccccagccagccccaccctgtaca
gctgaatgctggctcccagggtaatagaaatgaatataagctatatcctgagctttctagctatcatgaga
aaactggcaatttgaatcaaccaatagaagtgcagcattatactctttcgaaggacaacagccaggagac
ttgaattttcaagcaggagacagaatcatagttatatcaaagaccgactcaaattttgattggTGGGAAGG
aaaacttcgaggtcaaactggaattttccagccaactatgtaactatgaat **taa**agttcatgctatTTTG
ttactt 1603

Mfsd6 / cDNA clone from library plasmid pGADT7-recAB | NM_133829.2

4105 ggagacaggatcagctgtacagtgaaggcctctgtgtgaccgttctgcctgccccctgcctcgg
gagaaacattctacacctggatgcctagcttcaactacaaaacacagcttggaaatgatgggaacaattaagc
tgatggTTACTTTGCACTTGAATGGTACTGCAGTGTCAACCCCAAGGCTCATTTTAAGTGACCTTTAAA
atcagatgtatTTATTATGCTCGTGCAATTACAGAAATGAAGTGGGAGACAGGCTGAGCCCCACCTATGAA
tgtacagtatgtggattgtgaaagtgactgtagggaaatcagagcgttgatcttgtgtttacaattctgg
tgatttctttgaaaagctgctggTTTTGGGAAATGCACAGTGGGTGATTGAAATAAAAGGTAATAACCAT
TTAAATATTTGTAATGAAAAACAGTGCACAAACAAGAGAACATCCTCTGCTCTGTAATGAATGACAC
caaattcaatatgccttcgTTACAAAATGTTTACTGTGAGCGTCGATCCAACAGTGCAGTAATTTCTAGCC
TTTTGAGCTGACACCTTCAGAGTTTGTGGACTTTGTGACTTTTTCTTCTGTTCTTACAGTGCCATATGT
cacttgaaaaatattaaagtgaattccaattaaa 4770

Strn3 / cDNA clone from library plasmid pGADT7-recAB | NM_052973.2

1868 gatgcaaccattcagtggtggaatatgcctagtcctaattgtggatccctatgatacatatgag
tcaaacgttctagctggcacttttagttgctcatacagatgcagctctggggctcttgccatagtggcataaa
aaaccaattactctcttgctcagcagatggcactattaggttatggaaccacagaagaaaagctgccatgtg
tttgacttacaatggagacaaggaacatggaatacctacatcagttgattttataggctgtgatccagcc
catatggttacgtctttcaacactggtagtgcggtaatatgatttagaaacatcacagtcattagtgat
gctttcctcacaggtagattctggtttacaatctagtaatcacattaacagagtagtaagtcaccctacac
ttcctgttacaataactgctcatgaagacagacacatcaagtttttgacaataaaacgggtaaaatgatc
cattctatggtagctcatttggtgctgttacaagtttagcagtagatcccaatggaatctatttgatgtc
tggaagccatgactgttccattagactatggaatttgacagtaagacatgtgtacaagaaataacagctc
ataggaagaaattggatgagtcatttatgatgttgctttccatccatcaaaggcatatatcgccagtgca
ggagctgatgctcttgccaaagtatttggtg^{tga}accaacatagactcgcactcttagaaaaaaaagatttac
ttggtcagaaaggggtctgcatcactgccatcatgaaggttctctgacatgacactacatgtgatctgct
ggtgattggggcagggcagaaattgggaatcacatcctaattgtcaggtttattagtttaagtgtaat
gtattttgtgggacagaaagaaaaggactccagtatctgtgcctatactggatatgaactgagcgggtt
ttgtttttgttttttaaggtgtttaagccaatgtggagtctgctcttagggggaaggactttttgttgga
tctgtgtgctgccttagggttaggaatgtggtgctctggtggggaagcaagctccaagagtagctttgtt
atctcttagtgatcttatgttcatcagtgaaatgccacagattcccttttaagttattttgctttaaaaa
aaaaaagaaaaa 3079

LOC100046859 / cDNA clone from library plasmid pGADT7-recAB | XM_003084438.1

1857 gaagataatttgaaacaggctcagtcgtggattagaggcatcaagggtggaagttccacaaat
accctgaatgccctgaaaattgcttttgctgatgaagaaacacaagtaatctaccttctgacagatgggag
accggaccagccaccagaaatggtgatggaccacgtcaaactctttcagaacatccccatctgtgccatct
ccttcagttacaacgatgagggtgcaacgagttcttgaaggagcttgctgccttgaccggaggcgagttc
cgagcttataactttggctgcaaggatccattcaggatactcaggatgaagatctgaaccttttgcttca
ggaaatggagcaggggtcacagcgacctggagaagatgcaggagctctacatggagtccttagtcggttgact
ggtggtacaacgcagacaaggacacggatagcaaacacaaaaggaaatcttgtccatgggtttcaactcca
gaagagcgtgcaaactcccaaccgcgacgacgattcactggcttcttcccccaaatgtgtctacaggatc
atggaagtttttgaggaaaagacacagaaaaagaaaatcctccatgcagaatcaacaaaacgagcctcc
tcagaagccacatctccaacttcaagagcagcagcaacaaagacagctccaactccagctccaggagccac
acctcagctctcagcaacagag 2580

Htra2 / cDNA clone from library plasmid pGADT7-recAB | NM_019752.3

1161 gggagtttctgcatcgcggggaaaagaaaaattcctggtttggaaaccagtgggtcccagcgcc
gctacattggagtgatgatgctgaccctgactcccagcatccttattgaactacagctccgtgagccaagc
ttccctgatgttcagcatgggtgtcctcattcataaagttatcctgggctccccgcacacagggctggctc
gcggcctggatgatgatccttggccattggggagaaattggcacaataatgctgaagatgtttatgaagctg
ttcgaacccaatcacagctggcagtgccgatccggcgccgatcagagacactgaccttatatgtgacccc
gaggtcacagaa **tga**atgactggaccggcaagagtgtgaagctcttgccctgatctcctccttgccttctc
agcctaggttctgagtgcattgtgggttagaggaggagtcagtgaacctgcccaggaggcaagtcctcctaaccg
ctgcatcagtcctgggctccgaagaacacattttatataaaataaaattatacctagcaacatgtta
cagtcaaaaaaaaaaaaaaaaa 1737

Ces1d / cDNA clone from library plasmid pGADT7-recAB | NM_053200.2

1112 gtcccctacatagtgggcatcaacaagcaagagtttggctggatcattccaacgcttatgggc
tatccactcgctgaaggcaactggaccagaagacagccaattctctcttgggaagtcctaccaaacact
taaaatctctgagaatatgattccagtggtcgctgagaagtatttagggggacagatgacctcaccaaaa
agaaagacctgttccaggacttgatggctgatgtggtatttgggtgtcccatcagtgattgtgtctcgaagt
cacagagatgctggagcctccacctatatgtatgagtttgagtatcgccaagctttgtatcggccatgag
accaaggcagtaataggagaccatggtgatgagatcttctcagtatctcatttttaaaagatg
gtgcctcagaagaggagaccaacctcagcaagatgggtgatgaaattctgggccaactttgctcggaatggg
aaccccaatggtggagggtgccccactggccagaatatgaccagaaggaagggtatctgaagattggtgc
ctcaactcaggcagcccagaggctgaaggacaaagaagtgagtttttgggctgagctcagggccaaggagt
cagcccagaggccatcccacagggcaacatggtgagctc **tga**tcaggaggggtcagctgtgcttaagaacctg
gagtc aaaggagtattattccacagaagattttttagaaaaataaacacttatctttgaagctataacatt
atatggtattttatacaaatgcattaaaaaggaaatatttatctccttcaacttgtaaaaaataaaataatg
ttttgaaaatc 1966

Mlst8 / cDNA clone from library plasmid pGADT7-recAB | NM_001252464.1

186 acagtgcagcatcaggactctcaggtaaatgcattggagattactccggaccgaagcatgatt
gctgctgcaggttaccacatatccgcatgtatgatctcaactccaataacccaacccatcatcagttta
tgacggagtgcagtaagaacattgcatcagtggtgttccagaggatggctcgctggatgtatacaggtggcg
aggactgcacagctcgcatctgggacctcaggtcccggaaacttgacagtgatcagcgatcttccaggtgaac
gcaccattaattgctgtgtctgcatcccaaccaggcagaactcattgtgggtgatcagagcgggtgctat
ccacatctgggacctgaagacagaccacaatgagcagctgattcccagcctgagcttccatcacgtctg
ctcacatcgaccagatgctagctacatggcagccgtcaatagtgccggaaactgctatgtctggaacctg
acagggggcattggtgacgatgtgactcagctcatccctaagaccaagatcccagcccatacacgctatgc
cctgcaatgccgcttcagccctgattccacgcttcttggccacctgttcagctgaccagacatgtaaaatct
ggaggacatccaacttctcctgatgacagagcttagcatcaagagtagtaaccctggagagtcacccgt
ggctggatgtggggctgtgccttctcaggggattcccagtagcattgtcacagcttcttctgacaacctagc

ccggctctgggtgtgtagagactggagaaatcaagagagagtatgggtggccatcagaaagctgtcgtctgct
tggccttcaatgacagtgctgctgggttagacttggcccttgaggctgcattgggcaatcaggactgcctgg
tatagtgacgccaagaggatgtatctgaacaatacccggtccaagtgagactctcaggtagcatgtcag
gccagttggacctgaccggactatgcaggcccctcctggccaacctagactttttggctactctacgctgg
gactctttccatgcccagtttgttgtcagaaagctcactcactaagccagactggactgggagtctttgct
cctttagagagacttagacctagaggacttgggactggtgaggagggtcagaggttaatgcctgtattccagg
tatgttaccgacttgcttcagaaattaccattatggccaggcaatctgggtttattaatccctactgtc
agctgccttccataggtactgggtgacctggccagcttactgacctgtggggacaggactggcctatggaac
caaaggccaggagggttgggtaggggtcttagtctgggaggtaataaaagcagacagacacaca

1592

Atp6v1h / cDNA clone from library plasmid pGADT7-recAB / NM_133826.4

846 ggttttcaacttcaatacacaatgattttttcaatatggctcctggcattcagtcctcaaatg
tgtgagcaccttcgctcgctataatatcattcctgttctatcagacatccttcaagaatctgtcaaagagaa
agtaacaagaatcattcttgcagcattccggaatttcttagaaaaatcaacggaaagagaaactcgccaag
agtatgctctggctatgattcaatgcaaagtagtgaacagttggagaatttggagcagcagaagtatgat
gatgaagatatcagtgaagacatcaaatcttttggaaaaacttggtagagagtgtccaggaccttagctc
atgtgatgaatacagttcagaacttaaatctggaagattggaatggagccctgtacacaagtctgagaaat
tttgagagaaaaatgccgtgagggtgaaatgagaagaactatgaactcttgaaaatcttgacaaaacttctg
gaggatcagatgatccacaagtcttagctgttctgctcagatgttggagaatatgtccggcattatcc
ccggggaaaacgggttattgagcagcttgggtgaaagcagttgggtgatgaaccacatgcaccatgaagacc
agcaggttcgtacaatgctcttctggccgtgcagaagctcatggtgcacaactgggaatatcttggtaaa
caactacagtcaagcagcctcagactgctgctgctcggagctgagctgacctgttcagcctttctgcact
tcccatggaccagtggagtgagaacctcagctctttaggggttaaaagcaaatagtttttaatttaattgatta
cttcttttctgttgtatagcttttccctatggtaattcctgggagaataaaagtgtttgcttgttaaattg
tataaaattagatactgctgtattagagaaatattactgttacttataattctttatgatttttgtattta
ttgtcctctgaaaatgaatataattaaaggattctcactcacaacatgttcttaaatgtttgcttattccta
ttgtggactttgaataaacatcattttttcaataaaaaattgggagaagtgttcccagggtgatgatgaga
ag 1974